

***C. elegans* locomotion: an integrated approach**

by

Jordan Hylke Boyle

**Submitted in accordance with the requirements
for the degree of Doctor of Philosophy.**



UNIVERSITY OF LEEDS

The University of Leeds

School of Computing

December 2009

The candidate confirms that the work submitted is his own, except where work which has formed part of jointly-authored publications has been included. The contribution of the candidate and the other authors to this work has been explicitly indicated overleaf. The appropriate credit has been given where reference has been made to the work of others.

This copy has been supplied on the understanding that it is copyright material and that no quotation from the thesis may be published without proper acknowledgement.

Declarations

Some parts of the work presented in this thesis have been published in the following articles. In each case, details of the contributions by myself and other authors are detailed, as well as which chapters the contents of the articles feature in:

J. H. Boyle and N. Cohen, “The role of body wall muscles in *C. elegans* locomotion”, *Proc. IPCAT 7*, (2007) 364–375.

My contributions: The work in this paper is all my own.

Other author contributions: NC provided supervision, feedback and general guidance.

Chapters based on this work: Chapter 6.

J. H. Boyle and N. Cohen, “*C. elegans* body wall muscles are simple actuators”, *Biosystems*, 94 (2008) 170–181.

My contributions: The work in this paper is all my own.

Other author contributions: NC provided supervision, feedback and general guidance.

Chapters based on this work: Chapter 6.

J. H. Boyle, J. A. Bryden and N. Cohen, “An integrated neuro-mechanical model of *C. elegans* forward locomotion”, *LNCS: Neural Information Processing, Part 1*, 4984 (2008) 37–47.

My contributions: Principal author. Developed physical model and integration with neural model. Performed all simulations.

Other author contributions: JAB and NC previously developed and published the neural model. NC provided supervision, feedback and general guidance.

Chapters based on this work: Chapter 5 is heavily based on this work. The physical model presented in Part III is also an extension of this work.

S. Berri, J. H. Boyle, M. Tassieri, I. A. Hope and N. Cohen, “Forward locomotion of the nematode *C. elegans* is achieved through modulation of a single gait”, *HFSP J.*, 3 (2009) 186–193.

My contributions: Equal lead author. Developed motion simulator software, did majority of writing. Was a major contributor to the design of the research and interpretation of results.

Other author contributions: MT performed rheological experiments. SB performed behavioural experiments and developed skeletonizer and data analysis software. SB and NC

contributed to writing. SB, IAH and NC contributed to design of research and interpretation of results. NC also provided supervision and general guidance.

Chapters based on this work: Behavioural results are presented in Chapter 4 and the motion simulator is presented in Chapter 3. This work also heavily influenced the model presented in Part III.

N. Cohen and J. H. Boyle, “Swimming at low Reynolds numbers: a beginners guide to undulatory locomotion”, *Contemp. Phys.*, 51 (2010) 103–123.

Author contributions: This paper was an invited review, but it includes both scholarship and original contributions. NC and JHB contributed equally to this paper in a way that makes it very difficult to attribute specific parts to one author or the other. Almost all aspects of the paper were a true joint effort.

Chapters based on this work: The theory reviewed in this paper features in Chapter 2, while the original contributions (in the form of simulations) feature in Chapter 3.

Abstract

The popular model organism *Caenorhabditis elegans* is a tiny nematode worm with a largely invariant nervous system, consisting of exactly 302 neurons with known connectivity. Moreover, the behavioural roles of many of these neurons have been uncovered using experimental techniques including targeted cell killing and genetic mutations. The result is an organism in which the locomotion subsystem is mapped at cellular resolution. Despite its small size and the apparent simplicity of the underlying nervous system, the worm is capable of a surprisingly rich repertoire of behaviours including navigation and foraging, mating, learning, and even rudimentary social behaviour. Indeed, this humble worm provides us with the first tangible possibility of understanding the complex behaviours of an organism from the genetic level, right up to the system level. The focus of this thesis on the locomotion system is motivated at least in part by the fact that most, if not all, of the worm's behaviours are mediated by some form of locomotion. The main objective of this thesis is to help elucidate the mechanisms underlying *C. elegans* forward locomotion. In pursuit of this goal I apply an integrated methodology that emphasises collaboration between modellers like myself and experimentalists, ensuring that models are grounded in the biological reality and experiments are well designed and poignant.

In contrast to previous models of *C. elegans* forward locomotion, the starting point of this investigation is the realization that the ability of the worm to locomote through a variety of different physical environments can shed light on the mechanism of neural and neuromuscular control of this behaviour. This work therefore begins with the presentation of several stand-alone studies, both theoretical and experimental, aimed at answering a number of preliminary questions. These include the development of a suitable model of the worm's low Reynolds number physical environments; a preliminary study of the importance of body physics on the kinematics of locomotion; an electrophysiological modelling study of the worm's body wall muscles; and an experimental investigation of the worm's locomotion in different environments, ranging from liquid to dense gels. These results lead to a new perspective on the worm's locomotion. Indeed, the conventional wisdom is that two kinematically distinct *C. elegans* locomotion behaviours – swimming in liquids and crawling on dense gel-like media – correspond to distinct locomotory gaits. By analysing the worm's motion through these different media, we reveal a smooth modulation of the undulations from swimming to crawling, marked by a linear relationship between key locomotion metrics. These results point to a single locomotory gait, governed by the same underlying control mechanism.

The core of this thesis is an integrated neuromechanical model of *C. elegans* forward locomotion. This model incorporates the results of the preliminary investigation of mus-

cle, body and locomotion properties. The neural circuitry is grounded in the literature but simplified to a set of repeating units. Neuronal properties are modelled at different levels of abstraction, with a proof-of-concept continuous model that is used to ground assumptions in physiological data, and a simplified binary model that is then used to study the locomotion control in detail. A key property of the motor neurons in both these models is their bistable response, inspired by a recent publication demonstrating such properties in other motor neurons. Interestingly, the model is quite different to any that have come before, both in terms of its underlying neural dynamics and the behaviours that it addresses. The key achievement of this model is its ability to qualitatively and quantitatively account for locomotion across a range of media from water to agar, as well as in more complex (heterogeneous) environments. One particularly interesting result is the demonstration that a proprioceptive oscillatory mechanisms can account not only for the generation of the body undulation, but also the observed modulation in response to the changing physical environments. Indeed, this model lacks any form of centrally generated nervous system control.

Finally, the model makes a number of important predictions about neuronal functions, synaptic functions and the proprioceptive response to different physical environments. A number of experiments and experimental designs are suggested to test these predictions. Preliminary experimental results are then presented to address each of these predictions. To date, these results all appear to validate the model and uncover new information about the locomotion system, hence demonstrating the power of the holistic, integrated methodology of this work. Specifically I address the role of the inhibitory D-class neurons and find evidence suggesting that they are part of the core circuit for forward locomotion, but that the phenotype associated with their removal only manifests strongly in less resistive (more fluid) media. Furthermore, I shed light on the relative roles of neural and muscle inhibition and suggest that it may be an absence of neural inhibition that underlies the forward locomotion defect of GABA defective worms.

Acknowledgements

First of all, I would like to thank my supervisor Netta Cohen for the role she has played in this challenging journey. For one thing she has been very generous with funding, allowing me to attend more than my fair share of conferences and the like. But of far greater importance is all I have learned from her over these four years. She has helped me so much in becoming a confident and capable scientist. Netta, there is truly no supervisor I would rather have had. I would also like to thank my colleagues in the *C. elegans* group, without whom this project would have been far less exciting and productive. My thanks go specifically to Stefano Berri for the integral part he has played in my work, for staring at all those wriggling worms and for putting up with my quirks. Also to Ian Hope, for his quiet support and his faith in my crazy ideas, and to Sophie Bamps who, along with Ian, trusted my results enough to undertake the very significant job of testing them out in the lab.

Then there are the many people who have contributed to preserving what's left of my sanity. To the BioSystems group as a whole, thank you for being such a great, sociable bunch of people who have made Leeds feel like home over these recent years. Thanks for listening to my gripes over beers and putting up with my lunch time rants about some random thing. One of the main contributors to my mental and emotional well-being has been the unofficial BioSystems MMA group consisting of Marc de Kamps, Pete Appleby and Andy Handley. Guys, thank you so much for helping me to stay in shape, vent my frustrations and develop a broader base of skills.

To my wonderful parents, thank you for making me the man I am today and for making me feel loved even when you're so far away. To Jed, thank you for being such a great young man. I am truly proud to be your big brother and I know we will only get closer in the years to come. And finally to you Bonny, my darling wife, whose contribution is the greatest of all. Thank you so much for loving me as madly as you do, thank you for all you have been willing to sacrifice to follow me around the world and thank you for being the wonderful woman you are.

Contents

| | | |
|----------|---|----------|
| I | Setting the Stage | 1 |
| 1 | Introduction | 3 |
| 1.1 | An unlikely hero | 4 |
| 1.2 | Goal and approach | 6 |
| 1.3 | Thesis outline | 7 |
| 2 | Background | 9 |
| 2.1 | Biological background | 9 |
| 2.1.1 | General anatomy | 9 |
| 2.1.2 | <i>C. elegans</i> behaviour | 12 |
| 2.1.3 | Genetics | 13 |
| 2.1.4 | The neural circuit for locomotion | 15 |
| 2.1.5 | Neurons with unknown function | 26 |
| 2.1.6 | Control of locomotion | 27 |
| 2.2 | Physics background | 29 |
| 2.2.1 | Reynolds number | 29 |
| 2.2.2 | Undulatory locomotion | 32 |
| 2.2.3 | The worm's environment | 36 |
| 2.3 | Previous models | 38 |
| 2.3.1 | Niebur and Erdös | 38 |
| 2.3.2 | Bryden and Cohen | 40 |
| 2.3.3 | Sakata and Shingai | 41 |
| 2.3.4 | Suzuki et al. | 41 |
| 2.3.5 | Karbowski et al. | 42 |
| 2.3.6 | Rönkkö and Wong | 42 |
| 2.3.7 | Discussion | 43 |

| | | |
|-----------|--|-----------|
| II | Preliminary Investigation | 45 |
| 3 | Exploring the physics: motion simulator | 47 |
| 3.1 | Introduction | 47 |
| 3.2 | Methods | 48 |
| 3.2.1 | Solving the equations of motion | 48 |
| 3.2.2 | Estimating K | 50 |
| 3.3 | Validation against theory | 50 |
| 3.4 | Results | 50 |
| 3.4.1 | Numerical results versus simplified analytical treatment | 51 |
| 3.4.2 | Investigating the physics of turning | 51 |
| 3.4.3 | An unusual scallop | 53 |
| 3.5 | Discussion | 55 |
| 4 | Forward locomotion: a single behaviour | 57 |
| 4.1 | Introduction | 57 |
| 4.2 | Methods | 59 |
| 4.2.1 | Worm Culture and Behavioural Assay | 59 |
| 4.2.2 | Data analysis | 60 |
| 4.3 | Results | 60 |
| 4.3.1 | Swimming and crawling correspond to a single gait | 60 |
| 4.3.2 | The groove is not required for crawling | 64 |
| 4.3.3 | Gel media are adequately described by a single-parameter model | 65 |
| 4.4 | Discussion | 66 |
| 5 | Preliminary neuromechanical model | 69 |
| 5.1 | Introduction | 69 |
| 5.2 | Methods | 70 |
| 5.2.1 | The neural model | 70 |
| 5.2.2 | Physical model | 72 |
| 5.3 | Results | 77 |
| 5.3.1 | Single oscillating segment | 77 |
| 5.3.2 | Two phase-lagged segments | 77 |
| 5.3.3 | Extending to more segments | 78 |
| 5.4 | Discussion | 80 |

| | | |
|------------|--|------------|
| 6 | Conductance based muscle model | 83 |
| 6.1 | Introduction | 83 |
| 6.1.1 | Anatomy of body wall musculature | 84 |
| 6.1.2 | Typical effects of diffusive coupling | 85 |
| 6.2 | Methods | 86 |
| 6.2.1 | Electrical properties of the muscle body | 86 |
| 6.2.2 | Muscle arms | 88 |
| 6.2.3 | Coupling | 90 |
| 6.2.4 | Current stimuli | 91 |
| 6.2.5 | Signal-to-noise ratio | 92 |
| 6.3 | Results | 93 |
| 6.3.1 | Dynamics of the single cell model | 93 |
| 6.3.2 | Coupling between quadrants | 94 |
| 6.3.3 | Coupling within quadrants | 96 |
| 6.4 | Discussion | 102 |
| 6.4.1 | Single cell dynamics | 102 |
| 6.4.2 | Muscle coupling | 104 |
| 6.4.3 | Muscle stretch receptors | 105 |
| 6.5 | Conclusions | 105 |
| | | |
| III | An Integrated Model of <i>C. elegans</i> Forward Locomotion | 107 |
| | | |
| 7 | Integrated model: Introduction | 109 |
| 7.1 | Motivation and goal | 109 |
| 7.2 | Assumptions | 110 |
| 7.2.1 | Oscillatory mechanism | 110 |
| 7.2.2 | Neuron dynamics | 112 |
| 7.2.3 | Connectivity | 112 |
| 7.3 | Model overview | 114 |
| 7.3.1 | Physical model | 114 |
| 7.3.2 | Neuromuscular control | 118 |
| 7.3.3 | Integrated model | 121 |
| | | |
| 8 | Integrated model: Methods | 125 |
| 8.1 | Introduction | 125 |
| 8.2 | Physical model | 126 |

| | | |
|----------|---|------------|
| 8.2.1 | Structure | 126 |
| 8.2.2 | Properties of the Environment | 128 |
| 8.2.3 | Passive body forces | 130 |
| 8.2.4 | Active muscle forces | 131 |
| 8.3 | Neuromuscular control | 132 |
| 8.3.1 | Dynamics of model muscles | 132 |
| 8.3.2 | Neural circuit | 134 |
| 8.3.3 | Muscle inputs | 136 |
| 8.4 | Model variants | 137 |
| 8.4.1 | Rectangular body | 137 |
| 8.4.2 | Generic nematode circuit | 137 |
| 8.4.3 | L1 circuit | 138 |
| 8.4.4 | Minimal oscillator | 139 |
| 8.4.5 | Continuous neurons | 140 |
| 8.5 | Implementation | 141 |
| 8.6 | Data analysis | 142 |
| 9 | Integrated model: Results | 143 |
| 9.1 | Model components | 143 |
| 9.1.1 | Passive body properties | 143 |
| 9.1.2 | Muscle properties | 145 |
| 9.1.3 | Neuron properties | 145 |
| 9.2 | Integrated model | 146 |
| 9.2.1 | A single mechanism accounts for swimming and crawling | 146 |
| 9.2.2 | Evaluating the swim-crawl transition | 147 |
| 9.2.3 | The model works in artificial dirt environments | 151 |
| 9.2.4 | The model reproduces contact forces | 151 |
| 9.3 | Model analysis | 153 |
| 9.3.1 | Effects of coupling | 153 |
| 9.3.2 | Effect of neural inhibition | 156 |
| 9.4 | Model variants | 160 |
| 9.4.1 | Rectangular body | 161 |
| 9.4.2 | Generic nematode circuit | 161 |
| 9.4.3 | L1 circuit | 161 |
| 9.4.4 | Continuous neurons | 161 |

| | | |
|-----------|--|------------|
| IV | Closing the loop | 167 |
| 10 | Predictions | 169 |
| 10.1 | Introduction | 169 |
| 10.2 | A medium dependent GABA ⁻ phenotype | 170 |
| 10.2.1 | Model prediction | 170 |
| 10.2.2 | Experimental result | 172 |
| 10.3 | Importance of neural inhibition | 172 |
| 10.3.1 | Model prediction | 172 |
| 10.3.2 | Experimental result | 174 |
| 10.4 | Masking effect | 174 |
| 10.4.1 | Model prediction | 174 |
| 10.4.2 | Experimental result | 176 |
| 11 | Discussion and conclusions | 177 |
| 11.1 | Preliminary investigation | 177 |
| 11.2 | Model | 179 |
| 11.2.1 | Achievements | 179 |
| 11.2.2 | Limitations | 180 |
| 11.2.3 | Implications | 180 |
| 11.3 | Methodology | 183 |
| 11.4 | Future work | 184 |
| 11.5 | Concluding remarks | 185 |
| | Bibliography | 187 |
| A | Publications | 199 |

List of Figures

| | | |
|-----|---|----|
| 1.1 | A holistic approach to the study of biological systems. | 6 |
| 2.1 | Schematic of <i>C. elegans</i> showing dimensions and gross structure viewed A) from the left side and B) in cross section. Note that the worm bends in the dorso-ventral plane, and therefore lies on its left or right side when moving on a firm substrate. | 10 |
| 2.2 | Sequences of stills taken from movies of worms A) “swimming” in water and B) “crawling” on agar. The numbers correspond to the time (in seconds) at which the frame was taken. Note that the worm’s body bends in the dorso-ventral plane (i.e. up-down) and is therefore lying on its left or right side. (see Supplementary movies C2_1 and C2_2) | 13 |
| 2.3 | Gap junction connectivity among the core ventral cord motor neurons, created from the data of Ref. [26]. | 21 |
| 2.4 | Chemical synaptic connections among ventral cord motor neurons, created from the data of Ref. [26]. Here only neurons associated with forwards locomotion are shown to reduce the complexity of the figure. Arrows with filled heads represent inhibitory synapses while open heads indicate excitatory synapses. | 23 |
| 2.5 | Reciprocal synaptic connections in the ventral cord locomotion circuit, including neurons from both the forwards and backwards circuits, created from the data of Ref. [26]. Arrows with filled heads represent inhibitory synapses while open heads indicate excitatory synapses. | 24 |
| 2.6 | Inhibitory synaptic connections in the ventral cord locomotion circuit, including neurons from both the forwards and backwards circuits, created from the data of Ref. [26]. Red arrows indicate synapses that are were not present in Figure 2.5. | 25 |

| | | |
|-----|---|----|
| 2.7 | Chemical synaptic connectivity involving VC class neurons, created from the data of Ref. [26]. The sole synapse to VC class neurons from motor neurons of other classes is marked in red. | 27 |
| 2.8 | Chemical synaptic connectivity involving AS class neurons, created from the data of Ref. [26]. | 28 |
| 2.9 | The effect of K on propulsion. An undulating body propagates a sinusoidal wave to the right at velocity v_{wave} (red arrow). If $K = 1$, no motion will result (not shown). If $K > 1$ (A), the body moves at velocity v_{prog} in the direction opposite to v_{wave} , with $ v_{\text{prog}} \leq v_{\text{wave}} $. If $K < 1$ (B), the situation reverses and the body moves in the same direction as v_{wave} , with $v_{\text{prog}} < v_{\text{wave}}$ | 37 |
| 3.1 | Assessing the validity of Eq. (2.7) with a physics simulator (see text for details). A) The analytic result of Gray et al. [43] is an excellent approximation for an undulator with a perfectly sinusoidal wave, a wavelength that is short relative to the body length and of a low amplitude. B) A purely sinusoidal idealization of the <i>C. elegans</i> crawling wave. The same equation handles such a wave reasonably well but with small errors due to the increased amplitude and wavelength. C) A more realistic <i>C. elegans</i> crawling waveform in which the wavelength increases towards the tail introduces significant errors. D) A realistic <i>C. elegans</i> swimming waveform in which the wavelength is greater than the body length is very poorly described by the analytic approximation. | 52 |
| 3.2 | Schematic demonstration of turning in simulated worms. The key requirement for turning is a dorsal/ventral curvature bias. A) A virtual worm with a purely sinusoidal locomotion waveform (four representative times are shown) has zero curvature bias (dotted line). B) The resulting centre of mass trajectory (thick line) has an oscillatory component, but the overall motion is in a straight line (thin line). C) Another virtual worm is generated by superimposing a sinusoidal locomotion wave (as in A) onto a circle with radius R , leading to a dorsal curvature bias (dotted line). D) The resulting centre of mass trajectory is highly curved (thick line), and approximates a circle (thin line) with the same radius R as was used in creating the body wave. | 54 |

| | | | |
|-----|------|--|----|
| 3.3 | A) | <p>A variation on Purcell’s scallop in which the two arms have different lengths and are allowed to rotate freely (like a wheel). Arms are modelled as slender cylindrical bodies. The medium is modelled as Newtonian ($K = 2$). The path of the scallop’s “centre of mass” (CoM, red dot) is shown in black. After a few rotations, the CoM appears to undergo both translation and rotation. However, the CoM never leaves a circular area of small radius, as can be seen by following the trajectory over sufficiently many cycles (B). Each “petal” corresponds to one cycle of rotation through 2π.</p> | 55 |
| | | | |
| 4.1 | | <p>Calculating the wavelength λ and frequency f of the locomotion wave. Locomotion waveforms are expressed in terms of the time varying curvature along the length of the body (colours correspond to different values of curvature, according to the colour bar), with positive values denoting dorsal bending and negative values denoting ventral bending. The propagation of the wave from head to tail gives rise to the visible stripes of approximately constant curvature, to which we fit a linear approximation (diagonal black lines). Wavelength and frequency can then be obtained based on the vertical and horizontal spacing respectively.</p> | 61 |
| | | | |
| 4.2 | A-C) | <p>Proportionality of key locomotion parameters in a variety of environments (a range of gelatin concentrations, deformable agar surface, non-deformable membrane surface, with $n \geq 3$ replicates per environment). Lines show the best linear fits to the data. D-F) Frequency, wavelength and amplitude of the locomotion wave all decay smoothly with K in the different media (gelatin and agar, with $n \geq 3$ replicates per environment). Lines show the best power-law fits to the data. Note the doubly logarithmic scales. In all graphs, filled circles show gelatin data. Different colours represent different gelatin concentrations as indicated. Agar and membrane data are represented by black triangles and white squares respectively.</p> | 62 |

| | | |
|-----|--|----|
| 4.3 | Locomotion waveforms visualised in terms of the time varying curvature along the length of the body [13]. Colours correspond to different values of curvature (see colour bars on right), with positive values denoting dorsal bending and negative values denoting ventral bending. The propagation of the wave from head to tail gives rise to the visible stripes of approximately constant curvature. By comparing the plots for different media, it can be seen that the locomotion waveforms of swimming and crawling are qualitatively equivalent, differing only in the inclination of the stripes and the spacing between them. | 63 |
| 4.4 | Sequences of four midlines extracted from movies of worms moving in/on different media. A-C) Worm midlines have been displaced vertically, rotated and aligned for clarity, with the head to the left and time increasing from top to bottom in quarter-period steps. The scale bar corresponds to approximately 0.1 mm. Estimated K values are A) 35, B) 35 and C) 1.9. D) Same midlines as above (A-C), still rotated, with the head to the left, but without removing the centre of mass motion. | 64 |
| 4.5 | A) Similarity of simulated and recorded CoM trajectories for a worm moving on an agar surface. B) Histogram of the magnitude of total error per time step between the real and recorded motion. The right-most bin includes all errors greater than 10 %, which occur due to noise in the recorded CoM trajectory (visible as irregularities on the black trajectory in A). | 66 |
| 5.1 | A) Schematic diagram of the physical model illustrating nomenclature (see text for details). B) The neural model, with only two units shown (the tail and one body). AVB is electrically coupled to each of the motor neurons via gap junctions (resistor symbols). | 73 |
| 5.2 | Decomposition of forces applied to the solid rods of the physical model. Initially, forces are represented in terms of x and y components (left). They are then converted to a coordinate frame relative to the orientation of the rod, before further separating the tangential components into odd and even subcomponents. See text for details. | 75 |
| 5.3 | Oscillations of, A) the original neural model [21] and, B) the integrated model (with $C_{\perp} = 80 \times 10^{-6} \text{ kg}\cdot\text{s}^{-1}$). Note the different time-scales. C) Oscillation frequency as a function of variable $C_{\perp} = 100C_{\parallel}$. The zero frequency point indicates that the segment can no longer oscillate. | 78 |

| | | |
|-----|---|----|
| 5.4 | Phase lagged oscillation of two segments. A) Bending angles extracted from a recording of a forward locomoting worm on an agar substrate. The traces are of two points along the worm (near the middle and $\frac{1}{12}$ of a body length apart). B) Simulation of two coupled units in the neural model. C) Simulation of the integrated model. Take note of the different time scale in subplot B) | 78 |
| 5.5 | Oscillation of the model with two body segments ($i = 1,2$) and one tail segment ($i = 3$). While the model is still able to oscillate, the waveforms are distorted and the correct phase lags are not preserved. | 79 |
| 5.6 | Frames extracted from a movie of the 11 segment integrated model (See Supplementary movie C5_1). Numbers in the top right corners give the time in seconds at which each frame was taken. Notice that despite the lack of coordination, the model still moves forwards (to the left). | 79 |
| 6.1 | Schematic showing the layout of body wall muscles and the gap junctions that connect them, based on the data of Ref. [76]. Within each quadrant the muscles are arranged in two staggered rows (L1, L2 or R1, R2). Gap junction coupling (red 'I' shapes) occurs with a regular pattern both within and between quadrants, which straddle the nerve cord (thick black line). | 85 |
| 6.2 | Equivalent circuit diagram of the muscle model showing currents, voltages and parameters of the muscle body (bottom right of figure), muscle arms (with two of ten compartments of one arm shown and remaining arms appearing in parallel) and coupling. All labels correspond to those in the text. | 89 |
| 6.3 | Whole cell current (A) and voltage (B) clamp traces from body wall muscle cells reproduced with permission from [64], with stimulus protocols shown below the traces. The response of the model muscle cells to identical stimuli are shown in (C) and (D). | 94 |
| 6.4 | Current-voltage relationships for the peak calcium (A) and steady state potassium (B) currents taken with permission from [64] and [65] respectively. Currents are shown normalised by cell capacitance. In (B), the relevant curve is the one labelled control. The corresponding relationships produced by the model are shown in (C) and (D). | 95 |

| | | |
|-----|--|-----|
| 6.5 | Whole cell I-V curve for a model muscle cell. The cell was held at -70mV by injecting hyperpolarizing current and then stimulated with 400ms depolarising current steps. The membrane potential at the end of the stimulus was recorded. | 95 |
| 6.6 | A) Model structure used to investigate the effect of gap junctional coupling between left and right quadrant muscle cells that are innervated by the same set of motor neurons (MN). The left muscle cell (LM) receives the full stimulus of amplitude A , while the right cell (RM) receives an attenuated signal of amplitude $A' = \alpha A$. Simulations are performed with and without gap junctional coupling g_{inter} . B) The percent change (ϵ) in the voltage difference between the left and right cells increases with increasing attenuation. | 97 |
| 6.7 | Effect of inter-quadrant coupling in the extreme (unrealistic) case of 100 % attenuation. The left muscle arms are stimulated by a sinusoidal current with peak amplitude of 500 pA while the right muscle arms are unstimulated. This leads to significant depolarisation of the left muscle (middle), which in turn causes current to flow through the gap junction into the right muscle arms. The resulting depolarisation of the right muscle body is just under 1mV (bottom). | 97 |
| 6.8 | Gap junction coupling is too weak to propagate significant activity. A muscle quadrant is simulated (only three cells shown) and the first cell is stimulated with a strong current pulse (250 pA for 500 ms). This causes a large ($> 40\text{ mV}$) depolarisation of the first cell (V_1), and small ($< 3\text{ mV}$) depolarisation of the second (V_2). By the third cell the depolarisation is insignificant ($< 0.5\text{ mV}$). | 99 |
| 6.9 | The effects of intra-quadrant coupling for two candidate waveforms. Inputs are (A) sinusoidal and (B) “sawtooth” (similar to the outputs of the neural model in Refs. [20, 21]), with a frequency of 0.5 Hz and a phase shift of $\frac{\pi}{8}$ between adjacent cells. In each case the simulations were performed with a chain of 24 coupled cells. Each plot shows (from top) the input current, membrane potential with and without coupling, normalised internal calcium concentration ($[Ca^{2+}]_i / \max[Ca^{2+}]_i$) with and without coupling, and the difference between the coupled and uncoupled calcium concentrations ($\Delta[Ca^{2+}]_i = ([Ca^{2+}]_{i,\text{coupled}} - [Ca^{2+}]_{i,\text{uncoupled}}) / \max[Ca^{2+}]_i$) for two representative (neighbouring) cells from near the middle of the chain. Note the nearly identical waveforms with and without coupling. . . | 101 |

| | | |
|------|---|-----|
| 6.10 | The significance of muscle coupling depends strongly on the phase lag (ϕ) and weakly on the frequency (F) of the sinusoidal input waveform. The effect is quantified by the peak (A) and mean (B) value of the difference between the muscle potential traces in the coupled and uncoupled cases. Phase lags used range from 0 to π in steps of $\pi/24$ | 102 |
| 6.11 | Effect of intra-quadrant coupling in the most extreme case of square wave input with a depolarising bias, which increases the sensitivity of $[Ca^{2+}]_i$ to potential changes. Panels show (from top) the input current, membrane potential with and without coupling, normalised internal calcium concentration with and without coupling, and the difference between the coupled and uncoupled calcium concentrations, as in Figure 6.9. | 103 |
| 6.12 | Two stages of low-pass filtering occur in the muscles, having a large effect on SNR. The first stage has its effect on the membrane potential, and the second on the internal calcium concentration. Coupling results in a small further improvement due to a small change in the effective input impedance. | 103 |
| 7.1 | Structure of the physical model. The worm is represented by 49 solid rods (black lines) whose end points (black circles) are connected by lateral (red) and diagonal (blue) elements. | 116 |
| 7.2 | The worm's locomotion wave exhibits a posteriorly decreasing gradient in curvature, averaged over time ($\bar{\kappa}$). S is a measure of the position along the worm's body, with $S = 0$ corresponding to the head and $S = 1$ corresponding to the tail. A) Experimentally observed curvature gradient obtained by averaging the curvature at each point along the body, first over time and then over several worms ($n = 3$ for agar and $n = 5$ for water). Bars indicate the standard deviation over the n worms. B) Qualitatively similar curvature gradients exhibited by the model, due to the gradients in muscle efficacy and stretch receptor weighting. | 121 |
| 7.3 | Oscillation of the integrated model showing the total current input (top) and states (bottom) of the dorsal (black) and ventral (red) neurons. The blue lines represent the distinct thresholds for turning on (higher) and off (lower). When the red line in the top panel is dashed, this indicates that the ventral neuron is receiving inhibition from the dorsal neuron. The excitatory input from AVB is switched on at $t = 1$ second. | 122 |

| | | |
|-----|---|-----|
| 8.1 | A) Schematic diagram of the physical model illustrating nomenclature (see text for details). B) Schematic of the neuromuscular model, showing one of 12 repeating units making up a symmetrized circuit for forward locomotion control. The circuit includes a pair of B-class excitatory neurons (circles), a pair of D-class inhibitory neurons (squares) and four muscles (diamonds) on each side. Synapses are labelled either as excitatory (arrowhead) or inhibitory (circlehead). Posteriorly directed lines from B-class neurons denote the stretch receptor inputs. | 133 |
| 8.2 | Modified schematics for alternative model variants. A) Generic nematode circuit with two-way neural inhibition. B) L1 larva circuit in which only dorsal neurons are present. | 138 |
| 9.1 | Frames taken from a simulation showing the dynamics of the passive physical model, with frame times (in seconds) given in the corner. The model is manually bent either in water (A) or on agar (B) before being released at $t = 0$ | 144 |
| 9.2 | The force generated by model muscles is a function of their activation, length and rate of contraction. A) Force/length relationship obtained by holding the muscle at a specific length (preventing it from contracting. B) Force/velocity relationship obtained by allowing the muscle to contract at a specified rate and measuring the force it exerts at the moment it reaches its rest length L_{0L} . The model therefore provides a simple linear approximation of these properties of biological muscles. Note that in both cases $-f$ is plotted for simplicity, because contractile forces are defined as negative in the model. | 145 |
| 9.3 | Dynamics of A) binary and B) continuous model B-class neurons. Note the different thresholds for activation and deactivation. | 146 |
| 9.4 | Stills taken from movies of the model moving in (from left) water, intermediate gelatin, agar, a microfluidic environment as described in [90] and a microfluidic environment as described in [78] (see Supplementary movies C9_1 to C9_5). Frame times, in seconds, are given in the top right corner. | 148 |

| | | |
|-----|--|-----|
| 9.5 | A) Experimentally observed transition from swimming to crawling, from Chapter 4, showing locomotion in gelatin (circles; colours indicates percent gelatin concentrations as in Figure 4.2) and agar (black triangles). The grey line is the best linear fit to the data. B) The model reproduces the swim-crawl transition with reasonable quantitative agreement. Colours denote the product of tangential and normal drag coefficients, ranging from light yellow (virtual water) to dark red (virtual agar) and correspond to the colours in Figure 9.6. The data points representing water and agar are marked with squares of the appropriate colour. Wave properties are extracted as described in Section 8.6. The grey line is again the linear fit from panel A), provided for comparison. | 149 |
| 9.6 | Values of C_{\parallel} and C_{\perp} used to evaluate the swim-crawl transition. Values for each drag coefficient range from water (pale yellow square) to agar (dark red square), but only combinations that yield $1.5 \leq K \leq 40$ were used. Of those combinations for which simulations were performed, some yielded uncoordinated locomotion as described in the text. These values are marked with black dots. Data from the remaining combinations (filled circles) was used to generate Figure 9.5. Colours denote the product of tangential and normal drag coefficients, ranging from light yellow (virtual water) to dark red (virtual agar). | 150 |
| 9.7 | Stills taken from movies of the model moving in novel microfluidic environments. A) A square layout can also impose a crawling-like waveform if the posts are sufficiently closely spaced and with the addition of a ceiling effect as in Ref. [78]. B) With agar-filled chambers, which impose a crawling-like waveform, widely spaced posts can become obstacles. . . . | 152 |
| 9.8 | Effect of coupling in the minimal oscillator model with one DB (red) and one VB (black) neuron. A) No coupling is included, allowing the dorsal and ventral neuron to maintain their starting phase lag. B) The addition of neural inhibition ($w_{-}^V = 0.4$) efficiently imposes an anti-phase relationship. C) Physical coupling ($\alpha_{\text{physical}} = 0.3$) also imposes an anti-phase relationship, though it does so more slowly. D) Contrary to conventional wisdom, muscle inhibition ($\bar{w}_{\text{NMJ}} = 0.4$) tends to impose in-phase synchrony. | 154 |

| | | |
|------|---|-----|
| 9.9 | Interaction between multiple forms of coupling. A) With neural and muscle inhibition, the effect of neural inhibition wins. When combining physical coupling with muscle inhibition, different effects are possible. B) If physical coupling is sufficiently weak, muscle inhibition dominates, whereas if muscle inhibition is sufficiently weak (C), physical coupling dominates. D) If neither is sufficiently weak, oscillations are quenched. | 155 |
| 9.10 | State transition diagram for the B class model neurons. See text for an explanation. | 156 |
| 9.11 | Stills taken from movies of model variants, with the frame time (in seconds) given in the top right corners. The conditions are (from left) rectangular body model in water, rectangular body model on agar, L1 model in water, L1 model on agar, continuous model in water and continuous model on agar. | 160 |
| 9.12 | Postsynaptic currents in response to excitation of motor neurons, normalised by the maximum current. A) Postsynaptic currents in response to light stimuli reproduced with permission from Ref. [77]. Symbols indicate experimental data points and the solid lines are the best single exponent fits. B) Postsynaptic currents at the model NMJ in response to depolarising current injection to a VB motor neuron. Red squares are for comparison with (A). | 162 |
| 9.13 | Postsynaptic response of the model to hyperpolarizing and depolarising currents. The blue circle indicates the postsynaptic current at the neuron's rest potential. | 163 |
| 10.1 | Stills taken from movies of real and simulated GABA defective worms, with frame times (in seconds). Columns are (from left) <i>unc-30 (e191)</i> mutant worm in water, <i>unc-30 (e191)</i> mutant worm on agar, model GABA ⁻ worm in water and model GABA ⁻ worm on agar. | 171 |
| 10.2 | Stills taken from movies of real and simulated defective worms, with frame times (in seconds). Columns are (from left) <i>unc-8 (e49)</i> mutant worm in water, <i>unc-8 (e49)</i> mutant worm on agar, model worm with paralysed tail in water and model worm with paralysed tail on agar. | 175 |

List of Tables

| | | |
|-----|---|-----|
| 5.1 | Parameters for a self-oscillating tail unit ($j = N$), as in Ref. [21]. | 72 |
| 5.2 | Parameters for body units ($j < N$) and tail-body interactions as in Ref. [21]. All body unit parameters that are not included here are the same as for the tail unit. | 72 |
| 5.3 | Parameters of the physical model. | 74 |
| 6.1 | Parameters for the muscle body obtained by fits to experimental traces (see text for detail). Reported values are given where possible. The two values of C_A and C_B were used in the simulations for compatibility with voltage- and current-clamp data [64, 65] and coupling parameters [76] respectively. | 88 |
| 6.2 | Muscle arm compartment parameters, obtained from estimates of the cell properties and dimensions (see text). | 90 |
| 6.3 | Intra- and inter-quadrant coupling parameters. g_{intra} and g_{inter} were re- ported [76]. The remaining parameters were obtained by curve fitting to Figure 2 B of Ref. [76]. | 91 |
| 8.1 | Parameters of the physical model | 132 |
| 8.2 | Parameters of the neuromuscular model | 136 |
| 8.3 | Continuous model parameters. Any parameters not given here are the same as in the original model. | 142 |
| 9.1 | Locomotion metrics for real (top) and simulated (bottom) worms moving in water and on agar. Values are given as mean \pm standard deviation. Note that the standard deviation for simulated worms is always zero. . . . | 147 |
| 9.2 | State transitions and associated thresholds. See text for an explanation. . . | 159 |

Part I

Setting the Stage

Chapter 1

Introduction

Ever since we first realised that life is the result of processes that are ultimately comprehensible, scientists have strived to understand the apparent miracles of the natural world. Yet despite the truly remarkable advances that have been made, we have barely scratched the surface of this frontier. The problem we face is the phenomenal complexity of biological systems at every level of organisation. When one is touched by a work of artistic expression, be it music or literature, it is hard to believe that both the work itself and your emotional reaction to it are emergent properties of what is essentially three pounds of meat (albeit very well organised meat). Looking at a single one of the billions of neurons that make up the brain, one is struck simultaneously by its complexity and its simplicity. On the one hand, how can the human mind emerge from a network of units whose dynamics, to a first approximation, are those of an integrator. But on the other hand, if one looks more closely at that single neuron it becomes clear that it is an immensely complex system in its own right, whose “simple” dynamics are the result of an intricate molecular ballet that hardly seems less complex than the neuronal network of which it is a part. Directing this dance within each and every cell is the gene regulatory network, a dynamical system of great complexity that is the subject of extensive research. One of the big questions at this level of organisation is how the gene regulatory network gives rise to the myriad of distinct cell types that make up an organism, despite each cell containing an identical set of instructions encoded in its DNA. The discovery of DNA in the mid 20th century, and the realization that it somehow encodes all the information required to build a specific organism, was quite possibly the greatest scientific revelation of modern

history. Indeed, these molecules, consisting of nothing more than four distinct symbols called bases (adenine, thymine, guanine and cytosine), can be said to define all that we are. But again, despite incredible advances, the complexity of the genetic code means that we are still a long way from truly understanding how you or I have emerged from a sequence of 3 billion base pairs.

Whereas in some sense we are nothing more than an exquisitely complex set of chemical reactions, realistically we have no hope of understanding animal behaviour in these terms. Fortunately, while each level of organisation interacts with the others, they are still somewhat separable. Indeed great progress can be made in understanding cell function without being overly concerned with the atomic forces that ultimately hold it all together. We are therefore each free to study biological systems at the level that appeals to us most as individuals. Achieving the ultimate goal of a full understanding of life, from top to bottom and from bottom to top, will involve the parallel efforts of scientists in a great many fields. To me personally, the most interesting aspect is the neural basis of behaviour. But even within this area there is choice in terms of the scale and level of abstraction on which to focus.

In any organism, the sensory and motor components of the nervous system are relatively easy to study, because they interface directly with the outside world – sensory stimuli can be controlled and motor behaviour can be recorded. In higher animals like mammals, the input and output are coupled via a complex mind, whose internal state is likely to play a major role in sensory-motor response. For this reason it is simpler organisms, whose behaviour is much more sensory driven, that appeal to me most of all. These animals, whose nervous systems are relatively hard-wired and that generate useful, intelligent behaviour without comprehension, are far more tractable than their more impressive relatives. One such animal, that could almost be considered a biological robot, is the subject of this thesis. Its name is *Caenorhabditis elegans*, known to its friends as *C. elegans* or simply “the worm”.

1.1 An unlikely hero

Amidst the many fascinating members of the animal kingdom, a primitive 1 mm nematode worm is an unlikely hero indeed. Barely visible to the naked eye, this tiny transparent creature is the focus of a great many scientific careers, has been the subject of Nobel Prize winning work on three separate occasions [18,23,39,59,86,108,116,122] and is probably the best characterised of all animals. Many factors contribute to the worm’s lofty position, but it is primarily a combination of its anatomical simplicity and amenability to a variety

of experimental techniques that make it such an attractive organism to study [17]. Further details will be discussed in Section 2.1, so what follows is merely a brief overview.

C. elegans is, first and foremost, a genetic model organism. Thanks to the efforts of a great many molecular biologists, the *C. elegans* community is now at a point where the expression of specific genes, many of which have known functions, can be precisely controlled. One application of this is to silence the function of genes that would normally be expressed in a cell. By observing the resulting changes in the worm's behaviour, the roles of that gene (or rather, the protein that the gene codes for) can be inferred. Another application is to induce the expression of genes (either native or foreign) in specific cells. This is often used to express fluorescent proteins in certain cells, making them glow visibly under a suitable microscopy set-up. Fluorescent proteins can also be used to identify which cells express a particular gene. Recent advances have made it possible to encode proteins whose fluorescence is correlated with calcium levels within a cell (a good indicator of electrical activity), or that allow a cell to be electrically excited by an external light source. The application of such techniques is greatly facilitated by the worm's transparent body and very short life cycle.

While the techniques of genetic manipulation are undoubtedly the largest contributors to our detailed understanding of the worm, there are other factors of huge importance to studies of the neural basis of behaviour. Chief among these is the fact that the worm's nervous system consists of a mere 302 neurons and is essentially hard wired and invariant between individuals. Even more remarkably, the connectivity of this compact neural circuit has been experimentally mapped. With such a limited neural circuit, the worm is unlikely to have much by way of a mind, and instead operates more like a complex sensory-motor device. Accordingly, an unusually high percentage of neurons have sensory or motor function, with short neural pathways from input to output. But while the connectivity of the *C. elegans* nervous system is known to an unprecedented degree of accuracy, far less information is available on the dynamical properties of these neurons. Thus the question of the neural basis of the worm's behaviour is still an open and attractive one.

While this humble creature provides us with the first tangible possibility of understanding the complex behaviours of an organism from the genetic level, right up to the system level, achieving this grand goal is still no mean feat. It will help, however, to focus on a well defined subset of behaviour. Specifically our group has chosen to focus on locomotion, which is by far the worm's primary motor output and is involved in almost everything that it does.

1.2 Goal and approach

The main objective of this research project is to elucidate the mechanisms of *C. elegans* forwards locomotion. While the underlying neural control obviously plays a major role in locomotion, it is not the only component to be considered. As this thesis argues, it is important to study the worm's locomotion as an integrated whole, rather than focussing exclusively on certain subcomponents. This in turn requires that a broad base of knowledge be brought to bear.

This is perhaps a good time to address the fact that my work, despite being thoroughly biological in its subject matter, falls under the banner of the School of Computing. Indeed my background is neither biological nor experimental, so some might ask what exactly I have to offer the *C. elegans* community. After all, the vast majority of worm research is performed by “traditional” biologists, and this approach has yielded results of great significance. But for some aspects of biology, particularly the study of animal behaviour, a holistic approach has the potential to be more powerful. Specifically, the methodology I advocate is to augment the experimental approach through the use of computer assisted data analysis, computational modelling and theory, as illustrated in Figure 1.1. Assuming that the hurdle of finding a common “language” can be overcome, a multidisciplinary group has the advantage of combining members with diverse skills who can complement their colleagues and compensate for each others weaknesses.

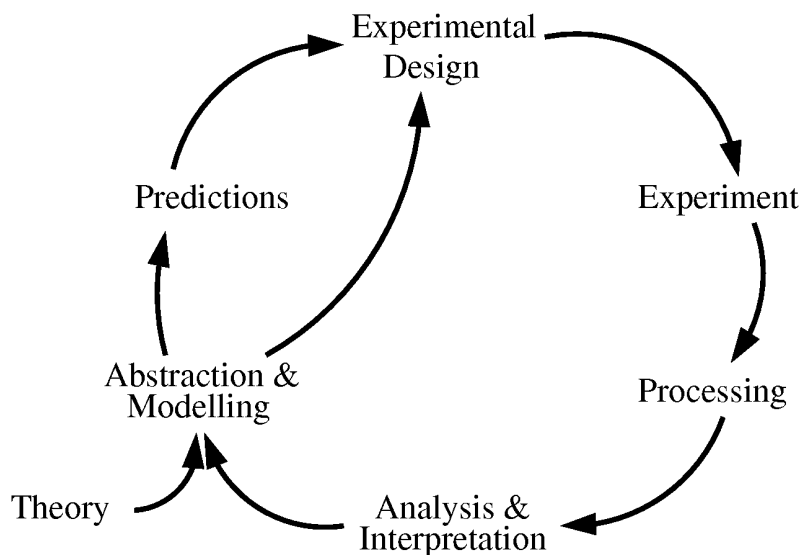


Figure 1.1: A holistic approach to the study of biological systems.

When tackling biological questions, it is vital to start with a large foundation of experimental data. This makes it possible to begin forming preliminary ideas as to how the

system is likely to function. These initial ideas are unlikely to be correct, because the complex nature of biological systems means this information is generally open to interpretation, is inevitably at least somewhat incomplete and represents a variety of different experimental approaches. But after suitable processing, analysis and interpretation, the data can be consolidated and abstracted to develop an initial model of the underlying system. In my case these models are computational, but they could just as easily be mathematical or more abstract and high level. It is also often possible to incorporate theory, such as a knowledge of body mechanics, to further guide the modelling effort. At this point it may become apparent that some crucial piece of information is missing, necessitating the design of new experiments aimed specifically at filling in these gaps. Alternatively (and with judicious use of assumptions) it may be possible to complete a working model of the system in question. Once a preliminary model has been formed it may yield predictions, which in turn will motivate the design of further experiments to test said predictions, and hence the model itself. The cycle can then continue, with each iteration refining both the model and the experimental design until a relatively complete understanding of the system is achieved.

Inevitably, no one person will have the necessary skills (or the time) to understand all of the components of Figure 1.1 completely. It is for this reason that a multidisciplinary group is so important. Complications arise from the fact that people with different backgrounds and expertise tend to look at the world a bit differently, and often speak somewhat different languages. But by ensuring that there is significant overlap among the roles of each group member, one can facilitate effective communication, interaction and cooperation towards the ultimate goal – in this case a complete understanding of *C. elegans* locomotion.

1.3 Thesis outline

The remainder of this thesis is organised as follows. In Chapter 2 I set the stage for my research by outlining the relevant background material. Section 2.1 provides an overview of *C. elegans* and its anatomy, behaviour and neural circuit for locomotion. Following this, Section 2.2 introduces the relevant physics, with special reference to undulatory locomotion of small organisms. Section 2.3 introduces the previous models of the worm's locomotion, before highlighting the key open questions in Section 2.3.7. Please note that while Chapter 2 is primarily a literature review, it also includes some of my own critique and interpretation of data.

Having established the foundations on which this work builds, Part II consists of sev-

eral largely independent preliminary studies aimed at addressing some of the key open questions identified in Chapter 2. Chapter 3 details a novel motion simulator and the results of its application to several basic questions related to undulatory locomotion in general. I also describe how the simulator can be used to estimate properties of the worm's environment, which is relevant to the following chapter. Chapter 4 presents the results of an important experimental investigation that demonstrates the effect of different physical environments on the worm's locomotion. Next, in Chapter 5, I present a preliminary neuromechanical locomotion model, the results of which significantly influence the work in Part III. Finally, in Chapter 6 I use a detailed, conductance-based model of the worm's muscles to investigate their possible contribution to the control of locomotion.

Part III of this thesis is dedicated to my primary contribution, which is an integrated model of *C. elegans* forwards locomotion. In Chapter 7 I begin by consolidating the ground work and outlining the key assumptions that go into the model. This is followed by a non-technical overview of the model that is intended to give an intuitive understanding of how it works. The details of the model are given in Chapter 8, leading to the results in Chapter 9.

In line with the approach outlined in Figure 1.1, the last part of this thesis aims to close the loop, relating my main results back to the biology. In Chapter 10 I present three predictions generated by the model, as well as the results of experiments used to test them. My final conclusions are then presented in Chapter 11, bringing this thesis to a close.

Chapter 2

Background

In this chapter I will introduce the background information that is relevant to the remainder of this thesis. I will begin with a review of *C. elegans*, with particular reference to the neural circuit for locomotion. I will then introduce the theoretical foundations that shape our understanding of the physics of the worm's locomotion. Finally I will briefly discuss the previous models of *C. elegans* locomotion.

2.1 Biological background

2.1.1 General anatomy

Caenorhabditis elegans is an extremely popular model organism and as such is the subject of several on-line resources including *WormBase*, which focusses on the worm's genetics and *WormAtlas*, with a focus on anatomy. In particular, the Handbook of *C. elegans* anatomy [5], freely available via *WormAtlas*, provides an excellent introduction to the worm's anatomy, along with more detailed sections on specific subsystems. It would be impractical to provide a similar level of detail here, so I will instead provide just a brief overview of the worm's general anatomy and refer the interested reader to the aforementioned work.

C. elegans is a species of non-parasitic nematode (roundworm). The vast majority of individuals are self-fertilizing hermaphrodites, but males are also found on occasion [17]. Much less is known about the male than the hermaphrodite, and this thesis will focus

exclusively on the latter. The adult hermaphrodite is about 1 – 1.2 mm long, and approximately $80\ \mu\text{m}$ in diameter, with a tubular body that is tapered at both ends (see Figure 2.1 A). The entire adult worm consists of exactly 959 cells (excluding those that will become sperm and eggs), of which 302 are neurons and 95 are body wall muscles [133]. The locomotion nervous system is of particular significance to this work and will be discussed in more detail in Section 2.1.4. Here I describe the gross structure of the body and nervous system.

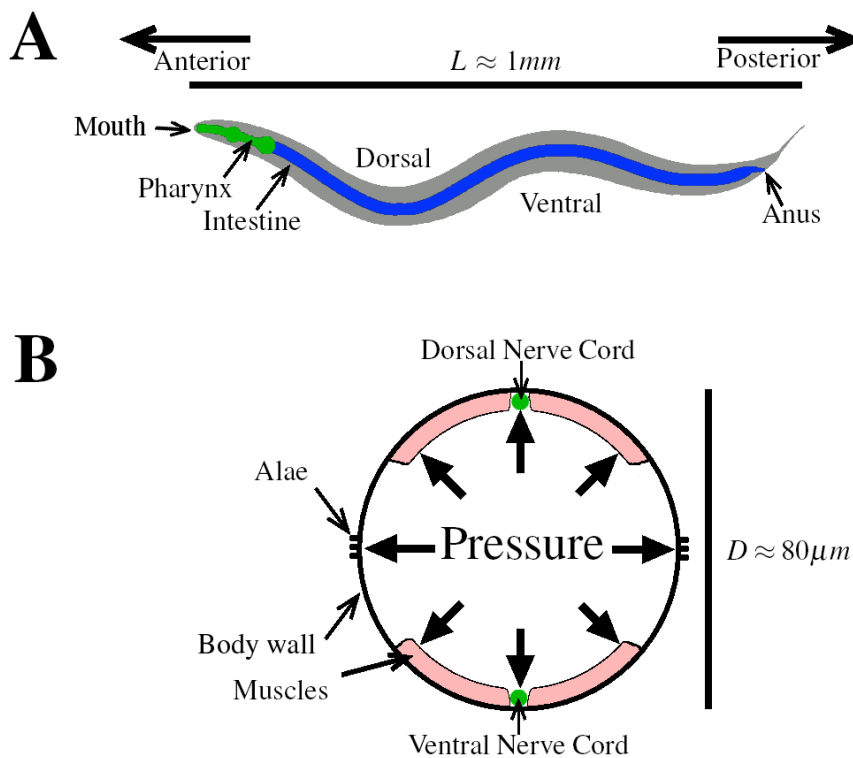


Figure 2.1: Schematic of *C. elegans* showing dimensions and gross structure viewed A) from the left side and B) in cross section. Note that the worm bends in the dorso-ventral plane, and therefore lies on its left or right side when moving on a firm substrate.

Like all nematodes, *C. elegans* has a non-segmented body and lacks any rigid components, instead relying on a “hydrostatic skeleton” which essentially consists of a flexible outer tube (consisting of the cuticle and hypodermis) filled with pressurised fluid (in addition to the gut and reproductive organs) [6]. The result can be likened to the balloons used to make animals at a children’s party – the combination of an external elastic sheath and internal pressure creates as firm yet pliable structure. Unlike a balloon, the cuticle (which is shed at the end of each larval stage) has a structured surface. Alternating circumferential ridges and furrows called annuli give a wrinkled appearance, while longitudinal

tread-like ridges called alae run along the left and right sides of the body [30].

Within the outer tube of the body is the inner tube of the digestive system. The worm survives primarily on a diet of bacteria, which enter through the mouth situated at the tip of the head and are sucked into an organ called the pharynx. The pharynx is a tubular structure with two bulbs and consists of muscles that are controlled by a dedicated nervous system of 20 neurons. Its role is that of a pump and grinder, preparing the bacteria for digestion by the intestine which runs from the back of the pharynx to the anus near the tail [4]. The body cavity also contains the gonads, uterus and eggs.

Bending of the body is achieved via the longitudinal contraction of body wall muscles that are arranged in four quadrants [7] (see Figure 2.1 B) and are anchored to the basal lamina (one of the layers making up the worm's body wall). The individual muscle cells are quite flat and, unlike vertebrate skeletal muscles that attach only at their end points, have one entire side attached to the basal lamina [22]. This is important because it allows muscle contraction to generate smooth bending, rather than causing kinks or folds in the cuticle. Each quadrant (dorsal left, dorsal right, ventral left and ventral right) consists of either 23 (ventral left) or 24 muscle cells. Along most of the body, muscles in the two dorsal quadrants (and similarly the two ventral quadrants) are controlled by the same set of neurons [135]. As a result, most of the body is only capable of bending in the 2D dorso-ventral plane. In contrast the head (first four muscles per row) and neck (next four muscles per row) receive input from head motor neurons that enable bending in 3D.

Of the worm's 302 neurons, 20 form the pharyngeal nervous system [4] and the remaining 282 form the somatic nervous system which is distributed throughout the body. Most *C. elegans* neurons have simple structure (either monopolar or bipolar¹) [136], though there are some exceptions with more complex, branching structures. The highest concentration of neurons is found in the nerve ring, which circles the pharynx in the head and is the closest the worm has to a brain. In addition, several ganglia² are found in the vicinity of the head and tail. In lieu of a spinal cord, the worm has two nerve cords which run along the dorsal and ventral sides of the body wall. While the dorsal nerve cord (DNC) contains only neural processes, the ventral nerve cord (VNC) also contains many neural cell bodies distributed along its length [135], most of which are motor neurons that innervate the body wall muscles. Unusually, nematode body wall muscles have several thin processes (muscle arms) which extend to the appropriate nerve cord where they form neuromuscular junctions [34].

¹A monopolar neuron has a single process extending from the soma (cell body), while a bipolar neuron has two processes, each extending from opposite sides of the soma.

²A ganglion is a cluster of nerve cell bodies, somewhat like a very simple auxiliary brain. These structures are significant features of many invertebrate nervous systems.

2.1.2 *C. elegans* behaviour

Despite its small size and relative anatomical simplicity, *C. elegans* is capable of a remarkably rich repertoire of behaviours which, although simpler, have close parallels in larger animals. Like all animals the worm exists to reproduce. Since the hermaphrodite, unlike the male, takes no active role in mating, its primary goal becomes survival which, in turn, necessitates eating and threat avoidance. The worm exhibits chemotaxis towards chemicals usually associated with food, while exhibiting a strong avoidance response to certain chemical repellents that are associated with danger [11]. The worm also has a thermotaxis behaviour, which manifests as a preference for temperatures at which the worm was previously fed and an avoidance of temperatures at which it was starved [53]. This is also an example of associative learning in *C. elegans*. Finally, mechanosensory stimuli elicit a variety of behavioural effects [40]. When the worm feels the sensation of bacteria (or similarly sized glass beads) [104] it slows its locomotion so as to stay in the food rich area. It also has separate pathways for detecting gentle and harsh body touch as well as nose and tail touch, all of which elicit changes in the direction or speed of locomotion.

The worm's locomotion is of particular interest due to its involvement in most higher level behaviours, as well as the fact that it is directly observable and easily quantifiable. Furthermore, as will be discussed in the following sections, the neural circuit for locomotion is relatively well understood. Yet despite the small underlying circuit, locomotion is an adaptive behaviour that changes significantly depending on the worm's environment and allows it to navigate effectively. In the laboratory *C. elegans* worms are typically grown in petri dishes containing a layer of agar gel³. The gel is quite firm, and worms tend to lie on the surface rather than burrowing into it. The locomotion behaviour observed under these conditions is referred to as *crawling*, and is characterized by a roughly sinusoidal waveform with a wavelength of about 2/3 of the body length (Figure 2.2 B). The undulation frequency is usually about 0.5 Hz, but various factors have been found to modulate it [66]. Worms typically crawl forwards most of the time, but also move backwards intermittently and when stimulated to do so. A reversal is often combined with a re-orienting manoeuvre called a pirouette, in which an asymmetric body undulation causes the worm to point in a new direction. Modulating the probability of performing these manoeuvres is one way that the worm navigates, performing a biased random walk. It can also perform gentle turns in response to stimuli while moving forwards.

Sometimes, worms are instead placed in a liquid medium called M9 buffer⁴, leading

³NG agar is the standard *C. elegans* culture medium, the composition of which is described in Ref. [17].

⁴M9 buffer is an aqueous salt solution, the composition of which is described in Ref. [17]. For convenience I will often refer to it simply as water.

to a significantly different locomotion behaviour dubbed *swimming* (or, in some older works, *thrashing*). A swimming worm typically undulates at about 2 Hz and there is also a significant difference in the wave form (Figure 2.2 A). This will be elaborated on in Chapter 4. In addition to swimming and crawling, recent methodological developments

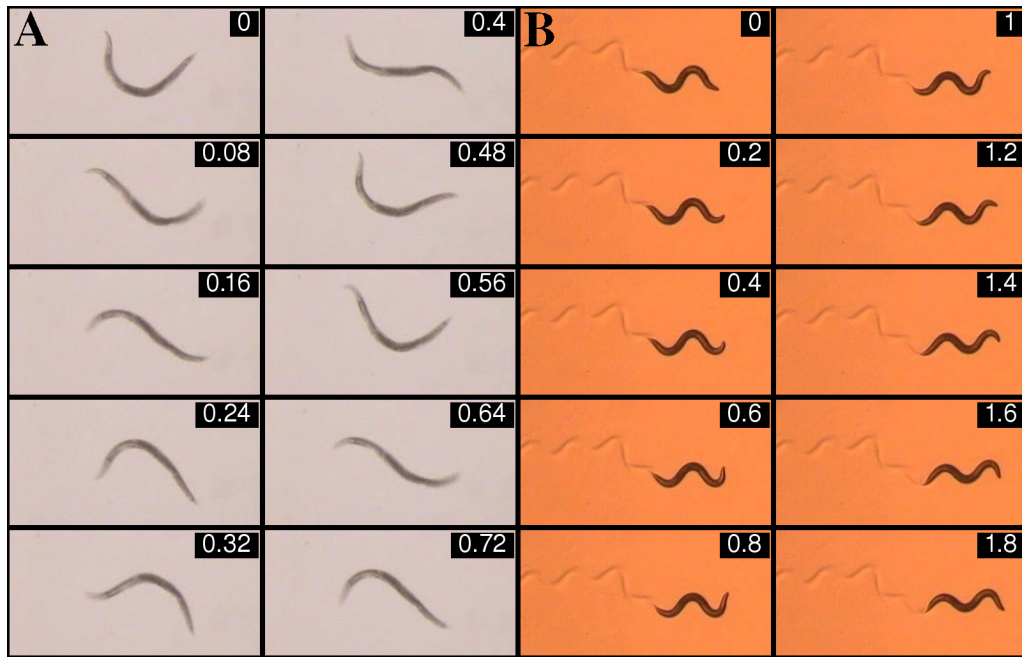


Figure 2.2: Sequences of stills taken from movies of worms A) “swimming” in water and B) “crawling” on agar. The numbers correspond to the time (in seconds) at which the frame was taken. Note that the worm’s body bends in the dorso-ventral plane (i.e. up-down) and is therefore lying on its left or right side. (see Supplementary movies C2.1 and C2.2)

have shown that the worm can adapt its locomotion according to external constraints. Specifically, Lockery et al. [78] have developed a technique whereby structured microfluidic environments can be fabricated from transparent elastomer. Using this technique they created channels of diameter slightly greater than the worm’s and with sinusoidal shapes of different wavelengths and amplitudes, such that a worm placed in the channel has a waveform imposed on it. The worm is able to cope with a variety of channel configurations, illustrating the robustness of its locomotion.

2.1.3 Genetics

C. elegans began its rise to fame when it was chosen by Sydney Brenner, a molecular biologist and future Nobel laureate, as a model organism for the study of molecular

and developmental biology. In his seminal 1974 paper “The Genetics of *Caenorhabditis elegans*” [17], Brenner described methods for the isolation and mapping of *C. elegans* mutants, along with a characterization of about 300 mutants affecting the worm’s behaviour or morphology. In the same issue of *Genetics*, John Sulston together with Brenner published a preliminary chemical characterization of the worm’s genome, including a measurement of the genome size [117].

Several factors contribute to the worm’s suitability as a genetic model organism. First of all the majority of *C. elegans* offspring are the result of self fertilization, which makes it possible to obtain “fully homozygotic” lines in which the offspring are essentially clones of the parent [17]. One therefore need not worry about a specific genotype being lost from generation to generation. Furthermore, the ability to self-fertilize means that even highly defective mutants can usually reproduce. Finally, worms can be easily grown in very large numbers and take only three days to reach sexual maturity, making genetic experiments much less time consuming than they would be in most multicellular organisms.

Since these early days, the worm has become and increasingly popular and important organism for molecular biologists. In 1998 it became the first organism to have a fully sequenced genome [29], paving the way for the human genome project. To this day the roles of and interactions between more and more genes are being elucidated. At present, there are over 3000 mutant strains available to researchers through the *Caenorhabditis* Genetics Centre (CGC) [112], which can be mail-delivered upon request.

Genetic nomenclature

Gene names in *C. elegans* consist of three letters followed by one or more numbers (i.e. *abc-123*), with the letters generally related to the phenotype associated with mutation of that gene. For example, mutants that exhibit defective or uncoordinated locomotion are dubbed *unc*, those whose bodies are longer than usual are dubbed *lon* and those that are short, or dumpy, are dubbed *dpy*. It should be noted that the distinction between genes, gene products and mutants can be a source of confusion for those new to the field. For example, a non-mutant (referred to as wild type, or N2) worm will have a functional copy of the imaginary gene *abc-123* which is expressed in certain cells to produce the protein ABC-123⁵. A worm in which the *abc-123* gene is defective is loosely referred to as an “*abc-123* mutant”, although strictly speaking the name of the mutant allele in question should be provided (i.e., *abc-123 (e456)*). In the case of a gene whose name implies a certain phenotype (*unc-30*), the phenotype is not associated with the wild type version of the gene, but rather the mutant.

⁵genes use lower case italics, while gene products use normal upper case

It is also worth noting that different mutant alleles can have a variety of effects on the expression of the gene product (typically a protein). A loss-of-function (or null) allele is one in which the mutation is so severe that a functional gene product is not produced at all. Alternatively, a reduction-of-function allele results either in reduced expression of the gene product or in a gene product that is only partially functional. Finally a gain-of-function allele is one that either causes the gene product to be produced in places that it would not normally be, or that affects the product in a subtle way that leaves its function intact, but prevents it from being inhibited as it should (resulting in overactivity)

2.1.4 The neural circuit for locomotion

C. elegans is an attractive subject for research on the neural basis of behaviour due to an invariant nervous system consisting of a mere 302 neurons. More importantly, the members and connectivity of this nervous system are largely known. This information was deduced by the painstaking work of several groups. John G. White and co-workers reconstructed the anterior nervous system from electron micrographs of thin slices of the worm [136]. The same technique was used by David Hall and Richard Russell to reconstruct the posterior nervous system [49]. Finally, this highly influential work was recently revisited by Beth Chen and colleagues, who used the published data, as well as White's original micrographs, to produce the most complete database of connectivity data to date [26]. In addition to this connectivity data, the role of many of the neurons of the locomotion circuit were investigated by Martin Chalfie and colleagues (including White) [24] using a technique called laser ablation, whereby specific identified neurons are selectively killed, leaving the worm alive and otherwise intact. Finally, because the worm's small size makes electrophysiological recordings difficult, information is sometimes inferred from studies of the much larger but closely related nematodes *Ascaris suum* and *Ascaris lumbricoides*, whose motor nervous systems are very similar to that of *C. elegans* [114]. After giving an overview of the worm's locomotion nervous system in the following paragraphs, I will describe the ventral cord locomotion circuit and how it is classically thought to work, based primarily on Refs. [24, 136]. This is followed by a discussion about the reliability of data before presenting a more detailed analysis of the ventral cord circuitry based on the consolidated data of Ref. [26].

Overview

The worm's neural circuit for locomotion is naturally divisible into two main sub-circuits that are located in the nerve ring (head) and in the ventral cord respectively. The first four

body wall muscles in each quadrant, the “head”, receive input only from the head circuit, while the next four muscles in each quadrant, the “neck”, receive combined input from the head and ventral cord circuits. The remaining 15 or 16 muscles in each quadrant are controlled solely by the ventral cord circuit [135]. The muscles of the head and, to a lesser extent the neck, are significantly shorter and overlap more than the rest, so the majority of the body ($> 80\%$) is controlled by the ventral cord circuit (based on “neuron fixed point data” from Ref. [26]).

While the connectivity of the head circuit for locomotion is known [136], the roles of the individual neurons are somewhat unclear. One contributing factor is that the dense packing of neurons in the nerve ring makes laser ablation of specific cells more difficult. Another major factor is that both the circuit itself and the behaviours that it controls are significantly more complex than its ventral cord counterpart [44]. For example the head, unlike the body, is capable of bending in 3D [135].

The head circuit has been included at various levels of abstraction in some of the models introduced in Section 2.3. A few of these models have assumed that the head circuit forms a primary central pattern generator⁶ (CPG) for locomotion and have modelled it abstractly [67, 89]. In contrast, the model due to Sakata and Shingai [102] is based on the detailed connectivity and includes 41 neurons, proposing a viable mechanism for head oscillation. Yet despite the increased complexity, it is plausible that there is a “core” head circuit with a similar motif to that of the ventral cord.

Unlike the head circuit, the ventral cord locomotion circuit is one of the better understood sub-circuits in the worm. While the roles of some neurons are still not known, we have a reasonable idea of what constitutes the “core” locomotion circuit. The cell bodies of the ventral cord neurons are fairly evenly distributed along the length of the cord, which facilitates laser ablation studies and fluorescence imaging. It must be noted however that laser ablation is usually performed on newly hatched larva, so only cells that are present at that stage are ablated. Nonetheless, by combining data from laser ablations [24] with the structural information from serial reconstruction [135, 136], a coherent picture of much of the circuit can be formed.

Ventral cord circuit: classic view

As mentioned earlier, muscles in the two dorsal quadrants (and similarly in the two ventral quadrants) receive input from the same set of neurons and can therefore be conceptually combined. While there are no cell bodies in the dorsal cord, certain cells in the ventral

⁶Loosely, a CPG is a neuron or neural circuit that is capable of generating oscillations without requiring rhythmic input.

cord send processes to the dorsal cord via commissures which then run along the dorsal cord and provide input to the muscles [136]. The core ventral cord locomotion circuit includes six classes of motor neuron called DA, DB, DD, VA, VB, VD. In each case the first letter (D or V) specifies which muscles (dorsal or ventral) the neurons controls. The second letter indicates the parent class to which the neuron belongs, which are defined primarily on morphological grounds. Thus for example DA and VA neurons have similar morphologies, but innervate opposite sides of the body. In terms of the neuron properties, the single most important thing to know is the synaptic polarity, i.e. whether the neuron is excitatory or inhibitory. Based on data from *Ascaris*, it was concluded that DA, DB, VA and VB are cholinergic and therefore excitatory, while DD and VD are GABAergic and therefore inhibitory [62,99,114]. It has subsequently been confirmed that DD and VD are indeed GABAergic [84]. Somewhat unusually, the worm appears to have two largely distinct circuits for forwards and backwards locomotion [8] that are structurally very similar but with inverse orientation [136]. In what follows I will describe primarily the forwards circuit, with equivalent neurons of the backwards circuit given in parentheses.

Excitatory input to ventral muscles is mediated by cholinergic neurons of class VB (VA) of which there are 11 (12) members. Similarly, excitatory input to dorsal muscles is provided by 7 (9) neurons of class DB (DA). The members of each of these classes are distributed quite evenly along the nerve cord. Furthermore, the regions over which members of each class make neuromuscular junctions (NMJs) do not overlap [136], so each member controls its own section of the body. These neurons generally make gap junctions with neighbouring members of the same class. Interestingly, while the NMJ regions do not overlap, the neurons themselves do. Specifically, both VB and DB (VA and DA) have long, posteriorly (anteriorly) directed processes that are devoid of synaptic connections and are generally thought to function as stretch receptors that would provide sensory feedback about body bending. This was first proposed by R. L. Russell and L. Byerly (personal communication cited by White et al. [136]), but has yet to be experimentally verified.

In addition to innervating muscles, the cholinergic neurons also stimulate GABAergic neurons of class DD (6 members) and VD (13 members). Specifically, both VB and VA output to DD neurons, which then run across to the dorsal cord and inhibit the dorsal muscles. Similarly the VD neurons receive input from both DB and DA, and inhibit ventral muscles. These cross inhibitor neurons are therefore implicated in both the forwards and backwards locomotion circuits [136]. Unlike the DB, VB, DA and VA neurons, DD and VD do not have long, undifferentiated processes. Instead each member ends abruptly where the next begins, typically forming gap junctions with its neighbours. They are typ-

ically described as contributing to locomotion by helping to ensure the correct antiphase relationship between dorsal and ventral muscles at the same position along the worm, but this will be further discussed in Section 9.3.1. While the connectivity of D-class neurons suggests an equivalent role in forwards and backwards locomotion, they are generally thought to be essential only for moving backwards [137] (this will be addressed in Section 10.2).

The neurons discussed so far are the only ventral cord motor neurons whose role in locomotion is largely known. However, the ventral cord circuit also includes 6 motor neurons of class VC, which innervate both body wall and vulval muscles, and 11 of class AS⁷, that innervate dorsal body wall muscles. Both of these classes are cholinergic [99], but their roles in locomotion are not at all clear as they have not been successfully ablated.

There are also several interneuron classes associated with the ventral cord locomotion circuit, some of which have known roles. When a healthy worm is touched on the nose, it will immediately start backing up [24]. Similarly if touched on the tail, it will reverse direction if currently backing up, and will accelerate if going forwards. The sensory neurons responsible for this behaviour are outside the scope of the present work, but the interneurons that directly input to the motor neurons are of more interest. Laser ablation evidence suggests that forwards (backwards) locomotion fundamentally requires only a single pair of interneurons called AVBL and AVBR (AVAL and AVAR) [24]. These (L)eft / (R)ight neuron pairs are coupled to each other by many gap junctions [136], and are generally treated as a single entity called AVB (AVA). When AVB (AVA) is ablated, worms still respond to touch stimuli, but while their backwards (forwards) locomotion is normal, forwards (backwards) locomotion is highly uncoordinated [24]. Thus AVB (AVA) appears to be required for activating the forwards (backwards) circuit. Another pair of interneurons called PVC (AVD) appear to be required for the touch response. When PVC (AVD) is killed, worms are still capable of coordinated locomotion in both directions, but fail to respond to tail (head) touch [24]. Finally when both AVB and PVC (AVA and AVD) are ablated, the body undulations⁸ for forwards (backwards) locomotion are completely abolished. Together this suggests that AVB (AVA) provides the main “on” signal for forwards (backwards) locomotion, but that inputs from PVC (AVD) can compensate to some minor extent in their absence. These interneurons all have processes that run the entire length of the ventral cord and pass through the nerve ring, although while AVA, AVB and AVD have cell bodies near the head, PVC has cell bodies near the tail [136]. Furthermore, AVB

⁷The name AS stands for A-like Short. These neurons have similar morphology to DA, but with shorter processes [136].

⁸In the case of forwards locomotion, the AVB/PVC ablated worms could still move somewhat using only head oscillations. In contrast, backwards locomotion of AVA/AVD ablated worms is totally abolished

and PVC (AVA and AVD) connect similarly to each member of classes DB and VB (DA and VA) using a combination of chemical and electrical synapses.

Two other interneuron classes called AVE and DVA feature in the ventral cord locomotion circuit [136], but their roles are somewhat unclear. DVA has been shown to be respond to body bending and appears to regulate the extent of body bending in a non-trivial manner [72]. Neurons of class AVE have similar connectivity to AVD, but their processes end before the vulva. While it is therefore implicated in backwards locomotion, its exact role has yet to be revealed.

Reliability and invariance

Before beginning the circuit analysis, it is important to consider the reliability of the data, both in terms of the connections themselves and the extent to which these connections will be invariant from animal to animal. It is often stated that the worm's nervous system is invariant, but this assertion appears to be based on relatively limited information. In their original work, White et al. used data from a total of five *C. elegans* individuals, with most of the data coming from three adult hermaphrodites designated the N2T series (covering the head including the nerve ring), the N2U series (covering most of the body anterior to the vulva, but excluding most of the head) and the JSE series (covering the tail). Together these cover most of the animal, excluding a section of the posterior body [136] which was instead covered by data from the male N2Y series. Finally the JSH series, taken from an L4 larva, covers the nerve ring and anterior ventral cord and was used primarily to validate the reconstruction of the nerve ring. White et al. were able to compare the overlapping parts of these series, concluding that "The structure was found to be sufficiently invariant for equivalent processes and cell bodies to be identified in the region of overlap of two series" [136]. In their earlier paper on the structure of the ventral cord, White et al. [135] present a more detailed comparison between the anterior ventral cords of two worms, designated the "S" and "U" series in that work, examining both the morphological and synaptic invariance. While they are certainly very similar, there are a few cases where the relative positions of neurons in the ventral cord varies between the two animals. Similarly, while the connectivity is largely shared between the two worms, there are several instances of connections that occur in only one series. Let us briefly consider the possible explanations for this discrepancy. Clearly, one possibility is that this is a true reflection of variability between worms. In fact, Varshney et al. state that the precise chemical and electrical synaptic connections "are stereotypical from animal to animal with more than 75% reproducibility" [123]. While this may account for many discrepancies, there is also the possibility of both false-positive and false-negative con-

nections. However, since great care was taken in the reconstruction, it seems reasonable to rule out any significant number of false-positives. With regard to the completeness and correctness of the data as a whole (disregarding the possible variability between animals), Varshney et al. estimate that the connectivity data is about 90 % complete [123]. A significant number of the missing connections are likely to be in the area of the ventral and dorsal nerve cords posterior to the vulva, where connectivity data for several motor neurons is missing.

Ventral cord motor neurons: detailed connectivity

In White's original work [136], much of the connectivity data is given on a class (rather than individual neuron) basis, and therefore includes generalizations. In fact, their consolidation of data into a class-based view of the locomotion circuit has been very helpful in allowing the community to build up a picture of how the worm's locomotion system is likely to work. However, now that Chen et al. have painstakingly re-examined the connectivity data and made it available on an individual neuron basis [26], a closer inspection may reveal motifs that have gone unnoticed. Based on the earlier works of White et al. [136] and Chalfie et al. [24], it seems likely that the motor neurons of the ventral cord are responsible for generating locomotion, with the interneurons serving primarily to activate and modulate these circuits. Therefore in what follows I will focus primarily on the connectivity among the motor neurons themselves.

Gap junctions

According to the latest connectivity data, the worm's nervous system includes 6393 chemical synapses, 890 gap junctions and 1410 neuromuscular junctions [123]. All three of these synapse types are present in the ventral cord locomotion circuit and here I will start by examining the gap junction connectivity. Gap junctions in the ventral cord can be separated into three basic classes: connections among interneurons, connections among motor neurons and connections between interneurons and motor neurons. The interneuron circuit responsible for switching between forwards and backwards locomotion was introduced in Section 2.1.4 and is largely outside the scope of the present work, so the connections among interneurons will not be considered here. However, the command interneuron pairs AVB and AVA, which activate forwards and backwards locomotion respectively [24], make extensive gap junction connections with the motor neurons of the corresponding circuits [136]. While AVA uses a combination of chemical and electrical synapses, AVB must rely exclusively on gap junctions to activate the B-class neurons so

these connections are clearly important. On the other hand, the study presented in Chapter 6 strongly suggests that the gap junctions among body wall muscles, while numerous, are unlikely to have a significant role in locomotion. Indeed gap junctions can have many roles besides mediating electrical signals, including functions in embryogenesis and nervous system wiring [110].

In their original work, White et al. specifically drew attention to the numerous gap junctions between adjacent motor neurons of the same class, suggesting that these may be used to reduce discontinuities in activity along the worm [136]. However, examination of the updated data, plotted in Figure 2.3, shows that many inter-class connections also exist. Considering that gap junction numbers are likely to be significantly underestimated [123], the circuit is highly connected indeed.

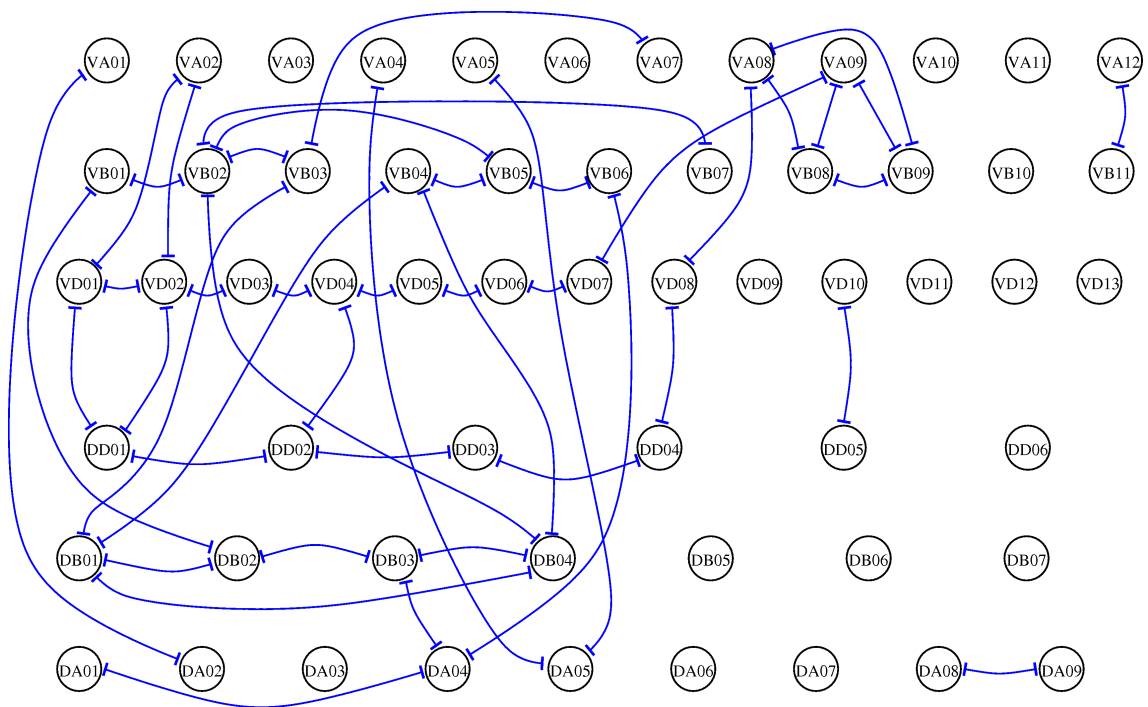


Figure 2.3: Gap junction connectivity among the core ventral cord motor neurons, created from the data of Ref. [26].

Purely in the interests of simplicity, it would be helpful if the extensive gap junction coupling among motor neurons could be omitted from the model presented in Part III. To shed light on the appropriateness of this simplification we can turn to genetic evidence. Of the 25 known innexins (gap junction genes) in the *C. elegans* genome, only *unc-7* and *unc-9* are extensively expressed in neurons [110], and mutations in both genes (all of which are thought to be null [12]) share a largely identical locomotion phenotype [92].

One potential clue comes from the fact that the forwards locomotion is far more severely affected than backwards [12]. Partial reconstruction of the ventral cord of an *unc-7* mutant revealed ectopic⁹ gap junction connections between B-class neurons and the backwards command neuron AVA [92]. Thus, one possible interpretation of the phenotype is that these connections somehow interfere with forwards locomotion. However, it is not clear whether these connections are functional, and it does seem somewhat unlikely that a loss-of-function mutation in an innexin gene could lead to extra, functional gap junctions. An alternative interpretation is that the ectopic gap junctions are non-functional and unimportant. In this case the forwards uncoordinated phenotype could be explained by the fact that while AVB connects to B-class neurons exclusively through gap junctions, AVA connects to A-class neurons with both gap junctions and chemical synapses (which would still be functional). Either way, the fact that both *unc-7* and *unc-9* mutants have smooth backwards locomotion [12] suggests that the coupling between motor neurons is not essential for backwards locomotion. Given that the motor neuron circuits for forwards and backwards locomotion are so similar [136], it seems likely that the coupling among forwards motor neurons is similarly non-essential. This conclusion is supported by the model due to Bryden and Cohen [21] (see Section 2.3), in which gap junction coupling among motor neurons was found to have minimal effect.

Chemical synapses

Of all the chemical synaptic connections among ventral cord motor neurons, the only ones that have been extensively discussed are the inputs from ventral (dorsal) A- and B-class neurons to DD (VD) neurons [136], where the D-class neurons are co-recipients of input at dyadic¹⁰ neuromuscular junctions. However, inspection of the detailed connectivity data reveals many other synaptic connections (see Figure 2.4), the pattern of which is not immediately obvious. Of particular interest are the various inhibitory connections, due to the importance of inhibition in pattern generating circuits. One of the major open questions in *C. elegans* locomotion is whether or not the neural circuit includes one or more central pattern generators (CPGs). CPGs are neural circuits that generate rhythmic outputs in absence of ascending or descending input [58], and are generally thought to underlie most, if not all, rhythmic motor behaviours. Of the previous models of the worm's locomotion (see Section 2.3) some have involved CPGs (located in the head) but others

⁹In this context, the meaning of ectopic is that these connections are not present in wild type worms.

¹⁰At a typical monadic synapse, the presynaptic neuron has a single postsynaptic partner. In contrast at a dyadic (or triadic) synapse, the presynaptic neuron has two (three) postsynaptic partners that are both activated by the released neurotransmitter.

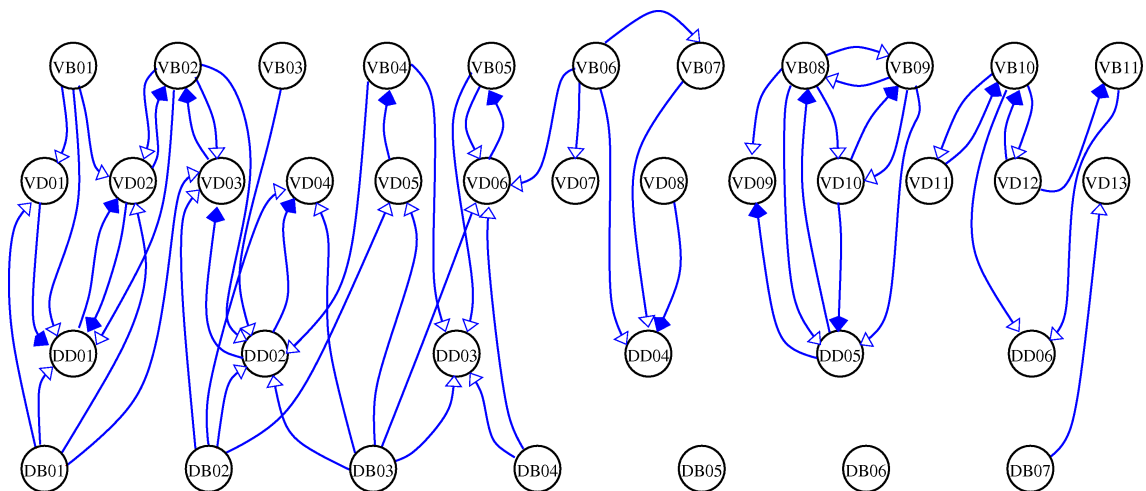


Figure 2.4: Chemical synaptic connections among ventral cord motor neurons, created from the data of Ref. [26]. Here only neurons associated with forwards locomotion are shown to reduce the complexity of the figure. Arrows with filled heads represent inhibitory synapses while open heads indicate excitatory synapses.

have instead relied purely on sensory feedback mechanisms that are essentially reflexive. Part of the reason why models have tended to rely, at least in part, on sensory feedback mechanisms is the fact that the ventral cord locomotion circuit, particularly as presented in Ref. [136], does not appear to support a CPG mechanism. However, in light of the new connectivity data, it is important to re-evaluate this conclusion.

The most basic motif typical of CPG circuits is reciprocal inhibition [58]. Examination of Figure 2.4 reveals only a single instance where this occurs, between DD01 and VD02. If one instead looks for any reciprocal connections between two neurons where at least one of them is inhibitory, more occurrences are found (see Figure 2.5). In principle, the motif of one excitatory and one inhibitory neuron, reciprocally connected, could generate oscillations. However, the period of any resulting oscillation would be of the same order as the combined neural time constant and synaptic delay. This is in contrast to a typical half-centre oscillator where the period is instead linked to the dynamics of escape or release from inhibition (which can be significantly slower). Thus, for the small *C. elegans* motor neurons with time constants of tens of milliseconds (see Section 8.3.2), the observed motif is unlikely to generate oscillations anywhere near behavioural time-scales (the fastest locomotion wave has $T \approx 500$ ms). One exception to this reasoning that cannot be ruled out is the possibility that the B-class (and A-class) neurons could function as pacemakers¹¹. However, in absence of any evidence to suggest that this is the

¹¹A pacemaker neuron's membrane dynamics allow it to generate rhythmic bursts of activity endoge-

case, I will not explore this idea any further. It would also be difficult to account for the observed modulation of locomotion frequency (see Chapter 4) with the aforementioned mechanisms. It therefore seems unlikely that the worm's locomotion would rely on a CPG in the ventral cord.

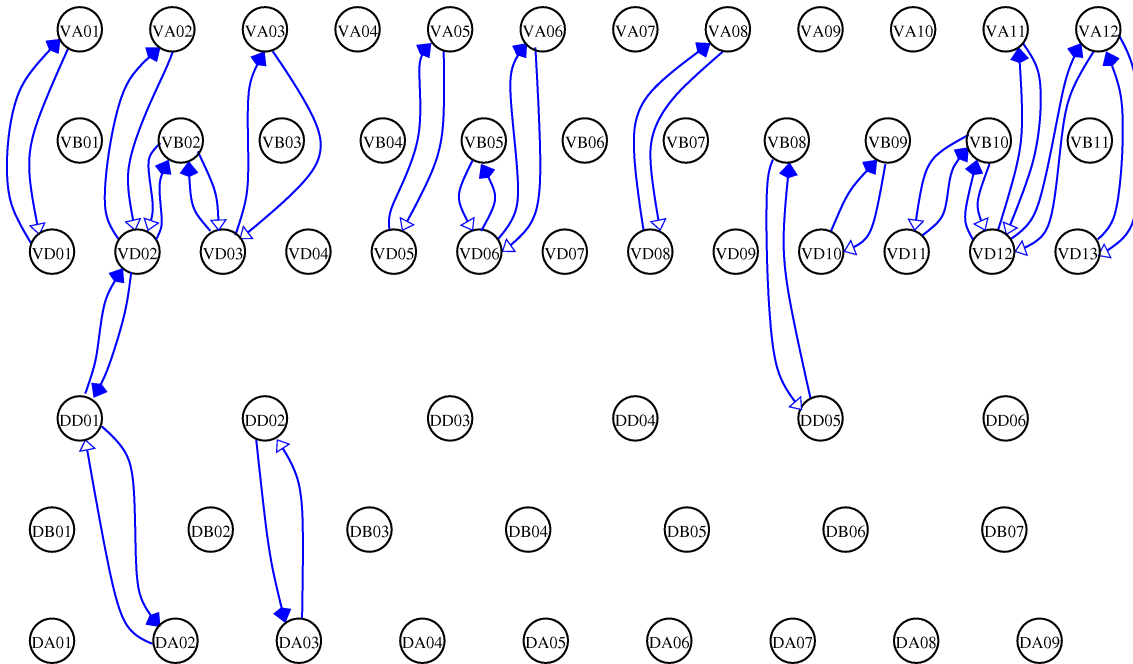


Figure 2.5: Reciprocal synaptic connections in the ventral cord locomotion circuit, including neurons from both the forwards and backwards circuits, created from the data of Ref. [26]. Arrows with filled heads represent inhibitory synapses while open heads indicate excitatory synapses.

In the context of a sensory feedback mechanism in which the excitatory neurons receive sensory feedback only from the side of the body that they innervate, one of the major requirements is to ensure the correct anti-phase relationship between dorsal and ventral neurons. It is generally accepted that D-class motor neurons perform this role by relaxing muscles on the opposite side of the body when one side contracts [84]. However, the analysis presented in Section 9.3.1 strongly suggests that, in the context of a sensory-feedback-based locomotion mechanism, inhibition of muscles is unlikely to have the desired synchronising effect on the motor neuron states. To ensure the correct phase relationship, what one instead requires is direct cross inhibition of the excitatory *motor neurons* themselves. In the closely related nematode *Ascaris suum*, whose motor nervous system is very similar to that of *C. elegans* [114], direct electrophysiological evidence

nously.

shows that DI and VI neurons (equivalent to DD and VD) do indeed inhibit DE and VE neurons (equivalent to DB and VB). In the original *C. elegans* connectivity data of Ref. [136] the equivalent connections are absent, but the same is not true of the updated data from Ref. [26]. Figure 2.6 shows all of the inhibitory synapses within the ventral cord locomotion circuit. What is immediately apparent is that D-class neurons make several of synapses with other motor neurons in the ventral cord.

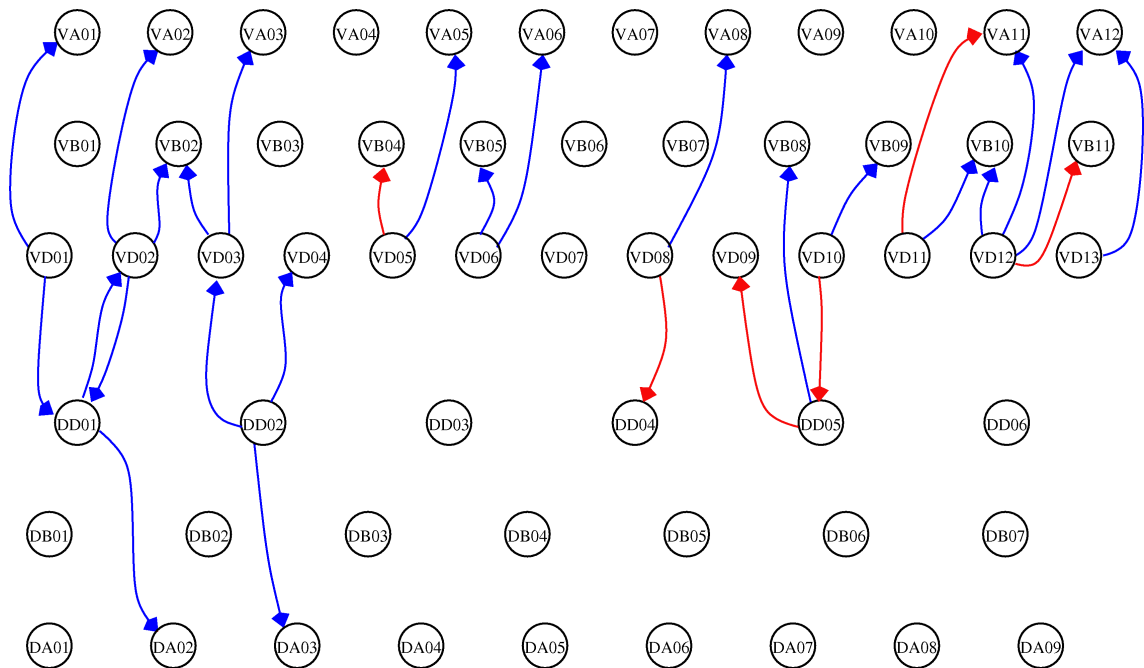


Figure 2.6: Inhibitory synaptic connections in the ventral cord locomotion circuit, including neurons from both the forwards and backwards circuits, created from the data of Ref. [26]. Red arrows indicate synapses that were not present in Figure 2.5.

Looking at this data in isolation, one might conclude that the pattern of inhibitory connections is too random to be significant. Indeed this is a particularly likely conclusion if one assumes that cross inhibition of muscles has the capacity to synchronize the oscillation of dorsal and ventral excitatory neurons in anti-phase, as is the standard interpretation. But if the results of Section 9.3.1 are valid, direct cross inhibition of neurons, as illustrated in Figure 8.2A, becomes much more important. Looking at Figure 2.6 again with this in mind, there is a striking difference between the dorsal and ventral connectivity. Indeed while none of the DB and only two DA neurons receive inhibition from DD, there are six VB and eight VA neurons that are inhibited by VD. If the forwards and backwards circuits are essentially equivalent it seems reasonable to examine the circuits together when looking for repeating motifs, in which case the ventral connections seem

more significant. But this raises two important questions. First, whether the prevalence of VD to VB/VA connections may be underestimated in the connectivity data and second, whether cross inhibition to ventral, but not dorsal neurons would be sufficient to synchronize the two sides.

With regard to the first point, Stretton et al. suggest that these connections may have been under-estimated since, in *Ascaris*, the excitatory motor neuron often receives its inhibitory input at a dyadic neuromuscular junction (NMJ), which could have been misinterpreted as a simple monadic NMJ [113]. It is also interesting that the majority of VB and VA neurons that do not receive inhibition appear to be in the area between the vulva and the pre-anal ganglion [136], which is likely to be less reliable [123]. It therefore seems plausible that inhibition of VB and VA neurons by VDs could be a regular motif. Of course, this is only useful if one way neural inhibition is sufficient, since the almost total lack of equivalent connections on the dorsal side could not realistically be explained in terms of missing connections. The hypothesized presence and sufficiency of ventral neural inhibition is one of the questions addressed by the model presented in Part III

2.1.5 Neurons with unknown function

In addition to the A-, B- and D-class neurons whose approximate role in locomotion is known [24], the ventral cord locomotion circuit includes two other classes of motor neuron, AS and VC, with largely unknown functions. While the VC neurons are known to be involved in egg laying, VC01-03 also have extensive synaptic connections to other motor neurons in the ventral cord (see Figure 2.7), as well as innervating body wall muscles. While their possible role in locomotion is totally unclear, they do have remarkably consistent connectivity. Specifically, while there is only a single synapse to a VC neuron from ventral cord motor neurons of other classes (shown in red in Figure 2.7), the first three VC neurons each synapse onto each of the D class neurons in the anterior half of the body (DD01-03, VD01-06), as well as to each other. VC04-06, on the other hand, have not a single synapse with motor neurons of other classes, although VC04 and VC05 are connected to VC01-03. Based on the connectivity pattern, it would seem that VC01-05 are likely to be coactive. Being cholinergic [99], activation of the VC neurons should lead to activation of the D-class neurons onto which they synapse, which in turn could be expected to relax the anterior half of the body. While this may be important for some behaviour, it seems unlikely that it would participate when the worm moves straight forwards or backwards. The VC neurons will therefore be omitted from the model presented in Part III.

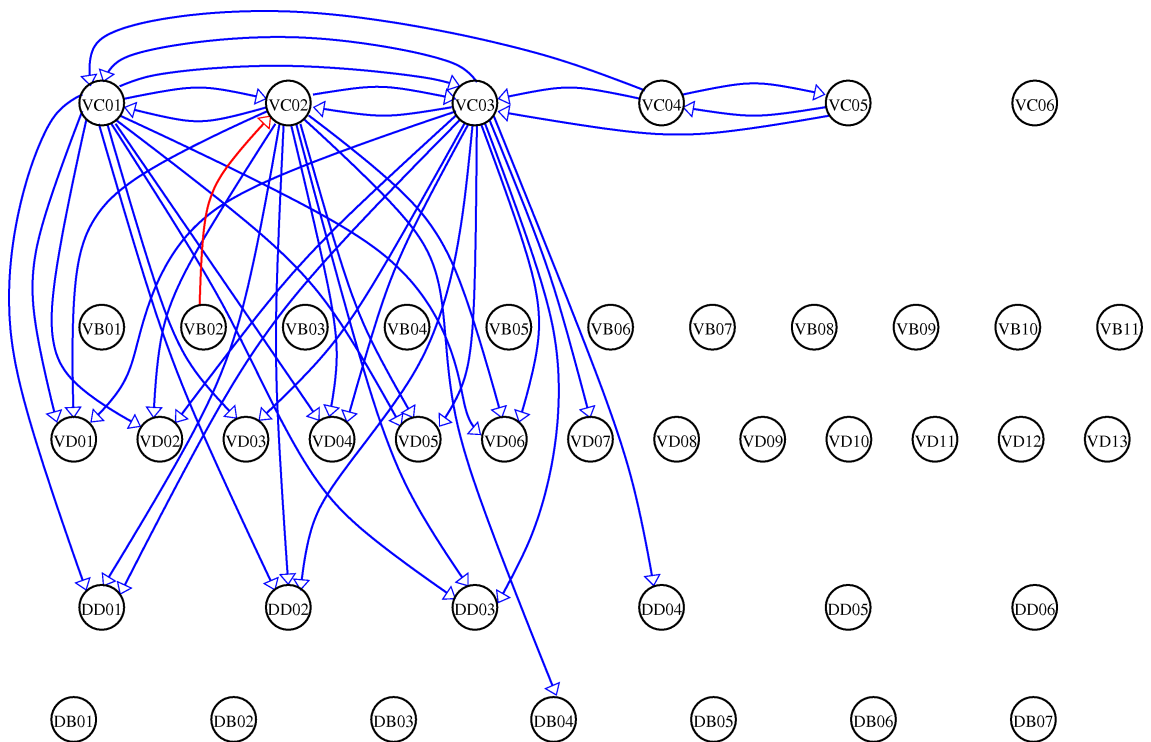


Figure 2.7: Chemical synaptic connectivity involving VC class neurons, created from the data of Ref. [26]. The sole synapse to VC class neurons from motor neurons of other classes is marked in red.

The other class of neurons with unknown function is AS, whose synaptic connectivity is shown in Figure 2.8. These cholinergic neurons [99] innervate dorsal muscles and have a structure similar to VA neurons, except that their processes in the dorsal cord are shorter [136]. This suggests that they might not have the proprioceptive function ascribed to A- and B-class neurons, and are more likely to be involved in backwards than forwards locomotion. Unfortunately the detailed connectivity does not shed any further light on their function. In absence of any information about their role in locomotion, the AS neurons will be omitted from the model presented in Part III.

2.1.6 Control of locomotion

One can think of a motor control system as consisting of a control signal that drives actuators or motor elements which in turn control the shape of the body, subject to environmental forces. In animals, the control signal is typically generated by the nervous system; the actuators are muscles; and feedback messages are generated either by the body (signals that sense the state of the muscles as well as the orientation and shape of the body, referred

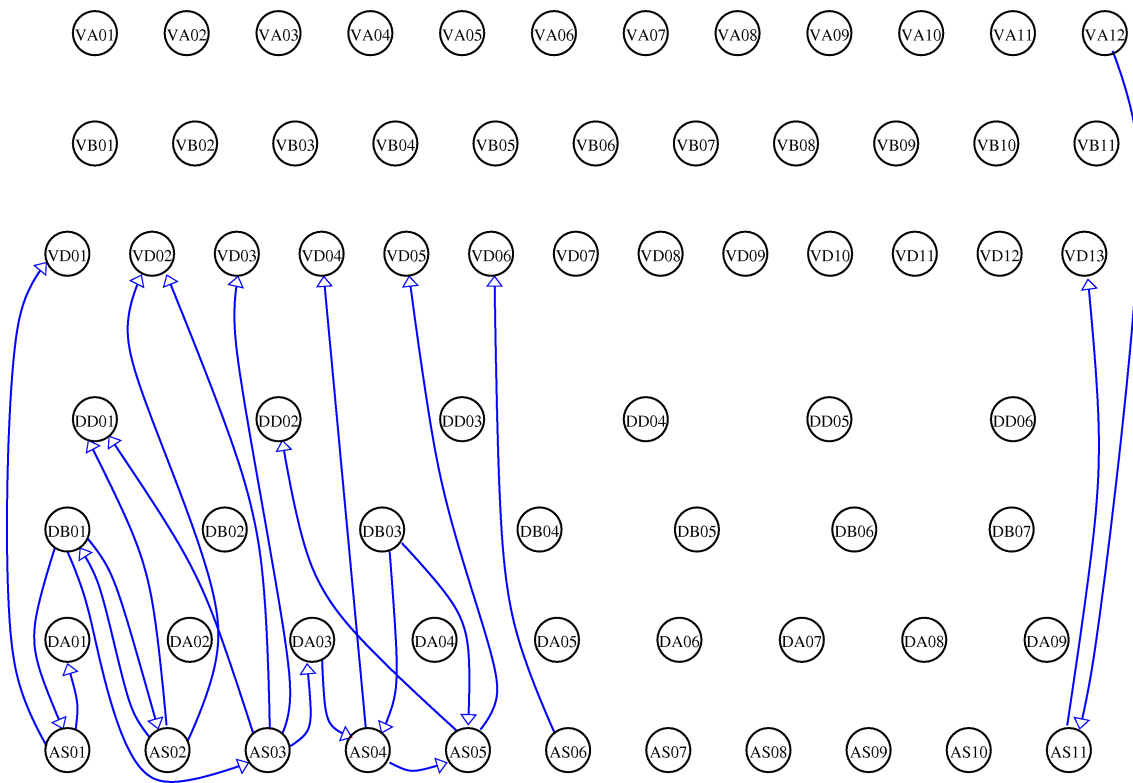


Figure 2.8: Chemical synaptic connectivity involving AS class neurons, created from the data of Ref. [26].

to as proprioception) or by other sensory perception (vision, etc.). For example, when we lift a heavy object or push against a wall, the body senses a strong resistance from the environment and can relay this to the nervous system, which, in turn, can alter or modulate the neural control. Thus, in this example the neural signal can be thought of essentially as a centrally controlled system with some feedback. It turns out that the vast majority of animal motor control systems contain such neural “control boxes”. Since most muscle behaviour consists of rhythmic motion, the underlying neural control generates rhythmic patterns of activity. Neural circuits that generate rhythmic patterns of activity even when completely severed from the rest of the body are dubbed *central pattern generating* or CPG circuits [52, 81, 82].

The fact that a CPG functions in isolation suggests that it can also be modelled in isolation. Indeed, traditionally, most animal motor control models (locomotion included) tended to be limited to a bottom-up model of internal neuronal or neuromuscular dynamics. These models are then complemented by top-down models of the physical aspects of locomotion (e.g., the aerodynamics of flight, the mechanics of legged locomotion and so on). The underlying assumption here is that, to a first approximation, the neuronal

control can be treated as a stand-alone control unit and hence decoupled from the physics of the body and environment. Over the course of this thesis I will demonstrate that, for *C. elegans* locomotion, a more integrated approach is required.

2.2 Physics background

To navigate its world, *C. elegans* uses undulatory locomotion, a means of self-propulsion that relies on the generation and propagation of waves along a body. As a mode of locomotion it is primitive and relatively simple, yet can be remarkably robust. No wonder then, that it is so prevalent across a range of biological scales from motile bacteria to gigantic prehistoric snakes. Key to understanding undulatory locomotion is the body's interplay with the physical environment, which the swimmer or crawler will exploit to generate propulsion. In this section I will introduce some of the theoretical foundations in fluid mechanics and their applications to self-propulsion in general and to undulatory locomotion in particular. As we will see in what follows, the size (and hence mass) of an organism has a significant affect on the physics of its interaction with the environment. I will therefore begin by introducing the concept of the Reynolds number, which captures the fundamental difference that size can have on locomotion in fluid media. The discussion will begin in the context of Newtonian fluids like water, but will later be extended to more complex fluids like gels.

2.2.1 Reynolds number

What is the Reynolds number?

Fluid mechanics has long been of interest to physicists. Already Isaac Newton postulated how fluids of different consistencies respond to forces. Perhaps, while taking a break from thinking about falling apples, he was holding a spoon over his cup of afternoon tea, and dragging it along the surface. He would have noticed that the top layer of the fluid was dragged along. How much more difficult would this be if he had done the same across a jug of honey? Newton postulated that the force required to keep a flat spoon moving at constant speed v would follow

$$F \propto A \left. \frac{dv}{dy} \right|_{\text{moving spoon}} \quad (2.1)$$

where A is the contact area of the spoon, and $v(y)$ is the speed profile of different slices of fluid as one moves a distance y away from the spoon. The proportionality constant is

called the viscosity of the fluid (or sometimes the dynamic or Newtonian viscosity) μ . The gradient of the velocity profile dv/dy reflects the strength of the dragging and indicates how nearby slices of fluid are differentially dragged¹². In fact, not all fluids obey the linearity of Eq. (2.1), but those that do are called Newtonian fluids. Examples include air, water and indeed honey with respective viscosities of $O(10^{-5})$ Pa·s, $O(10^{-3})$ Pa·s and $O(10^4)$ Pa·s.

Now if we change the speed with which we are moving the spoon (or stop it altogether), we must also consider the inertia of the fluid. Inertial effects will dominate over viscous forces when the spoon is sufficiently fast, or alternatively, when the fluid has sufficiently low viscosity. In this case, the force applied by the spoon on the fluid can result in non-linear convective and turbulent flows, which will then feed back and influence the motion. Let us try to determine when such inertial effects are important.

To do so, consider the motion of an object through a Newtonian fluid. Suppose the velocity v of the fluid drops off linearly away from the object. The viscous forces in the fluid around the object are given by $\mu A dv/dy$, which will then scale as $O(\mu \ell^2 v/\ell) = O(\mu \ell v)$, where ℓ is a characteristic size of the object. The inertial forces (due to the fluid's momentum in the same region mdv/dt) should scale as $O(\rho \ell^2 v^2)$ where ρ is the density of the fluid. The ratio of these two expressions is then characterized by a single dimensionless scaling parameter

$$\text{Re} = \frac{\rho \ell^2 v^2}{\mu \ell v} = \frac{\rho \ell v}{\mu}, \quad (2.2)$$

where Re is the conventional shorthand for the “Reynold’s number”. When $\text{Re} \gg 1$ inertial forces dominate. By contrast, if $\text{Re} \lesssim 1$ the viscous forces dominate the flow and the fluid largely responds to external forces in a passive manner. To give ballpark figures, a person swimming in water might experience a Reynolds number of $O(10^4)$. If we tried to swim through honey, we might feel a Re around $O(10^{-3})$ and bacteria swimming in water may feel Reynolds numbers as low as $O(10^{-5})$!

The Reynolds number can also be obtained from the governing equation in fluid dynamics, the so-called Navier-Stokes equation (given here in simpler form for incompressible fluids, i.e., $\nabla \cdot v = 0$)

$$-\nabla p + \mu \nabla^2 v = \rho \frac{\partial v}{\partial t} + \rho (v \cdot \nabla) v. \quad (2.3)$$

¹²In addition to being linear, Eq. (2.1) stipulates that fluid that is infinitesimally close to the spoon will travel at the same speed. This is often called the no-slip boundary condition.

Here, the left hand side describes pressure and viscous terms, and the right hand side describes inertial terms, which vanish at low Re¹³. In fact, it is easy to see here, that for an object with a characteristic length ℓ , we can recover the Reynolds number as the ratio of the inertial term $\rho(\mathbf{v} \cdot \nabla)\mathbf{v}$ to the viscous drag term $\mu\nabla^2\mathbf{v}$. In most of what follows, we will need only the low Re reduction of the Navier-Stokes equation

$$\mu\nabla^2\mathbf{v} = \nabla p. \quad (2.4)$$

Reynolds number for *C. elegans* locomotion

Here, both as an example and for the work that follows, let us calculate the approximate range of Reynolds numbers experienced by *C. elegans* during normal locomotion. First consider locomotion in water with viscosity $\mu \approx 10^{-3}$ Pa·s and density $\rho \approx 10^3$ kg/m³. The worm's characteristic length scale is $\ell \approx 10^{-3}$ and the characteristic velocity is $v \approx 2 \times 10^{-3}$ m/s (this is the peak value based on the 2 Hz lateral oscillation of the head). This yields a value of $\text{Re} \approx 2$ which is just below the upper limit of Re for which drag is approximately proportional to velocity [3, 9]. While the Reynolds number is strictly defined only for Newtonian media, one can still obtain an estimate of the relative importance of resistive and inertial effects on agar by using what we will refer to as the “effective viscosity” which is taken as one thousand times greater than the viscosity of water (see Section 8.2.2 for justification). If we further assume that the density of agar is equal to that of water and that the characteristic velocity will be lower, but of the same order of magnitude, we can conclude that the Reynolds number for a worm crawling on agar will be $O(10^{-3})$. Thus, in the remainder of this thesis, I will assume that the worm's motion obeys low Reynolds number physics.

Self-propulsion in low Re environments and the scallop theorem

Most of our intuition comes from our day to day experiences of the high Re world in which inertia must be overcome. When you pull away in your car, a torque is applied to the wheels, which in turn apply a backwards directed force to the surface of the road. The reactive (forwards directed) frictional force on the car gives rise to acceleration. At some speed this propulsive force is counter balanced by wind resistance and the velocity settles. The elimination of inertia at low Re means that *any* non-zero resultant force acting on an object will give rise to infinite acceleration. Thus, somewhat counter intuitively, the total net force and torque acting on an object moving in a low Re environment will at all

¹³Strictly speaking the Reynolds number is defined as the ratio of the viscous to the convective (non-linear) term, but in the low Re regime, both inertial terms can be neglected [97].

times be zero. As an example, suppose a small swimmer is moving at constant velocity, and then stops swimming. The above condition will result in immediate deceleration and the swimmer will stop. Swimming is indeed hard work at low Reynolds numbers. Curiously, low Reynolds number physics is remarkably reminiscent of the Aristotelian view of physics, in which objects will remain stationary in the absence of external forces. Aristotle's mechanics has long been dismissed as fundamentally flawed and superseded by Newtonian mechanics, so it is reassuring to see that this theory too has found its natural place.

Let us now consider a small swimmer (and hence at low Re). To have any chance of moving, it must be able to change its shape. The sum of all internal forces must clearly be zero (for the same reason you cannot lift yourself up by your boot straps). The change of shape will result in some motion of parts of the body in a global coordinate frame, which will then elicit reactive drag forces. But since these reactive forces *must* sum to zero, the organism as a whole will move in such a way that this is the case. This condition is sufficient to uniquely determine the motion of the whole organism given a known time series of body configurations and known environmental properties.

In fact the low Re physics imposes constraints on the possible shape changes that will result in progress. This was realized by Ludwig [80] and then by Purcell [97] who nicely formulated it as the scallop theorem. Consider a scallop that opens and closes its shell in water to move. At sufficiently high Re , the slow opening and rapid shutting of the shell pushes water out and propels the scallop in the opposite direction. At low Reynolds number, the flow of water into and out of the scallop over one cycle would be the same, regardless of the speed. As a result, scallops would make no net progress at low Re .

2.2.2 Undulatory locomotion

Spherical symmetry breaking for propulsion

While violating the time reversibility condition of the scallop theorem is necessary for successful propulsion at low Re , there is one other asymmetry that needs mentioning. Regardless of scale or Reynolds number, successful propulsion requires an asymmetry or anisotropy in the environmental resistance to the motion of the body. Consider a compact shape that undergoes a time-asymmetric cycle of shape changes, but remains at all times spherically symmetrical. It is trivial to see that such a shape would go nowhere. Thus, some form of spherical symmetry breaking is needed to achieve locomotion.

Indeed, nearly all life forms, from bacteria to mammals have a distinct body axis or polarity, which dictates the direction of motion. When a straight, elongated body is

moving forwards (parallel to its long axis) at low Re , it will displace less fluid per unit time than when moving sideways (normal to its long axis). Thus, it will encounter a smaller resistance from the fluid. Such an asymmetry in the level of resistance encountered by a body in different directions allows, in principle, for motion to be possible.

Slender body theory

In the context of low Reynolds number locomotion, some very general statements can be made within what is often dubbed slender body theory. We owe our understanding of the physics of undulatory locomotion in large part to the pioneering works of physicists and applied mathematicians (such as G. I. Taylor and M. J. Lighthill and his student G. J. Hancock) as well as zoologists (notably J. Gray, H. W. Lissmann and H. R. Wallace) in the 1950s [41, 51, 120, 121, 125–127]. These authors described the locomotion, analysed the physical forces and derived the mathematical framework that we still use today to understand low Re undulatory locomotion. (Incidentally, the theory developed for high Re undulations bears many similarities to slender body theory and is called elongated body theory [73]). In this section, I will present a brief overview of key results for slender body locomotion.

As I introduced above, two key asymmetries are required for an organism to be capable of low Re swimming. Not only must the undulation be asymmetric under time reversal, but some asymmetry in the environmental resistance is also required (the latter being a more general requirement of locomotion at any Re). Organisms that use undulatory locomotion are generally long and thin, guaranteeing asymmetry in the resistance to forward (or backward) and sideways motion. This is fairly clear in the context of an elongated body that is straight, but if it is instead curved into some arbitrary shape (so that the long axis is also curved) then the notion of forwards and sideways becomes less well defined. In this case it is helpful to think of the body cut up into thin slices along the long axis, much like a loaf of bread. Now instead of having a global definition of forwards and sideways, we consider the motion of each slice decomposed into components normal and tangent to the curved long axis at that point along the body. Similarly to before, motion in the normal direction will be more strongly resisted than in the tangential direction. This is because motion in the tangential direction involves the slice slipping into the space previously occupied by one of its neighbours. This is neatly illustrated by imagining the original body curved into a perfect circle with the head touching the tail. Now, if this body is rotated in place (like a steering wheel) then no extra fluid will be displaced and the slices will only move in the tangential direction. If the body is instead moved laterally, then fluid will have to be displaced and the resistance will be greater. In this case almost

all of the slices will have non-zero velocity in both the normal and tangential directions.

Now as already noted, analytically solving the motion of non-spherical shapes in a fluid is non-trivial. Slender body theory approaches this by deriving approximate solutions of the Navier-Stokes equation for no-slip boundary conditions applied to long cylindrical or similarly elongated shapes. These solutions take the form of force-velocity relations. Decomposing those into their vector components then leads to two different linear force-velocity relations along the major and minor axis of the object. It then becomes possible to write drag equations as

$$F_i = -C_i v_i, \quad (2.5)$$

where C_i are the effective drag coefficients for motion tangent (C_{\parallel}) and normal (C_{\perp}) to the body surface. Now, strictly speaking this should only be applied to the motion of a straight elongated body moving as a rigid object, but Lighthill [74] points out that it is often acceptable to approximate the fluid resistance in terms of local resistance coefficients. In this case the coefficients C_i are obtained per unit length so that each slice of the body can be assigned a small share of the total drag based on the components of its motion in directions normal and tangent to the *local* body surface.

Within this framework, R. G. Cox was able to derive equations approximating C_{\parallel} and C_{\perp} as functions of the length and radius of the body, and the viscosity of the Newtonian fluid [31]. Approximating the body shape as a prolate ellipsoid, J. Lighthill obtained similar but more accurate expressions for the effective drag coefficients [74]:

$$\begin{aligned} C_{\perp} &= L \frac{4\pi\mu}{\ln(2q/r) + 0.5} \\ C_{\parallel} &= L \frac{2\pi\mu}{\ln(2q/r)}, \end{aligned} \quad (2.6)$$

where L is the body length, r is the body radius, $q = 0.09\lambda$ (with λ being the wavelength of the undulation) and μ is the viscosity of the fluid. The requirement of asymmetric drag forces can be neatly expressed in terms of the ratio $K = C_{\perp}/C_{\parallel}$ which must have a value other than unity if progress is to be possible. Notice that the viscosity of the fluid has no effect on this ratio. Rather, it is completely determined by the geometry of the object. For worm-like shapes, K typically takes values around 1.5, whereas for infinitely long cylinders, $K \rightarrow 2$.

Undulations in rigid channels

To understand how propulsion is generated, consider the simple case of a cylindrical organism whose body undulates sinusoidally in a plane. From the scallop theorem we know that a standing wave will be unable to propel the organism, so instead consider a travelling wave that is propagated backward from head to tail, and is therefore not time symmetric. It is simplest to consider the limit $K \rightarrow \infty$, which could be achieved by placing the organism in a tightly fitting sinusoidal channel with the same amplitude and wavelength as the body wave but with rigid walls [41]. In the absence of any fluid or walls (i.e., in vacuum), the body wave could still propagate backwards at velocity v_{wave} , but the organism would stay stationary. However, when the organism is constrained by the channel, the wave is by definition stationary in global coordinates, forcing the organism forwards at a velocity $v_{\text{prog}} = -v_{\text{wave}}$.

Let us examine how propulsion is achieved down the channel. As the wave is propagated, the channel will apply a reactive force sufficient to prevent any motion in the normal direction. These reaction forces will only occur on the leading (i.e., backwards facing) edge of the wave. Now, the forwards directed components of these forces will add up, yielding a net propulsive force down the channel while any sideways directed components will cancel out. Hence, the organism will move forwards through the channel, with some velocity v_{prog} . As the organism slides forwards, it will rub against the sides of the channel and evoke reactive drag forces. Again the sideways directed components will cancel out over a cycle, but the backwards directed components will sum, yielding a net retarding force opposite to the direction of motion. The propulsive force exerted by the walls of the channel will be exactly sufficient to counteract this retarding force when the organism progresses at velocity $v_{\text{prog}} = -v_{\text{wave}}$.

Low Re undulations: “slip” formulation

Clearly, the $K \rightarrow \infty$ case can be trivially solved without recourse to fluid dynamics or slender-body theory. Now consider the same organism in a fluid, i.e., with finite K (the same reasoning will apply for any $K > 1$). However, now, the normal component of velocity v_{\perp} must be non-zero if the normal force F_{\perp} is to be non-zero. So, rather than the wave remaining stationary in the global frame, it will slip backwards at some velocity v_{slip} (with $|v_{\text{slip}}| \leq |v_{\text{wave}}|$) while the organism moves forwards at velocity $v_{\text{prog}} = -(v_{\text{wave}} - v_{\text{slip}})$. This is schematically illustrated in Figure 2.9A. An approximation of slender body theory can be obtained from the so called force resistivity theory and is due to Gray and Hancock [42]. Here, rather than solving the Navier-Stokes equations for a long and

slender body, the forces are approximated independently at each point (using equations of the form $F_i = -C_i v_i$ as before) and then integrated over the body length. Thus, any correlations in the fluid due to the spatially extended nature of the body are neglected. Applying this formalism to a perfectly sinusoidal body wave of low amplitude (A) and short wavelength ($\lambda \ll L$), Gray et al. [42, 43] were able to derive an expression relating v_{slip} to v_{wave} :

$$v_{\text{slip}} = v_{\text{wave}} \frac{B + 1}{KB + 1}, \quad (2.7)$$

where $B = 2\pi^2 A^2 / \lambda^2$.

In general, for a given locomotion waveform, the degree of slip depends only on K . Relating this back to the case of locomotion in a channel where we effectively have $K \rightarrow \infty$, we can see that for any B , we will have $v_{\text{slip}} \rightarrow 0$, so that over a single period of undulation the body travels a distance of one wavelength. Interestingly, this approach is valid for any $K > 0$. For $K = 1$ we obtain 100% slip (equivalent to a vacuum, or completely isotropic environmental resistance) and for $K < 1$ we observe direct wave propagation, with the body progressing in the same direction as the wave (Figure 2.9B). This mode of locomotion can be found in nature and is used, for example, by the polychaete worm *Nereis virens* [71].

While approximate, the simplicity and tractability of the force resistivity theory has led to its extensive application in biological domains, in particular for the study of flagellar propulsion in viscous fluids and nematodes in viscous and viscoelastic fluids (see below). In both cases, comparisons either against slender body theory [63] or against data [13] have concluded that the approximations are reasonable.

2.2.3 The worm's environment

It is remarkable how adept biological organisms are at adapting to different environments and modulating their behaviour. Many organisms exhibit enormous flexibility in navigating a wide range of environments, whether this involves changes of gait or continuous modulation of a single behaviour. At the same time, there are conditions in which organisms display very uncoordinated locomotion or else fail to make progress altogether. These may correspond to environments that are not usually encountered in an organism's natural habitat, or – more often in the geneticists' laboratory – to mutants that lack an essential protein. The investigation of biological forms of undulatory locomotion across different physical environments dates back to the early 20th century [43, 79, 125–127] and is playing an increasingly important role in genetics and in neuroscience [93].

This section's discussion has so far been largely limited to Newtonian fluids, which

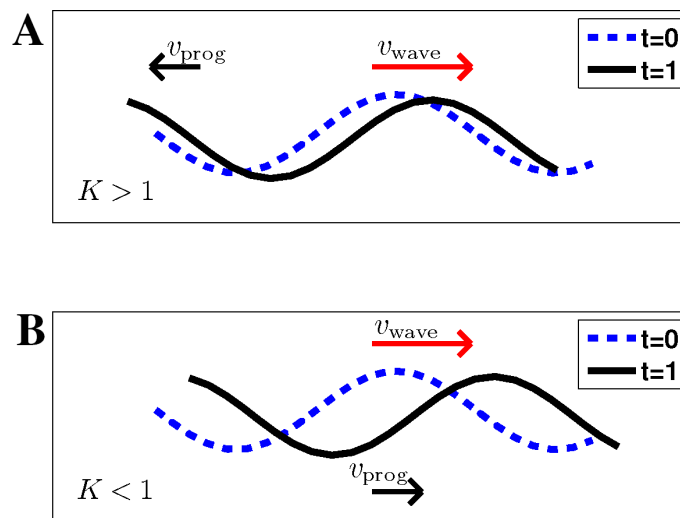


Figure 2.9: The effect of K on propulsion. An undulating body propagates a sinusoidal wave to the right at velocity v_{wave} (red arrow). If $K = 1$, no motion will result (not shown). If $K > 1$ (A), the body moves at velocity v_{prog} in the direction opposite to v_{wave} , with $|v_{\text{prog}}| \leq |v_{\text{wave}}|$. If $K < 1$ (B), the situation reverses and the body moves in the same direction as v_{wave} , with $v_{\text{prog}} < v_{\text{wave}}$.

are fully described by the viscosity of the medium. However, many low Re swimmers in fact move through complex fluids or other “soft” environments. For slender bodies in a Newtonian fluid, the ratio of drag coefficients K is fully determined by the geometry and cannot exceed 2. In contrast, in non-Newtonian environments, K (if and when it is well defined) is both a function of the geometry and of the medium. Strictly speaking, viscosity is not defined in non-Newtonian fluids, since the linearity of Eq. (2.1) is violated. Thus even the Navier-Stokes equation is not applicable. For example, the fluid may have some non-trivial structure, it may have energy storage capacity (e.g., elasticity), or perhaps the properties of the fluid may depend on the speed with which it is deformed. Of these cases, viscoelastic fluids (and viscoelastic approximations of gels) are probably the most relevant to biological swimmers. Slender body or resistive force theories can both be straightforwardly extrapolated to model viscoelasticity when the elastic properties of the fluid can be approximated by effectively stronger resistive drag coefficients in the normal direction, thus increasing the ratio K [43]¹⁴. Section 4.3.3 demonstrates that, in the context of *C. elegans* locomotion, this model is a reasonable approximation of gel media.

To the extent that slender body theory (and the simplified slip formulation thereof) may be extrapolated in this way, all of the above logic still holds, except that now the

¹⁴Note that viscoelasticity is typically modelled by adding time-dependent terms to the Navier-Stokes equation, so this parametrization by K is only valid in the limit where this time dependence can be neglected.

slippage parameter K is no longer determined solely by the geometry of the swimmer. As an example, consider *C. elegans* crawling on the surface of an agar gel. While the worm's mass is negligible, surface tension due to a thin film of water presses the worm firmly against the surface. As it moves, the worm breaks the network of the gel with its tapered head, forming a groove. Because the gel medium has memory, the groove persists over time and allows the rest of the body to slip forwards relatively easily. On the other hand, for the worm to move sideways, it must break the gel network over a much larger area. While a similar asymmetry exists when displacing fluid in a Newtonian media, the difference is that breaking the gel is a non-linear effect. The result is a significantly larger value of K (see Section 4.3.2 for values).

2.3 Previous models

To date, only a handful of models have focussed on the actual mechanism by which *C. elegans* generates and propagates the undulations responsible for locomotion. This is perhaps surprising given the relative wealth of information that we as worm scientists have access to. There are also some models that focus on higher level behaviours like thermotaxis, but these are outside the scope of the current work. This section provides a chronological account of the existing *C. elegans* locomotion models, drawing attention to their relative strengths and weaknesses.

2.3.1 Niebur and Erdös

Ernst Niebur and Paul Erdös were the first to develop a computational model of the worm's locomotion, publishing a series of papers in the late 80's and early 90's that have played a major role in shaping our understanding of the worm's locomotion. Three of these papers are of particular relevance to this thesis and will be discussed here.

The first paper, Ref. [88], focusses on the isolated nervous system and presents a model for electrotonic neurons in which excitation spreads passively. After developing the general model framework, the authors use reasonable estimates of membrane properties to simulate electrotonic propagation in *C. elegans* motor neurons and interneurons, as well as in *Ascaris* motor neurons. These simulations are used to address the hypothesis that the worm's travelling neuromuscular wave could be the result of electrotonically propagated activity travelling along the interneuron axons. Their simulations suggest that such propagation is about 50 times faster than the fastest observed neuromuscular wave, ruling out this hypothesis. The paper also argues that motor neuron stretch receptors

might be central to locomotion.

Next, in Ref. [36], the authors outline a discretized, two dimensional mechanical model of the worm. The model consists of a network of springs (representing the cuticle) in conjunction with outwards directed pressure forces (see Section 2.1.1). Abstract muscle forces articulate the body, while the environment is modelled in terms of local drag coefficients [74]. The authors then use this model to investigate the muscle excitation patterns that could potentially underlie locomotion on agar. They suggest that the worm's head is likely to contain an oscillatory mechanism to guide the body's sinusoidal trajectory. By assuming that such a mechanism exists, the authors present simulations demonstrating that stretch receptors could, in principle, generate a viable muscle activation pattern.

In Ref. [89], the authors extend the previous work, presenting the first integrated model of the worm's crawling on agar. Despite some limitations, the integrated model due to Niebur and Erdös is quite inspired and has greatly influenced the models that I will present in Chapters 5 and 8. Their model is controlled by an abstract central pattern generator (CPG) in the head, responsible for "steering" along the sinusoidal trajectory. A key feature of this model is that the trajectory of the head determines the shape of the body wave, via a very strong groove ($K = 10^4$). The contraction of muscles along the body is controlled by stretch receptors located approximately 1/5'th of a body length behind the muscle in question. However, because a muscle only contracts if both itself and the posterior segment from which it receives input are stretched beyond the average segment length, it can be inferred that the proprioceptive feedback is both local and posterior.

The work of Niebur and Erdös (specifically the integrated model of Ref. [89]) is surely the most significant and influential model of *C. elegans* locomotion, laying down much of the foundation on which future models, including my own, would be built. The model is quite successful in accounting for the worm's crawling behaviour on agar, and goes a long way to demonstrating the plausibility of a sensory feedback mechanism for controlling muscle contraction along the body. It also benefits from being an integrated model, in the sense that the body, environment and a neurally inspired control system are incorporated. However, as with any model, it also suffers from several limitations. Putting aside various minor issues that do not warrant mentioning, the main issues with the model are all related.

To put the model (and its drawbacks) in context, one must realise that it is generally believed that the worm's crawling on agar and swimming in liquids are distinct behaviours, each associated with a characteristic wavelength and frequency (this will be dealt with extensively in Chapter 4). The Niebur and Erdös model was therefore specifically a model

of crawling. Thus the single biggest limitation of the model – the fact that it does not address swimming and intermediate behaviours [13] – would not have been recognised at the time. Indeed, not only is the wavelength effectively hard coded through the combination of stretch receptor length and the properties of the head CPG, but the mechanism by which the head trajectory determines the shape of the body wave via a strong agar groove would fail entirely in less resistive environments like water. Furthermore, my work suggests that even agar may fail to support such a mechanism. The model assumes a value of $K = 10^4$, but states that similar results are obtained for lower values¹⁵, while section 4.3.2 shows that the actual value on agar is $K \approx 35$. The final drawback is the fact that the model incorporates an abstract CPG in the head, without providing any details or biological grounding. This perfectly justifiable limitation of scope takes on greater significance when one begins to ask how such an oscillator would be modulated to generate alternative locomotion behaviours. Of course these criticisms are not intended to detract from the breakthrough that the Niebur and Erdös model represented at the time, and the validity of much of the work to this day.

2.3.2 Bryden and Cohen

This model, by John Bryden and Netta Cohen, was first published in Refs. [19, 20] before being modified and extended as Ref. [21]. Following Niebur and Erdös, the model relies on sensory feedback mediated by motor neuron stretch receptors to generate and coordinate oscillations, and is restricted to the crawling behaviour. The focus of the model, however, is quite different. While Niebur and Erdös emphasise the mechanical aspects of locomotion, the Bryden and Cohen model emphasises the neural control and can therefore be considered the first true neural model of *C. elegans* locomotion. The authors forgo a true physical model in favour of a minimal physical framework in which each segment is represented by a single angle variable that evolves according to the relative activity in the dorsal and ventral neurons. This simplification represents an enormous computational saving, and allowed the authors to apply an automated optimization algorithm to obtain parameters for the neural circuit. Along with its restriction to crawling, the model's main drawback is the fact that its oscillation frequency is unrealistically high, and could not be sufficiently reduced while limiting neural parameters to a biologically plausible range. The authors acknowledge this limitation and suggest that the addition of a model of the body and environment would solve this problem. This will be addressed in Chapter 5.

¹⁵experimenting with an implementation of their model I found that as K is reduced from 10,000, undulations remain robust down to about $K = 1,000$ but gradually lose stability for lower values. For $K \leq 200$, I found that undulations were no longer sustained even for a single undulation period.

One of the main advantages of this model is the fact that it does not include a “black box” oscillator, instead accounting for the generation and propagation of oscillations in terms of biologically grounded model neurons.

2.3.3 Sakata and Shingai

The model due to Kazumi Sakata and Ryuzo Shingai [102] is different to the others discussed in this section in that it focusses exclusively on the neural circuit for head oscillations. The model does not include a physical component. Of all the model discussed here, this one is the most detailed and biologically accurate, incorporating 41 head neurons represented by compartmental, conductance based models with very little simplification of the connectivity. The authors use the model to make predictions regarding synaptic polarities in the circuit. For my purposes, the most important aspect of this model is its reliance on sensory feedback from neural stretch receptors, suggesting that the fundamental oscillatory mechanism may be shared between the head and ventral cord circuits.

2.3.4 Suzuki et al.

This model, created by Michiyo Suzuki et al. [118], is quite different to those discussed so far. The authors have created an integrated model that includes high level neural control (gentle touch response) and the generation of the actual locomotion wave. Moreover, the range of behaviours that the model aims to reproduce is much broader, including forwards and backwards locomotion, resting and both omega and coil turns. Thus the main strength of this model is its holistic approach. Unfortunately, this comes at the expense of realism and biological grounding.

Putting aside the higher level control which is outside the scope of the present work, the model includes both a physical body and local neural control. The body model is essentially the same as in Ref. [21], consisting of 13 rigid links with 12 joints. The angle of each joint is determined independently from the local neuromuscular activity meaning that the environmental forces are not modelled. Thus the forwards motion of the model does not actually emerge from the undulation of the body. The neural control is similarly simplified, consisting of a system of abstract, coupled oscillators that are not well grounded in the worm’s neural circuit. While the model successfully reproduces the aforementioned behaviours, it does so in a largely phenomenological manner that is unlikely to provide new insight into the worm’s locomotion system.

2.3.5 Karbowski et al.

The model by Jan Karbowski et al. is presented in Ref. [67], along with experimental work. The main strengths of this paper are the way in which they combine experiment and modelling in an attempt to make predictions and gain insight into the mechanisms underlying various mutant phenotypes, as well as the fact that it includes both the head and ventral cord sub-circuits. The authors use the model to make several specific predictions regarding the effects of changing various parameters, in some cases relating these to their experimental results. Although this is not explicitly stated, it would appear that the authors make the common assumption that crawling is a distinct behaviour, restricting their experiments and model to locomotion on agar. It is also assumed that the head circuit forms a primary CPG that is essential for locomotion. As with previous models, sensory feedback via motor neuron stretch receptors is found to be a vital component of the system.

One of the main drawbacks of this work is the fact that it lacks any form of physical framework. This is particularly problematic given the fundamental importance of sensory feedback. Instead, it appears that the authors have accounted for the delayed feedback provided by stretch receptors by low-pass filtering the relative dorsal/ventral muscle activation with a time constant of 350 ms, and using this as the feedback signal. However, the biggest drawback of the model is to do with the fundamental oscillatory mechanism in which a CPG in the head drives oscillations in the rest of the body via strong gap junctions between body wall muscles. While the model uses a gap junction conductance of equal magnitude to that of the muscle's self-exciting calcium channel, electrophysiological data [64, 76] suggests that this significantly over-estimates the coupling strength, suggesting that such a mechanism would not be possible. The role of gap junction coupling between muscles is investigated in detail in Chapter 6.

2.3.6 Rönkkö and Wong

The most recent model of *C. elegans* locomotion due to Mauno Rönkkö and Garry Wong [101] uses a formal particle system to model the worm and its environment, including attractants and repellents. The model focusses almost exclusively on the body and environment, including only a highly abstracted decision diagram to control the worm's behaviour. The model's main strength is that it is the first published work to investigate the effects of different environments (liquid, gel surface and "solid") on locomotion. Indeed the environment model they use is quite promising, as the use of particles means that the medium has a "memory" which allows the worm to deform the environment and form, for exam-

ple, a lasting groove.

Unfortunately the work as a whole suffers from a lack of biological grounding. The model does not include any form of motor nervous system, instead seemingly relying on externally applied forces to move the worm through space, while only the direction of the head is actively controlled. A sinuous locomotion waveform emerges from the interaction between the body and the large spherical particles that make up the environment. The fact that these particles have similar diameter to the worm somewhat undermines the model's realism.

2.3.7 Discussion

Despite sharing a common subject, the models discussed in the previous sections are surprisingly diverse in their approaches, and also in their strengths and weaknesses. Indeed, the only real consensus among these models is the requirement for proprioceptive feedback. One must therefore ask, does the world need another model of *C. elegans* forwards locomotion and, if so, what new angle should such a model take? Having read all these works carefully, my short answer is yes, there is still much room for improvement. Here I will motivate why this is the case.

One of the most obvious differences among these models is the extent to which the body and environment are taken into account. Indeed, two of the models that include only a minimal physical framework [21, 67] have found that neural properties alone lead to oscillations that are unrealistically fast. In Ref. [67], an abstract delay in the sensory feedback signal is used to slow the oscillations to a realistic speed. Such a delay cannot be justified in terms of neural properties and must therefore be assumed to account for the time taken for the body to change shape. These models therefore suggest that physical properties of the body and environment have a dominant effect on the frequency of the worm's undulation.

Related to the issue of physical models, a surprising observation is the fact that, with the exception of Ref. [101] (which lacks sufficient biological grounding to be of much interest to biologists), none of the models have considered locomotion in any medium besides agar. This could perhaps be explained by the fact that swimming, classically referred to as thrashing, has only quite recently been shown to be a purposeful goal directed behaviour [94]. While it is still not clear whether a single model should account for swimming and crawling, or whether these two behaviours rely on different underlying mechanisms, this question is one clear motivation for a new model. Furthermore, any model that sets out to investigate locomotion in more than one medium requires a physical

component of sufficient realism and detail to represent the properties of different environments. The existing models have also raised several questions with regard to the roles of various system components. Based on the work to date, I have identified the following key open questions:

- **Locomotion in different media:** One clear objective for a new model of locomotion is to extend the scope to include swimming. Before doing so, however, it is important to ascertain the relationship between swimming and crawling. Specifically, are they distinct behaviours produced by partially independent neural mechanisms, or are they simply different manifestations of a single behaviour.
- **The importance of body physics:** In order to investigate locomotion in different media, a physical model will probably be required. However, it would be helpful to first determine what sorts of effect a physical model is likely to have. One specific question is the extent to which the neural and physical components of a model can be developed and studied in isolation. It is also interesting to ask how a model such as Ref. [21] would react to the addition of a more realistic physical framework.
- **Role of body wall muscles:** The model due to Karbowski et al. [67] proposes an unusual mechanism whereby signals are propagated through coupling between muscle cells. It is therefore important to determine the role of the body wall muscles in locomotion.
- **The locomotion mechanism:** One of the biggest open questions is about the fundamental oscillatory mechanism. Specifically, it is not clear if the worm has, or requires, a primary CPG in the head, or even in the ventral cord itself. The role of the D-class inhibitory neurons in forwards locomotion is also unclear.

Overall, it seems that the details of the mechanism underlying *C. elegans* forwards locomotion are still quite unclear. A new model could therefore contribute to our understanding of the worm. However, given the current state of our knowledge, it would be beneficial to perform some preliminary studies aimed at addressing some of the open questions outlined above. This would help to guide the model and maximise its usefulness. Part II of this thesis consists of several such studies that contribute to the model presented in Part III.

Part II

Preliminary Investigation

Chapter 3

Exploring the physics: motion simulator

3.1 Introduction

The physics of low Reynolds number undulatory locomotion has been quite extensively studied, with some of the key work discussed in Section 2.2.2. With respect to this thesis, one of the most important results is the finding that the fluid forces acting on a small, elongate body can be approximated to a reasonable degree of accuracy in terms of local resistance coefficients for motion tangent and normal to the body surface [42, 74]. In the context of this representation, Gray et al. [42] were able to obtain analytical expressions for the propulsive thrust generated by sinusoidal locomotion waves of small, large, or variable amplitude, also extending to a filament propelling an inert head (e.g. a sperm). In their later work on nematode locomotion, Gray and Lissmann [43] used Equation 2.7 to infer the approximate ratio of drag coefficients $K = C_{\perp}/C_{\parallel}$ experienced by worms moving in a variety of media, based on the extent to which the locomotion wave slipped backwards while they moved.

Working on *C. elegans* locomotion, it has become clear that the utility offered by Gray's theory is extremely valuable. Not only can one infer the worm's velocity from its wave form and properties of the environment, but it is also possible to do the opposite, inferring properties of the environment (specifically K). However, to use an analytical equation requires that the locomotion wave itself can be expressed mathematically. Furthermore, it would be beneficial to be able to predict not only velocity, but also the detailed

trajectory of a locomoting worm. While a physical model such as that due to Niebur and Erdős [89] gives this detailed trajectory, it does so based on a pattern of muscle activation, rather than from an observed sequence of body shapes. Finding the correct muscle activation pattern to generate the observed shapes is far from trivial. What is instead required is a system that takes a numerical representation of an arbitrary body undulation and uses the approach of Gray et al. to compute the resulting trajectory, for a given value of K . The motion simulator described in Section 3.2.1 was developed to meet this requirement. Furthermore, as described in Section 3.2.2, it can also be used to estimate K numerically if the body undulation and trajectory are both known. This additional functionality was required for the “gelatin assay” presented in Chapter 4.

After presenting the details of the simulator below, it will be validated against Gray’s analytical results in Section 3.3. It will then be used to investigate the applicability of Equation 2.7 to body waves that resemble those used by *C. elegans* to varying degrees. Then, in Section 3.4, the simulator will be used to address some basic scientific questions as well as others of specific relevance to the worm.

3.2 Methods

3.2.1 Solving the equations of motion

The primary aim of this simulator is to predict the centre of mass (CoM) trajectory of a body based on its *known* sequence of shape changes. Being motivated primarily by an interest in *C. elegans* locomotion, the scope of the simulator is restricted to the low Reynolds number regime and to motion within a 2D plane. The body is represented by a curve embedded in this 2D space, but the shape of the worm can be taken into account by scaling the local drag coefficients for each of the N points according to the diameter of the body at that point along its length. Before starting a simulation it is necessary to set several parameters, namely the number of points N used to describe the body shape, the time step δt and the drag coefficients C_{\perp} and C_{\parallel} . However, since only the ratio $K = C_{\perp}/C_{\parallel}$ is relevant to determining the trajectory, the drag coefficients can be normalised so that $C_{\parallel} = 1$ and $C_{\perp} = K$. The choice of N should depend on the complexity of body shapes to be modelled, while δt should depend on the undulation frequency f . Both of these parameters offer a trade off between speed and accuracy. In most cases presented here, values of $N = 25$ and $\delta t = 1/(1000f)$ were used.

The locomotion waveform is entirely pre-determined and must be provided to the simulator as a time sequence of body shapes, described in terms of the relative locations

of N points along the body midline. The internal actuation forces required to achieve these shapes need not, therefore, be modelled. To obtain the input time series, worms are recorded at 25 frames per second (fps) and the midlines are extracted as described in Ref. [13], to obtain the time sequence of coordinates of N equidistant points along the body. Using spline interpolation over time, this input time series can be upsampled to $1/\delta t$ fps. The next step is to displace and rotate the midline in each frame such that the CoM is stationary and the head is to the left. The displacement and rotation used for each frame is recorded, allowing the worm's actual trajectory to be reconstructed if required. This yields a time series of body midlines $\mathbf{s}(t) = \{\mathbf{x}(t), \mathbf{y}(t)\}$ that can be used by the simulator, as well as the CoM trajectory $\mathbf{CoM}(t) = \{\mathbf{x}_{\text{CoM}}(t), \mathbf{y}_{\text{CoM}}(t), \theta_{\text{CoM}}(t)\}$. Alternatively, artificial body midlines with the desired properties can be generated. This is often useful for investigating specific questions, as in several of the examples in Section 3.4.

Having completed the preprocessing of the input data, the simulation itself can be performed as follows. In a typical, high Reynolds number physics engine, the net force on a body results in acceleration according to $a = F/m$. At low Re, the very small mass will result in large accelerations, leading to a stiff system requiring extremely short time steps to integrate. In the limit of $m \rightarrow 0$ and for $F \neq 0$, we would have the numerically problematic situation of $a \rightarrow \infty$. In the “real world”, this means that the velocity of the body will always be at steady state, at which the net force and similarly net torque are zero [74]. In absence of inertia, and in the context of our model of the environment, the CoM motion is not history dependent, so each time step can be handled independently. Thus to obtain the motion at time $t(i)$, we will only have to consider the body shape at times $t(i)$ and $t(i-1)$. For each time step, the velocities of the N points are resolved into normal and tangential components, assuming initially that the CoM does not move or rotate. This motion evokes reactive environmental forces of the form $F = -CV$, which are combined to yield a net force and torque on the CoM. Based on the directions and magnitudes of these vectors, the simulator applies a small displacement and/or rotation (in the direction of $-F_{\text{net}}$ and $-\tau_{\text{net}}$) and then recomputes the reactive forces to get the new resultant. This process is iterated, accumulating small displacements and rotations until the zero net force and torque conditions are met to within a specified tolerance (usually $|F_{\text{net}}| < 10^{-11}$ N and $|\tau_{\text{net}}| < 10^{-13}$ Nm), at which point the simulator combines the final displacement and rotation δx , δy and $\delta \theta$ with the CoM trajectory. Thus the simulator effectively performs a gradient descent on F_{net} and τ_{net} in order to find the correct motion for each time step, combining these to get the trajectory.

3.2.2 Estimating K

The simulator described above can also be used to estimate the ratio $K = C_{\perp}/C_{\parallel}$ associated with a given medium, based on a recording of a worm moving through it. Given an initial guess for K , the equations of motion for the recorded sequence of body shapes are solved, yielding a candidate trajectory. This candidate trajectory can then be compared to the experimentally recorded trajectory $\mathbf{CoM}(t)$, and the value of K adjusted up or down accordingly. This process can then be repeated until the best fit value of K is found.

3.3 Validation against theory

The simulator presented here relies on the same underlying model of environmental forces as was used by Gray et al. [42,43] in developing their analytic expressions. The simulator can therefore be validated by comparing its output to that of Equation 2.7, under conditions that fully satisfy the assumptions underlying the equation. These are that the locomotion wave is sinusoidal, that the wavelength λ is short compared to the body length L and that the amplitude A is sufficiently small that $\lambda \approx \lambda_{\text{conv}}$ (as defined in Section 4.2.2). Simulations were therefore performed in a variety of virtual environments (with K ranging from 1 to 10^4) using an artificially generated time series of a low amplitude sinusoidal midline spanning multiple wavelengths, as shown in Figure 3.1A (specifically $\lambda_{\text{conv}} = 0.125L$, $A = 0.016\lambda_{\text{conv}}$). Note that a value of $N = 100$ was used, in order to capture the many alternating curves in the body.

The comparison revealed that the average error per undulation cycle between the simulated and theoretical CoM velocities is at most 0.73 % (for $K = 1.5$) and improves slightly with increasing K . For $K > 20$ the error is less than 0.6 %. One can therefore conclude that the simulator presented here agrees closely with the theory, provided the assumptions underlying Equation 2.7 are met.

3.4 Results

The results of using the physics simulator to estimate K from recordings of worms are incorporated in Chapter 4. However, it can also be used to address questions related to slender body theory, low Re physics and *C. elegans* locomotion, the results of which are included below.

3.4.1 Numerical results versus simplified analytical treatment

Having found close agreement between the simulator and Equation 2.7 under certain conditions (see Section 3.3), the simulator can now be used to assess the scope of validity of the simplified analytical treatment. Simulations were performed for a range of K values using locomotion waveforms that (i) have larger, more realistic amplitude (Figure 3.1B), (ii) that deviate from perfect sinusoids and better match the observed shapes of the worm (Figure 3.1C) and (iii) span less than a complete wavelength (Figure 3.1D) as observed when worms are placed in water.

As expected, all of these changes lead to greater discrepancies between theory and simulation, due to the limited applicability of Equation 2.7. Specifically, when the waveform deviates from a sine wave in such a way that the wavelength increases towards the tail (as in the real worm), v_{wave} ceases to be constant along the worm¹. In high K environments, the maximum λ dominates while for lower K the average λ is more meaningful. Higher amplitude waves introduce errors, particularly in the low K regime, where B dominates in Equation 2.7. Shapes spanning less than a wavelength also pose a problem for the theory. This can be explained by considering an extreme case where $\lambda \rightarrow \infty$. While this would imply $v_{wave} = f\lambda_{conv} \rightarrow \infty$, and therefore infinite velocity, the body will actually be a straight line at all times, and no motion will result. This comparison suggests that for realistic *C. elegans* locomotion waves across a range of K values, a physics simulator is best suited to determining the CoM motion.

3.4.2 Investigating the physics of turning

Studies of *C. elegans* navigation have generally focussed on the process whereby improving conditions tend to increase the probability of forwards runs, while worsening conditions increase the probability of reorienting manoeuvres called pirouettes [95]. This can result in a biased random walk towards a chemical attractant. However, the worm is also capable of a “steering” behaviour while moving forwards, allowing it to track isotherms at its preferred temperature [54]. It must therefore be possible for the worm to modify its forwards locomotion waveform in such a way as to generate gentle turning in the desired direction. It is not clear, however, how this turning is achieved, both from a neuromuscular and a physical point of view. One of the main advantages of this simulator over an analytic approach is the ability to predict the CoM trajectory, as opposed to just the speed, from a particular sequence of body shapes. It is therefore well suited to inves-

¹Note that the issue of non constant v_{wave} is addressed by Gray and Hancock [42] in the context of a wave that increases in amplitude toward the tail.

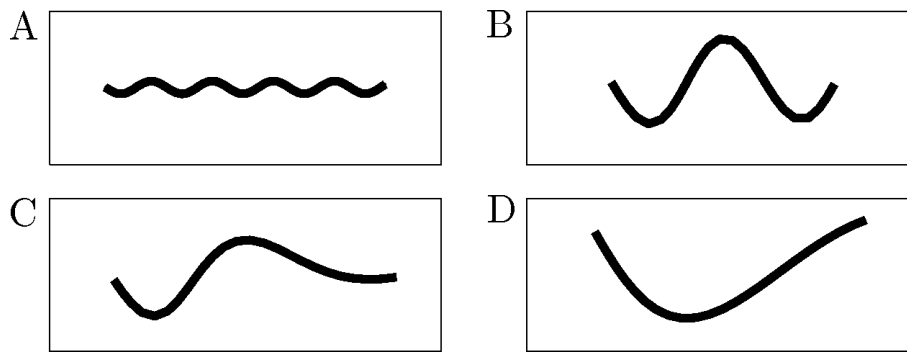


Figure 3.1: Assessing the validity of Eq. (2.7) with a physics simulator (see text for details). A) The analytic result of Gray et al. [43] is an excellent approximation for an undulator with a perfectly sinusoidal wave, a wavelength that is short relative to the body length and of a low amplitude. B) A purely sinusoidal idealization of the *C. elegans* crawling wave. The same equation handles such a wave reasonably well but with small errors due to the increased amplitude and wavelength. C) A more realistic *C. elegans* crawling waveform in which the wavelength increases towards the tail introduces significant errors. D) A realistic *C. elegans* swimming waveform in which the wavelength is greater than the body length is very poorly described by the analytic approximation.

tigating how the locomotion waveform should be modulated in order to generate gentle turning. Note that the simulations in this section were performed using an unrealistically strong groove ($K = 10^4$) in order to minimize slippage and clearly demonstrate the relevant effects. The same principles would apply with a weaker groove, but the resulting slippage would obscure the results somewhat.

Clearly any waveform that is totally dorso-ventrally symmetric (like a sine wave) will lead to a straight² CoM trajectory. However, there is also a large class of dorso-ventrally *asymmetric* waveforms that still fail to generate turning, such as a half-wave rectified sinusoid (a sine wave with all negative values clipped to zero). To understand why such a waveform fails to generate turning, consider the fact that the worm's shape at each time is effectively obtained by sliding a window along a periodic waveform, in the same way that idealized worms are often generated from a sine wave. Assume the worm is moving in an infinitely strong groove (which will have exactly the same shape as the original periodic waveform) we can see that the trajectory will have to be straight because the original waveform was straight (aligned with the long axis of the waveform). This suggests that the key requirement for gentle turning may be a locomotion wave with non-zero average curvature.

²Worm trajectories always have an oscillatory component with wavelength on the order of 1mm, but such trajectories can still be "straight". A trajectory will therefore be considered straight if it is possible to draw a straight line that is tangent with each of the peaks (or troughs) of the oscillatory CoM trajectory.

To illustrate this idea, let us compare the motion of a sinusoidal body shape with zero curvature bias (Figure 3.2A and B) with that of a worm with a strong dorsal curvature bias (Figure 3.2C and D). Specifically, by bending a sinusoidal wave pattern along the arc of a circle, the average curvature of the body is trivially equal to that of the corresponding circle (see Figure 3.2C). As the figure shows, in these simple cases, the virtual worm's trajectory matches the curvature bias of the body. To understand how the torque responsible for this turning is generated, consider two points P and Q on the body, such that $Q = P + \lambda$. We can see that the inclination of the body at these two points will not be equal, but will rather differ by some angle $\theta = \lambda/R$ where R is the radius of the underlying circle and λ is the wavelength of the underlying sine wave. In idealised environments, and after completing one undulation cycle, the point Q should occupy the space previously occupied by point P and have the same inclination that P had previously. This is only possible if the entire worm rotates by $-\theta$, which will result in a trajectory with radius of curvature R . Note that this excellent correspondence between body and trajectory bending occurs only in the case of an idealized environment with $k \rightarrow \infty$. For more realistic environments, some slippage is expected in the progress of the worm, leading to a more complex relationship between body curvature and trajectory curvature.

3.4.3 An unusual scallop

Consider a cyclical version of Purcell's scallop (introduced in Section 2.2.1), where instead of opening and shutting, the scallop's opening angle keeps increasing (at 2π per cycle). Shapere and Wilczek [106] have noted that the Scallop theorem assumes that the scallop cannot turn through more than 2π on its hinge. However, if we allow the scallop to do so, and assuming the two arms are identical, the resulting motion will be time symmetric so the scallop will still go nowhere. To break time reversal symmetry, one arm could be longer than (or otherwise different to) the other, and hence subject to a greater resistive drag force. This odd "creature" is illustrated in Figure 3.3A. While such a case would be difficult to address analytically, it can be easily handled by the simulator. The interesting result is that in this case the scallop rotates and displaces slightly with each rotation of its arms. At first this looks like an example of low Reynolds number locomotion with only a single degree of freedom, something that Purcell argues is impossible [97]. However, if the scallop is allowed to keep rotating, it eventually traces out a closed path through space, as shown in Figure 3.3B. Thus, while our hypothetical creature can rotate, it is still incapable of any ongoing translation.

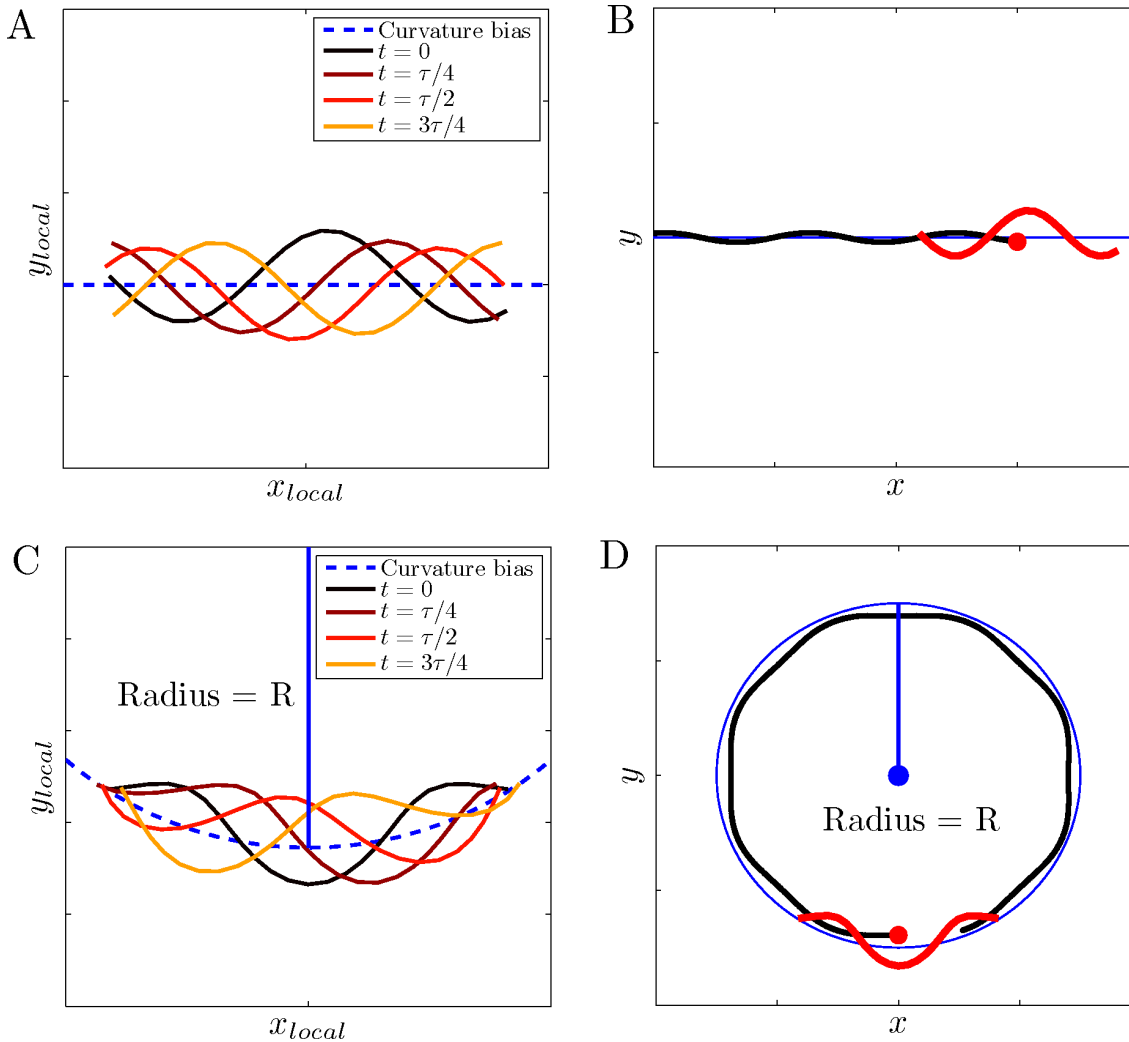


Figure 3.2: Schematic demonstration of turning in simulated worms. The key requirement for turning is a dorsal/ventral curvature bias. A) A virtual worm with a purely sinusoidal locomotion waveform (four representative times are shown) has zero curvature bias (dotted line). B) The resulting centre of mass trajectory (thick line) has an oscillatory component, but the overall motion is in a straight line (thin line). C) Another virtual worm is generated by superimposing a sinusoidal locomotion wave (as in A) onto a circle with radius R , leading to a dorsal curvature bias (dotted line). D) The resulting centre of mass trajectory is highly curved (thick line), and approximates a circle (thin line) with the same radius R as was used in creating the body wave.

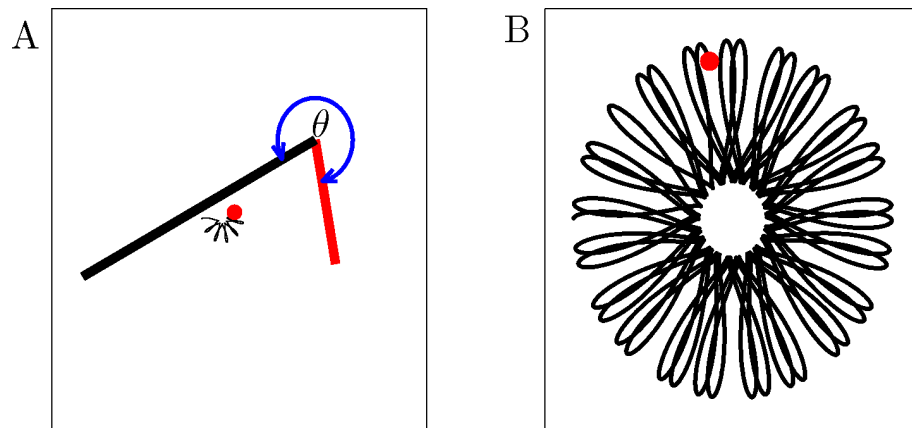


Figure 3.3: A) A variation on Purcell’s scallop in which the two arms have different lengths and are allowed to rotate freely (like a wheel). Arms are modelled as slender cylindrical bodies. The medium is modelled as Newtonian ($K = 2$). The path of the scallop’s “centre of mass” (CoM, red dot) is shown in black. After a few rotations, the CoM appears to undergo both translation and rotation. However, the CoM never leaves a circular area of small radius, as can be seen by following the trajectory over sufficiently many cycles (B). Each “petal” corresponds to one cycle of rotation through 2π .

3.5 Discussion

The novel motion simulator presented in this chapter extends the well established theory of Gray et al. [42] to arbitrary waveforms and allows the reproduction of curved CoM trajectories. Like the work it extends, this simulator relies on the assumption that the resistance offered by the fluid is well described by the local drag coefficients C_{\parallel} and C_{\perp} . However, the theory underlying this simplified representation was developed in the context of Newtonian fluids, so its validity for viscoelastic and gel media (whose properties are far more complex) could certainly be questioned. Thus one important result of this work is the finding, presented in Section 4.3.3, that the locomotion of worms in gel media can be quite accurately accounted for by this simple model of the environment, provided an appropriate value of K is used.

In the context of this thesis, the most important application of the simulator is the estimation of K values for the gelatin assay presented in Chapter 4. But the results in this chapter demonstrate that it is a useful, multi-purpose tool that can be used to address questions, not only in *C. elegans* science, but also more generally in low Reynolds number physics. Also, the insight offered into the mechanism of gentle turning will be valuable for future studies of taxis behaviours in the context of an integrated neuro-mechanical model.

Of course, the simulator also has its limitations. While it has been demonstrated that the environment model used here can account quite well for locomotion on or in a gel, this is still an approximation that could conceivably be a source of inaccuracy in the estimations of K . The simulator is also unable to represent the fact that gels have memory, something that might be of greater relevance when a worm reverses direction, slipping into a groove it has already formed. It would be beneficial if the simulator could account for friction (as opposed to drag) and inhomogeneities in the medium.

With regard to its role in K estimation, the simulator suffers somewhat due to noise in the recorded midlines and CoM trajectories. There is sometimes slight variation in the position of midline points relative to the image of the worm (due e.g. to lighting changes), which can introduce errors. Noise in the recorded CoM trajectory makes it impractical to independently obtain K values for each frame, meaning that the values obtained reflect an average over the entire clip. However, because the worms in the gelatin assay experience a non-homogeneous environment (due primarily to interactions with the slide and coverslip, see Section 4.2.1), it would be preferable if instantaneous K values could be reliably obtained. Yet despite these shortcomings, the simulator presented here has proven to be a very useful tool in the study of *C. elegans* locomotion.

Chapter 4

Forward locomotion: a single behaviour

4.1 Introduction

Until recently, our understanding of *C. elegans* locomotion has been largely restricted to the worm's so-called "crawling" behaviour that is exhibited on agar. This is most likely linked to the fact that worms are usually grown and maintained on agar plates, according to the protocols first described in Ref. [17]. Agar plates are also ideal for studying higher level behaviours, like chemotaxis or touch response, for various reasons. Among these is the fact that worms leave visible tracks on the gel surface, thereby recording where they have been, and the fact that controlled stimuli (chemical or physical) can be relatively easily administered. Furthermore, when a worm moves on agar it does so with very little slippage (see Section 2.2.2), due to the effect of the groove (see Section 2.2.3). As a result, there is very close correlation between body undulations and centre of mass motion which makes it particularly easy to identify reversals and turns. This lack of slippage also makes it clear that the worm's locomotion is purposeful and efficient.

But crawling is by no means the worm's only mode of locomotion. It has long been known that when *C. elegans* is placed in water¹, crawling is replaced by a new behaviour called "thrashing" or (more commonly in contemporary work) "swimming", characterized by a faster oscillation and different body shape often described as a "C" [48, 93] (as distinct from the "S" shape associated with crawling). The use of the term thrash-

¹Worms are actually placed in an aqueous salt solution called M9 buffer, described in Ref. [17], but this will be referred to as water for simplicity.

ing hints at the fact that this behaviour looks, at least at first glance, like a worm flailing helplessly as it tries in vain to locomote. This is not the case, however, and it has recently been demonstrated that worms in water are capable of purposeful, goal directed locomotion [94], leading to the increased use of the term swimming. Indeed, the reason swimming looks less effective than crawling is because the value of K in water is low, leading to a lot of slippage (see Section 2.2.2) and making it easier for the worm to be perturbed off its heading.

As noted in Section 2.3, previous models of the worm's locomotion have generally been restricted to the crawling behaviour [14, 21, 67, 89, 118]. To understand why this is, one must first be aware of the widely held notion that swimming and crawling are two fundamentally distinct behaviours [90, 93], each associated with a well defined waveform and (to a lesser extent) frequency [66, 67, 69]. This, combined with the fact that crawling is the more interesting and tractable of the two behaviours, certainly explains the limitation of scope in the models. None the less, swimming is also deserving of modellers' attention, so the model presented in Part III of this thesis will include swimming and crawling in its scope. But before embarking on such an endeavour, it is important to revisit the relationship between the two behaviours, particularly in light of the worm's limited neural circuit for locomotion. It would therefore be informative to examine the worm's locomotion in media whose properties are intermediate between those of water and agar.

Many animals exhibit kinematically distinct patterns of locomotion which differ qualitatively from each other, like the classic examples of a horse's walk, trot, canter and gallop, or a person's walk and run. In typical cases like these, gaits are defined in terms of how the parameters of locomotion change as a function of speed. Specifically, Alexander [2] gives the following definition: "A gait is a pattern of locomotion characteristic of a limited range of speeds described by quantities of which one or more change discontinuously at transitions to other gaits." However, gaits can also be defined in terms of the pattern of locomotion used in different media, such as the salamander's aquatic and terrestrial gaits [61], which differ qualitatively from each other. It therefore seems reasonable to take the essence of Alexander's definition and apply it to variable environments. Thus, if while changing the properties of the medium continuously from water-like to agar-like a discontinuous change in some property of the locomotion kinematics is observed, one could conclude that swimming and crawling were different gaits. Alternative gaits will typically rely on somewhat different neural mechanisms. This can be accomplished by recruiting different or additional neural populations, potentially through the action of neuromodulators or changes in descending input, or alternatively through the direct modulation of neural properties.

To address the relationship between swimming and crawling we undertook to map the transition from one behaviour to the other. To do so, we introduced a tunable environment in which the viscoelastic properties of the medium, and hence the stiffness of the groove (see Section 2.2.3), can be modulated from water-like Newtonian conditions (with K of order 1) to strongly non-Newtonian media. By recording and analysing the worm's locomotion in each medium we were able to quantitatively compare the observed body waves in terms of parameters like frequency and wavelength. If swimming and crawling really do represent fundamentally distinct behaviours, or gaits, we would expect to find some critical point in the transition where the worm stops swimming and begins to crawl. This would be marked by a discontinuous change in one or more locomotion metrics at some point during the transition. Conversely, a smooth transition through a continuum of intermediate behaviours would suggest that swimming and crawling are simply different manifestations of a single gait, much like a slow or fast walk in humans. This in turn would imply that the entire range of behaviours were the product of a single, modulated neural mechanism. The implication for future models of locomotion would be that a single model should be able to swim and crawl (and everything in between). The work in this chapter has already been published in Reference [13].

4.2 Methods

4.2.1 Worm Culture and Behavioural Assay

Wild type N2 *C. elegans* worms were cultivated using standard methods [17]. Experiments were performed on young adult hermaphrodites (4 days from hatching) at 20° C. We recorded the locomotion of freely moving worms fully immersed in gelatin solutions, where increasing concentrations correspond to more viscoelastic media that offer more resistance to motion and have a higher ratio of effective drag coefficients K . Specifically, gelatin (SIGMA G-8150) was dissolved in M9 and diluted to concentrations of 0.0 % (water), 0.5 %, 1.0 %, 1.2 %, 1.4 %, 1.5 %, 1.6 %, 1.8 %, 2.0 %, 3.0 % and 4.0 %. The inhomogeneous sampling of concentrations reflects the fact that the gel properties change rapidly between 1.0 % and 2.0 %. As will be shown in Section 4.3.2, 2.0 % gelatin is behaviourally equivalent to agar. We also added 2.5% (v/v) of swelled Sephadex beads (G-50 Medium MP Biomedicals 195580) to each sample in order to maintain the space between the glass slide and coverslip at 200 μ m. Gelatin solution filled the space between slide and coverslip, and a single worm was introduced. In addition to the range of gelatin solutions, we also recorded locomotion on agar and on a flat, non deformable surface,

namely a piece of moist dialysis membrane placed on a 2% agar gel pad. The recordings, taken at 25 frames per second, were then analysed as described in the following section.

4.2.2 Data analysis

To analyse the behaviour we began by using our specially developed “skeletonizer” software (described in Ref. [13]) to obtain the coordinates of 25 equidistant points along the midline of the worm for each frame. Using custom software, we then calculate locomotion metrics including the wavelength λ , amplitude A and frequency f of the body wave. Details of our method are provided in Ref. [13], so what follows is a brief overview.

The first step is to obtain the body curvature along the worm for each frame. A minimum of three points is required to calculate a curvature value (but these triplets can overlap) so the 25 point midline yields values for curvature at 23 points. This allows the changing body shape to be expressed in terms of curvature values in space (i.e. at 23 equidistant points along the body) and in time, as shown in Figure 4.1. Propagation of the body wave from head to tail gives rise to the diagonal stripes in the figure. The next step is to make linear fits to the regions of maximum curvature (diagonal black lines in Figure 4.1). At this point the undulation period $T = \frac{1}{f}$ is calculated as the average horizontal distance between the linear fits, while the wavelength (normalised by body length) is similarly obtained from the vertical distance. It is important to note that in cases where the wavelength is *greater* than the body length, it may be necessary to extend the linear fits beyond the end of the body in order to obtain the vertical distance between them. Also note that we use a physiologically grounded version of wavelength, defined as the *arc* length of a single period along the body, because this reflects the underlying pattern of muscle activation and more naturally links to neuromuscular locomotion models. Once the wavelength and frequency have been obtained, the amplitude is calculated as described in Ref. [13]. The time sequences of midlines and worm coordinates were also fed to the motion simulator described in Chapter 3 to obtain estimates of K , having been unable to do so through the rheological characterization described in Ref. [13].

4.3 Results

4.3.1 Swimming and crawling correspond to a single gait

Having collected data from locomotion in 11 different gelatin concentrations as well as on agar and a non-deformable surface (the latter will be addressed in Section 4.3.2), we were able to begin looking at the swim-crawl transition. Note that while locomotion on

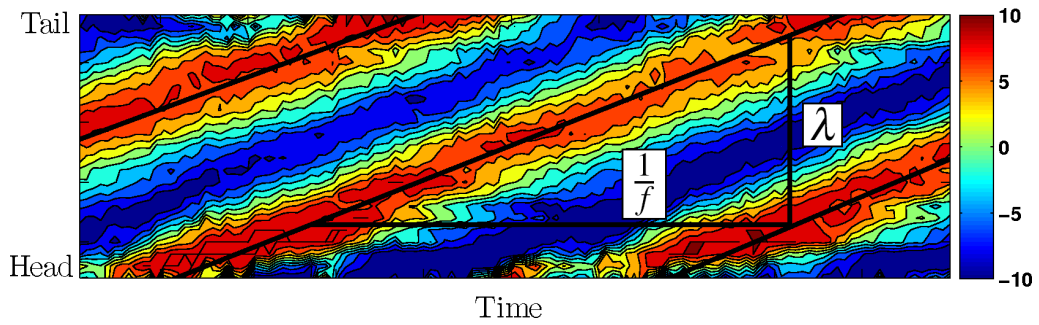


Figure 4.1: Calculating the wavelength λ and frequency f of the locomotion wave. Locomotion waveforms are expressed in terms of the time varying curvature along the length of the body (colours correspond to different values of curvature, according to the colour bar), with positive values denoting dorsal bending and negative values denoting ventral bending. The propagation of the wave from head to tail gives rise to the visible stripes of approximately constant curvature, to which we fit a linear approximation (diagonal black lines). Wavelength and frequency can then be obtained based on the vertical and horizontal spacing respectively.

agar is approximately equivalent to that in 2 % gelatin, our assay goes as far as 4 %. Thus the behaviours sampled by our experiment extend from swimming, through possible intermediate behaviours, to crawling and beyond. However, when we first looked at the locomotion metrics as a function of concentration we found that the behaviour was highly variable, concluding that the gelatin solutions were not homogeneous. We therefore decided not to group the data by concentration, rather treating each experiment independently. This turned out to be the key to interpreting the data, and the results are summarized in Figure 4.2, in which each point represents a single experiment.

To assess the continuity of the transition, we have visualised the data in two ways. Figure 4.2A-C shows the frequency, amplitude and wavelength as functions of each other, while Figure 4.2D-F shows each of these parameters as a function of K . If swimming and crawling were distinct behaviours, we would expect to see two clusters of points in each graph. In marked contrast to this, we find that across this entire range of environments there is a clear linear relationship between the frequency, amplitude and wavelength of undulations (Figure 4.2A-C), with no discontinuity in the transition. Moreover, when each of these locomotion metrics is plotted against our estimates of K (Figure 4.2D-F), we find that all three of them decay smoothly and continuously. One exception is the flat surface data which has not been included in plots D-F. The implications of this will be discussed in Section 4.4.

Thus, we find no evidence for the existence of distinct swimming and crawling behaviours, nor for a switch between different modes of locomotion. Rather, our results

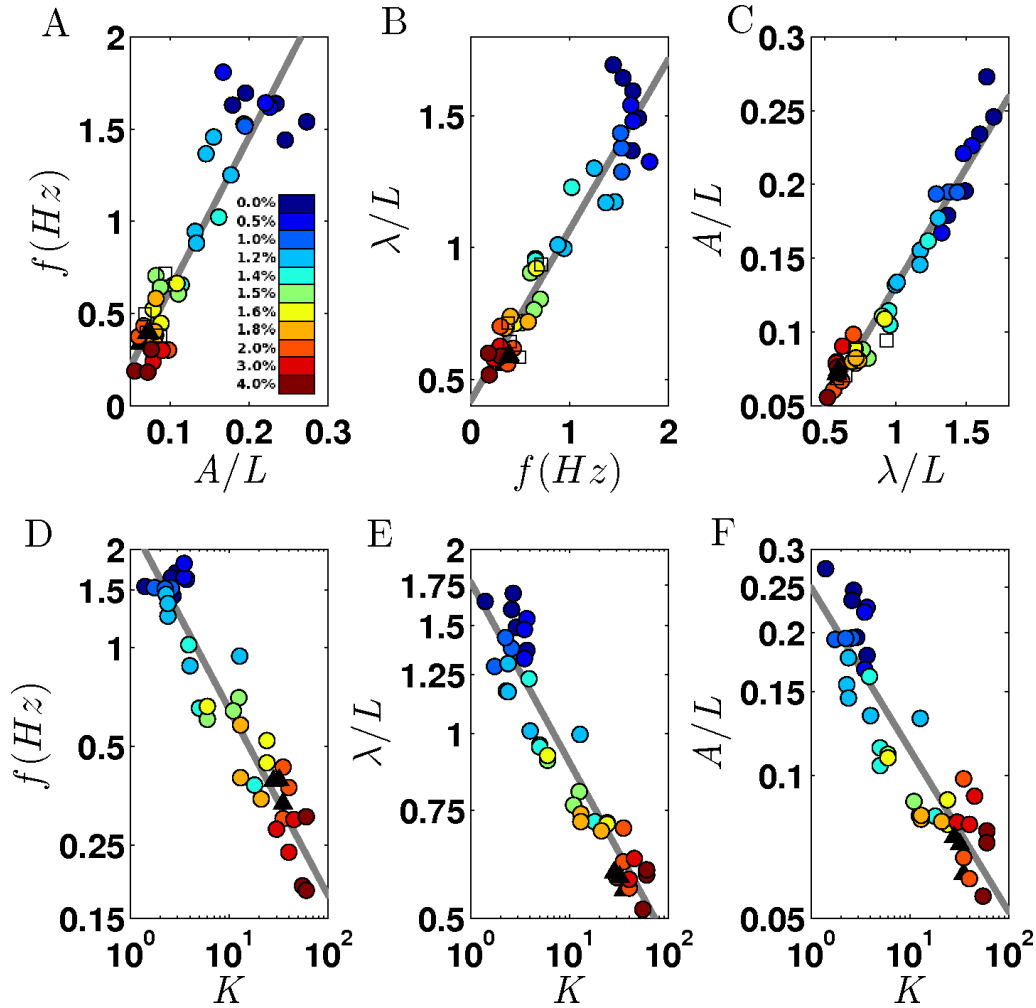


Figure 4.2: A-C) Proportionality of key locomotion parameters in a variety of environments (a range of gelatin concentrations, deformable agar surface, non-deformable membrane surface, with $n \geq 3$ replicates per environment). Lines show the best linear fits to the data. D-F) Frequency, wavelength and amplitude of the locomotion wave all decay smoothly with K in the different media (gelatin and agar, with $n \geq 3$ replicates per environment). Lines show the best power-law fits to the data. Note the doubly logarithmic scales. In all graphs, filled circles show gelatin data. Different colours represent different gelatin concentrations as indicated. Agar and membrane data are represented by black triangles and white squares respectively.

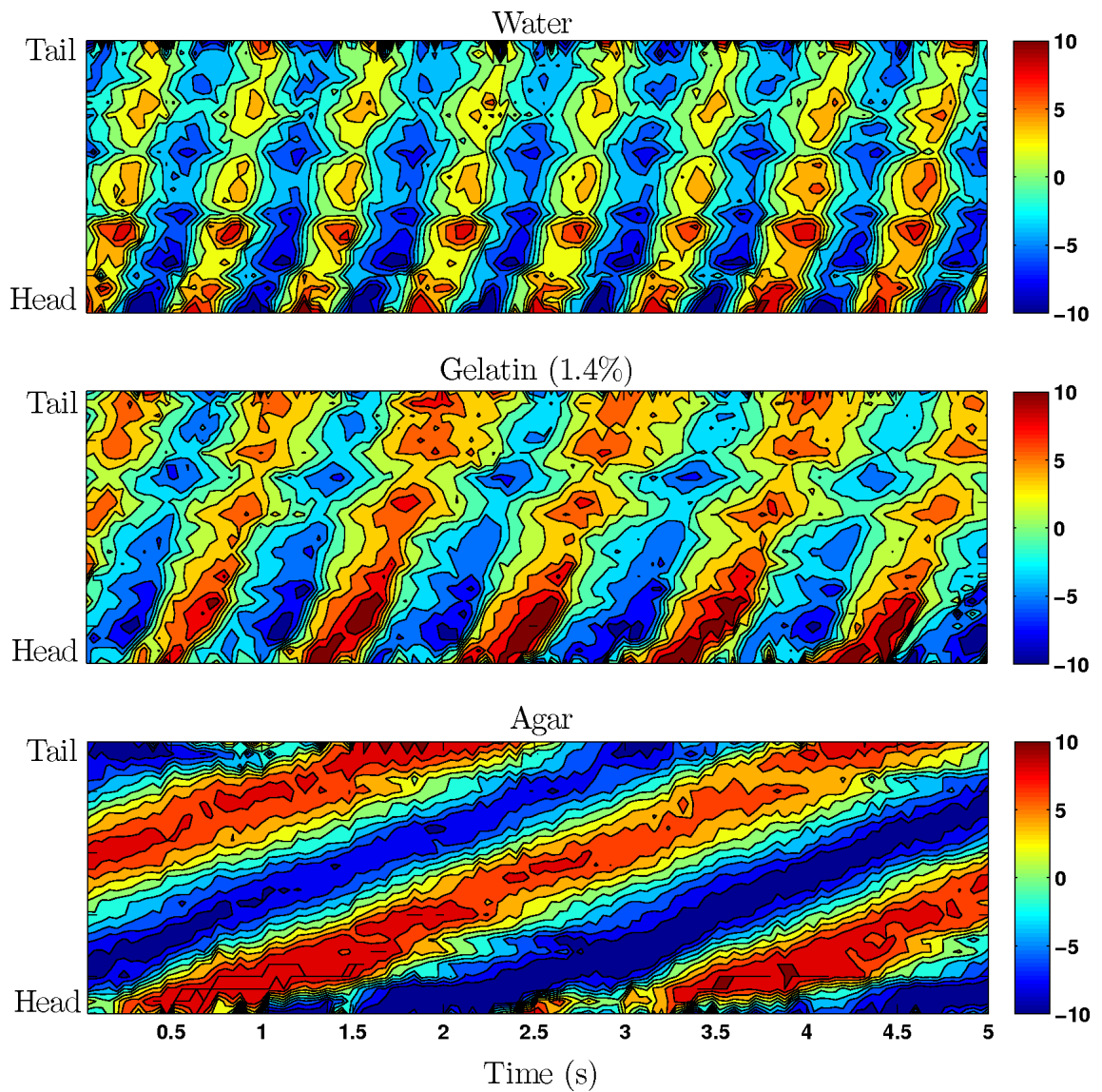


Figure 4.3: Locomotion waveforms visualised in terms of the time varying curvature along the length of the body [13]. Colours correspond to different values of curvature (see colour bars on right), with positive values denoting dorsal bending and negative values denoting ventral bending. The propagation of the wave from head to tail gives rise to the visible stripes of approximately constant curvature. By comparing the plots for different media, it can be seen that the locomotion waveforms of swimming and crawling are qualitatively equivalent, differing only in the inclination of the stripes and the spacing between them.

strongly suggest that all *C. elegans* forwards locomotion waveforms (see Supplementary movies C4_1 to C4_3 for examples) are achieved through a continuous modulation of a single gait. In light of this result, one would expect that the locomotion waveform would be qualitatively equivalent across different environments. This was confirmed by visualising the propagation of body curvature through both space (along the worm) and in time, as shown in Figure 4.3.

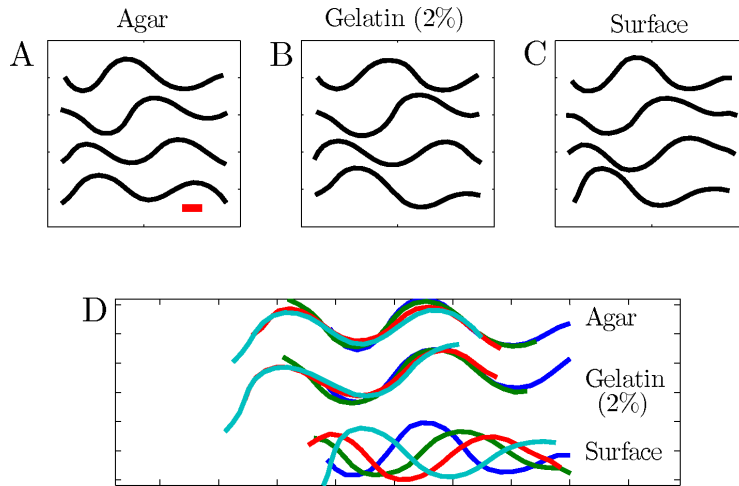


Figure 4.4: Sequences of four midlines extracted from movies of worms moving in/on different media. A-C) Worm midlines have been displaced vertically, rotated and aligned for clarity, with the head to the left and time increasing from top to bottom in quarter-period steps. The scale bar corresponds to approximately 0.1 mm. Estimated K values are A) 35, B) 35 and C) 1.9. D) Same midlines as above (A-C), still rotated, with the head to the left, but without removing the centre of mass motion.

4.3.2 The groove is not required for crawling

The results shown in Figure 4.2D-F suggest that the locomotion wave could potentially be changing in response to the groove strength parameter K . This is interesting in light of the Niebur and Erdős model [89] which, as noted earlier (see Section 2.3) relies on a very strong groove with $K = 10^4$ to allow the head trajectory to impose the body waveform. However, the relatively low values of K we obtain for motion on agar ($K = 32 \pm 4$), in the closest matching gelatin concentration of 2 % ($K = 37 \pm 3$) and even for 4 % gelatin ($K = 58 \pm 3$) are several orders of magnitude lower and might not support the proposed mechanism. None the less, our work raises an important question as to whether or not the groove strength is the key property of the environment with respect to determining the locomotion waveform. It is also plausible that, in the case of gelatin solutions, the

value of K happens to be proportional to another property that actually determines the waveform. Alternatively it could be some combination of factors that matters.

To address this question, we sought to eliminate the presence of a groove altogether, by placing worms on a flat, non-deformable surface (see Section 4.2.1). The resulting behaviour was recorded and compared to that of worms in other environments. Surprisingly, we found close agreement between the body waves produced on a surface and those produced on agar or in 2 % gelatin, as shown in Figure 4.4A-C. Specifically, we found that $\lambda_{\text{agar}} = (0.58 \pm 0.02)L$, $\lambda_{2\% \text{gel.}} = (0.63 \pm 0.07)L$ and $\lambda_{\text{surface}} = (0.65 \pm 0.06)L$, where L is the body length of the worm. To confirm that no groove is formed on the membrane surface, we note that the worm produces virtually no forwards motion in this case (Figure 4.4D, Supplementary movie C4.4), implying that K is close to unity. For $K = 1$ (an ideal surface with no forces except symmetrical surface friction), the theory presented in Section 2.2.2 predicts that the worm's centre of mass will remain stationary relative to the surface [42].

The above results strongly suggest that the shape of the worm is not determined by K , but rather by some other property of the environment. Furthermore, the fact that a crawling-like waveform can be produced on a surface with virtually isotropic resistance implies that the body shape must be determined by local muscle forces, rather than being physically imposed by the head trajectory.

4.3.3 Gel media are adequately described by a single-parameter model

Following slender body theory and the slip formulation of Gray and Lissmann [42,43], the motion simulator presented in Chapter 3 models the low Reynolds number environmental forces in terms of anisotropic local resistance coefficients (see Section 2.2.2). In our simulator, as in Equation 2.7, it is the ratio K (rather than the drag coefficients C_{\perp} and C_{\parallel} themselves), in conjunction with the locomotion waveform, that determines the actual motion of the worm. However, it is clear that this model only approximates the properties of fluids, particularly those of complex viscoelastic fluids and gels. However, the validity of this approximation can be assessed by comparing the simulated centre of mass motion of the worm (for the optimal value of K) to the corresponding experimental trajectory and computing the percent error for each time step of the simulation. For worms moving on agar or in 2 % gelatin, an average of 81 % of the simulation time steps had an error of less than 2 %, while 91 % had an error of less than 5 %. However, it should be noted that large error spikes occur at irregular intervals, due to noise in the experimental centre of mass recordings. The data from a representative clip of locomotion on agar is

illustrated in Figure 4.5. This suggests that indeed, *C. elegans* locomotion in gelatin and agar environments is adequately described by a single-parameter viscoelastic model of the environment. Such a representation is not suitable, however, for any study in which the forces responsible for bending the body will be modelled. In this case the actual drag coefficients C_{\perp} and C_{\parallel} would need to be used.

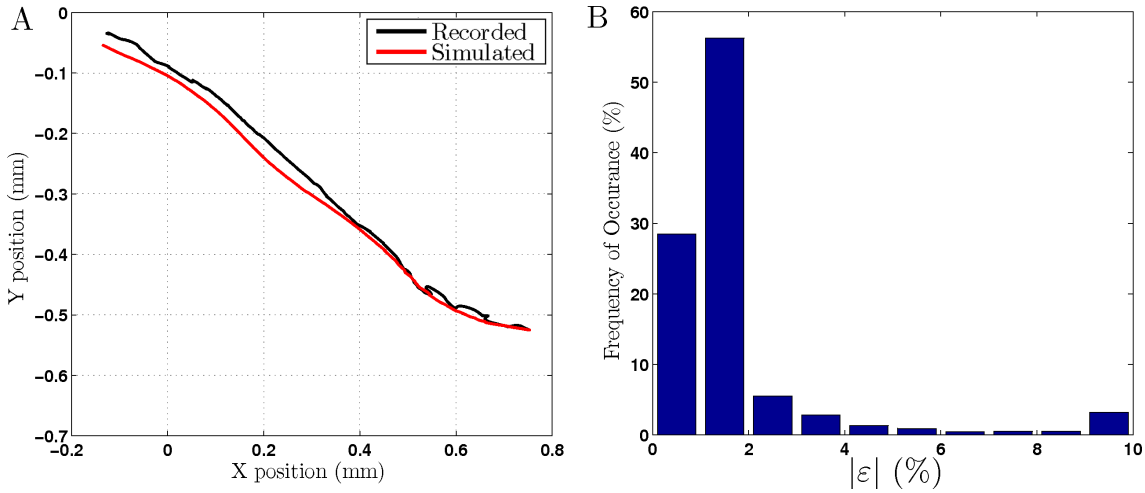


Figure 4.5: A) Similarity of simulated and recorded CoM trajectories for a worm moving on an agar surface. B) Histogram of the magnitude of total error per time step between the real and recorded motion. The right-most bin includes all errors greater than 10 %, which occur due to noise in the recorded CoM trajectory (visible as irregularities on the black trajectory in A).

4.4 Discussion

The primary result of this work is the demonstration of a smooth and continuous change between the so-called swimming and crawling waveforms, indicating that the whole range of behaviours corresponds to a single gait. In the *C. elegans* literature however, swimming is often described as having a “C” shape, as distinct from the “S” shape associated with crawling [48,93], implying a qualitative difference. By demonstrating a smooth transition between these behaviours, our work reveals that swimming and crawling are not qualitatively different and that the observed “C” shapes, rather than being universal, are simply the extreme phases of a roughly sinusoidal travelling wave with a wavelength longer than the worm’s body (see Figure 4.3).

Clearly the worm can (or must) change its locomotion waveform when exposed to different environments. Yet it is still not entirely clear what properties of the environment are

relevant, nor how exactly this modulation is achieved. The data presented here does shed some light on the matter, however. The gelatin results (Figure 4.2D-F) show a change correlated with K , but do not indicate which is the physically meaningful variable that the worm responds to. In fact, as K increases - in the gelatin assay - it is likely that not only the ratio of drag coefficients increases, but that the absolute resistance (in both directions) also increases. So which is it that really matters? The effective resistance to motion experienced by the worm, or the anisotropy in that resistance? The membrane experiments strongly suggest that the anisotropy (as captured by K) is not the key determinant of the worm's behaviour. This therefore suggests that the worm is responding to some function of the absolute resistance. Unfortunately, since we did not test the motion of surfaces of different resistances, we cannot confirm this hypothesis or shed light on what exact function that might be. However, the integrated neuromechanical model presented in Part III shows a smooth modulation of the undulation wavelength and frequency as a function of one such metric, namely the product of drag coefficients. If this is true, the worm must experience significant friction against the dialysis membrane surface.

The next question to ask is *how* the observed modulation of the locomotion wave is achieved. One possibility is that the worm senses some aspect of the environment and then actively modulates its neural circuit through the action of neuromodulators or peptides, or perhaps by recruiting additional neurons or changing the level of tonic input to some part of the circuit. However, in light of the worm's limited neural circuitry, the most parsimonious explanation would be that the waveform is passively modulated by the physics of the environment. But while purely passive, mechanical modulation could potentially explain changes in body shape, it is harder to imagine how such a mechanism would underlie the significant changes in frequency. One possible answer lies in the "stretch receptor hypothesis" that features to varying degrees in the models introduced in Section 2.3. If proprioceptive feedback from stretch receptors in A- and B-class motor neurons underlie a sensory feedback based oscillation mechanism (or at least make a sufficiently strong contribution to the oscillation mechanism) then direct modulation by the environment becomes more plausible. This will be further investigated in Chapter 5 and in Part III.

Regardless of the details of how and in response to what the worm's locomotion behaviour is modulated, the main implication of this work for future locomotion models is that they cannot address crawling (or swimming for that matter) independently. Indeed any future model should aim to reproduce the entire range of behaviours demonstrated here. As for the modulatory mechanism, a new model should be able to shed some light on the matter by testing one or more hypotheses. It seems logical to begin by attempting

to account for the observed modulation as simply as possible. The model presented in Part III will hopefully do just that.

Chapter 5

Preliminary neuromechanical model

5.1 Introduction

One of the more significant differences among previous *C. elegans* locomotion models (see Section 2.3) is the extent to which they have incorporated physical properties of the body and environment. In light of the investigation presented in Chapter 4, demonstrating that the worm's locomotion behaviour is strongly modulated (either directly or indirectly) by properties of the environment, it seems reasonable that any future locomotion model should include a physical component. As a starting point, one can ask what effect a physical model is likely to have when combined with a neuromuscular component. The main questions that will be addressed in this chapter are (i) whether a disembodied neural model can continue to function after the addition of a body with mechanical properties; and (ii) how the addition of these mechanical properties will alter the dynamics of said neural model.

The starting point for this investigation is a neural model previously developed by John Bryden and Netta Cohen [21], in the absence of a physical body. In isolation, this neural model produces a realistic locomotion waveform but suffers from the limitation that the undulations it produces are of significantly higher frequency than the observed behaviour of the crawling worm. A similar problem was encountered by Karbowski et al. [67], whose model similarly lacks a physical component. In their case the oscillations were slowed by including a time delay in the sensory feedback that is presumably an

abstraction of the effect of the body. This suggests that the dynamics of *C. elegans* neurons may be sufficiently fast that the physical dynamics become the limiting time-scale. The physical model that will be used here is adapted from a previous physical model due to Niebur and Erdős [89] and will also form the basis of a more complex and quantitative model presented in Part III.

Evaluation of the resulting integrated neuromechanical model will be performed in stages. First, the effects of physical forces on the frequency and waveform of oscillation will be investigated by simulating a single oscillating segment. This will be followed by an investigation of the physical interactions between segments, and the extent to which this perturbs the phase locking that underlies propagation of a travelling wave. Finally the results will be discussed in Section 5.4.

5.2 Methods

5.2.1 The neural model

The neural model is based on the work of Bryden and Cohen [19–21]. Specifically, it is a minor adaptation of the model (equations and parameters) presented in [21] which is itself an extension of Refs. [19, 20]. The model simplifies the neuronal connectivity presented by White et al. [136] into a minimal neural circuit for forward locomotion. This reduced model contained $N = 11$ repeating *units*, (one “tail” and ten “body” units) where each unit consists of one dorsal motor neuron (of class DB) and one ventral motor neuron (of class VB). A single command interneuron (representing a pair of interneurons of class AVB) provides the “on” signal to the forward locomotion circuit and is electrically coupled (via gap junctions) to all motor neurons of classes DB and VB. In the model, motor neurons also have sensory function, integrating inputs from stretch receptors, or stretch-sensitive ion channels, that encode each segment’s bending angle. Motor neurons receive both local and – with the exception of the tail – proximate sensory input, with proximate input received from the adjacent posterior segment. The sensory-motor loop for each unit gives rise to local oscillations which phase lock with adjacent units. The neural-only model used a minimal physical framework in which the bending angle of each segment is completely determined by the relative activation of the two neurons that control it. As a result there are no physical interactions between segments. Equations and parameters for the neural component of the integrated model are largely the same as those in Ref. [21], but are given below with new nomenclature. Figure 5.1B shows the neural model with only two units (a tail and one body unit) shown.

Neurons are assumed to have graded potentials [19–21]. In particular, motor neurons (VB and DB) and are modelled by leaky integrators with a transmembrane potential $V(t)$ following:

$$C \frac{dV_j^k}{dt} = -G^k(V_j^k - E_{\text{rev}}) - I_{\text{shape},j}^k + I_{\text{AVB},j}^k, \quad (5.1)$$

where $j = 1, \dots, N$ and $k = \{D, V\}$; C is the cell's membrane capacitance; E_{rev} is the cell's effective reversal potential; and G^k is the total effective membrane conductance. The sensory input from the local and posterior segment is given by

$$I_{\text{shape},j}^k = \sum_{q=j}^{j+1} (V_q^k - E_{\text{stretch},q}^k) G_{\text{stretch},q}^k \sigma_{\text{stretch},q}^k(\theta_q), \quad (5.2)$$

where $E_{\text{stretch},q}^k$ is the reversal potential of the ion channels, θ_q is the bending angle of segment q and $\sigma_{\text{stretch},q}^k$ is a sigmoid response function of the stretch receptors to the local bending, given by

$$\sigma_{\text{stretch},q}^k(\theta_q) = 1 / \left[1 + \exp \left(-(\theta - \theta_{0,q}^k) / \delta \theta_q^k \right) \right] \quad (5.3)$$

where the steepness parameter $\delta \theta_q^k$ and the threshold $\theta_{0,q}^k$ are constants given in Tables 5.1 and 5.2. Note however that since the tail unit ($j = N$) receives no posterior sensory input, any term in Equation 5.2 with $q > N$ is ignored. The command input current $I_{\text{AVB},j}^k = G_{\text{AVB}}^k (V_{\text{AVB}} - V_j^k)$ models gap junction coupling with AVB (with coupling strength G_{AVB}^k and denoting AVB voltage by V_{AVB}). Note that in the model, AVB is assumed to have a sufficiently high capacitance that the gap junction currents have a negligible effect on its membrane potential.

Segment bending in both the neural and neuromechanical models depends on a summation of the output function from each of the two neurons within a unit:

$$\frac{d\Theta_j}{dt} = \sigma_{\text{out}}^V(V_j^V) - \sigma_{\text{out}}^D(V_j^D), \quad (5.4)$$

where $\sigma_{\text{out}}^k(V_j^k) = \omega_{\text{max}}^k / [1 + \exp \left(-(V_j^k - V_0^k) / \delta V^k \right)]$ with constants ω_{max}^k , δV^k and V_0^k . Note that dorsal and ventral muscles contribute to bending in opposite directions (with θ and $-\theta$ denoting ventral and dorsal bending, respectively).

Table 5.1: Parameters for a self-oscillating tail unit ($j = N$), as in Ref. [21].

| Parameter | Value | Parameter | Value | Parameter | Value |
|-------------------------|-------------|--------------------------|-------------|--------------------------|----------|
| E_{rev} | -60 mV | V_{AVB} | -30.7 mV | C | 5 pF |
| G_N^V | 19.07 pS | G_N^D | 17.58 pS | G_{AVB}^V | 35.37 pS |
| G_{AVB}^D | 13.78 pS | $G_{\text{stretch},N}^V$ | 98.55 pS | $G_{\text{stretch},N}^D$ | 67.55 pS |
| $E_{\text{stretch},N}$ | 60 mV | $\theta_{0,N}^V$ | -29.68° | $\theta_{0,N}^D$ | -8.46° |
| $\delta\theta^V$ | 0.1373° | $\delta\theta^D$ | 0.4186° | ω_{max}^V | 6987°/s |
| ω_{max}^D | 9951°/s | V_0^V | 22.8 mV | V_0^D | 25.0 mV |
| δV^V | 0.2888 mV/s | δV^D | 0.0826 mV/s | | |

Table 5.2: Parameters for body units ($j < N$) and tail-body interactions as in Ref. [21]. All body unit parameters that are not included here are the same as for the tail unit.

| Parameter | Value | Parameter | Value | Parameter | Value |
|----------------------------|----------|--------------------------|----------|----------------------------|----------|
| $G_{j<N}^V$ | 26.09 pS | $G_{j<N}^D$ | 25.76 pS | $G_{\text{stretch},j<N}^V$ | 16.77 pS |
| $G_{\text{stretch},j<N}^D$ | 18.24 pS | $E_{\text{stretch},j<N}$ | 60 mV | $\theta_{0,j<N}^V$ | -22.14° |
| $\theta_{0,j<N}^D$ | -10.26° | $\delta\theta_{j<N}^V$ | 1.589°/s | $\delta\theta_{j<N}^D$ | 1.413°/s |

5.2.2 Physical model

The physical model is an adaptation of Ref. [89], a discrete, 2-D model consisting of a number of points arranged symmetrically in two rows (representing the dorsal and ventral sides of the worm). Each point is acted on by the opposing forces of the elastic cuticle and pressure, as well as muscle actuation force and environmental drag. The simplifications that have been introduced reduce the simulation time, in part by allowing the use of a longer time step.

The model, whose structure is illustrated in Figure 5.1A, represents a worm of length L and radius R by a total of P points labelled \mathbf{p}_i^k , where $i = 1, \dots, P/2$ and $k = \{D, V\}$. Each dorsal/ventral pair $\mathbf{p}_i^k, \mathbf{p}_i^{\bar{k}}$ (the notation \bar{k} denotes the opposite side to k i.e., if $k = D$ then $\bar{k} = V$) is connected by a rigid rod of length $2R$. Each of these rods is connected at its end points to each of the adjacent rods by four springs. Two lateral springs connect points on the same side of adjacent rods ($\mathbf{p}_i^k, \mathbf{p}_{i+1}^k$) and resist both elongation and compression. Two diagonal springs connect the dorsal side of the i^{th} rod to the ventral side of the $i+1^{\text{st}}$, and vice versa ($\mathbf{p}_i^k, \mathbf{p}_{i+1}^{\bar{k}}$). These springs strongly resist compression and have an effect analogous to that of pressure, in that they help to maintain constant “volume”. The model was implemented in C++, using a 4th order Runge-Kutta method for numerical integration, with a time step of 0.1 ms. The original model [89] required a time step of 0.001 ms with the same integration method. While the use of rods for the radial connections precludes changes in width, it has the advantage of allowing the forces acting on \mathbf{p}_i^k and

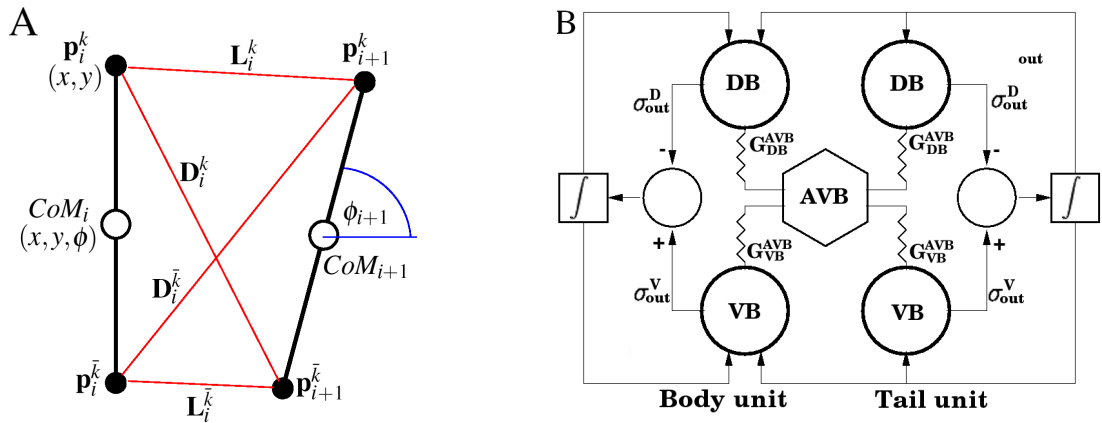


Figure 5.1: A) Schematic diagram of the physical model illustrating nomenclature (see text for details). B) The neural model, with only two units shown (the tail and one body). AVB is electrically coupled to each of the motor neurons via gap junctions (resistor symbols).

$\mathbf{p}_i^{\bar{k}}$ to be combined into a single force and torque acting on the rod's midpoint (that will loosely be referred to as the centre of mass, or CoM). This also means that the state of the i^{th} rod can be described in one of two ways: either by the (x, y) coordinates of the centre of mass (CoM_i in Fig. 5.1) and angle ϕ_i relative to the x axis, or by the (x, y) coordinates of its two end points (\mathbf{p}_i^k and $\mathbf{p}_i^{\bar{k}}$ in Fig. 5.1). Each formulation has its own advantages and will be used where appropriate.

Spring forces

The rigid rods are connected at their end points to each of their neighbours by lateral (L) and diagonal (D) springs that are indexed by $m = 1, \dots, M$, where $M = P/2 - 1$. These forces are directed along the vectors

$$\begin{aligned} \mathbf{L}_m^k &= \mathbf{p}_{m+1}^k - \mathbf{p}_m^k \\ \mathbf{D}_m^k &= \mathbf{p}_{m+1}^{\bar{k}} - \mathbf{p}_m^k. \end{aligned} \quad (5.5)$$

The lateral and diagonal spring forces $\mathbf{f}_{L,m}^k$ and $\mathbf{f}_{D,m}^k$ depend on the length of these vectors, $L_{L,m}^k = |\mathbf{L}_m^k|$ and $L_{D,m}^k = |\mathbf{D}_m^k|$ and are collinear to them. The magnitude of the lateral and

diagonal spring forces are piecewise linear functions

$$f_{L,m}^k(L_{L,m}^k) = \begin{cases} \kappa_L^{S2}(L_{L,m}^k - L_L^2) + \kappa_L^{S1}(L_L^2 - L_L^0) & : L_{L,m}^k > L_L^2 \\ \kappa_L^{S1}(L_{L,m}^k - L_L^0) & : L_L^2 > L_{L,m}^k > L_L^0 \\ \kappa_L^{C2}(L_{L,m}^k - L_L^1) + \kappa_L^{C1}(L_L^1 - L_L^0) & : L_{L,m}^k < L_L^1 \\ \kappa_L^{C1}(L_{L,m}^k - L_L^0) & : \text{otherwise} \end{cases}, \quad (5.6)$$

$$f_{D,m}^k(L_{D,m}^k) = \begin{cases} \kappa_D^{C2}(L_{D,m}^k - L_D^1) + \kappa_D^{C1}(L_D^1 - L_D^0) & : L_{D,m}^k < L_D^1 \\ \kappa_D^{C1}(L_{D,m}^k - L_D^0) & : L_D^1 < L_{D,m}^k < L_D^0 \\ 0 & : \text{otherwise} \end{cases}, \quad (5.7)$$

where spring (κ) and length (L) constants are given in Table 5.3.

Table 5.3: Parameters of the physical model.

| Parameter | Value | Parameter | Value | Parameter | Value |
|---------------------|------------------------------------|-----------------|---|-----------------|--------------------|
| R | $40 \mu\text{m}$ | L_L^0 | $50 \mu\text{m}$ | L_L^1 | $0.5L_L^0$ |
| L_L^2 | $1.5L_L^1$ | L_D^0 | $\sqrt{(L_L^0)^2 + (2R)^2}$ | L_D^1 | $0.95L_D^0$ |
| κ_L^{S1} | $20 \mu\text{N}\cdot\text{m}^{-1}$ | κ_L^{S2} | $10\kappa_L^{S1}$ | κ_L^{C1} | $0.5\kappa_L^{S1}$ |
| κ_L^{C2} | $10\kappa_L^{C1}$ | κ_D^{C1} | $50\kappa_L^{S1}$ | κ_D^{C2} | $10\kappa_D^{C1}$ |
| f_{muscle} | $0.005L_0^h\kappa_L^{C1}$ | C_{\perp} | $80 \times 10^{-6} \text{kg}\cdot\text{s}^{-1}$ | C_{\parallel} | $C_{\perp}/100$ |

Muscle forces

In the model, muscles are located between each pair of neighbouring points on the same side of the body (\mathbf{p}_m^k and \mathbf{p}_{m+1}^k), yielding a total of M muscles on each side. Muscle forces $\mathbf{f}_{M,m}^k$ are directed along the lateral vectors \mathbf{L}_m^k and have magnitude

$$f_{M,m}^k = f_{\text{muscle}} A_m^k, \quad (5.8)$$

where f_{muscle} is a constant (see Table 5.3) and A_m^k are scalar activation functions for the dorsal and ventral muscles, determined by

$$(A_m^D, A_m^V) = \begin{cases} (\Theta_m(t), 0) & \text{if } \Theta_m(t) \geq 0 \\ (0, -\Theta_m(t)) & \text{if } \Theta_m(t) < 0, \end{cases} \quad (5.9)$$

where $\Theta_m(t) = \int_0^t \frac{d\Theta_{j=m}}{dt} dt$ is the integral over the output of the $j = m^{\text{th}}$ unit of the neural model (given by Equation 5.4).

Total point force

With the exception of those on the first and last rods, each point \mathbf{p}_i^k is subject to forces from the springs and muscles connecting it to the anterior ($i-1$) and posterior ($i+1$) rod. Thus the net force \mathbf{f}_i^k acting on each point is given by

$$\mathbf{f}_i^k = (\mathbf{f}_{L,i}^k - \mathbf{f}_{L,i-1}^k) + (\mathbf{f}_{D,i}^k - \mathbf{f}_{D,i-1}^{\bar{k}}) + (\mathbf{f}_{M,i}^k - \mathbf{f}_{M,i-1}^k). \quad (5.10)$$

Since the first rod has no anterior body parts, and the last rod has no posterior body parts, all right hand side terms with $i=0$ or $i=P/2$ are taken as zero.

Equations of motion

Motion is calculated from the total force acting on each of the P points. Since the points \mathbf{p}_i^k and $\mathbf{p}_i^{\bar{k}}$ are connected by a rigid rod, it is convenient to convert the two forces \mathbf{f}_i^k and $\mathbf{f}_i^{\bar{k}}$ to a single force and torque acting on the rod's centre of mass. This requires a change from global coordinate space to local coordinates relative to the orientation of the rod, expressed in terms of its angle ϕ . See Figure 5.2 for a clarification of the text.

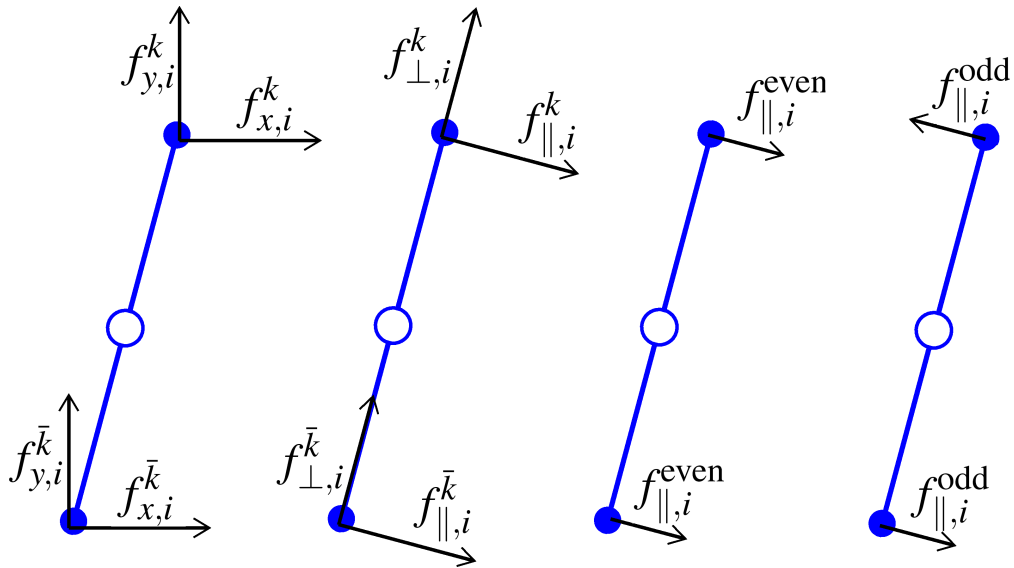


Figure 5.2: Decomposition of forces applied to the solid rods of the physical model. Initially, forces are represented in terms of x and y components (left). They are then converted to a coordinate frame relative to the orientation of the rod, before further separating the tangential components into odd and even subcomponents. See text for details.

Rotation by $\frac{\pi}{2} - \phi_i$ converts the coordinate system of $\mathbf{f}_i^k = (f_{x,i}^k, f_{y,i}^k)$ to a new system $\mathbf{f}_i^k = (f_{\parallel,i}^k, f_{\perp,i}^k)$ with axes tangent (\parallel) and normal (\perp) to the local body surface, which

is itself defined as being *normal* to the rod (see Figure 5.2 for clarification). This is accomplished by

$$\begin{aligned} f_{\parallel,i}^k &= f_{x,i}^k \cos\left(\frac{\pi}{2} - \phi_i\right) - f_{y,i}^k \sin\left(\frac{\pi}{2} - \phi_i\right) \\ f_{\perp,i}^k &= f_{x,i}^k \sin\left(\frac{\pi}{2} - \phi_i\right) + f_{y,i}^k \cos\left(\frac{\pi}{2} - \phi_i\right). \end{aligned} \quad (5.11)$$

The normal components can then be summed and applied to CoM_i , resulting in pure translation. The tangential components must be further separated into odd and even parts (giving rise to a torque and force respectively) by

$$\begin{aligned} f_{\parallel,i}^{\text{even}} &= \frac{(f_{\parallel,i}^V + f_{\parallel,i}^D)}{2} \\ f_{\parallel,i}^{\text{odd}} &= \frac{(f_{\parallel,i}^V - f_{\parallel,i}^D)}{2}. \end{aligned} \quad (5.12)$$

As in the motion simulator of Chapter 3, the model uses low Reynolds number physics and therefore disregards inertia. The resistance of the environment is modelled as Stokes' drag of the form $\mathbf{F} = -C\mathbf{V}$. Following the theory outlined in Section 2.2.2, the model uses different constants for drag in the tangential and normal directions, given by C_{\parallel} and C_{\perp} respectively. The motion of CoM_i is therefore given by

$$\begin{aligned} V_{\perp,i}^{(\text{CoM})} &= \frac{1}{C_{\perp}} (f_{\perp,i}^D + f_{\perp,i}^V) \\ V_{\parallel,i}^{(\text{CoM})} &= \frac{1}{C_{\parallel}} (2f_{\parallel,i}^{\text{even}}) \\ \omega_i^{(\text{CoM})} &= \frac{1}{RC_{\parallel}} (2f_{\parallel,i}^{\text{odd}}). \end{aligned} \quad (5.13)$$

Finally $V_{\parallel,i}^{(\text{CoM})}$ and $V_{\perp,i}^{(\text{CoM})}$ are converted back to (x,y) coordinates using

$$\begin{aligned} V_{x,i}^{(\text{CoM})} &= V_{\parallel,i}^{(\text{CoM})} \cos\left(\frac{\pi}{2} - \phi_i\right) + V_{\perp,i}^{(\text{CoM})} \sin\left(\frac{\pi}{2} - \phi_i\right) \\ V_{y,i}^{(\text{CoM})} &= -V_{\parallel,i}^{(\text{CoM})} \sin\left(\frac{\pi}{2} - \phi_i\right) + V_{\perp,i}^{(\text{CoM})} \cos\left(\frac{\pi}{2} - \phi_i\right). \end{aligned} \quad (5.14)$$

Feedback signal

In the neural model, the output of the neural unit $d\Theta_j/dt$ directly determines the bending angle θ_j for each segment. In the integrated model, Θ_j are taken as the inputs to the muscles. Muscle outputs (or contraction), in conjunction with the physical model, cause

the lengths of the lateral elements, and therefore the segment angle, to change over time. The effective segment bending angle θ_j (required for the feedback signal to the neurons) is then estimated from the dorsal and ventral lengths by

$$\theta_j = 36.2 \frac{L_{L,m=j}^D - L_{L,m=j}^V}{L_L^0}, \quad (5.15)$$

where L_L^0 is the resting length of the lateral elements. This value can then be fed back into the neural controller via Equation 5.2.

5.3 Results

5.3.1 Single oscillating segment

The neural model alone produces robust oscillations in segment bending angle (θ_j) with a roughly square waveform, as shown in Figure 5.3A. The model segment oscillates at about 3.5 Hz, as compared to frequencies of about 0.5 Hz observed for *C. elegans* locomotion on an agar substrate, or about 2 Hz in water (note that the Bryden and Cohen model generates a crawling-like waveform and should therefore ideally oscillate at 0.5 Hz). It was reportedly not possible to find parameters within reasonable electrophysiological bounds for the neural model that would slow the oscillations to the desired time-scales [21]. Oscillations of the integrated neuromechanical model of a single segment are shown in Figure 5.3B. All but four parameters of the neuronal model remain unchanged from Ref. [21]. However, the parameters $\theta_{0,j}^k$ used for the actuation step caused a slight asymmetry in the oscillations when integrated with a physical model, and were therefore modified to the values presented here. As can be seen from the traces in the figure, the integrated model is able to oscillate at about 0.5 Hz with a smooth, almost sinusoidal waveform. The frequency of oscillation can be smoothly modulated over quite a broad range by changing the drag parameters, as shown in Figure 5.3C.

5.3.2 Two phase-lagged segments

Parameters of the neural model are given in Table 5.1 for the tail segment, with alternative parameters given in Table 5.2 for the body segment. Figure 5.4 shows the bending waveforms recorded from a living worm (Figure 5.4A), simulated by the neural model (Figure 5.4B) and simulated by the integrated model (Figure 5.4C). With two segments the integrated model is able to oscillate realistically and with a suitable phase lag, although the

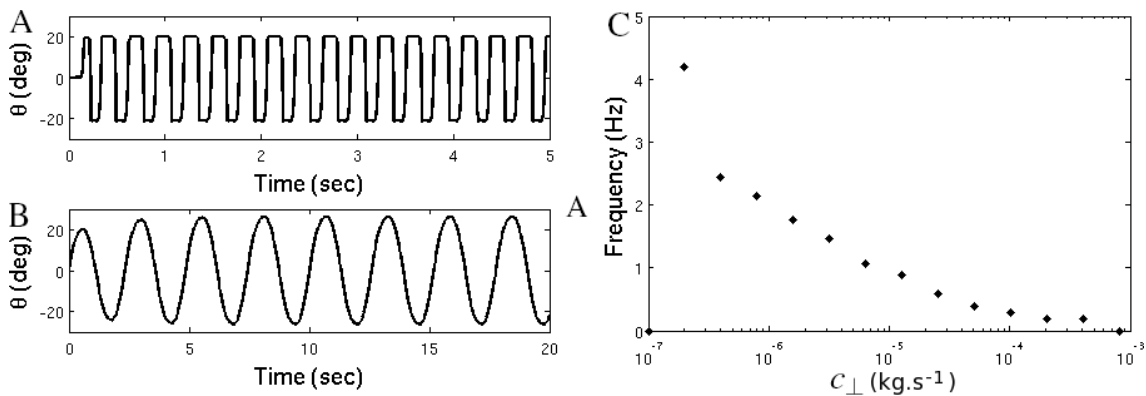


Figure 5.3: Oscillations of, A) the original neural model [21] and, B) the integrated model (with $C_{\perp} = 80 \times 10^{-6} \text{ kg}\cdot\text{s}^{-1}$). Note the different time-scales. C) Oscillation frequency as a function of variable $C_{\perp} = 100C_{\parallel}$. The zero frequency point indicates that the segment can no longer oscillate.

segment bending waveforms are not identical for the tail and body segment. Note however that during this oscillation, the middle of the three rods remains almost in place while the outer two rods do most of the moving (not shown).

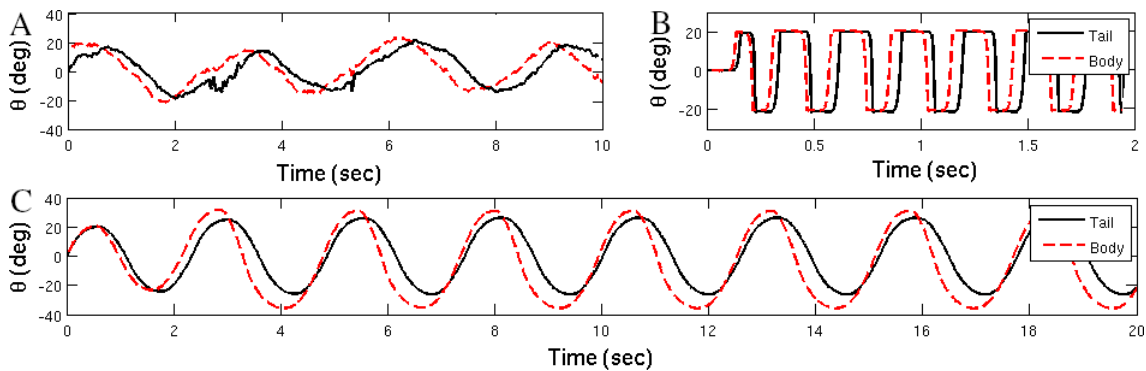


Figure 5.4: Phase lagged oscillation of two segments. A) Bending angles extracted from a recording of a forward locomoting worm on an agar substrate. The traces are of two points along the worm (near the middle and $\frac{1}{12}$ of a body length apart). B) Simulation of two coupled units in the neural model. C) Simulation of the integrated model. Take note of the different time scale in subplot B)

5.3.3 Extending to more segments

As more segments are added to the model, the significance of physical interactions between them will increase. This is particularly significant for segments near the middle of the worm, as the body parts attached to either side must be moved in order for the segment to bend, adding significant mechanical load. Furthermore, motion of a given segment will

generally deform its neighbours, interfering with the sensory feedback loop. A simulation of the model with three segments (adding an additional “body” segment) should begin to reveal whether the control system is robust to these perturbations. As demonstrated in Figure 5.5, the three segment model continues to oscillate robustly. However, it is immediately apparent that the physical interactions are detrimental to the model’s ability to synchronize, leading to a breakdown of the correct phase relationship. The bending waveforms of the individual segments are also affected.

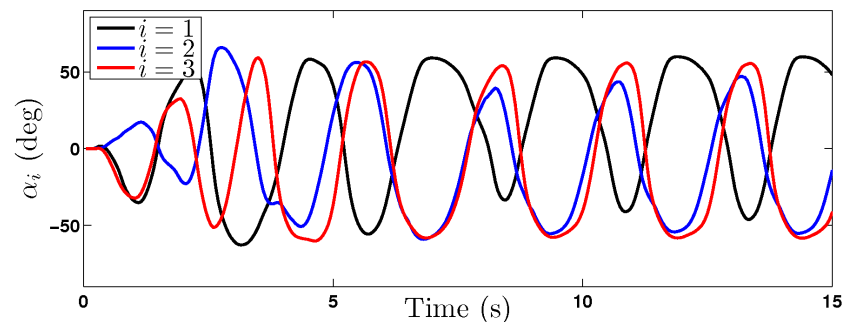


Figure 5.5: Oscillation of the model with two body segments ($i = 1, 2$) and one tail segment ($i = 3$). While the model is still able to oscillate, the waveforms are distorted and the correct phase lags are not preserved.

If the number of segments is increased to 11 (as in the original neural model) similar behaviour is observed. Oscillations continue and forward progress is still made, but the waveforms of individual segments are again distorted and the correct phase relationship is not preserved. Specifically, the phase lags between adjacent segments are too large, resulting in a very short wavelength as shown in Figure 5.6. In fact, the direction of bending (dorsal or ventral) typically alternates every two to three segments.

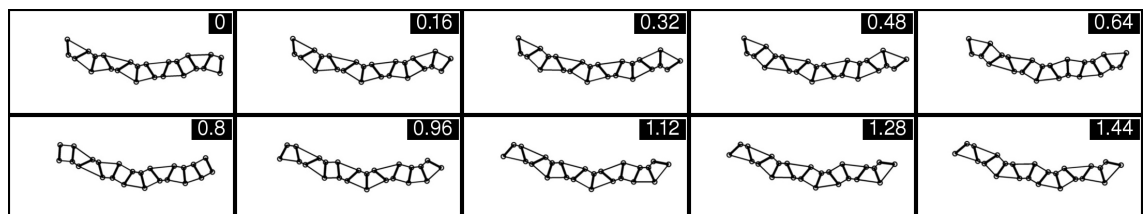


Figure 5.6: Frames extracted from a movie of the 11 segment integrated model (See Supplementary movie C5.1). Numbers in the top right corners give the time in seconds at which each frame was taken. Notice that despite the lack of coordination, the model still moves forwards (to the left).

5.4 Discussion

The model presented here, while only partially successful, provides valuable insight into the importance of body physics. First, it demonstrates that a neural model developed with only the most rudimentary physical framework can continue to function only partially when a more realistic embodiment is added. Second, it shows that the inclusion of body physics can have a dramatic effect on the oscillation dynamics. When only a short section (two segments or less) is simulated, these effects are beneficial. Indeed, both the waveform and frequency of oscillation are improved beyond what was possible for the isolated neural model [21]. However, when more segments are included the effect of the body becomes more detrimental, particularly to the inter-segment phase relationship.

To understand these different classes of effect it helps to consider the local and long range effects of the body separately. Locally the effect of the body and environment is primarily to filter the neural outputs, adding a delay to the sensory feedback loop with a similar effect to that used by Karbowski et al. [67]. In the original neural model, the frequency of oscillation depends only on the neural time-scale. Adding a physical model introduces an additional time-scale, as well as a nonlinearity in the mapping between neural activity and segment bending. When the neural states change, the body will begin bending at a rate that depends on the strength of the muscles relative to the resistance of the environment. The neural states depend critically on the stretch receptor feedback, which in turn is dependent on the body dynamics. Thus the neurons must “wait” for the body configuration to change. With the parameters used in this model, the frequency is dominated by the physical rather than the neural time-scale, so the oscillation slows down. The observed change in waveform from roughly square to roughly sinusoidal is caused by the nonlinearity introduced by the body. As the segment bends the muscle force is increasingly resisted by the elasticity of the stretched or compressed cuticle, reducing the net force and therefore the rate of bending. It is this effect that smooths the waveform. When a second segment is added, the effect remains largely unchanged. The middle rod stays roughly in place, while the oscillation of each segment causes the outer two rods (which are connected only to the middle rod) to move.

Let us now consider the long range effects. In the original model the angles of each segment were computed independently, and the resulting worm “shape” was visualized as a series of lines connected to each other at the specified angles. Adding a physical model means that bending of any of the inner segments applies forces to the adjacent segments. To accommodate this motion the nearby points must typically move laterally, but this is strongly resisted by the normal drag coefficient. If this load is too great, the

nearby points will not move and instead the body elements will have to stretch or compress to accommodate this force, often leading to unrealistic, contorted body shapes. The result is that the segments are constantly perturbing each other physically, with these deformations feeding back into the control system via the stretch receptors. The very short wavelength displayed by the 11 segment integrated model can also be explained by the fact that motion normal to the body surface is resisted more strongly than motion tangent to it. In the extreme case of zero phase lag (a standing wave), the net curvature of the body will be great and the ends of the worm would have to undergo large lateral displacement. If instead the phase lag between adjacent segments is 180° , the net curvature of the body will be approximately zero, so all segments would experience only small lateral displacements, thereby reducing the load.

There are two main conclusions to be drawn from this work. First, the physical effects of a body can be both beneficial and detrimental, but must certainly be taken into account. This should be incorporated at an early stage, as a control system developed in the absence of long range physical interactions is unlikely to work once they are introduced. Second, this investigation has shown that changing the physical drag is a viable method for modulating the frequency of oscillation.

Chapter 6

Conductance based muscle model

6.1 Introduction

Models of *C. elegans* locomotion generally focus on the worm's nervous system [20, 21, 118] or body mechanics [36, 89], but it is currently not clear which components of the locomotion subsystem are actively involved in generating and shaping locomotion. The candidates are the interneurons, head and ventral cord motor neurons, body wall muscles and the *C. elegans* body itself. While it was demonstrated in Chapters 4 and 5 that the body is an important part of the locomotion system, some other components of the system must generate the patterns of muscle activation required for locomotion. Thus the two alternatives are either that the patterned activity of the motor neurons activates the muscles which then act as actuators to deliver the mechanical contractions, or that in addition to neuronal activity, the muscles themselves are capable of generating oscillatory dynamics and/or of propagating such signals down the length of the worm. The former holds in most studied motor systems: the neural circuit generates a patterned output, and the muscles serve as actuators of that output. Interestingly, this division does not seem to be as clear in *Ascaris lumbricoides* [36, 131, 132] – a much larger but closely related nematode whose nervous system is structurally very similar to that of *C. elegans*. In *Ascaris*, the body wall muscles are electrically coupled by gap junctions and appear to form a functional syncytium which produces spontaneous myogenic activity: voltage spikes superimposed on slow depolarisations, which propagate independently of the nervous system [131, 132].

From this perspective, it may not be surprising if *C. elegans* muscles had a similar pattern generating (or pattern modulating) role in locomotion. In fact, a recent locomotion model due to Karbowski et al. [67] relies on a mechanism whereby oscillations generated in the head are imposed on the rest of the body in part via strong muscle gap junctions.

In the absence of a direct answer to this question, one may turn to behavioural evidence from locomotion-defective (or so called uncoordinated) mutant strains of the worm. Particularly instructive are mutations that might disrupt electrical signal flow between muscles. There are two gap junction genes that have been implicated in *C. elegans* locomotion, namely *unc-7* and *unc-9* [110]. Mutations in both of these result in virtually identical phenotypes [92] where locomotion is severely impaired. Both are widely expressed, but only *unc-9* is expressed in muscles. Liu et al. have shown that worms treated with *unc-9* RNA interference (RNAi) to suppress *unc-9* gene expression exhibit substantially reduced locomotion velocities [76]. The authors suggest that this effect could be attributed specifically to the reduction in gap junction coupling between body wall muscles, based in part on the fact that *C. elegans* neurons are partially resistant to RNAi [109].

In this chapter, which was previously published as Ref. [16], I rely on electrophysiological data recorded from body wall muscles in acutely dissected preparations [64,65,76] to construct a model of individual and coupled muscle cells. This model is then used to determine what possible active role may be attributed to individual *C. elegans* body wall muscles and, furthermore, to determine the consistency of such a model with the observed phenotype of gap junction defective worms. More specifically, I will attempt to address the following questions: Do the muscles typically fire action potentials? What is their contribution to the generation of rhythmic behaviour? And finally, how strong is the inter-muscular coupling, and to what extent does it affect locomotion?

6.1.1 Anatomy of body wall musculature

The body wall muscles of *C. elegans* are divided into four quadrants (ventral left, ventral right, dorsal left and dorsal right) each of which consists of 23 or 24 trapezoidal cells, arranged in two staggered rows as shown in Figure 6.1 (also see Section 2.1.1). When it locomotes, the worm lies on its side, with the pairs of ventral and dorsal muscle quadrants contracting in unison. Gap junctions couple cells within each quadrant, as well as between quadrants (ventral left with ventral right, and dorsal left with dorsal right). Within a quadrant, gap junctions are found between each muscle cell and the two overlapping cells from the other row [76] (see Figure 6.1).

Nematode muscles are unusual in that they extend thin, non-contractile processes to

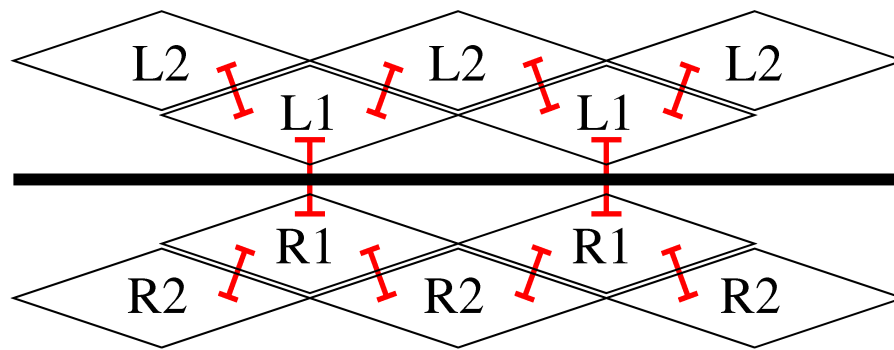


Figure 6.1: Schematic showing the layout of body wall muscles and the gap junctions that connect them, based on the data of Ref. [76]. Within each quadrant the muscles are arranged in two staggered rows (L1, L2 or R1, R2). Gap junction coupling (red ‘I’ shapes) occurs with a regular pattern both within and between quadrants, which straddle the nerve cord (thick black line).

the motor neurons in the nerve cord, where they receive their neuromuscular input. The gap junctions which couple cells from the two ventral (or dorsal) quadrants are found on these muscle arms, where they meet at the nerve cord [76]. Each muscle typically has three to five arms [34].

6.1.2 Typical effects of diffusive coupling

Gap junctions are found in a range of organs and cell types in vertebrates as well as invertebrate species and are very common in excitable tissue (e.g., heart muscle, pancreas, and the nervous system). Many gap junctions have fixed conductance and act as resistive elements. The current flowing through such a resistor would be proportional to the voltage drop across it, or the potential difference between the two coupled cells, j and k : $I_{j,k} = G(V_k - V_j)$ where G denotes a constant conductance (or inverse resistance). In *C. elegans*, it appears that the conductance of some gap junctions is itself a function of the potential difference between the coupled cells. Nonetheless, for the purposes of this introduction, it is sufficient to consider whether the coupling is relatively “weak” or “strong”, neglecting any functional dependence of the conductance.

If coupling is sufficiently strong, the coupled elements will fully synchronise, effectively becoming a single entity. Therefore the more interesting cases are those of weak and intermediate coupling. Weakly coupled limit cycle oscillators have been the subject of much theoretical investigation [37, 38, 68]. Typically, the frequencies of the oscillators are pulled towards each other, and full or partial entrainment may result, depending on the difference in natural frequency and the strength of the coupling. In certain situations

unexpected behaviour can result, such as antiphase oscillation [107], bursting [50] and even quenching [98].

Coupling between non-oscillating elements has received less attention, but here one would expect two main effects. First, gap junctions will allow diffusive currents to diminish potential differences between coupled cells. In addition, the input impedance of the cells will be affected, altering their frequency response [28].

6.2 Methods

The anatomy of the body wall muscles was described in Section 6.1.1. Each cell is represented by a compartmental conductance based model, with one compartment for the cell body and ten compartments for each muscle arm. All active currents are included in the main compartment, while the arms are modelled as passive cables.

To extend the model to an entire quadrant, the structure shown in Figure 6.1 was slightly simplified as follows. Each quadrant is reduced to a chain of identical, non-overlapping cells with nearest neighbour coupling, which is a reasonable simplification given the pattern of gap junction connectivity.

6.2.1 Electrical properties of the muscle body

The conductance based model of the muscle body is the first and most important component. This model contains three active currents [64, 65]: fast and slow potassium (K^+) currents (I_{Kf} and I_{Ks}) and a calcium (Ca^{2+}) current (I_{Ca}) that exhibits inactivation on both fast and slow time-scales, mediated by Ca^{2+} and voltage respectively. The model also includes a standard leak conductance I_L . A circuit diagram of the complete model is shown in Figure 6.2. The membrane potential for the i^{th} muscle in the chain is therefore given by

$$C \frac{dV_i}{dt} = -\Sigma I_{ion} + I_{in} + I_{i-1,i} + I_{i+1,i} \quad (6.1)$$

$$\Sigma I_{ion} = I_{Ks} + I_{Kf} + I_{Ca} + I_L,$$

where I_{in} is the input current from the muscle arms (see Section 6.2.2) and $I_{j,k}$ are gap junction currents (see Section 6.2.3). The membrane currents are given by

$$\begin{aligned} I_{Ks} &= g_{Ks}n(V - V_{Ks}) \\ I_{Kf} &= g_{Kf}p^4q(V - V_{Kf}) \\ I_{Ca} &= g_{Ca}e^2f(1 + (h - 1)\alpha_{Ca})(V - V_{Ca}) \\ I_L &= g_L(V - V_L), \end{aligned}$$

with activation variables e , n , p , and inactivation variables f , h , q . Gating kinetics are given in terms of a generic variable x

$$\frac{dx}{dt} = \frac{x_{\infty}(V, V_{\text{half}(x)}, k_{(x)}) - x}{\tau_x} \quad (6.2)$$

with a steady state given by

$$x_{\infty}(X, X_{\text{half}}, k) = \frac{1}{1 + \exp[(X_{\text{half}} - X)/k]}, \quad (6.3)$$

and the calcium mediated inactivation is given by

$$h = x_{\infty}([Ca^{2+}]_i, Ca_{\text{half}(h)}, k_{(h)}). \quad (6.4)$$

Finally, the intracellular calcium concentration $[Ca^{2+}]_i$ evolves according to

$$\tau_{Ca} \frac{d[Ca^{2+}]_i}{dt} = - ([Ca^{2+}]_i + \phi_{Ca} I_{Ca}) \quad (6.5)$$

where τ_{Ca} models the calcium time constant and ϕ_{Ca} scales the effect of I_{Ca} on $[Ca^{2+}]_i$.

In order to find values for the 29 parameters I simulated voltage clamp and current clamp traces of the model, fitting the parameters so that the traces matched the corresponding whole cell recordings of body wall muscle cells of acutely dissected worms [64] as closely as possible. I similarly fit the steady state I-V curves for I_K and I_{Ca} [64, 65]. Those parameters for which values were reported in the literature were limited to a range close to the reported values. Fits were obtained by an evolutionary algorithm (differential evolution [96]). The cost function used was the sum of the costs for the whole cell and I-V traces. The cost for each trace was obtained by sampling 20 points along the curve and combining the squared error between the real and simulated trace at each of these points. The parameters obtained are given in Table 6.1. Note that the value of $C = 30$ pF

was not evolved, but was taken from Ref. [76] and used to ensure the correct scaling with respect to the coupling parameters. All simulations were run with a 4th order Runge-Kutta method with a time step of 0.1 ms.

| Param. | Value | Reported Val. | Param. | Value | Reported Val. |
|---------------|----------------------|-------------------|-------------|----------------------|---------------|
| C_A | 72.3 pF | ~ 75 pF [64] | C_B | 30 pF | 29.6 pF [76] |
| g_{Ks} | 436 S/F | 399 S/F [65] | V_{Ks} | -64.3 mV | -67.9 mV [65] |
| g_{Kf} | 400 S/F | 423 S/F [65] | V_{Kf} | -55.0 mV | -47.0 mV [65] |
| g_{Ca} | 220 S/F | 199 S/F [64] | V_{Ca} | 49.1 mV | 50.0 mV [64] |
| g_L | 19.3 S/F | 22 S/F [76] | V_L | 10.0 mV | n/a |
| α_{Ca} | 0.283 | n/a | ϕ_{Ca} | $2.77 \cdot 10^{-8}$ | n/a |
| $V_{0.5n}$ | 19.9 mV | n/a | k_n | 15.9 mV | n/a |
| $V_{0.5p}$ | -8.1 mV | n/a | k_p | 7.4 mV | n/a |
| $V_{0.5q}$ | -15.6 mV | n/a | k_q | -10.0 mV | n/a |
| $V_{0.5e}$ | -3.4 mV | n/a | k_e | 6.7 mV | n/a |
| $V_{0.5f}$ | 25.2 mV | n/a | k_f | 5.0 mV | n/a |
| $Ca_{0.5h}$ | $64.1 \cdot 10^{-9}$ | n/a | k_h | -10 μ M | n/a |
| τ_n | 25.0 ms | n/a | τ_p | 2.3 ms | n/a |
| τ_q | 150 ms | n/a | τ_e | 0.10 ms | n/a |
| τ_f | 151 ms | n/a | τ_{Ca} | 11.6 ms | n/a |

Table 6.1: Parameters for the muscle body obtained by fits to experimental traces (see text for detail). Reported values are given where possible. The two values of C_A and C_B were used in the simulations for compatibility with voltage- and current-clamp data [64, 65] and coupling parameters [76] respectively.

6.2.2 Muscle arms

The muscles arms are modelled as passive cables, each characterised by membrane capacitance (c_m), membrane resistance (r_m) and longitudinal resistance (r_l) (see Figure 6.2). Each arm consists of $N = 10$ discrete compartments, with five arms per muscle. The membrane potential of each arm compartment evolves according to

$$c_m \frac{dv_n}{dt} = I_{in_n} - I_{out_n} - I_{m_n} \quad \text{for } n = 1 : N, \quad (6.6)$$

where I_{in_n} is the current flowing into the n^{th} compartment, I_{out_n} is the current flowing out of the n^{th} compartment and I_{m_n} is the current leaking through the cell membrane, according to

$$I_{m_n} = \frac{v_n - V_L}{r_m} \quad \text{for } n = 1 : N. \quad (6.7)$$

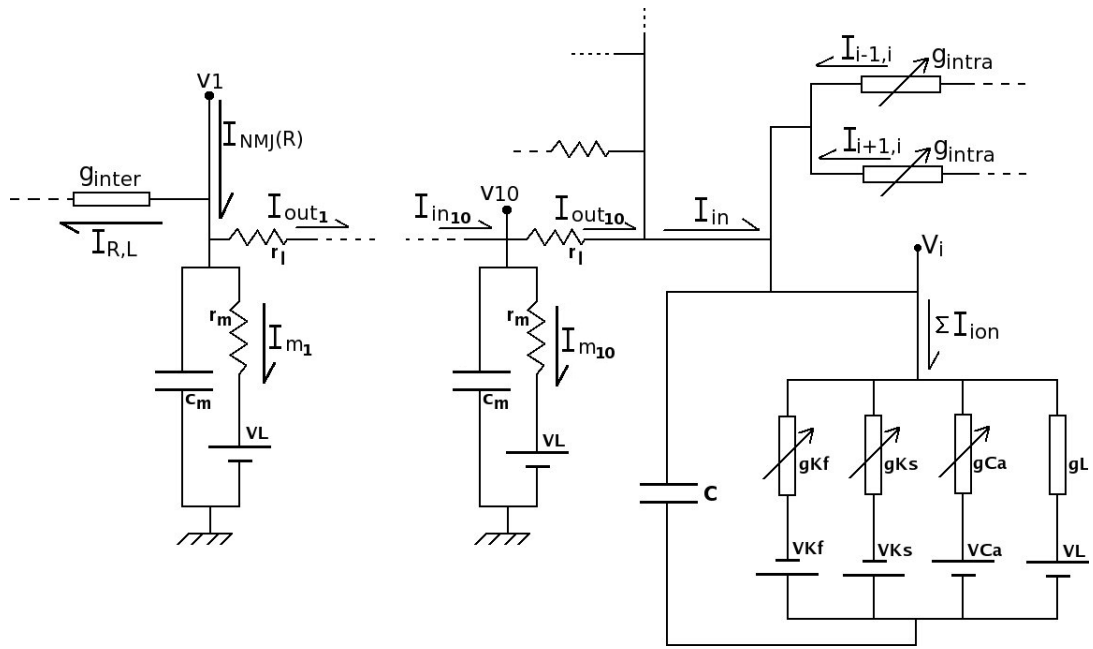


Figure 6.2: Equivalent circuit diagram of the muscle model showing currents, voltages and parameters of the muscle body (bottom right of figure), muscle arms (with two of ten compartments of one arm shown and remaining arms appearing in parallel) and coupling. All labels correspond to those in the text.

The current flowing out of compartment n into compartment $n + 1$ is

$$I_{\text{out}_n} = \frac{v_n - v_{n+1}}{r_l} \quad \text{for } n = 1 : N - 1$$

$$I_{\text{out}_N} = \frac{v_N - V}{r_l},$$

where V is the membrane potential of the muscle body. With the exception of the first compartment, the current that flows out of one compartment must flow into the next, so

$$I_{\text{in}_n} = -I_{\text{out}_{n-1}} \quad \text{for } n = 2 : N. \quad (6.8)$$

For two coupled muscles (whether on the dorsal or ventral side), the first compartment of arms on the right (left) muscle quadrant have

$$I_{\text{in}_1} = I_{\text{NMJ}} \pm I_{R,L}, \quad (6.9)$$

where I_{NMJ} is the neuromuscular junction (NMJ) input, and $I_{R,L}$ is the inter-quadrant gap junction current described in Section 6.2.3. Finally, the total current flowing into the

muscle body is the sum of currents flowing out of each of the five arms

$$I_{\text{in}} = -\sum I_{\text{out}_N}. \quad (6.10)$$

Since no data on the electrical properties of the arms was available, the cable parameters were based on estimates of the specific capacitance (C_m) and resistance (R_m) of the membrane, and the specific resistance of the cytoplasm (R_l), scaled by the arm dimensions. Using the standard value of $C_m = 1 \mu\text{F}/\text{cm}^2$, a cell with $C = 30$ pF (as in [76]) should have a surface area of $3 \times 10^{-3} \text{ mm}^2$. The same cell was reported to have $G_{\text{in}} = 1/R_{\text{in}} = 666$ pS, so $R_m = 45 \times 10^3 \Omega\text{cm}^2$. Finally a standard value of $R_l = 100 \Omega\text{cm}$ was chosen. Approximating each muscle arm as a cylinder with $l = 10 \mu\text{m}$ and $r = 0.75 \mu\text{m}$ (divided into ten compartments), yields:

$$c_m = C_m 2\pi r l \quad (6.11)$$

$$r_m = \frac{R_m}{2\pi r l} \quad (6.12)$$

$$r_l = \frac{R_l l}{\pi r^2}. \quad (6.13)$$

The resulting parameter values are given in Table 6.2.

| N | c_m | r_m | r_l |
|-----|-------|----------------|----------------|
| 10 | 47 fF | 950 G Ω | 570 k Ω |

Table 6.2: Muscle arm compartment parameters, obtained from estimates of the cell properties and dimensions (see text).

6.2.3 Coupling

The inter-muscular gap junctions are characterised in Ref. [76]. Intra-quadrant gap junction conductance was found to be a function of the potential difference across the junction. Coupling between quadrants was reported to have no voltage dependence (and a significantly smaller conductance). The intra-quadrant gap junction current introduced in Section 6.1.1 is given by

$$I_{j,k} = G_{ss}(V_j - V_k)(V_j - V_k), \quad (6.14)$$

where

$$G_{ss}(\Delta V) = g_{\text{intra}} \left[\frac{1 - \Gamma_{\text{min}}}{1 + \exp(A(|\Delta V| - V_0))} + \Gamma_{\text{min}} \right]. \quad (6.15)$$

The inter-quadrant coupling from Section 6.2.2 is simply

$$I_{R,L} = g_{\text{inter}}(v_1(R) - v_1(L)), \quad (6.16)$$

where $v_1(R)$ is the potential of the first compartment of a right muscle arm and $v_1(L)$ is the potential of the first compartment of a left muscle arm. Having defined the form of the coupling, the next step is to choose the parameters. As a conservative choice of g_{intra} , I used the peak value reported in Ref. [76]. The value of g_{inter} is the reported value of 75 pS divided evenly across the five arms of each muscle cell. The remaining parameters set the voltage dependence of the intra-quadrant coupling and were obtained by manual curve fitting to the experimental G/V curve in [76]. The parameters are given in Table 6.3.

| g_{intra} | g_{inter} | Γ_{min} | A | V_0 |
|--------------------|--------------------|-----------------------|-----|-------|
| 370 pS | 15 pS | 0.13 | 40 | 60 mV |

Table 6.3: Intra- and inter-quadrant coupling parameters. g_{intra} and g_{inter} were reported [76]. The remaining parameters were obtained by curve fitting to Figure 2 B of Ref. [76].

6.2.4 Current stimuli

Inter-quadrant coupling occurs between cells that would be expected to be coactive (either on the ventral or dorsal side). To investigate whether these gap junctions could contribute to equalising input to left and right muscles, the arms of the left and right muscle cells are stimulated with sinusoidal currents of different amplitudes while monitoring the resulting potential change in both left and right muscle bodies.

Intra-quadrant coupling is different, as it occurs between cells which would be expected to have slightly different input. The locomotion waveform of a worm is periodic in time, with a frequency of about 0.5 Hz for locomotion on agar. It is also approximately periodic in space, with a wavelength of about $\frac{2}{3}$ of the body length on agar. Given 24 cells in a muscle quadrant, a single wavelength should span $\frac{2}{3}24$ muscle cells. Therefore the inputs to adjacent muscles should be phase shifted by approximately $\frac{2\pi}{\frac{2}{3}24} = \frac{\pi}{8}$. It has been shown that the related nematode *Ascaris* has non-spiking neurons and graded synaptic transmission [32]. At the time this work was first published [15], it was believed that *C. elegans* motor neurons shared these properties. As a result, this study focussed on cases where the current input to each muscle was some smoothly varying function. The results

from two such functions are shown in Section 6.3.3. It has subsequently been shown [85] that at least some of the worm's motor neurons exhibit bistable behaviour. Fortunately the original study also addressed the possibility of square wave input (see Figure 6.11) and found that the conclusions were not altered by the choice of waveform.

This work will focus on locomotion as displayed on agar, as this is the medium on which the *unc-9* RNAi phenotype was described. For completeness I will also perform simulations using sinusoidal stimuli over a range of frequencies and phase lags, spanning the full range of locomotion behaviour (see Chapter 4). In water the worm oscillates with a frequency of about 2 Hz and often exhibits a characteristic “C” shape. The spatial wavelength of the body wave in water is approximately twice the body length, with only half a wave being visible at any one time. Therefore the inputs to adjacent muscles should be phase shifted by approximately $\frac{2\pi}{2 \times 24} = \frac{\pi}{24}$.

6.2.5 Signal-to-noise ratio

Another potential effect of coupling is on signal-to-noise ratio (SNR). Synaptic vesicle release is a stochastic process, so neuromuscular currents are likely to have a random component. Rather than explicitly modelling vesicle release, I have used an approximation where the input to each muscle consists of a periodic signal combined with additive white Gaussian (zero-mean) noise. I use spectral methods to calculate the signal-to-noise ratio (SNR) in a model muscle cell, stimulated with a superposition of a sinusoidal wave and white Gaussian noise. The input signal has a period $T = \frac{2\pi}{\omega_{in}} = 2$ s. Simulations were run for a total duration of $D = 8$ s with a time step of $\Delta t = 0.01$ ms.

The SNR is estimated from the power spectrum density (PSD) of the muscle output. For a signal $x(t)$, the PSD is given by

$$\text{PSD}(\omega) = X(\omega)X^*(\omega)/N,$$

where $X(\omega)$ is the Fourier transform of the signal (calculated with a fast Fourier transform or FFT, with $N = 2^{19}$), and the asterisk denotes complex conjugation.

To estimate the SNR from the PSD, we must first specify what frequency range will be considered “signal”. Ideally the input should appear in the frequency domain as a spike of zero width at 0.5 Hz. In reality the signals (particularly the “filtered” signals V_i and $[Ca^{2+}]_i$) will be smeared to some extent, leading to a peak of non-zero width. Based on visual inspection of the PSD, I have assigned all components on the range 0 – 5 Hz to the signal, and from 5 Hz to 50 kHz to noise. While there will be some noise in the 0 – 5 Hz range, this represents only 0.01% of the total bandwidth, and will not significantly affect

the results. Finally I will obtain values for the signal power, P_{signal} , the noise power P_{noise} and the ratio SNR as follows

$$P_{\text{signal}} = \frac{1}{N} \sum_{-5\text{Hz}}^{5\text{Hz}} \text{PSD}(\omega) \quad (6.17)$$

$$P_{\text{noise}} = \frac{1}{N} \left[\sum_{5\text{Hz}}^{50\text{kHz}} \text{PSD}(\omega) + \sum_{-50\text{kHz}}^{-5\text{Hz}} \text{PSD}(\omega) \right] \quad (6.18)$$

$$\text{SNR} = \frac{P_{\text{signal}}}{P_{\text{noise}}}. \quad (6.19)$$

The SNR is then calculated for different values of the input noise variance.

6.3 Results

6.3.1 Dynamics of the single cell model

It is important that the single cell model reproduces the dynamics of a body wall muscle cell under voltage- and current-clamp conditions. Figure 6.3 shows the experimental voltage- and current-clamp traces [64] along with corresponding traces produced by simulation of the model with matching inputs. Likewise Figure 6.4 shows I-V curves for I_K and I_{Ca} (recorded and simulated). The model output is quantitatively very similar to the experimental data.

Having verified the validity of the model under these controlled conditions, I went on to investigate whether the cell could produce action potentials. In contrast to *Ascaris* body wall muscles [131], the model muscles are incapable of sustained spiking, either spontaneously or in response to current injection. Even when the fitness function for the parameter optimisation was altered to reward oscillatory behaviour, sustained spiking could not be achieved for realistic values of g_{Ca} . The non-spiking nature of the model is consistent with the recently observed behaviour of the muscles in semi-intact worms [130]. The steady state I-V curve for an entire model muscle cell is shown in Figure 6.5. The voltage response diminishes as current increases, giving rise to a concave I-V relationship.

The model predicts that *C. elegans* body wall muscles respond to stimuli with graded potential changes. The model reproduces the observed electrophysiological characteristics of voltage and current clamped body wall muscle cells well [64], providing an excellent starting point for investigating the effect of inter-muscular coupling.

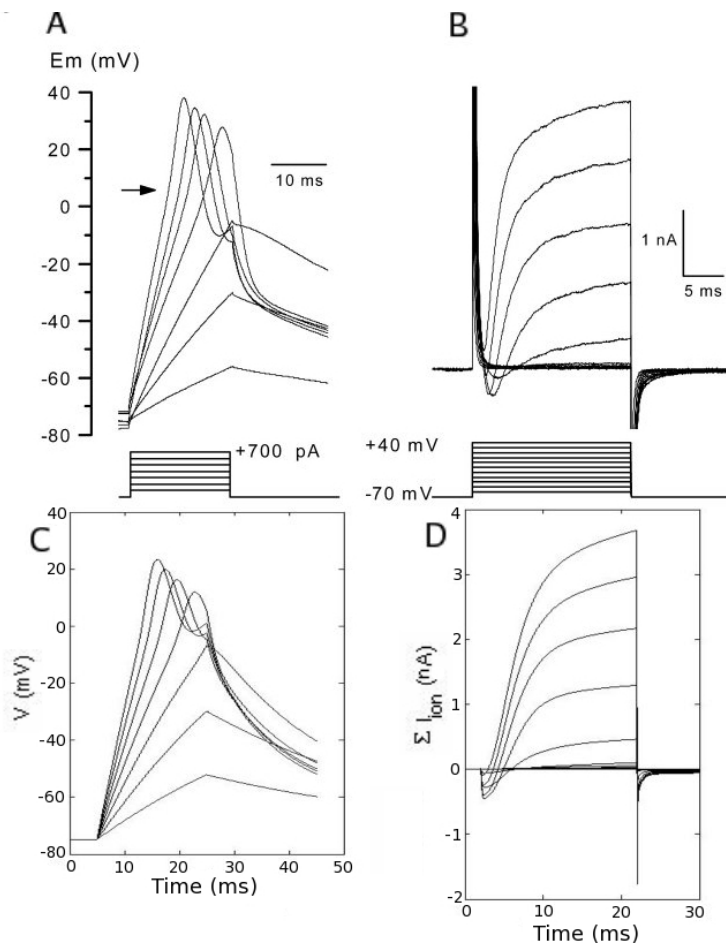


Figure 6.3: Whole cell current (A) and voltage (B) clamp traces from body wall muscle cells reproduced with permission from [64], with stimulus protocols shown below the traces. The response of the model muscle cells to identical stimuli are shown in (C) and (D).

6.3.2 Coupling between quadrants

Given that inter-quadrant coupling occurs between cells which are expected to be coactive, I sought to determine whether these gap junctions could help to synchronise activity in the left/right cell pairs. While inter-quadrant coupling has been reported to have very low conductance (75 pS versus 370 pS for intra-quadrant coupling) [76], it is plausible that the location of these junctions on the tiny muscle arms might increase their significance.

Although the cell pairs in question are innervated by the same neurons, properties of the individual neuromuscular junctions could cause the cells to receive slightly variable input. This could take the form of an amplitude difference or a time delay in the inputs.

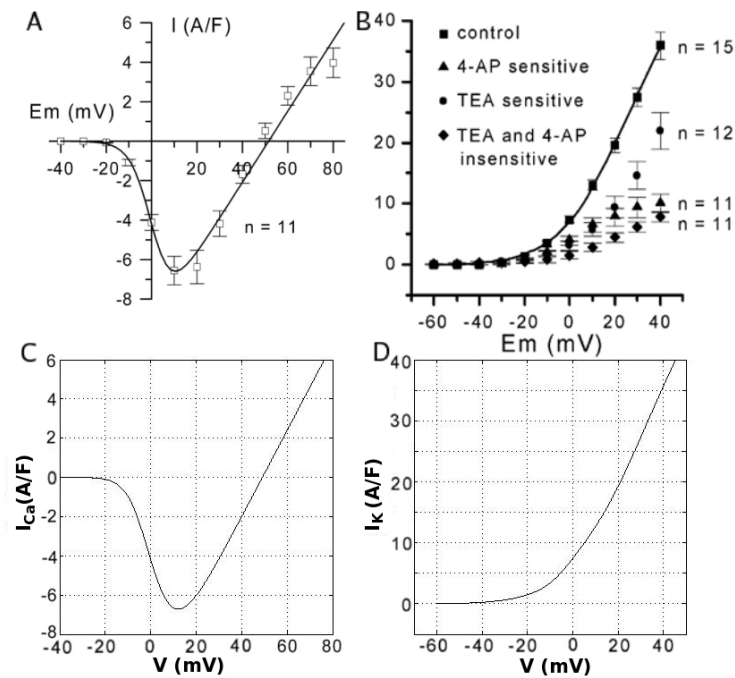


Figure 6.4: Current-voltage relationships for the peak calcium (A) and steady state potassium (B) currents taken with permission from [64] and [65] respectively. Currents are shown normalised by cell capacitance. In (B), the relevant curve is the one labelled control. The corresponding relationships produced by the model are shown in (C) and (D).

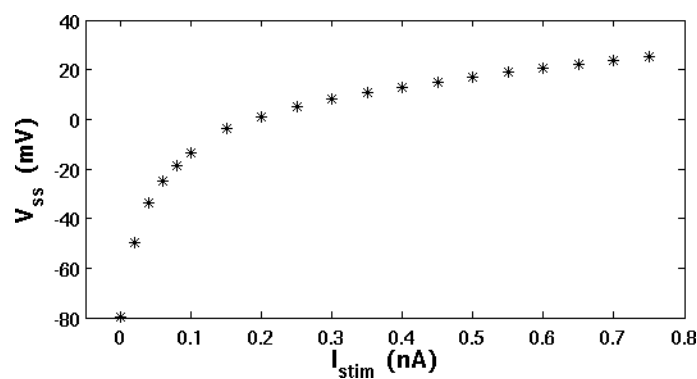


Figure 6.5: Whole cell I-V curve for a model muscle cell. The cell was held at -70mV by injecting hyperpolarizing current and then stimulated with 400ms depolarising current steps. The membrane potential at the end of the stimulus was recorded.

The effect of coupling when inputs to adjacent cells are phase shifted by an amount ϕ is dealt with in Section 6.3.3, for the stronger intra-quadrant gap junctions. Here I will consider the case where the cells receive input of different amplitude.

I simulated two cells (each with five arms as described in Section 6.2.2) and stimulated the arms of both muscles with depolarising current. One cell (left) receives the full stimulus with amplitude A , while the other (right) receives input A' (as shown schematically in Figure 6.6 A) attenuated by α such that $A' = \alpha A$. For each α I ran the simulation with and without gap junction coupling and in each case calculated the difference in the membrane potential between the left and right cells as an average absolute deviation (denoted δ)

$$\delta = |V_{left} - V_{right}|. \quad (6.20)$$

The effect of the coupling ε is then obtained by comparing δ between coupled and uncoupled muscle cell pairs

$$\varepsilon = \frac{\delta_{uncoupled} - \delta_{coupled}}{\delta_{uncoupled}}. \quad (6.21)$$

The results are shown in Figure 6.6 B. As can be seen, the percent change induced by the gap junctional coupling increases with the level of attenuation. This is not surprising, since depolarisation of the cells causes their total membrane conductance to increase (see concave relationship in Figure 6.5), thereby making the relative contribution of gap junction currents smaller by comparison. However, note that while the stimulated muscle responds strongly, the potential of the coupled cell is only weakly affected (under 3% even for the maximal attenuation). Finally, for this most extreme (and unrealistic) case of 100 % attenuation, Figure 6.7 shows the membrane potentials in the body compartments of both cells. When the potential of each compartment was plotted (not shown), I observed virtually no decrement in voltage down the arms, consistent with experimental observations [100].

It seems clear from these simulations that inter-quadrant coupling is too weak to contribute any significant current flow between left and right coupled muscle cells.

6.3.3 Coupling within quadrants

The next step is to determine the role of the stronger intra-quadrant coupling in locomotion. There are several possible avenues which must be investigated and I will address these in turn.

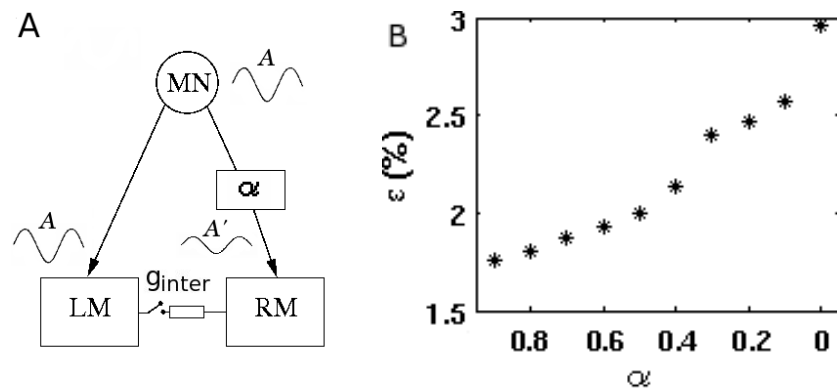


Figure 6.6: A) Model structure used to investigate the effect of gap junctional coupling between left and right quadrant muscle cells that are innervated by the same set of motor neurons (MN). The left muscle cell (LM) receives the full stimulus of amplitude A , while the right cell (RM) receives an attenuated signal of amplitude $A' = \alpha A$. Simulations are performed with and without gap junctional coupling g_{inter} . B) The percent change (ϵ) in the voltage difference between the left and right cells increases with increasing attenuation.

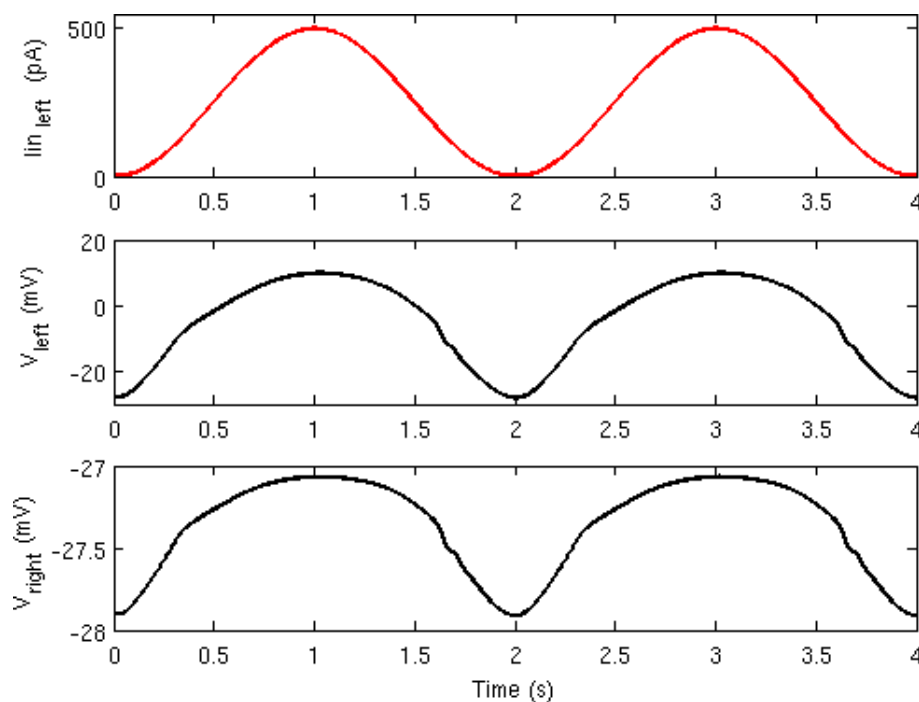


Figure 6.7: Effect of inter-quadrant coupling in the extreme (unrealistic) case of 100 % attenuation. The left muscle arms are stimulated by a sinusoidal current with peak amplitude of 500 pA while the right muscle arms are unstimulated. This leads to significant depolarisation of the left muscle (middle), which in turn causes current to flow through the gap junction into the right muscle arms. The resulting depolarisation of the right muscle body is just under 1mV (bottom).

Propagating activity

A key question is whether the combination of active, excitatory currents and electrical coupling might allow regenerative propagation of activity down the chain of muscles, as reported in *Ascaris* [132]. Not only does the absence of spikes make this unlikely, but the model indicates that the coupling is also insufficiently strong. Experiments with the model suggest that an increase of four fold in g_{Ca} (required to allow spiking) and about six fold in g_{intra} would be required to allow regenerative propagation (not shown).

Even if true regenerative propagation is not possible, stimulation at one end of the chain of muscles could still propagate significantly, albeit with attenuation. To investigate to what degree this occurs, I simulated a chain of cells and stimulated the first cell with a strong (250 pA for 500 ms) current pulse, observing the resulting depolarisation in all cells in the chain. As shown in Figure 6.8 the first (stimulated) cell is strongly depolarised. There is a peak depolarisation of only about 2 mV in the second cell and almost no signal propagates to the third cell (peak depolarisation < 0.5 mV).

The model therefore suggests that for the reported conductance values [64, 65, 76], signal propagation through a muscle quadrant can be ruled out as a mechanism for generating the locomotion waveform.

Waveform modulation

The next question is whether the coupling within muscle quadrants could be involved in modulating the waveforms of muscle activation produced by neural inputs. I began by simulating a chain of 24 muscle cells with nearest neighbour coupling, as described in Sections 6.2.1 and 6.2.3. Current stimuli were applied as discussed in Section 6.2.4. Simulations were repeated with $g_{intra} = 0$ so that the resulting waveforms could be compared for the coupled and uncoupled cases.

Figure 6.9 A and B show the results of these simulations for two different input current waveforms. Traces are shown for two representative neighbouring cells from near the middle of the chain. For all the input waveforms tested, removing the coupling led to a barely noticeable change in the membrane potential traces. Looking closely, one can see that the difference in coupled and uncoupled potential becomes smaller as the cells are depolarised. This is not surprising, since depolarisation of the cells causes their total membrane conductance to increase, thereby making the relative contribution of g_{intra} smaller.

For any input waveform without discontinuities, the potential difference across the gap junctions will increase as the phase lag increases over the range 0 to π . To investigate the

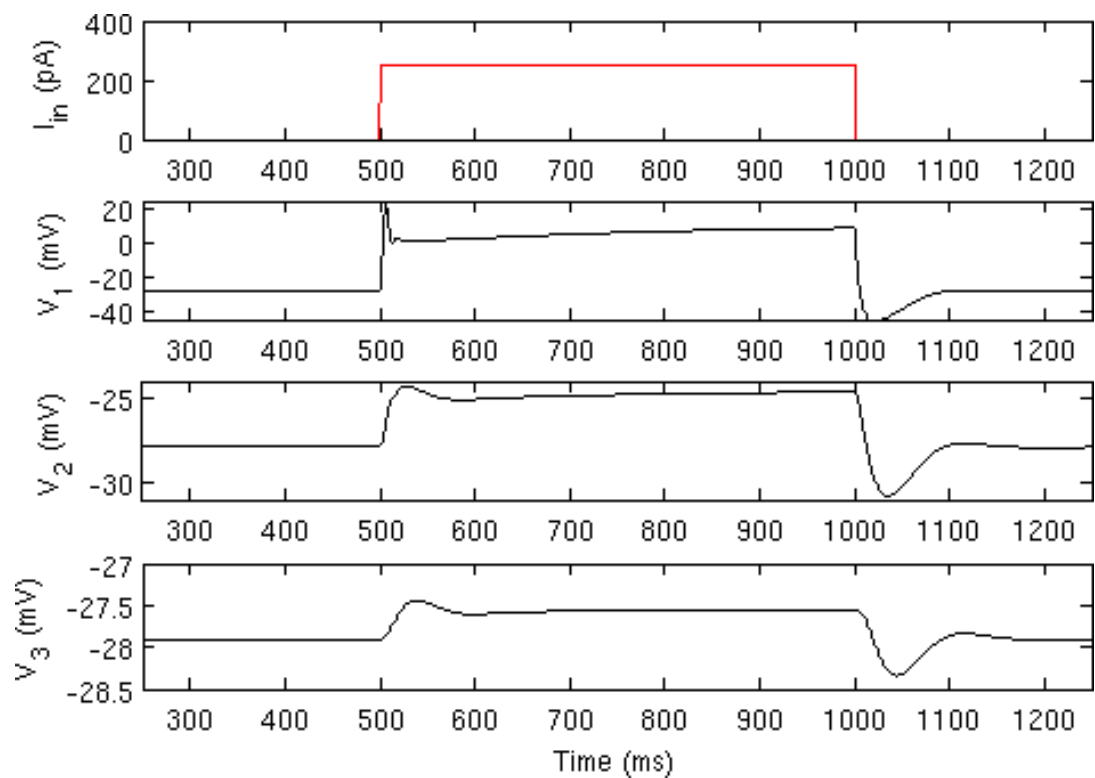


Figure 6.8: Gap junction coupling is too weak to propagate significant activity. A muscle quadrant is simulated (only three cells shown) and the first cell is stimulated with a strong current pulse (250 pA for 500 ms). This causes a large (> 40 mV) depolarisation of the first cell (V_1), and small (< 3 mV) depolarisation of the second (V_2). By the third cell the depolarisation is insignificant (< 0.5 mV).

dependence of coupling significance on both frequency (F) and phase lag (ϕ), I performed simulations using sinusoidal input currents over a range of frequencies and phase lags, chosen to cover the range of locomotion behaviours exhibited by the worm. To quantify the effect of the coupling for each F , ϕ pair, I began by calculating the magnitude of the voltage difference for the coupled and uncoupled muscle potential waveforms at each time step. Figure 6.10 shows both the mean and the peak values of this difference, taken over two periods of the input wave. As can be seen, the frequency of the input wave has little effect on the significance of coupling, while increasing the phase lag does have a large effect. Since the phase lag is smaller for locomotion in water than on agar, an investigation of the latter is better suited to revealing possible coupling effects.

The effect of coupling on $[Ca^{2+}]_i$ levels is generally even smaller than the effect on membrane potential. This is because changes in V below the threshold for I_{Ca} have no effect on $[Ca^{2+}]_i$. As a final test I stimulated the muscles with an input waveform specifically designed to maximise the effect on $[Ca^{2+}]_i$, a square wave input that maximises

the potential difference across the gap junctions, which in turn maximises the resulting current. I also added a depolarising bias current to give the cells a new resting potential of around -10mV where the gradient in the I-V curve for I_{Ca} starts to become steep (see Figure 6.4). As can be seen in Figure 6.11, the effect of coupling on $[Ca^{2+}]_i$ is indeed larger in this case, peaking at about 15% for a crawling waveform. However this peak is a brief transient and is followed by a negative trough of similar amplitude. Thus the average effect on $[Ca^{2+}]_i$ is small and would be unlikely to result in a detectable behavioural change.

Overall, the simulations presented here strongly suggest that the intra-quadrant coupling has too small an effect on the activation of body wall muscles to result in any observable change in the worm's locomotion.

Role of coupling in noise reduction

In all the simulations so far, it has been assumed that the neuromuscular inputs are clean signals untarnished by noise. However, since the release of neurotransmitter at chemical synapses is a stochastic process, one would expect that the real neuromuscular inputs would exhibit fluctuations. This then begs the question whether the coupling between muscles could have an effect on signal-to-noise ratio (SNR). Electrically, the cell can be approximated as a capacitance in parallel with a resistance (see Fig. 6.2) which makes the cell membrane behave much like a simple low-pass filter with time constant $\tau = \frac{C_{\text{mem}}}{G_{\text{mem}}}$. Since G_{mem} is dynamic τ will also be. Coupling will change the effective impedance of the cells, thereby changing the properties of this filter.

To determine the extent to which this occurs, I performed simulations with a current stimulus consisting of a periodic signal with an additive noise component (as described in Section 6.2.5). Simulations were run both with and without coupling, for various values of noise variance σ . I then estimated the SNR of the input current and of the resulting V and $[Ca^{2+}]_i$ waveforms (as described in Section 6.2.5). In the absence of coupling, the low-pass characteristics of the cell lead to a significant improvement in the SNR of the membrane potential over that of the input current signal. The additional low-pass effect of $[Ca^{2+}]_i$ leads to an even better SNR in the calcium waveform. When coupling is added, however, there is only a very small further improvement in SNR, as illustrated in Figure 6.12. One can therefore conclude that the impedance of the individual muscle membrane is by far the dominant factor in determining the frequency response of the muscle quadrant as a whole.

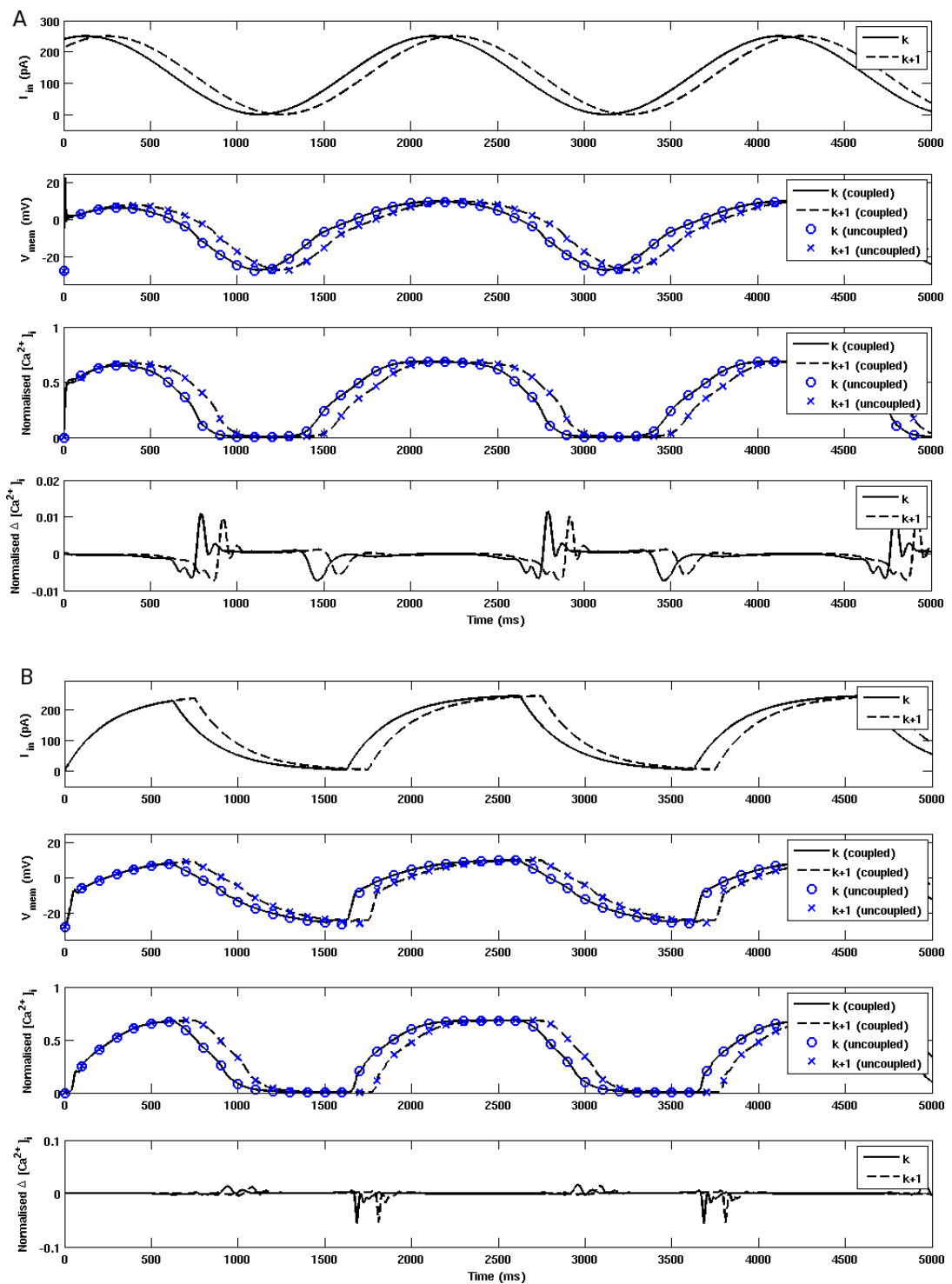


Figure 6.9: The effects of intra-quadrant coupling for two candidate waveforms. Inputs are (A) sinusoidal and (B) “sawtooth” (similar to the outputs of the neural model in Refs. [20, 21]), with a frequency of 0.5 Hz and a phase shift of $\frac{\pi}{8}$ between adjacent cells. In each case the simulations were performed with a chain of 24 coupled cells. Each plot shows (from top) the input current, membrane potential with and without coupling, normalised internal calcium concentration ($[Ca^{2+}]_i / \max[Ca^{2+}]_i$) with and without coupling, and the difference between the coupled and uncoupled calcium concentrations ($\Delta[Ca^{2+}]_i = ([Ca^{2+}]_{i,coupled} - [Ca^{2+}]_{i,uncoupled}) / \max[Ca^{2+}]_i$) for two representative (neighbouring) cells from near the middle of the chain. Note the nearly identical waveforms with and without coupling.

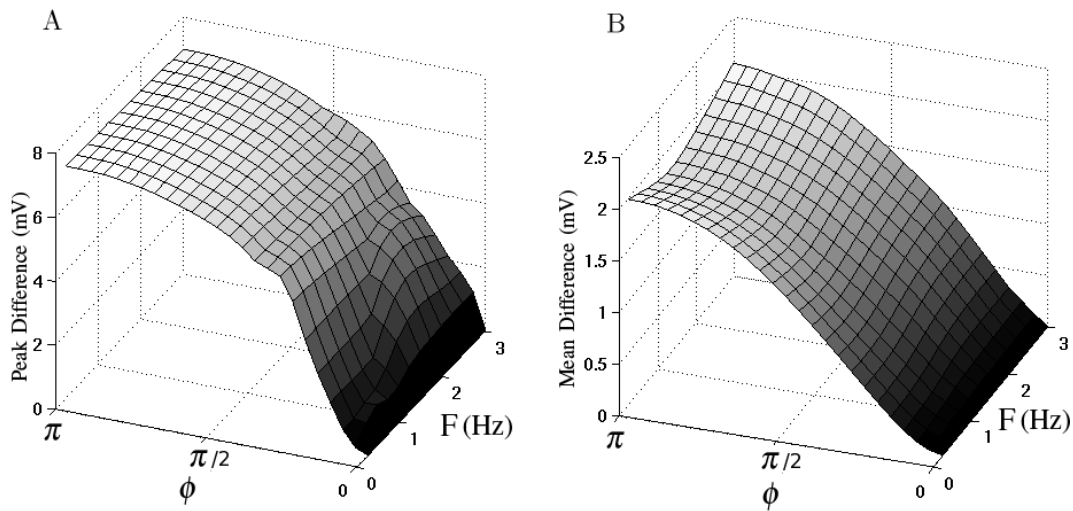


Figure 6.10: The significance of muscle coupling depends strongly on the phase lag (ϕ) and weakly on the frequency (F) of the sinusoidal input waveform. The effect is quantified by the peak (A) and mean (B) value of the difference between the muscle potential traces in the coupled and uncoupled cases. Phase lags used range from 0 to π in steps of $\pi/24$.

6.4 Discussion

In this chapter I have presented a first detailed electrophysiological model of *C. elegans* body wall muscles, that was used to test several hypotheses about the possible role of these muscle cells in the locomotion of the worm. Model parameters were found such that the membrane properties of the cell bodies matched experimental recordings. A possible caveat on those parameters is the lack of relevant *in vivo* data to date. Nonetheless, the model presented is likely to provide a valid first approximation of muscle dynamics in a behaving worm.

All of the results presented here strongly suggest that in fact, *C. elegans* muscles are most likely to act only as actuators, and are not capable of communicating signals in a sufficiently effective manner, either to participate in pattern generation, or to propagate electrical oscillations.

6.4.1 Single cell dynamics

First, I have ruled out the possibility of sustained calcium action potentials for parameters anywhere within the ballpark of the model I have presented. The fact that conductances would have to increase many fold to yield any oscillations in the model cells suggests that such behaviour is unlikely *in vivo*. This is an interesting result and contrasts with reported

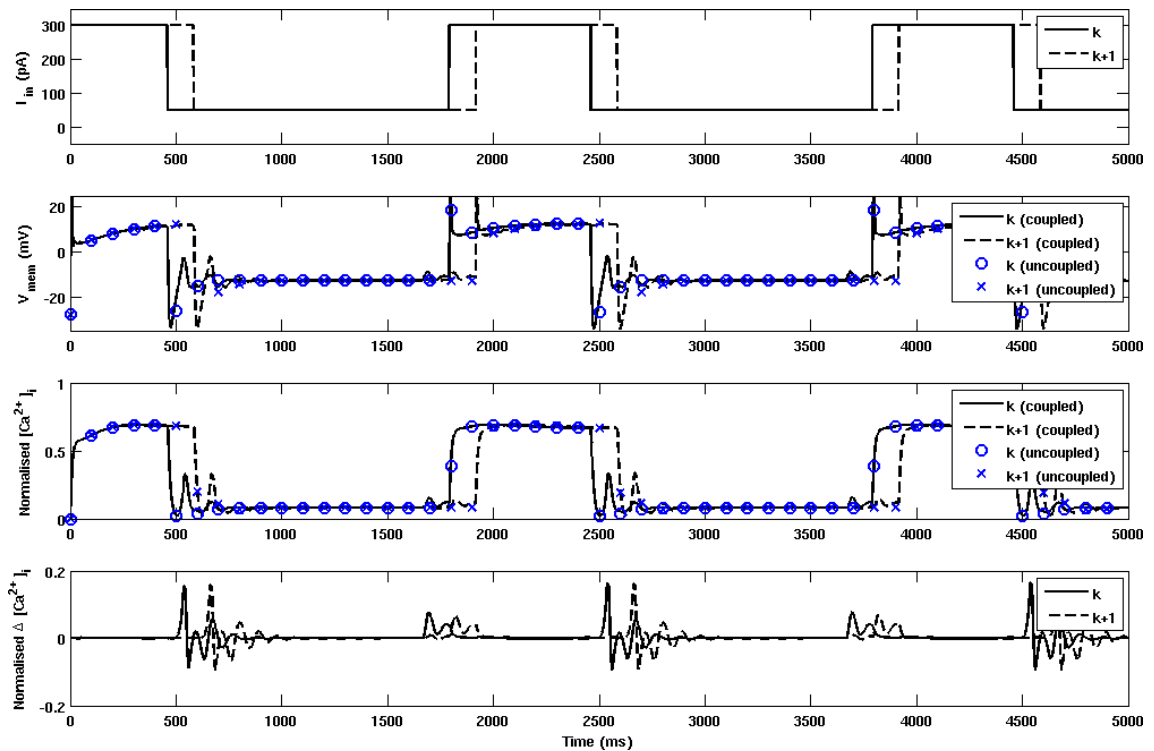


Figure 6.11: Effect of intra-quadrant coupling in the most extreme case of square wave input with a depolarising bias, which increases the sensitivity of $[Ca^{2+}]_i$ to potential changes. Panels show (from top) the input current, membrane potential with and without coupling, normalised internal calcium concentration with and without coupling, and the difference between the coupled and uncoupled calcium concentrations, as in Figure 6.9.

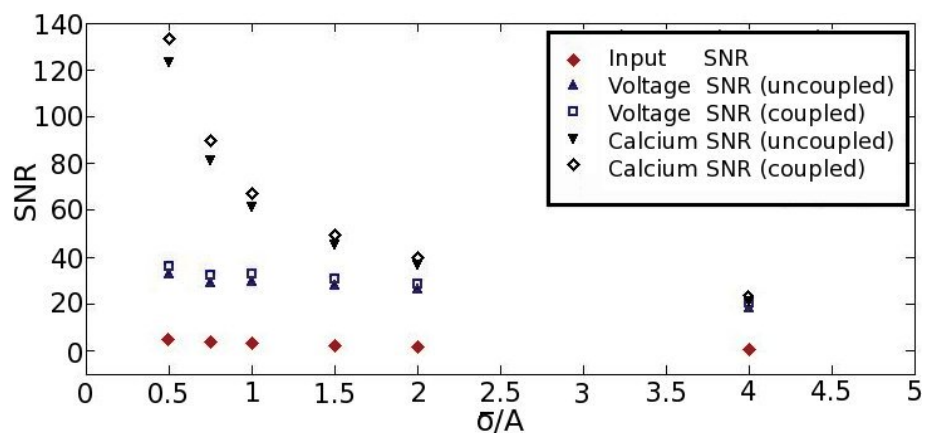


Figure 6.12: Two stages of low-pass filtering occur in the muscles, having a large effect on SNR. The first stage has its effect on the membrane potential, and the second on the internal calcium concentration. Coupling results in a small further improvement due to a small change in the effective input impedance.

results for the related nematode worm *Ascaris lumbricoides* but appears to be consistent with recent experiments on *C. elegans* body wall muscles [130]. One possible explanation for this difference between the two nematodes is their relative sizes and cell numbers. While the two worms have almost identical motor nervous systems [114], *Ascaris* can be over two orders of magnitude longer than *C. elegans*. Thus the amount of muscle tissue that must be innervated will be far greater in *Ascaris*, possibly requiring regenerative propagation within the muscle syncytium. That said, the absence of action potentials in body wall muscles does not, in itself, preclude a possible role of these muscle cells in rhythmic pattern generation.

Another question is what role the muscles may have in shaping locomotion. Figure 6.9 shows that the waveform of electrical activity in muscles closely follows the waveform of the input. This holds true both with and without inter-muscular coupling. The muscles therefore seem to be little more than actuators. Possibly interesting properties of the muscle cells are the concave I-V relationship shown in Figure 6.5 (which could endow them with an extended dynamic range) and their capability for some (limited) low-pass filtering. The extended dynamic range and low-pass characteristics should, if anything, improve robustness to changes in levels of neural activity and stochasticity of neurotransmitter release respectively.

6.4.2 Muscle coupling

To determine the possible roles of the body wall muscle coupling, first, in pattern generation, second, in the propagation of signals along the worm, and third, in waveform shaping, I have presented simulations of chains of coupled muscle cells (modelling a single quadrant of body wall muscles in the worm) and pairs of coupled muscle cells (modelling inter-quadrant coupling). In these simulations, the limiting factor is the strength of the gap junctional coupling. In fact, it appears that the reported conductance values are too low to support effective signal transmission between adjacent muscle cells. While this may initially seem to be inconsistent with the *unc-9* RNAi data of Liu et al. [76], a recent publication by the same group [25] strengthens this conclusion. In one experiment, mutant worms lacking *unc-9* mediated gap junctions were reported to have this genetic defect selectively rescued in either neurons or muscles. This was done by expression of functional (wild-type) *unc-9* under the control of promoters specific to neurons (*Prab-3*) or muscles (*Pmyo-3*) respectively. Selective rescue attempts in neurons “largely rescued the locomotion defect”, while the selective rescue attempts in muscles “showed no obvious effect” [25].

6.4.3 Muscle stretch receptors

It has been suggested that *C. elegans* body wall muscle cells also possess so called stretch receptor channels, that depolarise the cell in response to bending or stretching of the body [75]. If so, in a rhythmically bending or undulating worm, the muscles may, in principle, have the capacity to respond to the alternating body posture actively (but still with graded potential changes) thus aiding and maintaining this oscillatory behaviour. Such a sensory-feedback mechanism mimics closely existing models of sensory feedback driving neuronal activation in the ventral cord [20,21,89] (and see Chapter 5 and Part III). However, if this were true, such a mechanism would operate effectively independently from any neurally generated oscillations, since the only points of contact between muscles and the nervous system (the neuromuscular junctions) only allow information flow in one direction – from the neurons to the muscles. Thus, to be interesting (i.e. to contribute significantly to pattern generation), muscles distributed along the body of the worm would need to coordinate their oscillations. The results presented here suggest that the weakness of the gap junctional coupling precludes the communication of such signals along a chain of muscles.

6.5 Conclusions

The model and simulations presented here suggest that the neural circuit is the active component generating the rhythmic patterns of locomotion (though this work sheds no light on the neural mechanism of generating such patterns – whether via a central pattern generating circuit, or via sensory feedback from stretch receptor channels). The model also suggests that the phenotypes of *unc-7* or *unc-9* mutation, or of *unc-9* RNAi, cannot be explained in terms of muscle gap junctions. One may therefore speculate as to which gap junctions (elsewhere in the locomotion system) may account for the reduced velocity observed in these mutant and RNAi treated worms. A likely candidate is the gap junctional coupling between the forward locomotion command interneurons AVB and forward locomotion motor neurons of classes VB and DB. Overall, this study strongly suggests that the body wall muscles are, for all intents and purposes, simple actuators. It should be noted however that the work in this chapter has addressed only the electrical properties of the muscles and their coupling. Gap junctions can have important, non-electrical roles such as mediating vital metabolic coupling [60] and contributing to development [111]. Furthermore, the mechanical properties of the muscles are likely to be important, and are included in the integrated model presented in Part III.

Part III

An Integrated Model of *C. elegans* Forward Locomotion

Chapter 7

Integrated model: Introduction

7.1 Motivation and goal

Despite the relative simplicity of the *C. elegans* locomotion system, it is clear that our communal understanding of it is still incomplete [124]. This is due in part to a lack of low level information regarding such factors as neuron dynamics and synaptic weights. Furthermore, while the information obtained from behavioural studies, serial reconstruction, laser ablation and genetic manipulations is a great asset, such information is never 100 % accurate (and often much less so) due to the very nature of biological systems and experimental techniques. We as a community are faced with the task of sorting through a huge body of information – no single piece of which can be taken as gospel – and distilling it into a complete and consistent picture of how the system functions. In the pursuit of this goal, one of our most powerful tools is computational modelling. Models contribute to our understanding in two equally important ways. First, the very act of building a model forces one to ignore much of the distracting information, focussing instead on what will hopefully be the essential components of the system. At the same time, building a model is an important reality check for existing hypotheses that seem viable superficially, but may fall apart when the time comes to implement them. Second, once a model is completed it can hopefully be used to generate testable predictions, the results of which will refine our understanding. In many cases the model itself will be a hypothesis, proposing a candidate mechanism for achieving some behaviour. Assessing the success of the

model in reproducing behaviours can then give some indication as to the validity of the hypothesis.

To date, several models of *C. elegans* locomotion have been published (these are introduced in Section 2.3), so it would be foolish to undertake the task of developing a new model without considering its novelty with respect to this body of work. In fact, the model presented here is quite timely, as two recent developments have set the stage for a new generation of models. Of most fundamental importance is our experimental finding, presented in Chapter 4, that the worm's swimming and crawling correspond to a single gait. The implication – that the entire range of locomotory behaviours are produced through modulation of a single neural mechanism – extends the scope of this model well beyond that of any of its predecessors. The second revelation that motivates this model is the recent finding by Mellem et al. that RMD motor neurons exhibit bistable dynamics [85]. While the ventral cord motor neurons have yet to be characterized, the demonstration of strongly non-linear neural dynamics in *C. elegans* stands in stark contrast to the previously held belief that the worm's neurons were incapable of active responses of this sort. This finding therefore opens up a whole new realm of possibility for locomotion models.

The goal of this model is, from a behavioural point of view, to reproduce *C. elegans* forward locomotion in a range of media from water to agar. In doing so, I aim to assess the plausibility of the proposed oscillatory and modulatory mechanisms. Finally, I hope to use this model to guide experiments that will shed light on the worm's locomotion.

7.2 Assumptions

As with any model, particularly one of a biological system, assumptions will have to be made. While the smaller assumptions are too numerous to mention, here I will outline those that are particularly interesting, significant or controversial.

7.2.1 Oscillatory mechanism

One of the most important unanswered questions about *C. elegans* locomotion is whether it involves a central pattern generator (CPG) and if so, whether this CPG is essential. While it is generally believed that CPG circuits underlie most rhythmic behaviours [82], there is an alternative hypothesis in the case of the worm. Specifically, it has been suggested that the worm may rely entirely on sensory feedback, mediated by postulated stretch sensitive channels on A- and B-class motor neurons [124], to generate the undulations required for its locomotion [21, 33]. It is quite widely accepted that the proposed

motor neuron stretch receptors are involved in locomotion (despite a lack of direct evidence that they actually exist) but this certainly does not preclude the involvement of a CPG. After all, sensory feedback usually provides vital modulation of CPG activity [47] and some of the models described in Section 2.3 rely on the combination of a CPG in the head and a sensory feedback based mechanism in the ventral cord [67, 89]. It has also been suggested that the role of the CPG circuit may be to filter noisy sensory signals rather than to generate motor commands [70].

For the present model I will make the common assumption that the B-class (and A-class) ventral cord motor neurons have stretch sensitive channels on their axons. In absence of information about their properties, they will be given only very simple linear behaviour with elongation leading to excitation and compression leading to inhibition. Rather than requiring different types of channels, this assumes that the stretch receptors are partially active at their rest length, so the inhibition is mediated by a reduction in excitation. Also, it has been speculated in the past that the stretch sensitive channels may be localized to certain areas on the axon, but for this model it is assumed that the channels are evenly distributed along its entire length.

With regard to the mechanism of oscillation, this model will be built according to the hypothesis that *C. elegans* locomotion does not require a CPG circuit. There are several reasons motivating this choice. First, the circuit analysis presented in Section 2.1.4 suggests that the ventral cord locomotion circuit is unlikely to support a CPG. With regard to the head circuit, all the motor neurons for which the neurotransmitter assignments are known are either cholinergic or GABAergic [99]. It therefore seems likely that GABA is the main inhibitory neurotransmitter in the locomotion circuit. Since inhibition is a key requirement for a CPG, the fact that forwards locomotion of GABA pathway defective mutants (e.g. *unc-25* and *unc-30* [83]) is largely normal on agar suggests that, if such a circuit exists, it is unlikely to be essential [124].

The second motivation for a pure sensory feedback mechanism comes from the observed modulation of the locomotion wave in different environments (see Chapter 4). While it is certainly common for CPG circuits to be modulated to produce different motor patterns [105], there is no obvious pathway for such modulation in *C. elegans* locomotion. In the context of the worm's tiny nervous system, the most parsimonious explanation for the behavioural changes would be direct modulation of the sensory feedback loop via the changing physical interaction of body and environment.

To summarise, the model presented here will incorporate the assumption that a sensory feedback based mechanism is sufficient to account for *C. elegans* locomotion in a range of media from water to agar, without recourse to a CPG circuit. It will also be

assumed that no explicit modulation is necessary, instead relying purely on the changing physical properties of the environment and the associated changes in sensory feedback. The success of the model in reproducing the observed behaviour will be used to assess the plausibility of these assumptions.

7.2.2 Neuron dynamics

To date, the dynamics of the ventral cord motor neurons have not been characterized. It has generally been assumed that the worm's neurons respond passively to stimulation, based in large part on the absence of voltage gated sodium channels in the *C. elegans* genome [10]. Recently, however, Mellem et al. [85] were able to perform an electrophysiological characterization of the RMD motor neurons in the head, finding them to exhibit bistable behaviour mediated by a self exciting calcium conductance. This is a very important result, showing that the worm's neurons are capable of more interesting behaviour than a simple graded response. Such dynamics are desirable in the context of a locomotion model since non-linearity is a key requirement for a system to be capable of self-sustained oscillations [115].

Based on the RMD data and in absence of evidence to the contrary, it would be reasonable to assume that either or both the B- and D-class neurons possessed non-linear behaviour. In fact, the D-class equivalent neurons in *Ascaris* have even been shown to produce spontaneous oscillations [113]. In *C. elegans* however, evidence from a variety of sources suggests that while B-class neurons are essential for coordinated forwards motion [24], D-class neurons are not required for coordinated forwards locomotion on agar [84, 129, 138]. It is therefore unlikely that the D-class neurons alone have important non-linear dynamics. While it would be perfectly reasonable to assume that both classes have similar dynamics, I am concerned that this would overcomplicate the model. Therefore, in the interests of simplicity, I will begin by assuming that the B-class motor neurons exhibit bistable behaviour similar to the RMD neurons while the D-class neurons respond linearly to input. If the results of this model suggest that further complexity is warranted, the D-class dynamics could be re-evaluated. Note that in the context of a model in which the only input to D-class neurons comes from the bistable B-class neurons, the behaviour would remain unchanged even if the D-class neurons were given bistable dynamics.

7.2.3 Connectivity

One of the main advantages of *C. elegans* as a subject for neural models is the fact that its nervous system has been reconstructed in detail. However, as discussed in Section 2.1.4,

the connectivity data is not entirely complete and can be quite difficult to interpret. As a result, it has been necessary to make some assumptions about the connectivity in order to facilitate the modelling process.

First, the model does not include a distinct head circuit, instead focussing on the ventral cord. This is motivated primarily by the fact that the ventral cord circuit is better understood (see Section 2.1.4). This limitation of scope is clearly not ideal, but was necessary given time constraints. However, this limitation brings in some related issues that could be scientifically interesting. The main implicit assumption is that, for the purposes of simple forwards locomotion, the head circuit does not make a special contribution. This is in contrast to the Niebur and Erdős [89] and Karbowski et al. [67] models in which the head functions as a primary pattern generator that is essential for locomotion. Thus I am assuming that the simple ventral cord circuitry is sufficient to generate coordinated locomotion without extra help. But it is also worth noting that while the head circuit is clearly more complex and is capable of more varied behaviour than its ventral cord counterpart, this does not preclude the possibility that the core oscillatory mechanism is the same as that of the ventral cord. Indeed the head neurons exhibit a similar (albeit more complicated) motif where excitatory neurons innervate muscles on each side and also stimulate cross inhibitory GABAergic neurons [99, 102, 136]. Also, previous models involving the head circuit have found that sensory feedback is a necessary component [67, 102]. If a model based on the simple but relatively well understood ventral cord circuit is successful in reproducing the desired behaviours, this might suggest that the head circuit includes a component that is equivalent to the ventral cord motif.

The ventral cord locomotion circuit includes major asymmetries in the number of members in each neural class (13 VD, 11 VB, 7 DB and 6 DD). Also, the neural connectivity is actually quite irregular (see Section 2.1.4). Thus the second important assumption I have made is that the ventral cord circuit can be approximated as a number of largely identical repeating units (each containing one neuron of each class) without losing the essence of its operation. This is clearly a very significant assumption that should be removed from future versions of the model. However, at this stage it was essential to allow the model to be developed in stages. It seems likely that the real worm compensates for the asymmetries by having slightly different “parameters” for different neurons and synapses. However, trying to optimise the model as a single entity, without being able to first build and test the individual oscillator units, would not have been practical at this stage.

The final assumption I have made about the connectivity, discussed in Sections 2.1.4 and 9.3, is that the inhibitory connections from VD to VB neurons are both functional,

significant and under-represented in the connectivity data [26]. Specifically, despite VD to VB connections only having been identified between about half the members of these classes, they have been included as a feature of the repeating neural units in the model. This is potentially quite a controversial assumption, but is also an interesting prediction of the model that is currently being investigated experimentally (see Section 10.3).

7.3 Model overview

The model is described by a fairly complex set of equations which are presented in Chapter 8. However, before delving into the mathematical details, the reader is likely to benefit from a more intuitive description of the model and its various sub-components, as provided in this section.

7.3.1 Physical model

The research conducted so far has led to the conclusion that the physics of the worm's body, together with the environment in which it is embedded, is a vital component of the locomotion system. The physical model therefore provides an indispensable interface not only between the worm's neural control system and the outside world, but also between the muscle output and sensory feedback. While the neural control cannot be evaluated without a body, the behaviour of the body can, at least to an extent, be evaluated without the neural control. The physical model was therefore developed first.

Environment

At the crudest level the physical model consists of two components: the body and the environment. The role of the fluid environment (for the purposes of this model gels will be approximated as fluids, as justified in Section 4.3.3) is to apply loads to the body, thereby modulating the worm's behaviour and providing thrust to allow it to progress. The environment will only apply a force to an object (or part of the body) that is moving through the fluid, and this force will be proportional to the velocity. If an object with negligible mass is pulled through a fluid by an external force of fixed magnitude, the object's velocity will immediately reach the steady state at which the fluid drag exactly counteracts the external force [74]. Due to the linearity of the drag force equation used here ($F = -CV$), the velocity of the object will be inversely proportional to the drag coefficient C . Thus the resistivity of the environment effectively scales the physical "time constant" of the locomotion system. Further to this scaling effect (that could also be

achieved in a Newtonian medium), the model is able to represent the “grooviness” of the environment (the value of K , see Section 2.2.3), thereby modulating the worm’s ability to get traction (see Section 2.2.2). To express both of these properties requires only two parameters: the normal and tangential drag coefficients $C_{\perp} = KC_{\parallel}$. In the context of this simplified model, these two parameters fully describe any fluid environment.

With regard to quantification of the model, values for the drag parameters are very important indeed. Direct measurement of properties like body elasticity are not available, but environmental properties are easier to measure and have therefore been reported to some degree. This is only the case for the two “standard” *C. elegans* environments of water and agar, making it impossible to model *specific* gelatin concentrations. Water, being a Newtonian fluid with known viscosity, can be handled analytically. Specifically I will use Equation 2.6 due to Lighthill [74]. Agar is a more complex fluid that has not been as well characterized. It was therefore necessary to rely on direct (but inevitably less accurate) measurements of resistance reported in the literature, in combination with the estimate of K reported in Section 4.3.2. Thus while the parameters for agar may be less accurate than those for water, both are well grounded and provide a good starting point for quantification of the physical model. Note that the resistivity of agar is three orders of magnitude greater than water when comparing tangential drag coefficients (four orders of magnitude if comparing normal components). In lieu of parameters for specific gelatin concentrations, values will be interpolated as described in Section 8.2.2.

Passive body

The body model includes the passive properties of the worm’s hydrostatic skeleton, as well as the active properties of the muscles. While it is clearly a drastic simplification, the model hopefully captures the important aspects of the *C. elegans* body. The use of a 2D model is justifiable given that the body undulations are confined to the dorso-ventral plane [135], and an extension to 3D would dramatically increase the complexity. In absence of muscle activation the body is effectively a flexible elastic beam that can be easily bent, but will naturally return to a straight posture when left to its own devices. The body model is schematically illustrated in Figure 7.1 and consists of a row of solid rods, whose end points are connected by a network of damped springs, or “elements”. Clearly the discrete representation of a continuous body is an approximation, but with sufficiently fine graining this approximation should be satisfactory. The network of lateral and diagonal elements are used to represent the worm’s elastic cuticle, as well as the internal pressure. The lengths of the solid rods and the rest lengths of the springs are such that the model’s default shape is an ellipsoid with a length of 1 mm and a diameter of 80 μm .

The damping combined with each spring accounts for the fact that no real material will be purely elastic, and is used to increase the numerical stability of the model in less resistive environments, as well as limiting the maximum rate at which the body can bend.

This representation incorporates two main simplifications. First, the use of solid rods for the circumferential connections precludes any possible change in diameter, but simplifies the model. However, removing this simplification would only help if there was more detailed, quantitative data on which to base the parameters of the model. For the purposes of the present investigation, only the macroscopic behaviour of the body is relevant. It should also be noted that *C. elegans* does appear to be more compliant in the longitudinal than the circumferential direction [91]. The second simplification is the approximation of pressure forces by diagonal springs. While these springs do a good job of maintaining constant area within each segment, the main drawback is that this makes the area in each segment independent of the others. In addition to simplifying the model, this approach also has the advantage of preventing a section of the body from “ballooning” in response to hypercontraction elsewhere (something that, in the biological worm, would be prevented by the nonlinearity of cuticle elasticity). The diagonal elements also fulfil a second role, which is to prevent adjacent rods from sliding out laterally (like how a cardboard box can be folded flat when the top and bottom are open). Indeed without the diagonal elements it would potentially be possible for the length of the model worm to collapse to zero without changing the lengths of the lateral elements. The *C. elegans* cuticle contains crossed helical fibres [1] that would have a similar effect.

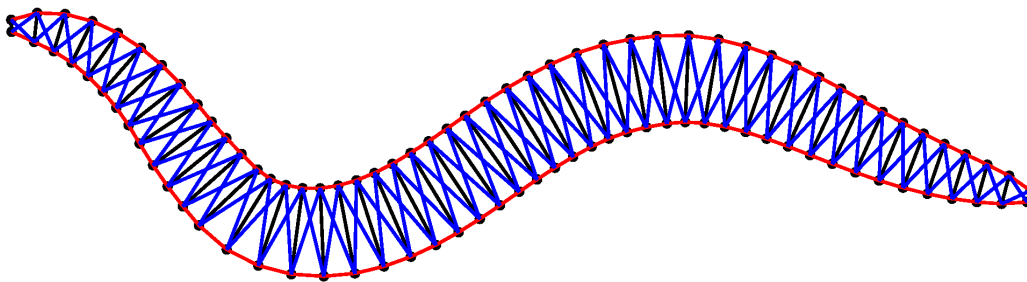


Figure 7.1: Structure of the physical model. The worm is represented by 49 solid rods (black lines) whose end points (black circles) are connected by lateral (red) and diagonal (blue) elements.

Quantification of the body model is unfortunately much less direct than for the environment, and is done based on behavioural criterion. Specifically, I use experiments

performed by Pascal Sauvage [103] on worms paralysed with muscimol (which activates GABA receptors and therefore fully relaxes the muscles). The experiments show the worm being manually bent and allowed to passively straighten in water or on agar. It is at this stage that the environmental parameters come into play, allowing me to simulate the body in a quantitative model of water or agar and compare this to the real behaviour. Basically, the elasticity of the passive body model is such that water applies an almost negligible load (the worm straightens in less than 100 ms), while agar applies a very significant load (the worm straightens over a matter of minutes).

Muscles

Clearly, the body model is not particularly interesting without active muscle forces. In the model, dorsal (ventral) muscles are located between each pair of adjacent dorsal (ventral) points. Activation of a muscle generates a contractile force that pulls its two end points closer together. Assuming the opposing muscle is relaxed, the passive body properties will cause the opposite side of the body to elongate simultaneously. This causes the angle between the two adjacent rods to change, leading to bending of the body at that point. Thus by contracting specific muscles, the body can be made to take on a large class of curved shapes. Like the passive body elements, muscles are modelled as a spring in parallel with a damper. Unlike the passive elements, the spring constant, spring rest length and damping constant all depend on the muscle's level of activation (clipped to the range $0 \rightarrow 1$ to prevent negative or excessive forces). I chose this model as a simple way to endow the muscles with the length/tension and velocity/tension relationships exhibited by real muscles [55] (see Section 9.1.2). While the velocity/tension relationship has only a quantitative effect, the length dependence has an important qualitative role as described below.

The role of the damping component is to implement the velocity/tension relationship. If the muscle is held at a fixed length, the spring will exert some force F and the damper will have no effect. If the muscle is then allowed to contract with some velocity V , the damper will apply a force that opposes contraction. Thus the net force exerted by the muscle will be reduced by a factor proportional to the shortening velocity and the damping constant. Conversely if the muscle is forced to elongate while trying to contract, the sign of the damping term will switch and it will instead add to the contractile force. The damping constant is taken to be proportional to the time-varying muscle spring constant to ensure that the velocity dependence scales with the overall muscle activation.

The spring component of the muscle model is responsible for generating force and implementing the length/tension relationship. When the muscle activation is zero, the

stiffness of the spring is also zero and the rest length is equal to the segment rest length. Conversely, when the muscle activation equals or exceeds unity, the spring stiffness takes on its maximum value κ_{0M} while the rest length takes on its minimum value L_{\min} . For intermediate activation, these parameters vary linearly between their extreme values. By implementing the muscle as a spring, a simple linear length/tension relationship is included “for free”. As the muscle contracts (i.e., the spring shortens towards its current rest length) the force that it exerts will diminish. Similarly, over-stretching the muscle will increase the force. The main reason the length/tension relationship is so important to include is that it prevents the very unrealistic case of a body element shortening to zero length.

7.3.2 Neuromuscular control

In this section I will describe the neuromuscular control of the model, including the neuron model, neural circuit and muscle dynamics.

Muscle dynamics

From a dynamic point of view, the muscles are the simplest component of the model. Their input/output relationship is that of a simple low pass filter with a time constant of 100 ms (in crude agreement with the dynamics of obliquely striated muscle of a squid [87]), and the muscle state is represented by a unitless activation variable $A_{M,m}^k$. It is important to note, however, that this muscle time constant does not represent just the membrane time constant, but rather the dynamics of the entire process of excitation-contraction coupling.

Neuron dynamics

The model includes three distinct types of neuron, namely B-class and D-class motor neurons as well as the AVB interneuron pair. The dynamics of AVB are outside the scope of this model, so its only role is to switch the entire locomotion circuit on and off. The gap junction current from AVB into the B-class neurons is approximated as a constant excitatory current term I_{AVB}^k , which has different values for DB and VB neurons. The need for different values arises from the asymmetry of the circuit (one way neural inhibition). When these current terms are included, the model will oscillate and generate locomotion. When they are set to zero however, all neurons will switch off and locomotion will cease.

For the reasons outlined in Section 7.2.2, the B-class neurons are modelled as bistable units while the D-class neurons have a linear input-output relationship, except that their

output is inhibitory. In both cases the model is simplified by approximating the fast dynamics of these tiny neurons as instantaneous. In the case of the B-class neurons this means that the states change based on whether or not the total input current exceeds the neuron's threshold at that moment, while for the linear D-class neurons the output depends only on the input at that moment. To approximate the dynamics of the RMD neurons on which they are based, the model B-class neurons are fully binary, having distinct “on” and “off” states $S_n^k = 1$ and $S_n^k = 0$. The hysteresis exhibited by RMD neurons is implemented by making the transition threshold state dependent, with the threshold for switching off being lower than the threshold for switching on. Both of these properties are key features that make it possible, at least in principle, for the model to produce self-sustained oscillations. The bistability adds a vital threshold to the system [115] while the hysteresis, by introducing a history dependence, effectively adds a second dimension to the state space of the oscillators¹. Finally, the combined effect of a physical body and stretch receptor feedback provides delayed inhibition, satisfying the requirements for self-sustained oscillation.

Proprioception

In combination with the B-class dynamics, stretch receptor mediated proprioception forms the fundamental oscillatory mechanism of the model. Each DB (VB) neuron receives stretch receptor input from the dorsal (ventral) side of local and posterior segments. For neurons in the front half of the body, the stretch receptors sum over half the body length. For neurons in the back half of the body the receptive field runs to the tip of the tail and is therefore shorter, but these inputs are more strongly weighted to compensate for this reduction. Stretch receptors contribute to the total neural input by means of a current term $I_{SR,n}^k$, which can be positive or negative.

For each B-class neuron, the proprioceptive current is proportional to the total length change (compared to a relaxed worm) along the stretch receptor's receptive field. If the worm is uniformly bent, all segments within the receptive field will be stretched (compressed), leading to a large positive (negative) current. However, if the worm displays alternating dorsal and ventral bends, the receptive field will include some stretched segments and some compressed segments. These contributions will partially cancel out,

¹To illustrate this point consider the simpler case of a single neural oscillator unit connected to a single segment of the physical model. Now, while the DB and VB states and the dorsal and ventral lengths are somewhat independent, the properties of the model as a whole impose relationships between them. Specifically, without the inclusion of hysteresis, the states of all neurons in a unit would basically just be a function of the bending angle (θ) of the physical segment. Thus in this case the only independent variable would be θ , and the system would effectively be one dimensional. The theory of non-linear dynamics shows us that oscillation is not possible in a one dimensional system [115].

leading to a relatively small stretch current despite the tight curvature. This is a subtle point, but is central to the model's ability to adapt its waveform in different environments.

The general description above applies to all neural units, but the model also requires modifications to the proprioceptive properties of different neurons. These are due to the lateral and longitudinal variability of the model. First, the dorsal and ventral stretch receptors have been given slightly different properties. This was required to achieve symmetric oscillation with an asymmetric neural circuit. Specifically, while the ventral stretch receptors respond symmetrically to stretch and compression, the dorsal stretch receptors are slightly less sensitive to stretch and more sensitive to compression. Second, there is a variable longitudinal weighting term that is required due to the elliptical shape of the worm. As the radius decreases towards the head and tail, the length change associated with a certain amount of body curvature will decrease, leading to a weaker proprioceptive signal. By compensating for this change I ensure that the stretch receptors in each segment have a similar response to *curvature*. Finally, I include another weighting term that increases linearly from head to tail. This is required to compensate for the posteriorly decreasing gradient in average body curvature that is characteristic of the worm's locomotion waveform (see Figure 7.2 A) and is included in the model as described below.

Neural circuit

The neuromuscular connectivity in the model is longitudinally symmetric, so it suffices to describe the connectivity of a single neural oscillator unit. Each unit includes one neuron of each class (DB, VB, DD and VD). The model has $M = 48$ physical segments and $N = 12$ neural units, so each neuron controls four muscles. Dorsal (ventral) muscles receive excitatory input from DB (VB) and inhibitory input from DD (VD), which in turn receives excitation from VB (DB). Furthermore, the VB neuron receives inhibition from VD. I will show in Section 9.3 why this neural inhibition is a particularly important part of the model. The model includes no communication between neural units, except indirectly via the body and associated proprioceptive feedback. Another essential property of the model is a posteriorly decreasing gradient in the muscle efficacy. In combination with the inverse gradient in stretch receptor weight, this grants the model a qualitatively realistic curvature gradient as shown in Figure 7.2 B. More importantly however, it is essential for ensuring that the body will move in the correct direction (forwards) when initiating motion from a relaxed, straight posture.

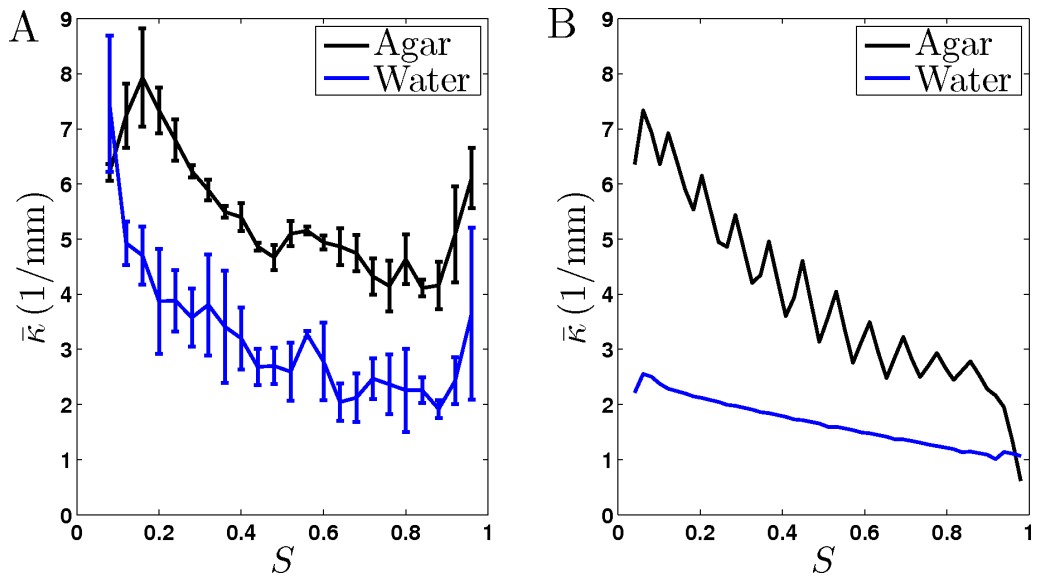


Figure 7.2: The worm’s locomotion wave exhibits a posteriorly decreasing gradient in curvature, averaged over time ($\bar{\kappa}$). S is a measure of the position along the worm’s body, with $S = 0$ corresponding to the head and $S = 1$ corresponding to the tail. A) Experimentally observed curvature gradient obtained by averaging the curvature at each point along the body, first over time and then over several worms ($n = 3$ for agar and $n = 5$ for water). Bars indicate the standard deviation over the n worms. B) Qualitatively similar curvature gradients exhibited by the model, due to the gradients in muscle efficacy and stretch receptor weighting.

7.3.3 Integrated model

Here I will give an intuitive explanation of how the embodied neural circuit generates oscillations (see Figure 7.3 for clarification). Consider a single neural unit connected to a short section of the body. Initially both DB and VB are off, and the body is in the relaxed, straight posture. When the AVB input is switched on, the total input current I^V to VB is sufficient to drive it above threshold, turning it on. This causes the ventral muscles to start contracting, thereby lengthening the dorsal side. At some point the dorsal stretch input will be sufficient to switch on DB, which will activate VD to inhibit VB, driving it below threshold and turning it off. At this stage the direction of bending will reverse, with the dorsal side contracting and the ventral side lengthening². This continues until the dorsal side is sufficiently contracted that the input to DB falls below threshold, turning it off and indirectly releasing VB from inhibition. The removal of inhibition pushes VB over

²Note that this only leads to oscillation because the B-class hysteresis causes the threshold to change at this point. Without it, the input to DB would fall below threshold almost immediately and oscillation would stop.

its threshold, turning it on and again contracting the ventral side, repeating the cycle. It should be noted that the frequency of oscillation depends entirely on the physical “time constant” of the body and environment, because the model will bend in each direction until a certain level of elongation/compression is reached – the nervous system has no internal sense of time, although the B-class neurons do have a sense of history.

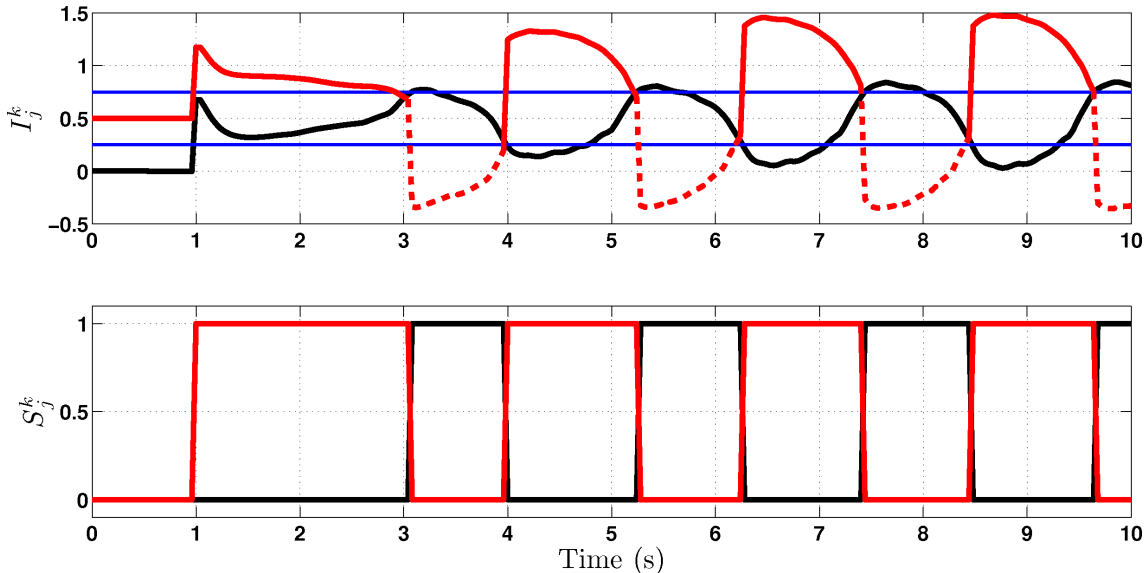


Figure 7.3: Oscillation of the integrated model showing the total current input (top) and states (bottom) of the dorsal (black) and ventral (red) neurons. The blue lines represent the distinct thresholds for turning on (higher) and off (lower). When the red line in the top panel is dashed, this indicates that the ventral neuron is receiving inhibition from the dorsal neuron. The excitatory input from AVB is switched on at $t = 1$ second.

Let us now consider the complete model, with multiple oscillators and a full length body. Coupling between oscillators is mediated in two related but slightly different ways. First, the stretch receptors respond to the combined elongation/compression of a long section of body. While this grants each unit the ability to sense something about the posterior segments, it must be noted that this is combined with information about the local segments, obscuring the latter. But even if the stretch receptors were purely local, the oscillator units would still be able to influence each other. This is thanks to the second mode of communication, in which parts of the body affect each others shapes through physical forces applied via the environment. In some cases this will deform a segment, while in other cases it can prevent a segment from changing shape. The relative importance of these two contributions will depend on the properties of the worm’s environment.

When the worm is in a less resistive environment like water, the external mechanical load is fairly insignificant compared to internal forces. In this case, interactions via

physical forces are minimized because the body parts connected to either side of a given segment are largely free to move. As a result the effect of the long range stretch receptor inputs will dominate. Their effect will be to gently push the oscillators towards in phase synchrony. Indeed when the gradients in muscle efficacy and stretch receptor weight are omitted, the resulting oscillation is virtually a standing wave. When the gradients are reintroduced, the slight gradient in natural frequencies combined with weak coupling will lead to frequency entrainment with a slight phase lag. Moreover, because the phase lag between units is small, length changes within the proprioceptive field will be well synchronized and will therefore “cooperate”, leading to a reduction in average curvature.

If the worm instead moves in a highly resistive environment like agar, the direct physical interactions will become dominant. Indeed, while developing the model I found that local proprioceptive feedback is sufficient to achieve realistic crawling on agar. To understand how the locomotion waveform emerges in this case, consider the model initiating locomotion from a straight configuration. Initially all VB neurons are active, so all ventral muscles exert a contractile force (with a decreasing gradient towards the tail). However, for a segment near the middle of the body to bend, the body parts connected to it must move sideways. This is resisted so strongly by the environment (specifically C_{\perp}) that bending is hardly possible at first. Instead the head will begin to curve ventrally from the tip, pulling the worm forwards slightly and thereby allowing a few more segments to bend (as they move forwards into the groove). At some point the head will be bent sufficiently that the neural states switch and bending in the other direction commences, leading to further propulsion and allowing still more segments to bend. It is this delay in bending (rather than in actuation) that gives rise to the crawling wavelength. Also, because the wavelength is shorter, the neurons’ proprioceptive fields will integrate over both dorsally and ventrally bent segments. These contributions will partially cancel out, so tighter curvature will be required to cause a change in bending direction. As Figure 7.2A shows, the average curvature is greater when a worm moves in agar than in water.

Chapter 8

Integrated model: Methods

8.1 Introduction

In the previous chapter I gave an overview of the components of the integrated model, as well as highlighting some of the important assumptions. Here I will present the model in detail, starting with the version from which the main results in Chapter 9 are obtained. Consistent with the order in which the model was developed, the physical model is presented first, starting with the representation of the environment. After fixing environmental parameters based on experimental data, the next step is the passive body model. By embedding the body in a well grounded model of the medium, suitable parameters can be chosen based on behavioural data without requiring direct knowledge of body properties like cuticle elasticity. The last component of the physical model is the muscle force model (the dynamics of muscle activation are included in the neuromuscular model), which is based on known properties of biological muscles.

Having built the physical model, the next step is to imbue it with neuromuscular control. The preliminary muscle model presented in Chapter 6 suggests that the details of muscle dynamics are not relevant to locomotion so a new, simpler model is used here. The model of the nervous system includes bistable B-class neurons and linear D-class neurons. The states of these neurons completely determine the activation levels of local muscles, with each neuron controlling only adjacent muscles on its own side. One particularly important part of the model is the proprioceptive input provided to the B-class

neurons via model stretch receptor channels which respond to lengths of sections of the body, extracted from the physical model.

Having completed the description of the main version of the model, I will go on to present several interesting model variants in Section 8.4. Lastly I will present the computational methods used to simulate the model in Section 8.5.

8.2 Physical model

The physical model presented here builds on an earlier model presented in Section 5.2.2, which in turn was inspired by the model due to Niebur and Erdős [89]. Briefly, each muscle is located in the gap between two points of the physical model. Thus, 49 dorsal/ventral point pairs numbered $i = 1, \dots, P/2$ form the boundaries of $M = 48$ segments numbered $m = 1, \dots, M$ (see Figure 7.1 for an overview) articulated by muscles on each side ((D)orsal and (V)entral). The hydrostatic skeleton and muscles are represented by a combination of damped springs and solid rods which connect these points and apply forces to them. The topology of the model is described first.

8.2.1 Structure

In the model, a worm of length L and maximum radius R is represented by $P = 2(M + 1) = 98$ discrete points \mathbf{p}_i^k , where $i = 1, \dots, P/2$ and $k = \{D, V\}$. In the previous version of the model presented in Section 5.2.2 (and see the variant in Section 8.4.1), the radius was taken as constant along the body, giving a rectangular outline. For increased realism, and specifically for the benefit of locomotion in microfluidic post arrays, the model has been adapted to approximate the tapered shape of the worm as a prolate ellipse with major radius $\approx L/2$ and minor radius R . In fact, to avoid having zero-valued radii at the ends (which would be numerically problematic) I take the major radius to be slightly greater than $L/2$ and obtain the radii according to

$$R_i = R \left| \sin \left(\cos^{-1} \left(\frac{i - M/2}{(M + 1)/2.0 + 0.2} \right) \right) \right|. \quad (8.1)$$

One of the simplifying assumptions of this model is that the worm's radial elasticity can be neglected, instead maintaining a fixed diameter over time. Thus, as in the model of Section 5.2.2, opposite points \mathbf{p}_i^k and $\mathbf{p}_i^{\bar{k}}$ are connected by a solid bar of length $2R_i$. The notation \bar{k} denotes the opposite side to k (i.e., if $k = D$ then $\bar{k} = V$). Each point \mathbf{p}_i^k is connected to adjacent points \mathbf{p}_{i-1}^k and \mathbf{p}_{i+1}^k on the same side by *lateral elements* representing

passive cuticle forces and active muscle forces. The volume-preserving effect of internal pressure is approximated by *diagonal elements* that connect \mathbf{p}_i^k to $\mathbf{p}_{i+1}^{\bar{k}}$. Together, these elements (described in Sections 8.2.3 and 8.2.4) yield a net force \mathbf{f}_i^k acting on each point. However, because solid rods are used for the radial connections, the forces acting on \mathbf{p}_i^k and $\mathbf{p}_i^{\bar{k}}$ can be combined into a net force and torque acting on the “centre of mass”¹ (CoM) of the i^{th} rod. The first step is to convert the forces \mathbf{f}_i^k from the global (x, y) coordinate frame to a local coordinate frame aligned with the rod. This conversion is also necessary so that the anisotropic drag coefficients C_{\parallel} and C_{\perp} (see Section 2.2.2) can have their effect. Note that the tangential and normal directions are defined with respect to the body surface, meaning that the rod is aligned with the *normal* axis (see Figure 5.2). Making this conversion requires only a rotation through an angle $\frac{\pi}{2} - \phi_i$ (where ϕ_i is defined as the angle of the i^{th} rod to the x axis, as shown in Figure 8.1A), using

$$\begin{aligned} f_{\parallel,i}^k &= f_{x,i}^k \cos\left(\frac{\pi}{2} - \phi_i\right) - f_{y,i}^k \sin\left(\frac{\pi}{2} - \phi_i\right) \\ f_{\perp,i}^k &= f_{x,i}^k \sin\left(\frac{\pi}{2} - \phi_i\right) + f_{y,i}^k \cos\left(\frac{\pi}{2} - \phi_i\right). \end{aligned} \quad (8.2)$$

Having decomposed the net force, the normal components can simply be summed and applied to CoM_i as a pure force. The tangential components of the force can cause both rotation and translation of the rod and must therefore be further decomposed into even and odd components (which will give rise to a torque and a force respectively) using

$$\begin{aligned} f_{\parallel,i}^{\text{even}} &= \frac{(f_{\parallel,i}^D + f_{\parallel,i}^V)}{2} \\ f_{\parallel,i}^{\text{odd}} &= \frac{(f_{\parallel,i}^D - f_{\parallel,i}^V)}{2}. \end{aligned} \quad (8.3)$$

The next step is to determine the motion that these forces will induce. Typically, forces give rise to accelerations which are then integrated to obtain velocities. However, the low Reynolds number assumption (see Section 2.2.1) significantly simplifies this process. First, as discussed in Section 3.2.1, the fact that inertia is negligible means that the net force and torque (including the environmental resistance) acting on each CoM must at all times be zero. To satisfy this requirement the drag force must be equal but opposite to the sum of the internal forces. Again invoking the low Reynolds number physics, the environmental forces are modelled as Stokes’ drag of the form $\mathbf{F}_{\text{drag}} = -\mathbf{C}\mathbf{V}$. Combining

¹Since this model uses low Reynolds number physics and is mass-free, the rod’s CoM is not strictly defined, and should instead be called the “centre of drag”. In what follows the CoM is defined as the midpoint between \mathbf{p}_i^k and $\mathbf{p}_i^{\bar{k}}$.

these two properties means that $\mathbf{F} + \mathbf{F}_{\text{drag}} = \mathbf{F} - C\mathbf{V} = 0$, so $\mathbf{V} = \mathbf{F}/C$. As a result, the drag force need never be explicitly calculated since for each point, $V_{(\parallel,\perp),i}^k = f_{(\parallel,\perp),i}^k/C_{(\parallel,\perp)}$. When the forces on \mathbf{p}_i^k and $\mathbf{p}_i^{\bar{k}}$ are combined and applied to the CoM, we get an analogous expressions for the velocity and angular velocity of the rod:

$$\begin{aligned} V_{\perp,i}^{(\text{CoM})} &= \frac{1}{C_{\perp}}(f_{\perp,i}^D + f_{\perp,i}^V) \\ V_{\parallel,i}^{(\text{CoM})} &= \frac{1}{C_{\parallel}}(2f_{\parallel,i}^{\text{even}}) \\ \omega_i^{(\text{CoM})} &= \frac{1}{R_i C_{\parallel}}(2f_{\parallel,i}^{\text{odd}}). \end{aligned} \quad (8.4)$$

The final step is to convert $V_{\parallel,i}^{(\text{CoM})}$ and $V_{\perp,i}^{(\text{CoM})}$ back into global (x,y) coordinates with

$$\begin{aligned} V_{x,i}^{(\text{CoM})} &= V_{\parallel,i}^{(\text{CoM})} \cos\left(\frac{\pi}{2} - \phi_i\right) + V_{\perp,i}^{(\text{CoM})} \sin\left(\frac{\pi}{2} - \phi_i\right) \\ V_{y,i}^{(\text{CoM})} &= -V_{\parallel,i}^{(\text{CoM})} \sin\left(\frac{\pi}{2} - \phi_i\right) + V_{\perp,i}^{(\text{CoM})} \cos\left(\frac{\pi}{2} - \phi_i\right). \end{aligned} \quad (8.5)$$

8.2.2 Properties of the Environment

As discussed in Section 4.3.3, the resistive forces applied by the worm's fluid environment in our experiments can be well represented by local drag coefficients resisting motion tangential (C_{\parallel}) and normal (C_{\perp}) to the local body surface. In this section I will present the derivation of values for these parameters in various environments. The modelling approach I am using requires that these parameters be well grounded, as they are essential to the quantification of the entire physical model. For Newtonian fluids of known viscosity, this is a relatively straightforward task. Using equations from slender body theory due to James Lighthill [74] combined with the known viscosity of water and the dimensions of the worm, we can write

$$\begin{aligned} C_{\parallel,\text{water}} &= L \frac{2\pi\mu}{\ln(2q/a)} = 5.2 \times 10^{-6} \text{ kg} \cdot \text{s}^{-1} \\ C_{\perp,\text{water}} &= L \frac{4\pi\mu}{\ln(2q/a) + 0.5} = 3.3 \times 10^{-6} \text{ kg} \cdot \text{s}^{-1}, \end{aligned} \quad (8.6)$$

where $\mu \approx 1 \text{ mPa} \cdot \text{s}$ is the dynamic viscosity of water and $q = 0.09\lambda = 135 \times 10^{-6} \text{ m}$ is proportional to the wavelength (λ) of the body wave (typically about 1.5 mm in water). Note that the values calculated above are for the whole worm, so the drag coefficient experienced by each of the P points is C/P .

Unfortunately the same approach cannot be used in more complex viscoelastic or gel-like (non-Newtonian) media, so a less direct method is required. For agar, H. R. Wallace estimated the tangential drag coefficients $C_{\parallel, \text{agar}}$ by directly measuring the force required to pull glass fibres of similar dimension to *C. elegans* across the surface [128]. Based on this measurement, Niebur and Erdős [89] estimated $C_{\parallel, \text{agar}} = 3.2 \times 10^{-3} \text{ kg}\cdot\text{s}^{-1}$. However, an estimate of the normal drag coefficient $C_{\perp, \text{agar}}$ was not given by Wallace, and Niebur and Erdős used an unrealistically high value of K . Instead, since $C_{\perp} = KC_{\parallel}$, the value of $C_{\perp, \text{agar}}$ can be obtained from the groove strength K which I previously estimated from recordings of wild type worms using the motion simulator (see Section 4.3.2), and found to be in the range 30 – 40. Taking a value of $K_{\text{agar}} = 40$ gives $C_{\perp, \text{agar}} = 40 \times C_{\parallel, \text{agar}} = 128 \times 10^{-3} \text{ kg}\cdot\text{s}^{-1}$, which will be used in what follows.

To model intermediate environments (gelatin solutions with a range of concentrations, or Newtonian media of increasing viscosity) requires a knowledge of the corresponding drag coefficients. Non-specific Newtonian media of increasing viscosity can be easily modelled by simply increasing C_{\parallel} and imposing $K = 1.5$ to get C_{\perp} . Intermediate gelatin environments (introduced in Chapter 4) are more difficult. In absence of direct measurements or a detailed model, the only option is to interpolate between the values for water and agar. However, interpolating both C_{\parallel} and C_{\perp} linearly between their water and agar values implicitly interpolates K in a way that may or may not be valid. Unfortunately the values of K obtained in Section 4.3.2 for specific gelatin concentrations are quite variable from experiment to experiment, and cannot be used to assess the validity of this interpolation. Rather than impose a relationship that might not be valid, I chose to allow all combinations of drag coefficients C_{\parallel} and C_{\perp} , such that (i) the minimum drag coefficients correspond to a water environment; (ii) the maximum drag coefficients correspond to estimates of agar properties; and (iii) the ratio of drag coefficients falls within the range $1.5 \leq K \leq 40$. The specific combinations used are shown in Figure 9.6.

While local drag coefficients are a suitable model of homogeneous fluid media, they cannot represent solid objects such as the posts in a microfluidic chip. In order to represent circular microfluidic posts, the model stores an array of post locations (x_p, y_p) and radii r_p . When any of the points \mathbf{p}_i^k comes within a distance $D_{i,p}^k < r_p$ of a post centre, it experiences a repulsive radial force of magnitude

$$f_{\text{post},i}^k = \kappa_{\text{post}} \left(\left(r_p - D_{i,p}^k \right) + 0.01 \left(\frac{r_p - D_{i,p}^k}{0.01} \right)^2 \right). \quad (8.7)$$

The spring constant $\kappa_{\text{post}} = 10\kappa_{\text{L}}$ (see Section 8.2.3 for κ_{L}) is sufficient to prevent the

worm from encroaching on the posts, while being compliant enough to avoid numerical issues. The post layouts simulated in Section 9.2.3 are taken from Refs. [78, 90]. Note however that Lockery et al. [78] use microfluidic chips in which the worm is squeezed between the top and bottom surfaces, while Park et al. [90] use chips with a higher ceiling (in both cases the gaps between posts are filled with water). To represent the latter case I use posts embedded in water. To approximate the friction forces due to the squeezing effect in the former, I set $C_{\perp} = C_{\parallel} = C_{\parallel, \text{agar}}/2$.

8.2.3 Passive body forces

In the absence of muscle activation, passive body forces capture the combined effect of the cuticle and internal pressure. As discussed in Section 7.3.1, I have chosen not to directly model the pressure forces, instead using diagonal elements which strongly resist compression to represent the effect of pressure. For the model to work in a highly resistive environment such as agar, spring forces suffice [14, 89]. However, to model motion in liquid, damping terms must also be included. I therefore model each lateral and diagonal element as a spring in parallel with a damper. Forces applied by the passive lateral elements ($m = 1, \dots, M, k = \{D, V\}$) are given by

$$f_{L,m}^k = \begin{cases} \kappa_L(L_{0L,m} - L_{L,m}^k) + \beta_L v_{L,m}^k & : L_{L,m}^k < L_{0L,m} \\ \kappa_L((L_{0L,m} - L_{L,m}^k) + 2(L_{0L,m} - L_{L,m}^k)^4) + \beta_L v_{L,m}^k & : \text{otherwise,} \end{cases} \quad (8.8)$$

where κ_L , β_L and $L_{0L,m}$ denote the lateral spring constant, damping constant and rest length, respectively. Note that, due to the non-constant radius, the rest lengths vary along the worm according to $L_{0L,m} = \sqrt{L_{\text{seg}}^2 + (R_m - R_{m+1})^2}$. The length of lateral element m , k is $L_{L,m}^k$ and $v_{L,m}^k = \frac{d}{dt}L_{L,m}^k$.

Similarly, the forces exerted by diagonal elements are given by

$$f_{D,m}^k = \kappa_D(L_{0D,m} - L_{D,m}^k) + \beta_D v_{D,m}^k, \quad (8.9)$$

where κ_D , β_D and $L_{0D,m}$ denote the diagonal spring constant, damping constant and rest length, respectively. The diagonal rest lengths are given by $L_{0D,m} = \sqrt{L_{\text{seg}}^2 + (R_m + R_{m+1})^2}$. The length of diagonal element m is $L_{D,m}^k$, while $v_{D,m}^k = \frac{d}{dt}L_{D,m}^k$.

The parameters for the passive body were chosen by comparing the behaviour of the passive physical model embedded in virtual water and agar environments (see Section 8.2.2) to that of a flaccid *C. elegans* in water or on agar [103] (see Section 9.1.1 for passive model behaviour). These parameters are given in Table 8.1.

8.2.4 Active muscle forces

The worm's muscles are anchored to the inside of the cuticle and are effectively grouped into dorsal and ventral sets, as discussed in Section 2.1.1. In the model, muscles connect adjacent points on the same side of the body, and therefore act in parallel with the passive lateral elements. Following Hill's relations [55], muscle forces are modelled as a function of the muscle activity level $A_{M,m}^k$, the length of the muscle and the muscle's speed of contraction or elongation. Specifically, (i) as a muscle shortens the maximum force it can develop will decrease, eventually reaching saturation, and (ii) the force it generates varies inversely with the speed of contraction, such that a muscle that is stretched while attempting to contract will generate a greater force. To capture these muscle properties, I model the muscle as a variable lateral element (again consisting of a spring acting in parallel with a damper), whose spring constant $\kappa_{M,m}^k$, spring rest length $L_{OM,m}^k$ and damping coefficient $\beta_{M,m}^k$ all depend on the muscle activation level. Finally, one particularly important feature is a gradient in the maximum muscle efficacies implemented by the parameter $F_{\max,m}$ that decreases linearly from head to tail. This gradient makes the shape of the worm more biologically realistic (see Figure 7.2) and is an essential feature for the model to work without a primary oscillator in the head (see Section 7.3.3). The most anterior muscles receive somewhat weaker innervation to prevent the tip of the head from displaying unrealistically strong bending.

These muscle forces are given by

$$f_{M,m}^k = \kappa_{M,m}^k (L_{OM,m}^k - L_{L,m}^k) + \beta_{M,m}^k v_{L,m}^k, \quad (8.10)$$

where

$$\begin{aligned} \kappa_{M,m}^k &= \kappa_{0M} F_{\max,m} \sigma(A_{M,m}^k) \\ L_{OM,m}^k &= L_{OL,m} - F_{\max,m} \sigma(A_{M,m}^k) (L_{OL,m} - L_{\min,m}) \\ \beta_{M,m}^k &= \beta_{0M} F_{\max,m} \sigma(A_{M,m}^k) \end{aligned} \quad (8.11)$$

where κ_{0M} and β_{0M} are constants. The function σ , used to clip muscle activation to the allowable range, is a piecewise linear approximation of a sigmoid and is defined as

$$\sigma(x) = \begin{cases} 0 & : x < 0 \\ x & : 0 < x < 1 \\ 1 & : x > 1. \end{cases} \quad (8.12)$$

The parameter $L_{\min,m}$ is included to prevent the muscles from contracting to an unrealistically short length. However, to facilitate the modular development of the model, it is desirable for the maximum attainable curvature to be the same for all m . For this reason I modulate this parameter according to the shape of the worm (see Table 8.1). This model qualitatively accounts for Hill's relations, as will be shown in Section 9.1.2. Muscle parameters were chosen such that the worm was strong enough to bend its body on agar, but could not generate unrealistically tight curvature. Clearly, these criteria do not strongly constrain the muscle parameters. However, the comparison of simulated to real contact forces presented in Section 9.2.4 suggests that the values used here are at least reasonable. These parameters are given in Table 8.1.

Table 8.1: Parameters of the physical model

| Param. | Val. | Param. | Val. | Param. | Val. |
|---------------|--|------------------------|--|------------------|-----------------------------------|
| M | 48 | P | $2(M+1)$ | R | $40 \mu\text{m}$ |
| L | 1 mm | Δ_M | 0.65 | L_{seg} | L/M |
| κ_L | $\frac{M}{24} 0.01 \text{ kg} \cdot \text{s}^{-1}$ | $L_{0L,m}$ | $\sqrt{L_{\text{seg}}^2 + (R_m - R_{m+1})^2}$ | β_L | $\kappa_L \times 0.025 \text{ s}$ |
| κ_D | $\kappa_L \times 350$ | $L_{0D,m}$ | $\sqrt{L_{\text{seg}}^2 + (R_m + R_{m+1})^2}$ | β_D | $\kappa_D \times 0.01 \text{ s}$ |
| κ_{0M} | $\kappa_L \times 20$ | $L_{\min,m}$ | $L_{0L,m} (1 - \Delta_M \frac{R_m + R_{m+1}}{2R})$ | β_{0M} | $\kappa_D \times 100$ |
| $F_{\max,1}$ | $0.7 \times (2/3)$ | $F_{\max,m=2,\dots,M}$ | $0.70 - 0.42 \frac{m-1}{M}$ | | |

8.3 Neuromuscular control

The neural model consists of $N = 12$ neuronal units numbered $n = 1, \dots, 12$ with n increasing from head to tail. Each unit consists of two B-class neurons, one ventral and one dorsal, as well as two D-class neurons. The circuitry is identical in all N units, but one of the parameters varies along the worm (Table 8.2). Specifically, to obtain similar levels of stretch receptor input along the body, despite the induced gradient in body curvature (see Section 8.2.4), the stretch receptor conductances are made to increase from head to tail. Parameter values are given in Table 8.2.

8.3.1 Dynamics of model muscles

C. elegans body wall muscles are arranged in four quadrants, each of which consists of a chain of semi-overlapping muscle cells with nearest neighbour gap junction coupling [76]. While several factors hinted that the muscles might actively participate in pattern generation, the investigation presented in Chapter 6 strongly suggests that the muscles are well

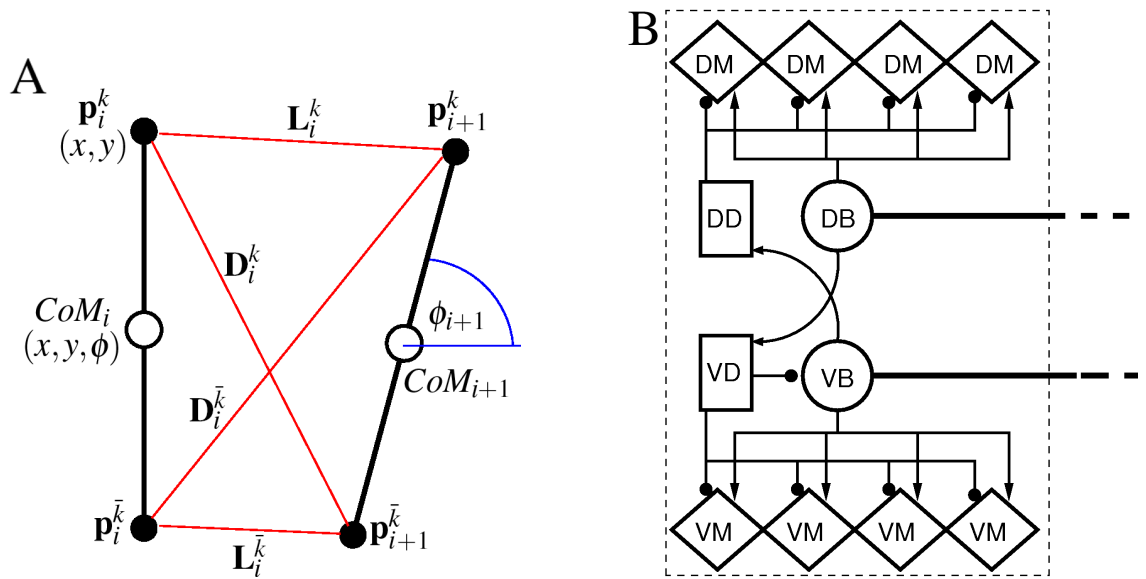


Figure 8.1: A) Schematic diagram of the physical model illustrating nomenclature (see text for details). B) Schematic of the neuromuscular model, showing one of 12 repeating units making up a symmetrized circuit for forward locomotion control. The circuit includes a pair of B-class excitatory neurons (circles), a pair of D-class inhibitory neurons (squares) and four muscles (diamonds) on each side. Synapses are labelled either as excitatory (arrowhead) or inhibitory (circlehead). Posteriorly directed lines from B-class neurons denote the stretch receptor inputs.

characterized by passive conductances with a membrane time constant on the order of tens of milliseconds. In line with this prediction, the main role of the model muscles is to generate force according to the mechanical properties described in Section 8.2.4. However, real muscles cannot respond instantaneously to inputs. Not only is the response time limited by the membrane time constant, but also by the time scales of the sequence of events that couple depolarization to force generation. For the purposes of the present model, I combine all these effects and model the muscle dynamics as a leaky integrator with a characteristic time scale of $\tau_M = 100$ ms, which crudely agrees with response times of obliquely striated muscle estimated from Ref. [87]. The muscle activation is represented by the unitless variable $A_{M,m}^k$ and evolves according to

$$\frac{dA_{M,m}^k}{dt} = \frac{1}{\tau_M} (I_{\text{NMJ},m}^k - A_{M,m}^k), \quad (8.13)$$

where $I_{\text{NMJ},m}^k$ is the total NMJ “current” driving the muscle. The parameters are given in Table 8.2.

8.3.2 Neural circuit

Currently there is no direct evidence as to the membrane dynamics of the worm's ventral cord motor neurons. Following the discussion in Section 7.2.2, the B-class neurons are schematically modelled as bistable RMD neurons [85]. I have attempted to reproduce the RMD dynamics qualitatively, with all variables treated as dimensionless. Parameter values are chosen to yield desired dynamics (with particular attention to the hysteresis band) rather than to match physiological values. Furthermore, two important simplifications have been introduced. First, based on the recordings in Figure 2 of Ref. [85] I have estimated the time constant of RMD neurons as $\tau \leq 10$ ms, in agreement with the value estimated by Niebur and Erdős in Ref. [88]. Because this time constant is so fast relative to behavioural time scales, I have approximated the model neurons as instantaneous. Second, the membrane potential of these neurons is represented by a binary state variable with states 0 and 1 denoting *off* and *on* states (and abstractly representing polarized and depolarized membrane potentials). However, a continuous version of the model is presented in Section 8.4.5 which exhibits the same basic behaviour despite being more difficult to tune due to the increased number of parameters. The success of that model variant suggests that the simplifications introduced here do not fundamentally alter the mechanism of the model.

Incorporating the above simplifications, the state variables for model B-class neurons evolve according to

$$S_n^k = \begin{cases} 1 & : I_n^k > 0.5 + \varepsilon_{hys}(0.5 - S_n^k) \\ 0 & : \text{otherwise,} \end{cases} \quad (8.14)$$

where S_n^k is the neuronal state variable for B-class neuron $n = 1, \dots, N$, $k = \{D, V\}$ (denoting (D)orsal or (V)entral); ε_{hys} sets the width of the hysteresis band; and I_n^k is the total input (or “electrical current”) into the neuron in question. Hysteresis is a key feature of the RMD behaviour and is achieved here by introducing state-dependent activation and deactivation thresholds $0.5(1 \pm \varepsilon_{hys})$. This prevents oscillations of arbitrarily small amplitude and, in conjunction with the stretch receptor weight, controls the extent of body bending. Because the D-class neurons are modelled as linear, with each member receiving input only from a single B-class neuron, it is not necessary to model their states explicitly. Instead they are represented simply by a negative synaptic weight applied to the state of the B-class neuron that innervates them.

The input term I_n^k for B-class neurons is given by

$$I_n^k = I_{\text{AVB}}^k + I_{\text{SR},n}^k + w_-^k S_n^{\bar{k}},$$

where I_{AVB}^k represents a constant input current from forward locomotion command interneurons AVB, which has different values for dorsal and ventral neurons; $I_{\text{SR},n}^k$ is the stretch receptor (SR) current flowing into the cell; w_-^k sets the inhibitory (GABAergic) synaptic weight; and \bar{k} denotes the opposite side to k as before. Note that since only ventral neurons receive inhibitory synaptic inputs, I have set $w_-^D = 0$.

The stretch receptor current

$$I_{\text{SR},n}^k = A_n G_{\text{SR},n} \sum_{m=1+(n-1)N_{\text{out}}}^s h_m^k \quad (8.15)$$

sums over contributions from a number of segments of the *physical* model (see Section 8.2.1). Here N_{out} is the number of muscles controlled by each neuron (in this case four) and the index s denotes the most posterior segment over which proprioceptive signals are integrated, with $s = \min\{M; N_{\text{SR}} + (n-1)N_{\text{out}}\}$. Thus for anterior segments, SR input is summed over N_{SR} segments of the physical model while for more posterior segments the SR input can only be summed to the end of the worm. To compensate for the different number of contributing segments, the weighing prefactor

$$A_n = \begin{cases} 1 & : (n-1)N_{\text{out}} \leq M - N_{\text{SR}} \\ \sqrt{\frac{N_{\text{SR}}}{(M-(n-1)N_{\text{out}})}} & : (n-1)N_{\text{out}} > M - N_{\text{SR}} \end{cases} \quad (8.16)$$

is used. The conductance parameter $G_{\text{SR},n}$ linearly increases from head to tail to compensate for the decreasing curvature of undulations down the worm, imposed by the gradient in muscle efficacy (see Section 8.2.4).

Finally, h_m^k is the effective mechanosensory activation function. For simplicity, I take this function to be operating over a linear (bilinear) regime on the ventral (dorsal) sides:

$$h_m^k = \lambda_m \gamma_m^k \frac{L_{\text{L},m}^k - L_{\text{OL},m}}{L_{\text{OL},m}}, \quad (8.17)$$

where $L_{\text{OL},m}$ is the segment rest length and $L_{\text{L},m}^k$ is the current length of the k^{th} side of the m^{th} segment with $m = 1, \dots, M$. The first weighting term:

$$\lambda_m = \frac{2R}{R_m + R_{m+1}} \quad (8.18)$$

is required due to the elliptical shape of the body model (see Section 8.2.1), and is a function of the variable radius R_i . The second weighting term:

$$\gamma_m^k = \begin{cases} 1 & : k = V \\ 0.8 & : (k = D) \& (L_{L,m}^k > L_{0L,m}) \\ 1.2 & : (k = D) \& (L_{L,m}^k < L_{0L,m}) \end{cases} \quad (8.19)$$

modifies only the dorsal stretch receptors and is used to ensure that the worm will move straight despite the asymmetry in the neural circuit. This completes the description of the neuronal model.

8.3.3 Muscle inputs

Muscles are labelled by an index $m = 1, \dots, M$ that increases from head to tail. Ventral (dorsal) muscle cells m receive an excitatory current input from one local VB (DB) neuron $n(m) = \text{ceil}[m/N_{\text{out}}]$ (i.e., m/N_{out} rounded up, with each neuron outputting to $N_{\text{out}} = 4$ muscles) as well as an inhibitory input from the corresponding VD (DD) neuron. The total input ‘‘current’’ to the muscles is therefore given by

$$I_{\text{NMJ},m}^k = w_{\text{NMJ}} S_{n(m)}^k + \bar{w}_{\text{NMJ}} S_{n(m)}^{\bar{k}}, \quad (8.20)$$

where w_{NMJ} are the excitatory neuromuscular junction weights and \bar{w}_{NMJ} denote the GABAergic neuromuscular weights (modelling direct muscle inhibition by D-class neurons).

Table 8.2: Parameters of the neuromuscular model

| Parameter | Value | Parameter | Value |
|------------------|--------|------------------------|---|
| N | 12 | ϵ_{hys} | 0.5 |
| M | 48 | I_{AVB}^V | 1.175 |
| N_{SR} | $M/2$ | I_{AVB}^D | 0.675 |
| N_{out} | M/N | $G_{\text{SR},n}$ | $\frac{(0.224+0.056n)}{N_{\text{out}}}$ |
| w_-^V | -1 | w_-^D | 0 |
| w_{NMJ} | 1 | \bar{w}_{NMJ} | $-w_{\text{NMJ}}$ |
| τ_M | 100 ms | | |

8.4 Model variants

While the majority of the results presented in the next Chapter are produced by the model described above, I have also developed several variants of the model that have their own advantages or applicability to certain situations.

8.4.1 Rectangular body

The physical model presented in Section 8.2 above was initially developed with a rectangular outline (i.e. constant radius) and only $M = 24$ muscle segments. Note that the number of neural units remains unchanged. While the increased number of segments and more realistic outline are generally advantageous, this comes at the cost of increased simulation times. Thus for some purposes it may be better to revert to the previous version in the interests of efficiency. Here I will briefly present the required minor modifications.

Most of the required changes are achieved indirectly by modifying two key “primary” parameters. Specifically, M is reduced from 48 to 24, and Equation 8.1 reduces to $R_i = R$. After making these changes, the values of the “secondary” parameters (those which were given as expressions dependent on other parameters) will need to be updated, but these will still follow the expressions given previously. One exception is the value of κ_D (given in Table 8.1) which must be changed to $\kappa_D = \kappa_L \times 100$. This is due to the change in the angle of the diagonal elements relative to the rods, that is associated with the altered segment aspect ratio.

8.4.2 Generic nematode circuit

As mentioned in Section 2.1.4, there are other nematodes that have similar nervous system structure to *C. elegans*. One such nematode, *Ascaris suum*, has been shown to have inhibitory connections going to both dorsal and ventral excitatory ventral cord motor neurons [113], and forms the basis of the “generic nematode” circuit shown in Figure 8.2A. In fact, the present model was initially developed based on this more symmetrical circuit, before discovering that one way neural inhibition was sufficient. Reverting the present neural model to this previous version can be easily accomplished. All that is required is to set $w_-^D = w_-^V$, $I_{AVB}^D = I_{AVB}^V$ and to reduce Equation 8.19 to $\gamma_m^k = 1$. However, as the model is then completely symmetric, it must be initialized with the states of all dorsal (or alternatively all ventral) neurons set to one, otherwise the symmetry will not be broken and no neurons will ever turn on.

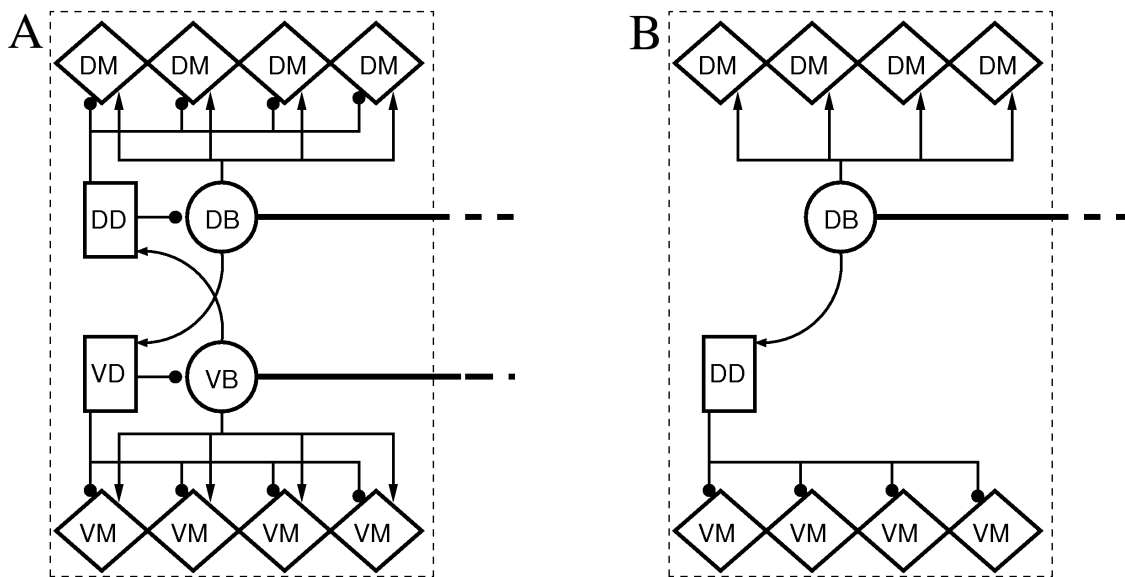


Figure 8.2: Modified schematics for alternative model variants. A) Generic nematode circuit with two-way neural inhibition. B) L1 larva circuit in which only dorsal neurons are present.

8.4.3 L1 circuit

At the time of hatching, L1 larva have significantly fewer neurons than the adult. A partial reconstruction of the L1 ventral cord [134] revealed that, at this developmental stage, the ventral cord locomotion circuit is significantly different and consists of only DA, DB and DD neurons (the VA, VB and VD neurons having not yet developed). In addition, the polarity of the DD neurons is different in that they receive input from DA and DB neurons and innervate muscles on the *ventral* side. Yet despite this circuit being hugely incomplete (relative to the adult), the L1 worm is capable of coordinated locomotion. While too little is known about the L1 circuit to model it accurately, it would still be interesting to test if the proprioceptive locomotion mechanism presented here could potentially work in the absence of ventral neurons, as in the circuit of Figure 8.2B.

In absence of information to the contrary, I will assume that the DD neurons are inhibitory at this developmental stage. I will also assume that the muscles on the ventral side of the L1 worm have a resting potential that is above the threshold for contraction (due either to their intrinsic dynamics or to tonic input from some other source). Both of these assumptions are very strong, and clearly mean that any results from this model variant must be taken as speculative. Under these assumptions the model is modified as follows. First, the model VB neurons are omitted, and the muscle input function previously given

by Equation 8.20 is replaced by

$$\begin{aligned} S_{\text{NMJ},m}^D &= w_{\text{NMJ}} S_{n(m)}^D \\ S_{\text{NMJ},m}^V &= 1 + \bar{w}_{\text{NMJ}} S_{n(m)}^D. \end{aligned} \quad (8.21)$$

Finally, the stretch receptor function given in Equation 8.19 is reduced to $\gamma_m^k = 1$, removing the stretch receptor bilinearity.

8.4.4 Minimal oscillator

Each unit of the neural model includes one DB and one VB neuron (in addition to the D-class neurons) which should oscillate in antiphase. In principle however, each of these neurons is capable of independent oscillation, provided it has a muscle to control and some associated tissue to receive feedback from. Thus each unit of the neural model actually consists of two semi-independent oscillators that communicate with each other via several pathways. First, the VB neuron is inhibited by DB via VD. Second, both VB and DB inhibit muscles on the other side of the body, via DD and VD respectively. Finally, there is indirect physical coupling via “internal pressure” (represented by the diagonal elements) that tends to extend one side when the other contracts. In order to test the effects of these different types of coupling, I have constructed a simplified version of the model with only a single neural unit consisting of one neuron of each class. Furthermore, the realistic body and environment are omitted in favour of a single pair of springs (dorsal and ventral), with each B-class neuron receiving stretch receptor feedback based on the length of the spring that it controls. These springs can be independent, but can alternatively be physically coupled by a “force” that attempts to maintain a constant sum of dorsal and ventral lengths. The strength of this coupling is set by the parameter α_{physical} . The length of the springs evolve according to

$$\frac{dL_{\text{spring}}^k}{dt} = (L_{0\text{spring}} - L_{\text{spring}}^k) - \alpha_{\text{physical}}(L_{\text{spring}}^k + L_{\text{spring}}^{\bar{k}} - 2) - f_M^k, \quad (8.22)$$

where L_{spring}^k is the length of the dorsal or ventral spring, $L_{0\text{spring}}$ is the rest length of the springs and f_M^k is the simplified muscle force given by

$$f_M^k = R(S^k + \bar{w}_{\text{NMJ}} S^{\bar{k}}). \quad (8.23)$$

Here the negative valued parameter \bar{w}_{NMJ} is the strength of the muscle inhibition and $R(x)$ denotes the ramp function whose value for positive x is x , and for negative x is zero

(used to prevent outwards directed muscle forces). The stretch receptor function is also simplified, being replaced by

$$I_{\text{SR}}^k = L_{\text{spring}}^k - 1. \quad (8.24)$$

Equations 8.14 and 8.15 are still used for the state transitions and total current input respectively.

8.4.5 Continuous neurons

The neural model presented in Section 8.3.2 makes use of two key simplifications, namely treating the neurons as binary (B-class) or linear (D-class) and instantaneous (both classes). However, it could certainly be argued that a mechanism that works with simple binary neurons would not necessarily work with more realistic continuous valued (and non-instantaneous) neurons. To validate the binary model I have developed an alternative version that uses more realistic neural dynamics and is presented here.

The most significant modification in this version of the model is to the dynamics of the B-class neurons themselves. Here I replace the binary neural states S_n^k , which were updated according to Equation 8.14, with continuous valued membrane potentials $V_{\text{mem},n}^k$ which evolve according to

$$\frac{dV_{\text{mem},n}^k}{dt} = \frac{1}{C_{\text{mem}}} \left(G_{\text{mem}} \left(V_{\text{rest}} - V_{\text{mem},n}^k \right) + I_n^k + I_{\text{act}} \right), \quad (8.25)$$

where C_{mem} , G_{mem} and V_{rest} are the membrane capacitance, membrane leak conductance and reversal potential respectively (see Table 8.3 for values). As before, I_n^k is the total input to the neuron while I_{act} models the active, self-exciting membrane current responsible for bistability and is given by

$$I_{\text{act}} = \frac{G_{\text{act}}}{1 + e^{-k_{\text{act}}(V_{\text{mem},n}^k - V_{\text{act}})}}, \quad (8.26)$$

where G_{act} is the maximum conductance of this channel. The parameters k_{act} and V_{act} determine the activation function for this channel and are given, along with G_{act} , in Table 8.3. These parameters were chosen to give realistic whole cell dynamics, as shown in Section 9.1.3.

The input term I_n^k follows a similar relationship to Equation 8.15, and is given by

$$\begin{aligned} I_n^D &= G_{AVB}(V_{AVB} - V_{\text{mem},n}^D) + I_{\text{SR},n}^D \\ I_n^V &= G_{AVB}(V_{AVB} - V_{\text{mem},n}^V) + I_{\text{SR},n}^V - \frac{G_{\text{GABA}}}{1 + e^{-k_{\text{GABA}}(V_{\text{mem},n}^D - V_{0,\text{GABA}})}} + I_{\text{bias}}, \end{aligned} \quad (8.27)$$

where G_{AVB} is the gap junction conductance from AVB neurons, whose (depolarized) membrane potential is given by V_{AVB} . The stretch receptor current is $I_{\text{SR},n}^k$ as before. The neural inhibition depends on the maximum synaptic conductance G_{GABA} , the activation parameters k_{GABA} and $V_{0,\text{GABA}}$ and the bias current I_{bias} . The values of all these parameters were chosen based on the behaviour of the model and are given in Table 8.3. The stretch receptor current $I_{\text{SR},n}^k$ is calculated similarly to before, with the parameter changes given in Table 8.3 and a new expression for γ_m^k that replaces Equation 8.19:

$$\gamma_m^k = \begin{cases} 2 & : (L_{\text{L},m}^k > L_{0\text{L},m}) \\ 1 & : (L_{\text{L},m}^k < L_{0\text{L},m}). \end{cases} \quad (8.28)$$

The muscle inputs previously given by Equation 8.20 are replaced by

$$I_{\text{NMJ},m}^k = \left(\frac{w_{\text{ACh}}}{1 + e^{-k_{\text{NMJ}}(V_{\text{mem},n(m)}^k - V_{0,\text{NMJ}})}} + \frac{w_{\text{GABA}}}{1 + e^{-k_{\text{NMJ}}(V_{\text{mem},n(m)}^k - V_{0,\text{NMJ}})}} \right), \quad (8.29)$$

where the w_{ACh} and w_{GABA} set the weights of the excitatory (ACh) and inhibitory (GABA) neuromuscular junctions, and the parameters $V_{0,\text{NMJ}}$ and k_{NMJ} determine the NMJ activation function. Finally, there is also a slight modification to the maximum muscle efficacies $F_{\text{max},m}$. All the modified parameters for the continuous model are given in Table 8.3. While the model is capable of coordinated locomotion (see Section 9.4.4), the increased complexity makes it much harder to tune for the desired behaviour. I have therefore treated it as a proof of concept, and have left the focus of my work on the binary model, whose relative simplicity better illustrates the fundamental principles of locomotion.

8.5 Implementation

The integrated model is implemented in C++. While the neural model is numerically straightforward, the physical model forms a stiff set of differential algebraic equations and is numerically more demanding, requiring an implicit solver. Rather than develop my own solver, I have made use of SUNDIALS IDA (version 2.3.0) [56], a freely available solver written in C and providing methods that are easily incorporated into C++ code.

Table 8.3: Continuous model parameters. Any parameters not given here are the same as in the original model.

| Param. | Val. | Param. | Val. | Param. | Val. |
|-------------------|----------------|-------------------|--|---------------------|--------------------------|
| G_{mem} | 500 pS | C_{mem} | 1 pF | V_{rest} | -72 mV |
| G_{act} | 20 pS | k_{act} | 500 | V_{act} | -60 mV |
| G_{GABA} | 10 pS | k_{GABA} | 100 | $V_{0,\text{GABA}}$ | V_{rest} |
| w_{ACh} | 3 | k_{NMJ} | 50 | $V_{0,\text{NMJ}}$ | -22 mV |
| w_{GABA} | -0.5 | G_{AVB} | 150 pS | V_{AVB} | -87.5 mV |
| I_{bias} | 8 pA | $G_{\text{SR},n}$ | $\frac{(5.12+1.28n)}{N_{\text{out}}}$ pS | $F_{\text{max},m}$ | $1 - \frac{0.4(m-1)}{M}$ |
| N_{SR} | $\frac{2M}{3}$ | Δ_M | 0.75 | | |

For efficiency, I have effectively separated the integration of the neural and physical models. The neuromuscular model is evolved using Euler integration with an integration time step of 1 ms (or 0.1 ms for the continuous model). For consistency, the solver of the physical model generates an output for every neural time step (but implicitly integrates with smaller, adaptive time steps). I use a base relative error tolerance of 10^{-12} . The absolute error tolerance for X and Y positions is set to 10^{-9} while for the rod angle ϕ (defined in Sections 5.2.2 and 8.2.1) I use an absolute tolerance of 10^{-5} . However, it is necessary to reduce all tolerances by a factor of 10 when simulating motion of the model with $M = 48$ in less resistive media $C_{\parallel} \leq 27.3 \times 10^{-6}$ or $C_{\perp} \leq 51.2 \times 10^{-6}$, as without this modification the integration fails (the model variant with $M = 24$ does not suffer from this problem).

8.6 Data analysis

In order to compare the behaviour of the model to that of the real worm, data analysis similar to that used in Chapter 4 was applied. It was not necessary to skeletonize the model's outputs because the (x, y) locations of the rod CoMs are readily available. To obtain a suitable "skeleton" required only that the model outputs were down sampled from 49 to 25 points by skipping every second point. However, as will be discussed in Section 9.2.2, some values of C_{\parallel} and C_{\perp} (indicated in Figure 9.6) resulted in uncoordinated locomotion characterised by a mismatch between head and tail frequencies. The resulting skeletons were excluded from the data analysis. The remaining skeletons were fed to the data analysis software developed by Stefano Berri so that locomotion parameters could be extracted as was done for experimentally obtained skeletons [13].

Chapter 9

Integrated model: Results

9.1 Model components

The model presented in Chapter 8 consists of several interlinked components. Here I will demonstrate the behaviour of some of these isolated components for independent validation.

9.1.1 Passive body properties

The first component of the model is the worm's passive body, embedded in a virtual environment. My modelling approach relies on the independent validation of each component (where possible) before integrating with the rest of the model. This way one reduces the number of simultaneous free parameters and takes advantage of as much information as possible. The behaviour of the passive model is based on experiments reported in a PhD thesis by Pascal Sauvage [103], which are the only such experiments that I have been able to find. Two key figures from that work show the body dynamics of a flaccidly paralysed worm in water and on agar. They show that a bent worm on an agar surface will remain in this bent shape indefinitely. Conversely, a bent worm in water straightens incredibly quickly upon release, taking approximately 20 ms to do so. However, it was necessary to make certain compromises when reproducing these behaviours. First, the worm can only remain bent *indefinitely* on agar because of the gel's yield stress (roughly equivalent to static friction), which must be overcome before any motion will occur. Since I model the

gel with local resistance coefficients, the yield stress is outside the scope of the model. Instead I have chosen the model parameters so that the passive worm on agar straightens slowly over several minutes (see Figure 9.1 B). In water, the worm is observed to straighten fully in a mere 20 ms. When I attempted to obtain this same behaviour from the model, I found that the equations became extremely stiff, causing problems for the integrator. I therefore increased the internal damping so that the passive model straightens in about 80 ms, thereby solving the numerical problems (see Figure 9.1 A). While this is four fold slower than the real worm this approximation should be acceptable since, in either case, the passive body straightens much faster than the body of an actively locomoting worm.

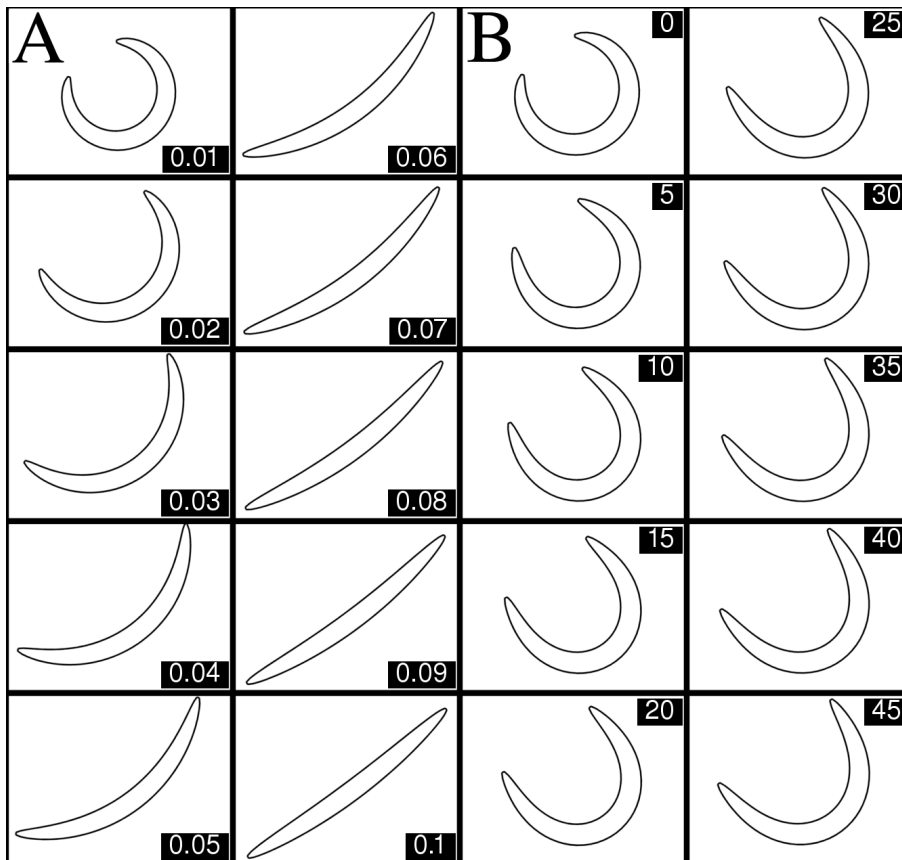


Figure 9.1: Frames taken from a simulation showing the dynamics of the passive physical model, with frame times (in seconds) given in the corner. The model is manually bent either in water (A) or on agar (B) before being released at $t = 0$.

9.1.2 Muscle properties

The muscle force model presented in Section 8.2.4 was designed as a simple way to reproduce two key qualitative properties of biological muscle [55]. Specifically, the force a muscle exerts depends on both its length and rate of contraction in addition to the level of activation. Figure 9.2 shows the force/length and force/velocity relationships for the muscle model, which are qualitatively similar to those of a typical biological muscle. Note, however, that I have not been able to find a characterization of nematode muscle. Having imbued the muscles with these properties, they are integrated with the passive body to yield the complete physical model.

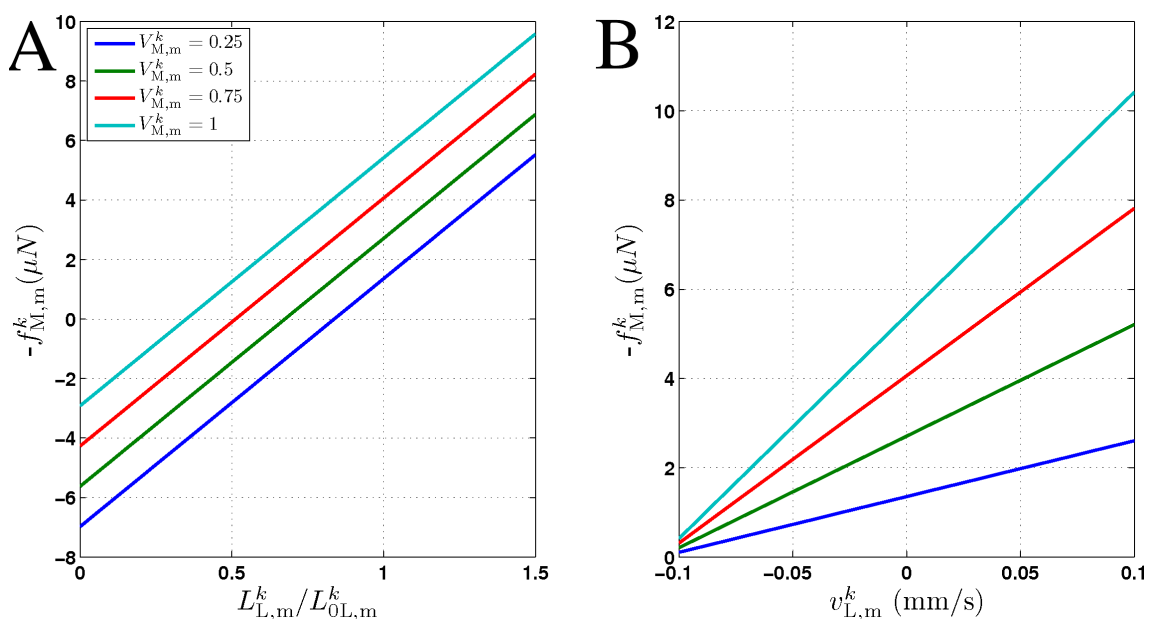


Figure 9.2: The force generated by model muscles is a function of their activation, length and rate of contraction. A) Force/length relationship obtained by holding the muscle at a specific length (preventing it from contracting). B) Force/velocity relationship obtained by allowing the muscle to contract at a specified rate and measuring the force it exerts at the moment it reaches its rest length L_{0L} . The model therefore provides a simple linear approximation of these properties of biological muscles. Note that in both cases $-f$ is plotted for simplicity, because contractile forces are defined as negative in the model.

9.1.3 Neuron properties

The dynamics of the model B-class neurons approximate those of recently characterized RMD motor neurons in the head [85]. The key properties that my model incorporates are bistability and hysteresis. The dynamics of the model neurons is shown in Figure 9.3 for

both the binary and continuous versions.

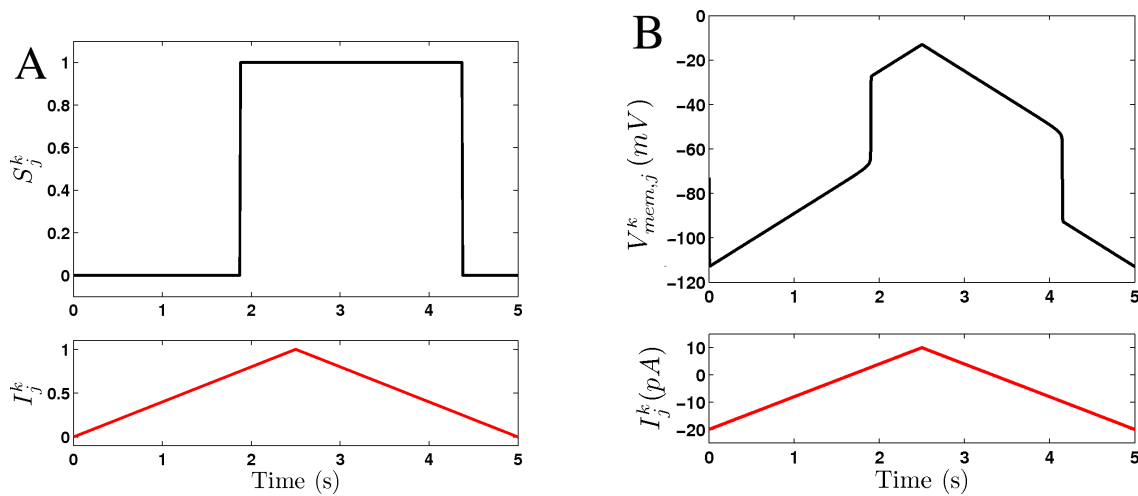


Figure 9.3: Dynamics of A) binary and B) continuous model B-class neurons. Note the different thresholds for activation and deactivation.

9.2 Integrated model

I have begun with the premise, grounded in *C. elegans* behaviour (see Chapter 4) and circuitry (see Section 2.1.4), that a single neural circuit is responsible for all of the worm’s forward locomotion, from slow, short wavelength sinuous “crawling” patterns to fast, long wavelength “swimming” patterns. With this in mind, I set out to develop a model of this neural circuit and its modulation that can account for the entire range of behaviours demonstrated in Section 4.3.1. Here I will present the results of this integrated neuromechanical model. Note that all simulations use the same initial conditions, with the body initialized in a straight line and all neuron states set to zero, unless stated otherwise.

9.2.1 A single mechanism accounts for swimming and crawling

The parameters given in Chapter 8 were chosen based on the behaviour of the integrated model in virtual water and agar environments. In fact it was remarkably easy to find parameters that gave realistic locomotion on agar, while more effort was required to make the model behave correctly in water. This suggests that the crawling behaviour may be more robust than swimming. None the less, I was able to find a single set of parameters that allow the model to reproduce locomotion in both environments with quite realistic undulation frequencies and waveforms (Table 9.1, Figure 9.4, Supplementary movies C9_1 and C9_3). Crucially, this is accomplished without any explicit modulatory mechanism

(beyond the proprioceptive feedback). Indeed, the *only* changes necessary to obtain these two locomotion behaviours are to the drag coefficients C_{\parallel} and C_{\perp} that define the model environment.

Unfortunately the results are not perfect, as the model oscillates about 40% faster than it should in water. I was unable to find parameters for the neural model that slowed the oscillations sufficiently without degrading other aspects of the behaviour. While the problem could have been solved by changing parameters of the physical model, I had already decided that I would not allow modifications of the physical parameters after fixing them as described in Section 7.3.1. The implications of this problem will be further discussed in Section 11.2.2. None the less, despite its imperfections, the model certainly captures the essence of swimming and crawling so the next step is to investigate the extent to which it generalises to other environments. Having chosen parameters based on the behaviour in these two specific media, this will be an important test of the model’s predictive power.

Table 9.1: Locomotion metrics for real (top) and simulated (bottom) worms moving in water and on agar. Values are given as mean \pm standard deviation. Note that the standard deviation for simulated worms is always zero.

| | | | | | | | |
|------------------------------------|-----------------|--------------------|-----------------|-----------------------------------|-----------------|-------------------|-----------------|
| $\frac{\lambda_{\text{water}}}{L}$ | 1.56 ± 0.13 | F_{water} | 1.59 ± 0.10 | $\frac{\lambda_{\text{agar}}}{L}$ | 0.58 ± 0.02 | F_{agar} | 0.38 ± 0.03 |
| $\frac{\lambda_{\text{water}}}{L}$ | 1.56 | F_{water} | 2.27 | $\frac{\lambda_{\text{agar}}}{L}$ | 0.65 | F_{agar} | 0.41 |

9.2.2 Evaluating the swim-crawl transition

Having experimentally mapped the worm’s transition from swimming to crawling in Chapter 4 and found it to be characterized by a smooth and monotonic frequency-wavelength relation (Figure 9.5), the obvious next step is to see how well the model reproduces this transition. One difficulty, discussed in Section 8.2.2, is an absence of data regarding the properties (C_{\parallel} and C_{\perp}) of the gelatin solutions used in the experiment. At this stage it is not clear if the observed linear relationship between frequency and wavelength depends on the way the drag coefficients change with increasing concentration. To address this question I have performed simulations in a large class of virtual media with drag coefficients ranging from water to agar as illustrated in Figure 9.6. It is important to stress, however, that this was essentially a 2D parameter sweep, where no relationship between C_{\parallel} and C_{\perp} was imposed ¹.

¹While no relationship was imposed, certain combinations of C_{\parallel} and C_{\perp} were excluded based on the ratio K . Since it is not possible for a gelatin solution to have $K < K_{\text{water}} \approx 1.5$, I have only performed

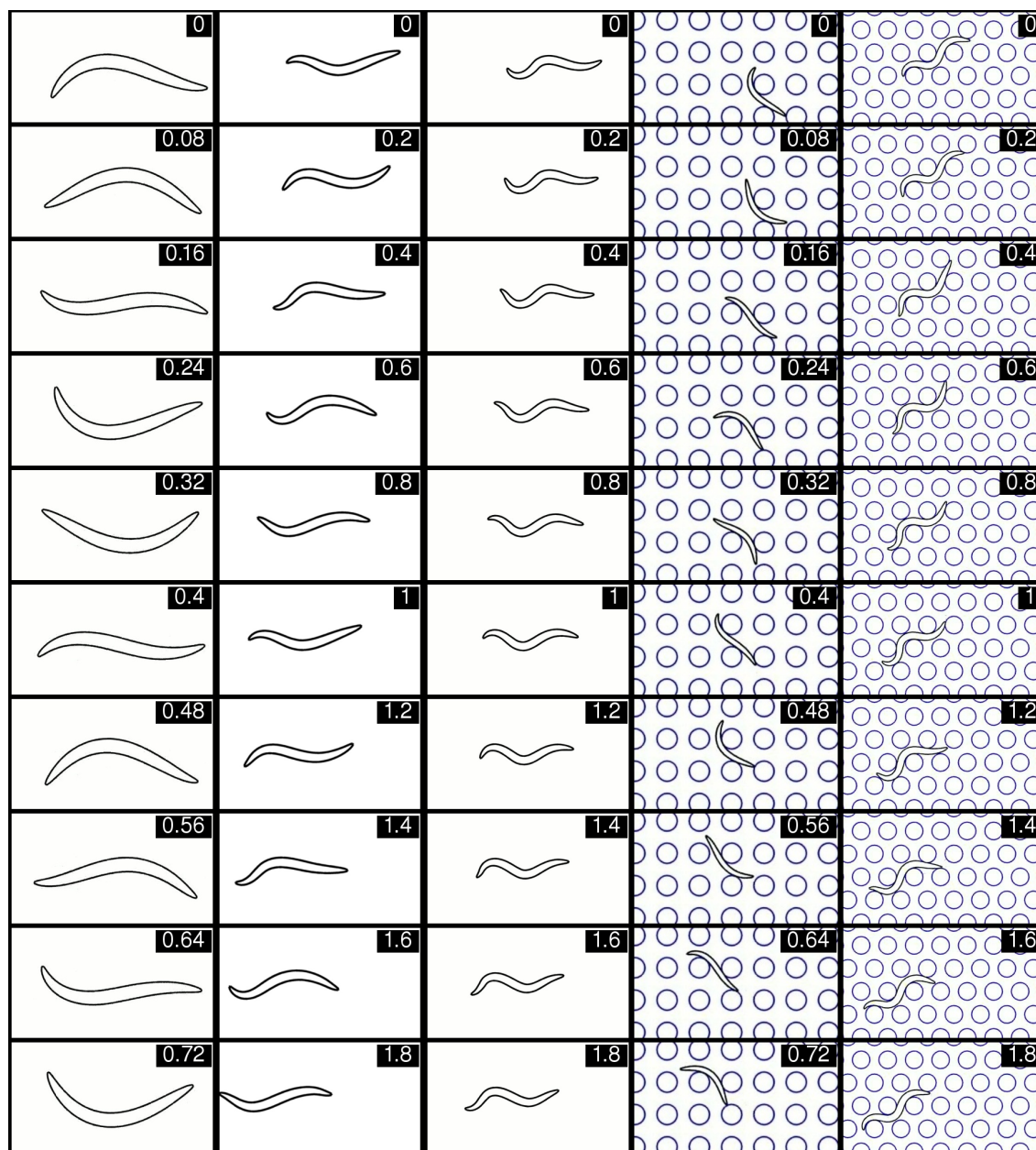


Figure 9.4: Stills taken from movies of the model moving in (from left) water, intermediate gelatin, agar, a microfluidic environment as described in [90] and a microfluidic environment as described in [78] (see Supplementary movies C9_1 to C9_5). Frame times, in seconds, are given in the top right corner.

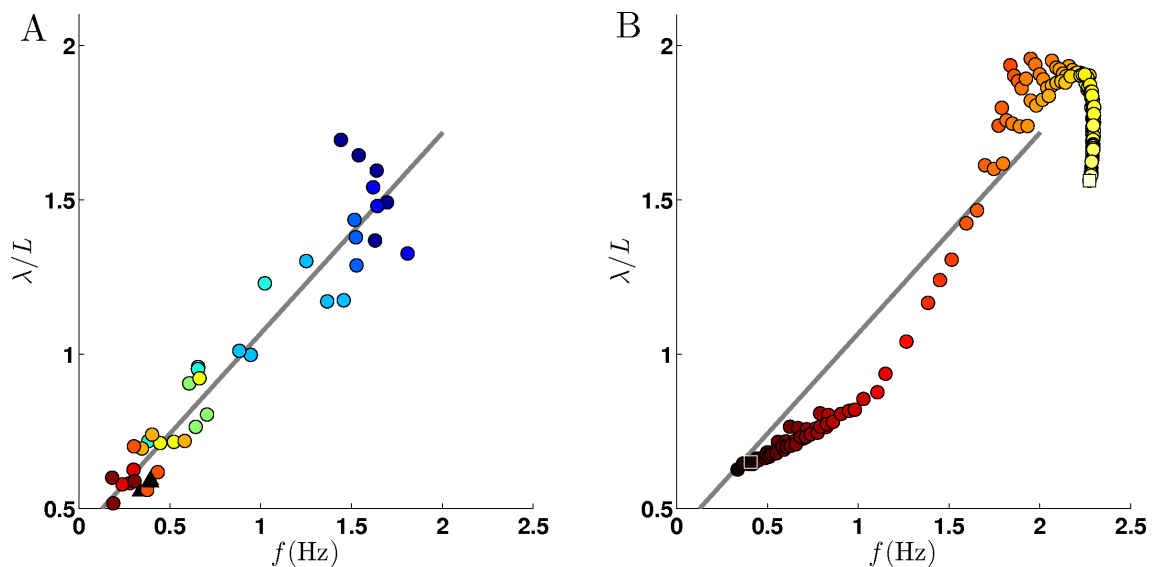


Figure 9.5: A) Experimentally observed transition from swimming to crawling, from Chapter 4, showing locomotion in gelatin (circles; colours indicates percent gelatin concentrations as in Figure 4.2) and agar (black triangles). The grey line is the best linear fit to the data. B) The model reproduces the swim-crawl transition with reasonable quantitative agreement. Colours denote the product of tangential and normal drag coefficients, ranging from light yellow (virtual water) to dark red (virtual agar) and correspond to the colours in Figure 9.6. The data points representing water and agar are marked with squares of the appropriate colour. Wave properties are extracted as described in Section 8.6. The grey line is again the linear fit from panel A), provided for comparison.

Overall the results are very promising, although there is certainly room for improvement. The model is indeed capable of intermediate behaviours (Figure 9.4 and Supplementary movie C9_2) and qualitatively reproduces the continuous transition (see Figure 9.5) from swimming to crawling. Indeed it is quite remarkable that this can be achieved without any direct modulation of the neural circuit. Furthermore, the relationship between wavelength and frequency is preserved for all combinations of C_{\parallel} and C_{\perp} that were tested (except those that yield uncoordinated locomotion, as described below), suggesting that this is a fundamental property of the locomotion system.

With regard to limitations, there are two main issues that warrant mentioning. The first of these is immediately apparent from Figure 9.5. While the experimentally observed transition is monotonic, the model's transition exhibits an initial increase in wavelength as the frequency decreases. Following this anomaly, the transition continues largely how it should. Unfortunately I have been unable to determine the cause of this problem, but

simulations where $1.5 \leq K \leq 40$.

this issue will be revisited in the discussion in Section 11.2.2.

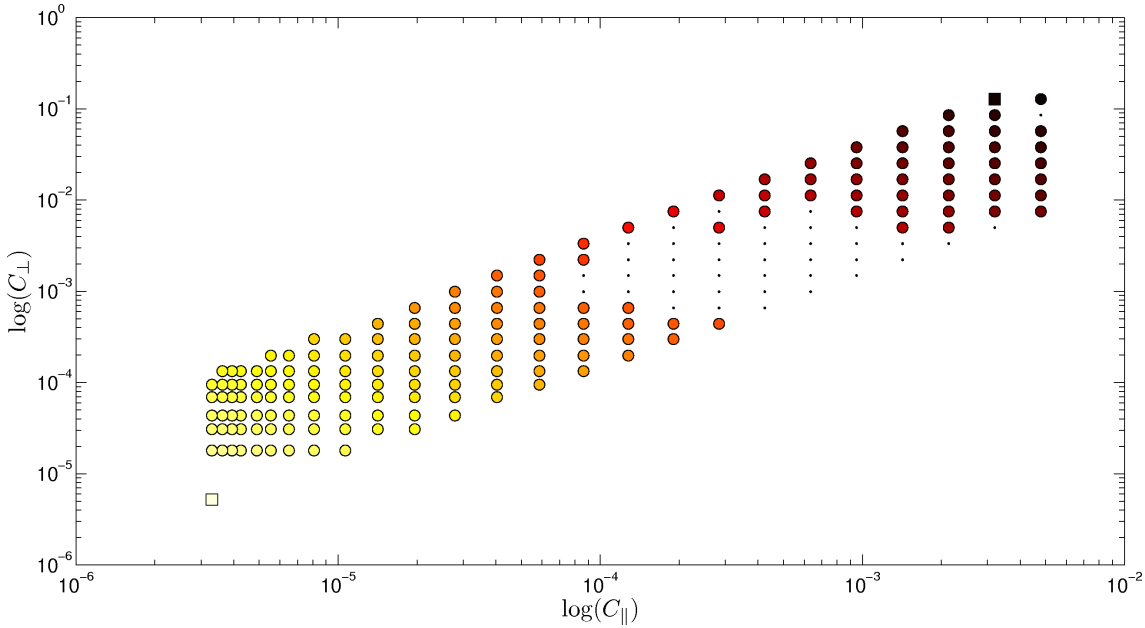


Figure 9.6: Values of C_{\parallel} and C_{\perp} used to evaluate the swim-crawl transition. Values for each drag coefficient range from water (pale yellow square) to agar (dark red square), but only combinations that yield $1.5 \leq K \leq 40$ were used. Of those combinations for which simulations were performed, some yielded uncoordinated locomotion as described in the text. These values are marked with black dots. Data from the remaining combinations (filled circles) was used to generate Figure 9.5. Colours denote the product of tangential and normal drag coefficients, ranging from light yellow (virtual water) to dark red (virtual agar).

The second issue is that some combinations of C_{\parallel} and C_{\perp} for which simulations were performed yield uncoordinated locomotion. Specifically, the inter-unit coupling fails to maintain the correct phase relationship along the body, leading to phase slips every few cycles. The result is that the locomotion wave becomes periodic over several cycles of local undulation – the waveform looks coordinated most of the time, but strange contortions pass down the body each time a phase slip occurs (see Supplementary movie C9_6). These uncoordinated simulations were identified by comparing the head and tail frequencies and were omitted from the data analysis and therefore from Figure 9.5. The C_{\parallel} , C_{\perp} combinations for which this occurred are marked with black dots in Figure 9.6. It is not clear why this phenomenon occurs when it does, but it would be interesting to know what trajectory is taken through the C_{\parallel} , C_{\perp} landscape when the gelatin concentration is gradually increased.

Despite these problems, it is reassuring to see that the model does not break down

in media besides water and agar. The model's behaviour suggests that some significant aspects of the worm's locomotion mechanism have been successfully captured, but that further refinement is required. Possible avenues for improvement will be discussed in Section 11.4.

9.2.3 The model works in artificial dirt environments

In addition to studying *C. elegans* locomotion in homogeneous media, locomotion in complex environments with solid obstacles can shed light on the worm's proprioceptive response and closed loop motor control. In particular, arrays of micro-fluidic posts ("artificial dirt") have recently been developed specifically for this purpose [78,90]. I recreated model microfluidic chambers (see Section 8.2.2) with the same quasi-2D hexagonal arrays as in Ref. [78] and square arrays as in Ref. [90] and used these to perform simulations of the integrated model. I found that the model copes well with these environments, producing remarkably realistic locomotion (Figure 9.4, Supplementary movies C9_4 and C9_5) when compared to the (admittedly sparsely) reported behaviour [78,90].

As in the reported experiments, the model yields crawling-like behaviour in the hexagonal post configuration [78] and swimming like motion in the cubic configuration [90]. To investigate whether the difference in behaviour can be attributed to the layout of the posts or increased resistance (due to the ceiling effect described in Section 8.2.2), I performed simulations with variable post sizes and inter-post separations; with either water- or agar- filled chambers; and with or without an effective ceiling [78]. I found that in either square or hexagonal post configurations, closely spaced posts tend to impose crawling-like body shapes on the model worm (see Figure 9.7 A and Supplementary movie C9_7), with amplitude and wavelength depending on the post size and configuration. Diluting the environment (and removing any effective resistance from a ceiling) leads to a modulation of the frequency, but has only a minor effect on the waveform (not shown). Interestingly, I found that locomotion is difficult to achieve in some configurations with agar-filled chambers (see Figure 9.7 B and Supplementary movie C9_8). Here, the agar imposes a crawling-like waveform which is incompatible with the post layout, so the posts essentially become obstacles.

9.2.4 The model reproduces contact forces

At the time I developed the present model, no direct measurements of the force exerted by a moving worm had been reported. It was therefore necessary to rely on behavioural observations in conjunction with quantitative estimates of the environmental properties in

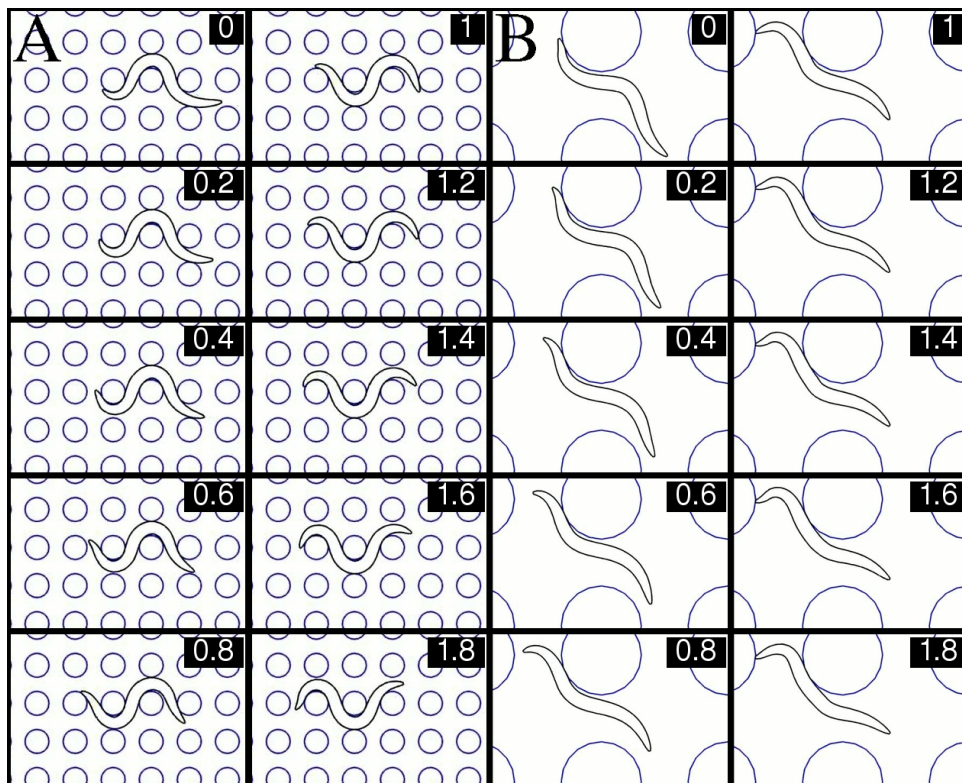


Figure 9.7: Stills taken from movies of the model moving in novel microfluidic environments. A) A square layout can also impose a crawling-like waveform if the posts are sufficiently closely spaced and with the addition of a ceiling effect as in Ref. [78]. B) With agar-filled chambers, which impose a crawling-like waveform, widely spaced posts can become obstacles.

order to set the parameters of the physical model. However, a measurement of the force exerted by *C. elegans* as it moves against a microfluidic pillar was recently reported in Ref. [35]. This provided an unexpected opportunity to perform an independent validation of the physical model (on agar at least), and thereby also of the method used to develop it.

I recreated an equivalent setup in the model, using the framework for artificial dirt simulations but with only a single post. I measured the contact force between the model worm and the post by recording the reactive force exerted by the latter. I analysed $n = 17$ examples of worm/post interactions, most of which involved the worm brushing past the post. Peak forces within each clip are $0.84 \pm 0.22 \mu\text{N}$. To estimate the maximum force, I simulated a worm moving straight into a large post, giving a peak force of $1.27 \mu\text{N}$. These values are remarkably close to the experimentally reported value of $2.5 \pm 2.5 \mu\text{N}$ [35]. While the experimental data was clearly very noisy (with standard deviation equal to

the mean), it would appear that the forces exerted by the model are slightly less than they should be. Thus, despite this test providing an important validation that the model parameters are approximately correct, any future version of the model would benefit from having access to this data at an earlier stage of development.

9.3 Model analysis

9.3.1 Effects of coupling

In the integrated model, communication between DB and VB neurons is mediated by a combination of muscle inhibition, neural inhibition and physical forces of the body and environment. This coupling is responsible for maintaining the correct antiphase relationship between dorsal and ventral neurons. In order to investigate the effects of these three forms of coupling, I developed a stripped down version of the model that is presented in Section 8.4.4. The model has three coupling parameters \bar{w}_{NMJ} , w_{-}^{V} and α_{physical} which determine the strength of the muscle inhibition, neural inhibition and physical interaction respectively. When all of these parameters are set to zero, the dorsal and ventral sides oscillate totally independently, as shown in Figure 9.8 A. I will begin by demonstrating the effect of each form of coupling independently. The effect of neural inhibition is intuitive and very robust. Over a wide range of values for w_{-}^{V} (from 0.1 to 10 was tested), neural inhibition imposes an antiphase relationship (see Figure 9.8 B). For values of 1 or more, this even works in the face of an inherent frequency difference. One way neural inhibition imposes synchrony very effectively – the main difference when compared to two way inhibition is that the amplitude and offset of the dorsal and ventral oscillations are different, but this is compensated for in the full model.

The effect of physical coupling is also quite intuitive. In the real worm, the pressure of the internal fluid will tend to maintain a constant volume in the body. In my physical model, this effect is approximated by the diagonal springs. The physical coupling in this simplified model is implemented differently (see Section 8.4.4), but has an equivalent effect. Whenever the sum of the dorsal and ventral lengths is greater than (less than) two, the coupling will tend to shorten (lengthen) both sides. As expected, physical coupling effectively imposes an antiphase relationship over a wide range of α_{physical} (see Figure 9.8 C). For $\alpha_{\text{physical}} \geq 0.2$, synchrony occurs within two or three cycles, except that oscillations break down for $\alpha_{\text{physical}} > 1.45$. However, it is not clear how strong this synchronizing effect would be in the context of the full physical model. As it turns out, there are some cases where physical coupling is sufficient to synchronise the dorsal and

ventral oscillations correctly in the full model. This will be shown in Section 10.2.

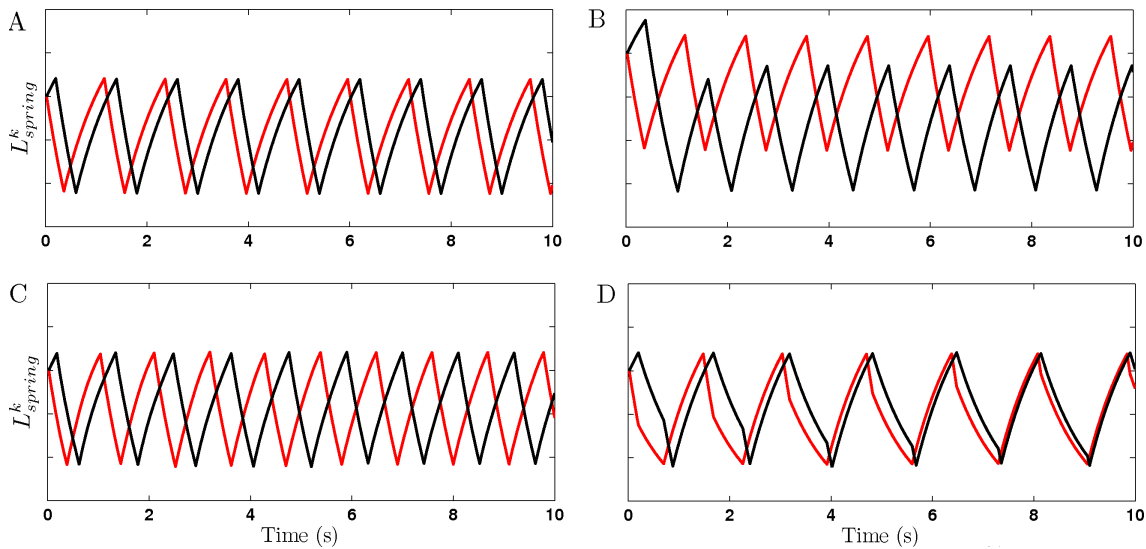


Figure 9.8: Effect of coupling in the minimal oscillator model with one DB (red) and one VB (black) neuron. A) No coupling is included, allowing the dorsal and ventral neuron to maintain their starting phase lag. B) The addition of neural inhibition ($w_-^V = 0.4$) efficiently imposes an anti-phase relationship. C) Physical coupling ($\alpha_{\text{physical}} = 0.3$) also imposes an anti-phase relationship, though it does so more slowly. D) Contrary to conventional wisdom, muscle inhibition ($\bar{w}_{\text{NMJ}} = 0.4$) tends to impose in-phase synchrony.

The last effect to investigate is that of muscle inhibition. Contralateral inhibition of muscles by D class neurons is generally believed to contribute to locomotion by imposing the required antiphase relationship [84]. But in contrast to this hypothesis, I have found that muscle inhibition actually pushes the neurons towards *in phase* synchrony, as shown in Figure 9.8 D. The speed at which this happens depends on the strength of the coupling. However, for $\bar{w}_{\text{NMJ}} > 0.53$ the oscillations are quickly quenched. For slightly lower values, oscillation continues but at significantly reduced frequency. Both of these effects are due to the fact that once the neurons are in phase, they inhibit each other while they are on, thereby reducing the total output to the “muscles”.

To explain this counter intuitive result, one must carefully consider what is happening. Assume that the neurons are oscillating with a phase lag close to 180° . At the instant that the dorsal neuron switches on, the ventral neuron is slightly behind schedule and has not yet switched off. Now, if the dorsal neuron was inhibiting the ventral neuron directly, the onset of the inhibition would push the ventral neuron *closer* to its “off” threshold, thereby causing it to switch off sooner and hence reducing the phase error. If instead the dorsal neuron inhibits the ventral muscle, the effect of the inhibition is to relax the muscle.

Superficially this looks like the correct effect – the dorsal muscle is relaxing too late, and this makes it relax sooner. But what effect does this have on the underlying neural state? Causing the muscle to relax and therefore lengthen will increase the stretch input into the dorsal neuron, pushing it *further* from its “off” threshold, thereby causing it to switch off later and hence making the phase error larger. The only time this would not happen is when the neurons are already in exact antiphase. Muscle inhibition is likely to have this effect in the context of any model that relies on stretch receptors that cause depolarization in response to elongation.

Next one can ask which effect would dominate when multiple forms of coupling are present. Physical coupling and neural inhibition have the same effect, so combining them is not particularly interesting. When muscle inhibition and neural inhibition are both included, neural inhibition is dominant. Even for the maximum value of $\bar{w}_{\text{NMJ}} = 0.53$, weak neural inhibition ($w_-^V \geq 0.1$) is sufficient to impose a nearly antiphase relationship. For $w_-^V = 0.5$, the muscle inhibition has no detectable effect on the phase lag (see Figure 9.9 A). The interaction of muscle inhibition with physical coupling is more complex. There are ranges of combinations for which oscillations die out, for which the muscle inhibition dominates and for which the physical coupling dominates. Examples of these are illustrated in Figure 9.9 B-D.

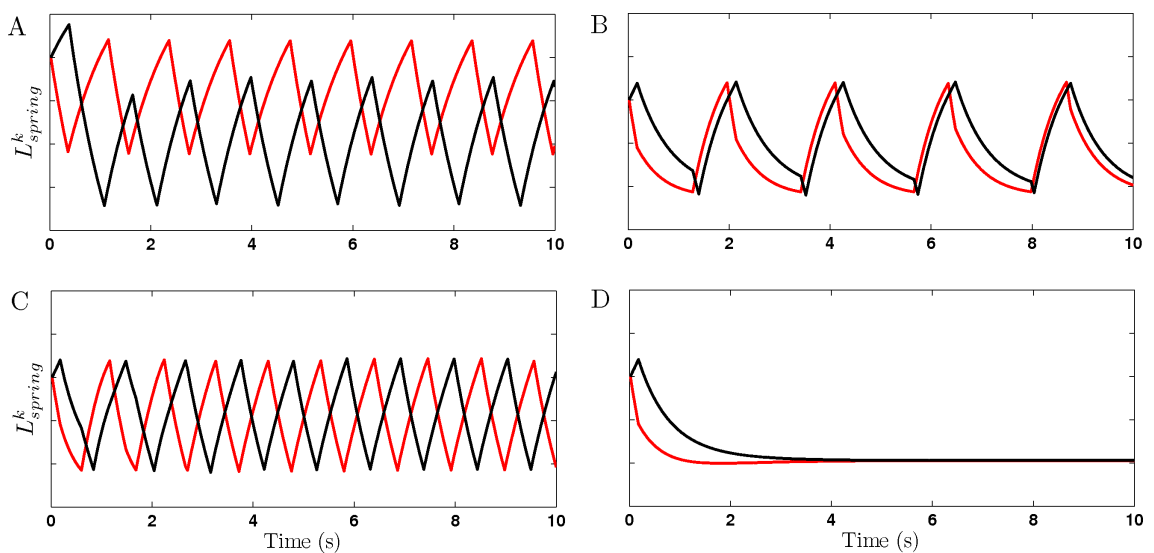


Figure 9.9: Interaction between multiple forms of coupling. A) With neural and muscle inhibition, the effect of neural inhibition wins. When combining physical coupling with muscle inhibition, different effects are possible. B) If physical coupling is sufficiently weak, muscle inhibition dominates, whereas if muscle inhibition is sufficiently weak (C), physical coupling dominates. D) If neither is sufficiently weak, oscillations are quenched.

9.3.2 Effect of neural inhibition

In the previous section I demonstrated the synchronizing effect of several forms of coupling. In light of the results therein, it is less surprising that I have found it necessary to include neural inhibition in the model. It would appear that muscle inhibition cannot take the place of neural inhibition, and although the physical coupling also pushes the dorsal and ventral neurons towards antiphase, its effect was found to be less robust. Here I will further investigate the effect of neural cross inhibition by means of a simple state analysis of a single oscillator unit.

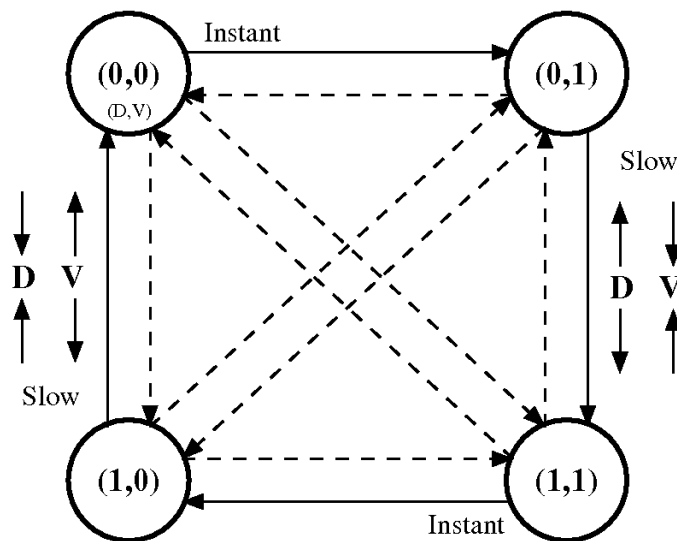


Figure 9.10: State transition diagram for the B class model neurons. See text for an explanation.

Figure 9.10 shows the state transition diagram for the B class model neurons. For each dorsal/ventral neuron pair, there are four possible states, represented by the large circles in the figure. In order to generate the alternating dorsal/ventral bending required for locomotion, the model must periodically cycle between the (0,1) and (1,0) states. While it is technically possible to make this transition directly, this would require that both neurons reached their respective thresholds at exactly the same moment. This is highly unlikely (and unstable), particularly in the full integrated model where segments are continually perturbing each other. Instead, the model will tend to go via either the (0,0) or (1,1) states. If we assume that both neurons cannot change state at exactly the same time, all four diagonal transitions become impossible. Stable oscillation will therefore require either a clockwise or anticlockwise path through the diagram. As we will see, with inhibition going only to ventral neurons the steady state behaviour will be

to cycle clockwise through the state diagram, following the solid arrows. If it was the dorsal neurons that received inhibition, the model would cycle counter-clockwise instead.

Because the model relies on sensory feedback, state transitions will only occur in response to a change in stretch receptor input. This in turn will only occur when the body changes its configuration. One must therefore consider how the body will move when the system is in each of the four states. When in the $(0, 1)$ state, the ventral muscle will contract while the dorsal muscle elongates, leading to ventral bending (the opposite occurs in the $(1, 0)$ state). Thus the model will dwell in these states while the body shape changes, until one of the stretch inputs I_{SR}^k reach the critical value $\sigma_{(S_D, S_V)}^k$ (see Table 9.2). However, when the model is in the $(0, 0)$ or $(1, 1)$ state, no predictable change in body shape will occur. This imposes the additional constraint that any body configuration that causes a transition $(0, 1) \rightarrow (1, 1)$ (or $(1, 0) \rightarrow (0, 0)$) must also immediately satisfy the conditions for a transition $(1, 1) \rightarrow (1, 0)$ (or $(0, 0) \rightarrow (0, 1)$). In order to cycle correctly through the state diagram, certain asymmetries in the transition thresholds are required. First, it is essential that the thresholds for all transitions $A \rightarrow B$ are different to that for $B \rightarrow A$, otherwise the system would tend to “bounce back” whenever it made a transition. This asymmetry is provided by the B-class hysteresis, which makes the transition threshold for each neuron depend on its own state.

In addition to this self-dependence, further asymmetry is required. Without dorso-ventral communication, the transition thresholds for a given neuron are not affected by the state of the opposite neuron. Consequently the two vertical branches in the figure will be identical to each other, as will the two horizontal branches. While it may not be immediately obvious, this is a fatal flaw. Let us assume the system is in the $(1, 0)$ state. At a certain time the dorsal side will have contracted enough that the dorsal neuron will switch off (alternatively the ventral side could have stretched enough that the ventral neuron switches on, but that would simply reverse the path through the graph), leading to a transition to $(0, 0)$. To avoid getting stuck in this state, it is essential that the transition to $(0, 1)$ be made immediately. However, if the conditions for $(0, 0) \rightarrow (0, 1)$ are met, then so are the conditions for $(1, 0) \rightarrow (1, 1)$, which means that this transition would have occurred before $(1, 0) \rightarrow (0, 0)$. This is further illustrated in Table 9.2. The first column gives the transitions that must be made in sequence (again, an equivalent result is obtained for counter-clockwise rotation by switching all dorsal and ventral neuron properties) and is expanded into individual neuron transitions in column 2. Based on these transition requirements the total stretch input into each neuron (I_{SR}^k) must either exceed or not exceed the critical values $\sigma_{(S_D, S_V)}^k$, according to column 3. These thresholds are state dependent, with $\theta_+ = \frac{1}{2}(1 + \epsilon_{hys})$ and $\theta_- = \frac{1}{2}(1 - \epsilon_{hys})$. When neural inhibition

is included, the thresholds on the ventral side also depend on the dorsal state. Finally, the physical model imposes a relation between dorsal and ventral lengths, and therefore also the stretch currents. Specifically, $I_{SR}^k = -\bar{I}_{SR}^k \pm \delta_{SR}$, where the error δ_{SR} depends on body properties and external perturbations. The maximum allowable δ_{SR} depends on the relative values of the thresholds $\sigma_{(S_D, S_V)}^k$. When direct neural inhibition is included, it is possible to satisfy all the requirements on $\sigma_{(S_D, S_V)}^k$ simultaneously. Without this neural inhibition, however, certain values of $\sigma_{(S_D, S_V)}^k$ (indicated in red) fail to meet the requirements. By changing other parameters these violations can be moved around the graph, but they cannot be eliminated.

It should also be noted that, with one way neural inhibition, the role of the dorsal and ventral neurons are actually quite different. Under normal conditions, the dorsal neuron acts as the “master”, and is responsible for triggering both the $(1, 0) \rightarrow (0, 0) \rightarrow (0, 1)$ and the $(0, 1) \rightarrow (1, 1) \rightarrow (1, 0)$ transitions.

Table 9.2: State transitions and associated thresholds. See text for an explanation.

| Transition | Transition | Condition on I_{SR}^k | Requirements on $\sigma_{(S_D, S_V)}^k$ | Value with GABA | Value without GABA |
|---------------------------|-------------------------|---|--|-----------------------------|-----------------------------|
| $(0,0) \rightarrow (0,1)$ | $S_D : 0 \rightarrow 0$ | $I_{SR}^D \leq \sigma_{(0,0)}^D = \theta_+ - I_{AVB}^D$ | $\sigma_{(0,0)}^D > \sigma_{(1,0)}^D$ | $\sigma_{(0,0)}^D = 0.075$ | $\sigma_{(0,0)}^D = 0.075$ |
| | $S_V : 0 \rightarrow 1$ | $I_{SR}^V > \sigma_{(0,0)}^V = \theta_+ - I_{AVB}^V$ | $\sigma_{(0,0)}^V < \sigma_{(1,0)}^V$ | $\sigma_{(0,0)}^V = -0.425$ | $\sigma_{(0,0)}^V = -0.425$ |
| $(0,1) \rightarrow (1,1)$ | $S_D : 0 \rightarrow 1$ | $I_{SR}^D > \sigma_{(0,1)}^D = \theta_+ - I_{AVB}^D$ | $\sigma_{(0,1)}^D > 0$ | $\sigma_{(0,1)}^D = 0.075$ | $\sigma_{(0,1)}^D = 0.075$ |
| | $S_V : 1 \rightarrow 1$ | $I_{SR}^V > \sigma_{(0,1)}^V = \theta_- - I_{AVB}^V$ | $\sigma_{(0,1)}^V < -\sigma_{(0,1)}^D - \delta_{SR}$ | $\sigma_{(0,1)}^V = -0.925$ | $\sigma_{(0,1)}^V = -0.925$ |
| $(1,1) \rightarrow (1,0)$ | $S_D : 1 \rightarrow 1$ | $I_{SR}^D > \sigma_{(1,1)}^D = \theta_- - I_{AVB}^D$ | $\sigma_{(1,1)}^D < \sigma_{(0,1)}^D$ | $\sigma_{(1,1)}^D = -0.425$ | $\sigma_{(1,1)}^D = -0.425$ |
| | $S_V : 1 \rightarrow 0$ | $I_{SR}^V \leq \sigma_{(1,1)}^V = \theta_- - I_{AVB}^V + w_-$ | $\sigma_{(1,1)}^V > \sigma_{(0,1)}^V$ | $\sigma_{(1,1)}^V = 0.075$ | $\sigma_{(1,1)}^V = -0.925$ |
| $(1,0) \rightarrow (0,0)$ | $S_D : 1 \rightarrow 0$ | $I_{SR}^D \leq \sigma_{(1,0)}^D = \theta_- - I_{AVB}^D$ | $\sigma_{(1,0)}^D < 0$ | $\sigma_{(1,0)}^D = -0.425$ | $\sigma_{(1,0)}^D = -0.425$ |
| | $S_V : 0 \rightarrow 0$ | $I_{SR}^V \leq \sigma_{(1,0)}^V = \theta_+ - I_{AVB}^V + w_-$ | $\sigma_{(1,0)}^V > -\sigma_{(1,0)}^D + \delta_{SR}$ | $\sigma_{(1,0)}^V = 0.575$ | $\sigma_{(1,0)}^V = -0.425$ |

9.4 Model variants

Here I will present results from the alternative model variants introduced in Section 8.4. These variants, while interesting, are not the focus of this work. The results will therefore be presented only briefly.

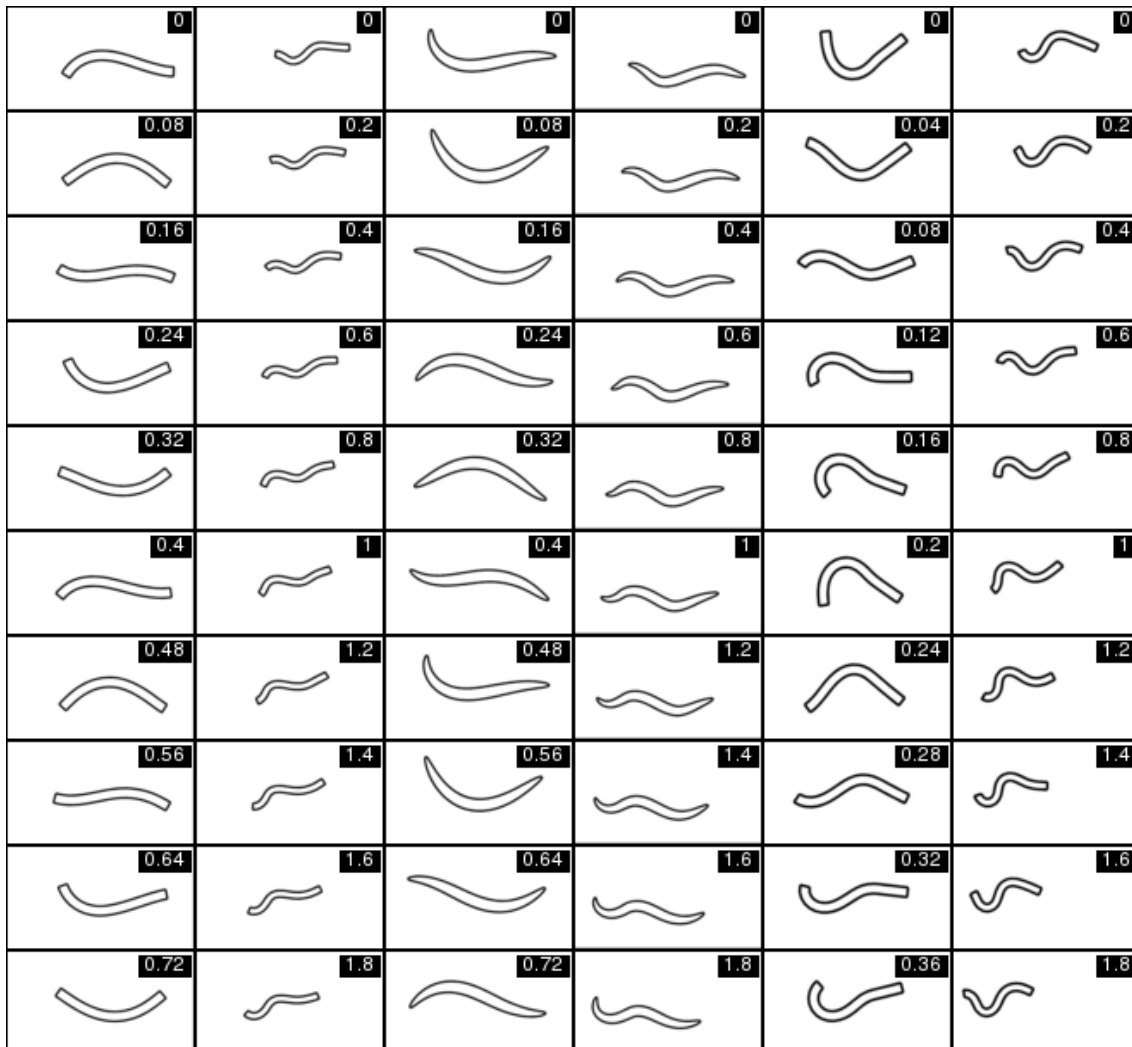


Figure 9.11: Stills taken from movies of model variants, with the frame time (in seconds) given in the top right corners. The conditions are (from left) rectangular body model in water, rectangular body model on agar, L1 model in water, L1 model on agar, continuous model in water and continuous model on agar.

9.4.1 Rectangular body

In most cases the behaviour of the integrated model is largely unchanged when the rectangular body is substituted for the more realistic ellipsoidal body (see Figure 9.11). The simulation time saved by reverting to this simpler model is 72% on agar and 94% in water. However, there are certain situations, namely when simulating environments with small objects, where the simpler version will not function correctly due to the flat head and greater separation between points. Since simulation time is not normally an issue, the ellipsoidal body will be used in most cases.

9.4.2 Generic nematode circuit

The model was initially developed with cross inhibition to both the VB and DB neurons. The idea was to first get the model to work, without being too concerned about biological realism. My intention was to look for a plausible implementation at a later stage. Somewhat surprisingly, I found that one way cross inhibition had an effect very similar to two way inhibition. It is therefore quite unremarkable that the generic nematode model is also capable of coordinated locomotion (not shown).

9.4.3 L1 circuit

In Section 8.4.3 I presented a modification to the model that is consistent with what we know about the neural circuit of the L1 larva that lacks VB and VD neurons. Because of this, the L1 model must rely entirely on the DB neurons to generate oscillations. The DB stretch receptor input must be responsible for triggering both the on and off transitions, with the ventral side of the body controlled in “open loop” by switching the DD mediated inhibition on and off. Interestingly, the basic mechanism of the model still works in this configuration, as shown in Figure 9.11 and Supplementary movies C9_9 and C9_10. However, in contrast to the standard model, the L1 model fails totally in the absence of GABA inhibition (see Supplementary movie C9_11), even on agar.

9.4.4 Continuous neurons

A version of the model using more realistic neurons with continuous dynamics was introduced in Section 8.4.5. This variant has more parameters than the binary model, and early attempts to make it work suggested that it is also more sensitive to parameter values. In fact, when using the continuous neural model and the elliptical physical model, the resulting integrated model failed to work in water. This raised an important question

as to whether this is a fundamental problem of the neural model, or simply a matter of optimization. To begin answering this question I reverted to the rectangular body physical model and found that having done so, the integrated model was capable of locomotion in water (albeit with a slightly uncoordinated waveform) as well as on agar (see Figure 9.11, Supplementary movies C9_12 and C9_13). So, if the continuous version of the neural model is capable of swimming and crawling when given a rectangular body, one can ask why it fails to swim with the elliptical body while the binary model works in both cases. The difference suggests that the binary model is more robust than the continuous model, and that crawling on agar is a more robust behaviour than swimming in water (also see Sections 10.2 and 10.4). The need for robustness, in this context, comes from the fact that the changing radius of the elliptical body gives different segments slightly different properties, as opposed to the rectangular model in which segments have identical properties. Although I attempted to compensate for this variation, it would appear that some inhomogeneity remains that is too much for the fragile continuous model to handle.

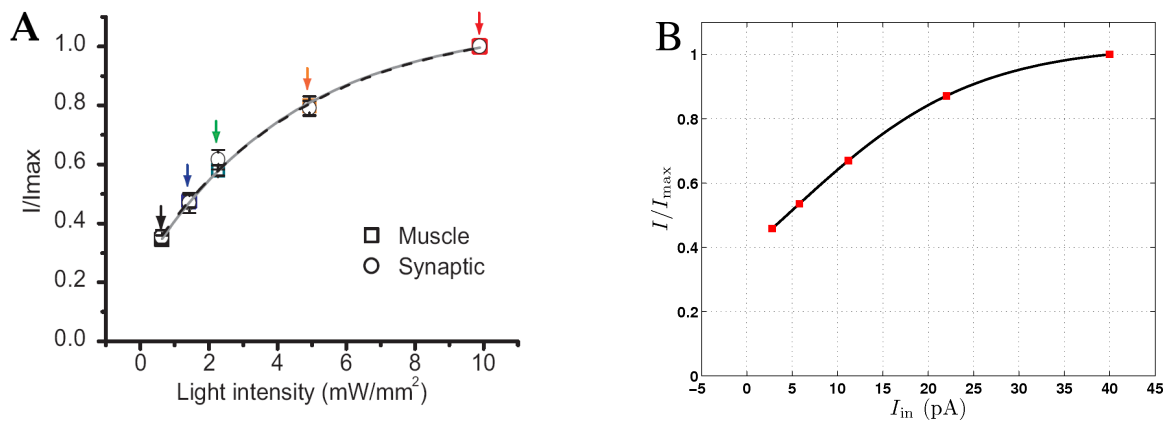


Figure 9.12: Postsynaptic currents in response to excitation of motor neurons, normalised by the maximum current. A) Postsynaptic currents in response to light stimuli reproduced with permission from Ref. [77]. Symbols indicate experimental data points and the solid lines are the best single exponent fits. B) Postsynaptic currents at the model NMJ in response to depolarising current injection to a VB motor neuron. Red squares are for comparison with (A).

With regard to the imperfect locomotion waveform exhibited by the rectangular body continuous model in water, note that the uncoordination is largely restricted to the tail. This is an interesting observation, and suggests that the problem may be linked to imperfect compensation for the reduced length of the posterior stretch receptors by Equation 8.16, combined with the greater sensitivity of this variant. It is quite likely that the behaviour of the continuous model could be greatly improved by tuning the parameters with an automated optimization algorithm.

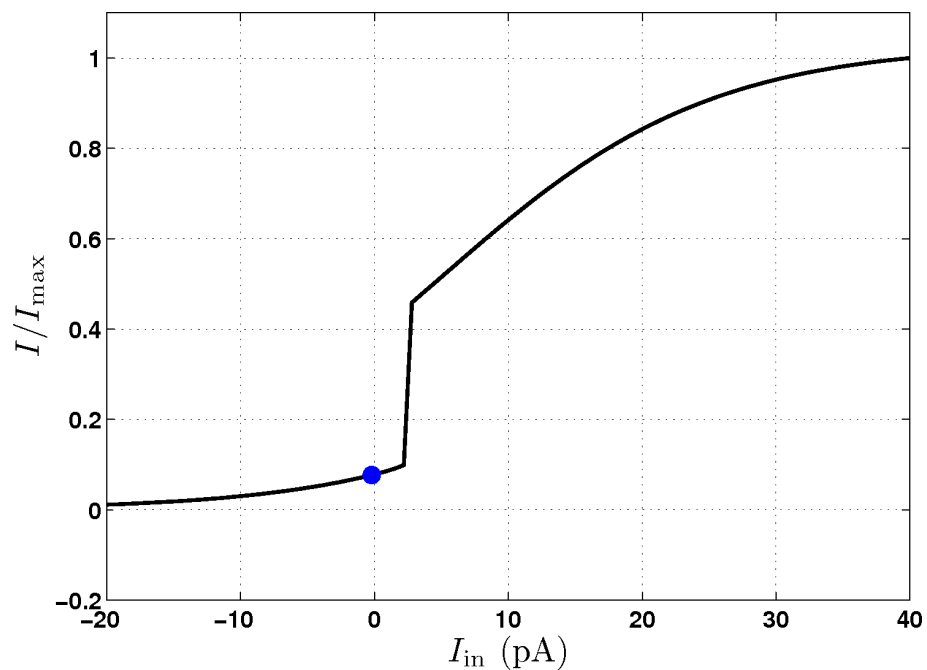


Figure 9.13: Postsynaptic response of the model to hyperpolarizing and depolarising currents. The blue circle indicates the postsynaptic current at the neuron's rest potential.

Despite its imperfect locomotion, the continuous model is still useful for addressing certain questions that are outside the scope of the binary model. Specifically, the simplified dynamics of the binary neurons, with totally discrete on and off states, make it impossible to evaluate their behaviour against electrophysiological data in a meaningful way. Until recently this was a moot point due to a lack of relevant data. However, a recent publication by Liu et al. [77] has provided an unexpected opportunity to evaluate some of the assumptions that went into the model, in particular the assumption of bistable behaviour in B-class (cholinergic) ventral cord motor neurons. The paper presents an innovative set of experiments, a subset of which I will briefly describe below.

The aim of the study was to investigate the nature of synaptic transmission at the *C. elegans* neuromuscular junction. Specifically, while a typical neuron fires all-or-nothing action potentials that trigger the release of a fixed quantity of neurotransmitter, some neurons rely on passive propagation of activity and graded synaptic transmission (in which the amount of neurotransmitter released depends on the level of depolarization). Neurons of this type often exhibit tonic release of neurotransmitter, such that some transmission occurs even when the neuron is at rest [77]. To characterise the neuromuscular junction, Liu et al. use cutting edge optogenetic techniques that make it possible to confer light sensitivity to a cell. Channelrhodopsin-2 is a light-activated excitatory ion channel that

can be genetically encoded. This is expressed in the cholinergic ventral cord motor neurons, making it possible to variably excite them with light stimuli of different intensities. This is complemented by similar experiments using halorhodopsin, a genetically encoded light-activated chloride pump that allows the cell to be hyperpolarized by light stimuli. In both cases the authors stimulate the cholinergic motor neuron while recording the evoked postsynaptic currents at the neuromuscular junction, in a preparation that eliminates the contribution of the GABAergic neurons. By directly applying light stimuli to B-class motor neurons and recording the response from body wall muscle cells, this paper provides electrophysiological data that can shed light both on the neuromuscular junction and, indeed, the activation properties of B-class motor neurons.

First, using channelrhodopsin, Liu et al. stimulate the presynaptic neuron with light of increasing intensity, finding that the postsynaptic current increases smoothly as shown in Figure 9.12A. They also use halorhodopsin to inhibit the presynaptic neuron, finding that the postsynaptic current is reduced. Looking at these results, the obvious interpretation is that the cholinergic motor neurons exhibit tonic, graded release of neurotransmitter. This elegant result is an important contribution to understanding (and modelling of) this and other neural circuits in *C. elegans*. Moreover, the results suggest that the motor neuron dynamics are similarly graded. Indeed, if the neurons fired classical all-or-nothing action potentials, then one might expect the postsynaptic currents to be similarly binary, or at least strongly non-linear. It appears, therefore, that the findings of Ref. [77] do not support the model proposed here. However, while the binary model cannot be used to address questions of this type, the continuous version can.

At the time the present model was initially developed, this data was not yet available. Instead, I based the neural dynamics on those of the RMD neurons [85] while the synaptic properties were loosely based on those of *Ascaris* neuromuscular junctions, which also exhibit graded transmission with tonic release [32]. After reading Ref. [77], I compared the behaviour of the model to this new data². Figure 9.12B shows that the postsynaptic current in the model muscles (as a function of the presynaptic current stimulus, which is functionally equivalent to the light intensity in the experiment) is quantitatively similar to the experimental currents in Figure 9.12A. With regard to tonic release, Figure 9.13 shows that the postsynaptic current in the model also decreases significantly in response to presynaptic hyperpolarization.

While the data of Ref. [77] is certainly consistent with an interpretation in which the motor neurons lack any form of active response, the results presented above suggest that

²In order to reproduce the experimental data, it was necessary to make some minor adjustments to the parameters for the synaptic activation function (Equation 8.29). These modified values were used for all simulations of the continuous model and are provided in Table 8.3.

the data is also consistent with the model presented here. Unlike the binary model, which approximates the RMD-like behaviour in terms of discrete high and low states, the very nature of the continuous model allows for significant changes in membrane potential in either “state”. Indeed, it is clear from Figure 1 of Ref. [85] that this is also the case for RMD. Thus, in the context of the interpretation proposed here, the smooth increase in postsynaptic current with increasing light intensity reflects variability in the neuron’s high (depolarized) state.

The fact that the Liu et al. results do not contain sufficient information to determine whether B-class neurons are graded or bistable suggests what further experiments may be able to address this question. First, as Liu et al. used only a single intensity of light in the polarizing (halorhodopsin) experiments, the resulting change in current could not be quantified in the same way as for the depolarizing (channelrhodopsin) experiments. Second, it is not clear whether light intensities used in the channelrhodopsin experiments induce a sufficiently full range of possible cell responses, or whether even the lowest intensities used already induce substantial depolarization. Therefore, in order to determine which interpretation is correct, a first step would be to repeat the channelrhodopsin experiments using lower light intensities. A smooth, linear response even at low stimulus intensity would suggest a linear, passive motor neuron response, whereas a strong non-linear response may point to an effective threshold, in line with a bistable response of the motor neurons. These results could potentially be integrated with data from halorhodopsin experiments, mapping the synaptic transmission properties over a wider range of input (as in Figure 9.13).

Part IV

Closing the loop

Chapter 10

Predictions

10.1 Introduction

While the very act of developing a model can be quite instructive, the ultimate aim of biological models is to generate testable predictions that guide new experiments. Creating the model presented in Part III has caused me to re-evaluate several assumptions about the worm's locomotion, while the model itself has provided an avenue for assessing the plausibility of the proposed oscillatory and modulatory mechanism. Indeed the promising results presented in Chapter 9 suggest that the model is sufficiently well grounded to have captured some aspects of the fundamental mechanism of *C. elegans* locomotion. It therefore seems reasonable to expect (or hope for) the model to have predictive power. Up to now this thesis has been mostly “feed forward”, with experimental data guiding the modelling work. But now it is the model's turn to feed back and influence the work in the laboratory.

In this chapter I will present three specific predictions that were generated by the model. Not only does this demonstrate the important contribution that computational modelling can make to biology, but it also stresses the importance of an integrated approach. It is at this point that we truly close the loop and reap the benefits of our multidisciplinary group. Finally, by testing the model predictions experimentally we further evaluate the model itself and guide future work.

10.2 A medium dependent GABA⁻ phenotype

In the worm's ventral cord locomotion circuit, cholinergic neurons of class B and A mediate forward and backward locomotion respectively. The only inhibition in this circuit is mediated by D-class GABAergic neurons. Individual D-class neurons receive input from both A- and B-class neurons on one side of the body and inhibit muscles, and in some cases also motor neurons (see Section 2.1.4), on the opposite side. The connectivity of these inhibitory D-class neurons suggests involvement in both forward and backward locomotion [26, 136]. The function of D-class neurons can be knocked out through mutation of genes required in the GABA pathway [84], by targeted killing of D-class neurons [129] and by laser axotomy [138], yielding essentially the same so-called *shrinker* phenotype [57] in all cases. These worms seem to be largely incapable of backward locomotion. In contrast to wild type worms which back up when touched on the head, GABA pathway defective (or GABA⁻) worms contract muscles along both sides of their bodies and therefore “shrink”. Forward locomotion of these GABA defective worms, on the other hand, is generally described either as wild type [129, 138], or nearly wild type with a reduction in amplitude [84] (see Supplementary movie C10_3). This leads to the commonly held conclusion that D-class neurons are not essential for forward locomotion [21].

10.2.1 Model prediction

Based on the GABA⁻ phenotype as reported, it seemed that the model should continue to work in the absence of inhibition. Consistent with the analysis presented in Section 9.3, removal of muscle inhibition has only a minor quantitative effect on the model's behaviour (not shown). Neural inhibition, on the other hand, plays a much more important role. In fact, I discovered quite early on in the development of the model that removal of VD mediated inhibition of VB motor neurons leads to grossly normal crawling behaviour on model agar, but a total inability to swim in water (see Figure 10.1, Supplementary movies C10_1 and C10_2). At first I was quite concerned about this result and made a concerted effort to tune the model parameters such that inhibition would not be required in any medium, but to no avail. On closer inspection of the literature, however, it became apparent that in every case where forward locomotion of GABA pathway defective worms was reported [84, 129, 138], the assay had been performed on agar. The model therefore suggests a novel prediction that these worms will exhibit a much stronger defect in forwards locomotion when placed in less resistive media.

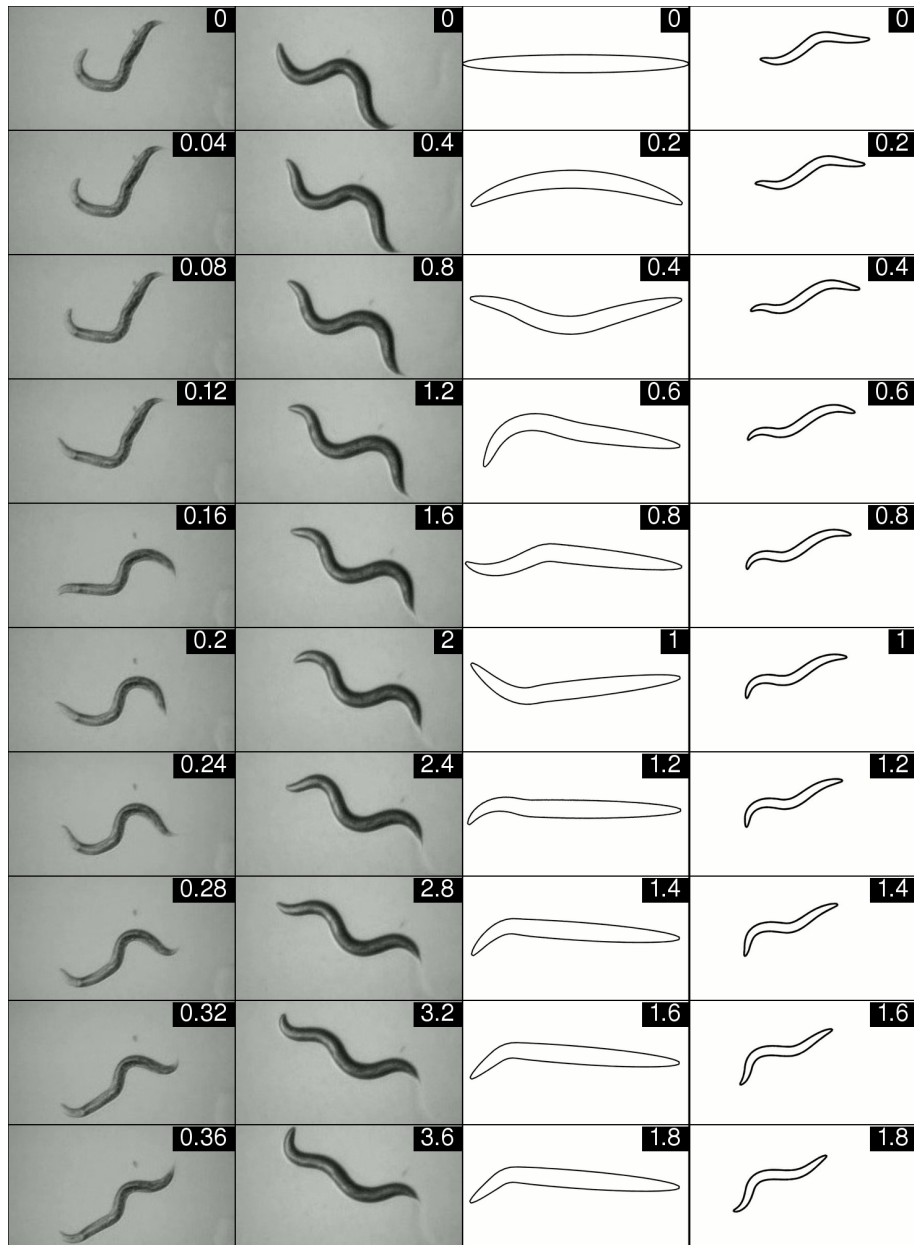


Figure 10.1: Stills taken from movies of real and simulated GABA defective worms, with frame times (in seconds). Columns are (from left) *unc-30 (e191)* mutant worm in water, *unc-30 (e191)* mutant worm on agar, model GABA⁻ worm in water and model GABA⁻ worm on agar.

10.2.2 Experimental result

To test the model's prediction, we placed a variety of GABA pathway defective mutants (*unc-25 (e156)*, *unc-30 (e191)* and *unc-47 (e307)*) in water, recording their behaviour (see Figure 10.1 and Supplementary movie C10_4). We found that all mutants tested exhibited highly dysfunctional locomotion when attempting to swim in water (there were some differences in the observed phenotypes, but all were highly uncoordinated). These worms were often frozen for extended periods of time in a very loopy configuration. Undulations, when they did occur, appeared to be independent in different sections of the body, with bending initiated at random locations and only rarely propagating from head to tail. Forward-like locomotion was only rarely observed, and involved the anterior body undulating while the posterior body was dragged behind. In light of our finding that swimming and crawling are likely to correspond to a single modulated gait (see Chapter 4), we conclude that D-class GABAergic neurons are an essential component of the forwards locomotion circuit. The fact that the phenotype associated with their removal is partially masked in more resistive media will be revisited in Section 10.4.

10.3 Importance of neural inhibition

While the results of Section 10.2 suggest that inhibition from D-class neurons may be important to forward locomotion, they do not shed any light on the relative contributions of neural and muscle inhibition. It has long been known that the GABAergic D-class neurons receive input from excitatory neurons on one side of the body and inhibit muscles on the opposite side [84, 135]. For efficient undulations, we would expect to see anti-phase activity all along the worm: i.e., the ventral neuron should repolarize soon after the corresponding dorsal neuron depolarizes and D-class neurons have often been described as contributing to this anti-phase relationship. One of the advantages of a computational model such as that presented here is that it allows an idea like this to be put to the test.

10.3.1 Model prediction

Contrary to the typical view of their role in locomotion, the model presented here has suggested that, in the context of a sensory feedback based oscillatory mechanism in which B-class neurons are depolarized in response to local stretch, direct muscle inhibition would not impose anti-phase synchrony between dorsal and ventral neurons. In fact, the analysis presented in Section 9.3.1 suggests that they will have the opposite effect: When a given neuron becomes depolarized and inhibits the opposite muscle, the resulting re-

laxation would indirectly excite the opposite neuron (via stretch receptors) thus delaying, rather than accelerating, its repolarization. It therefore seems likely that some direct inhibitory synaptic interaction is required between neurons on the ventral and dorsal sides. This is precisely the case in the model, which includes VD to VB inhibition in rough agreement with the known connectivity data [26] (see Sections 2.1.4 and 7.2.3).

What then would be the role of D-class muscle inhibition? One possibility is that the binary neurons in our model eliminate the need for muscle inhibition. In vivo, the “on” and “off” states of neurons are ultimately continuous rather than discrete valued, and there is thought to be tonic release of neurotransmitter at the neuromuscular junctions (based on data from *Ascaris* [32]). Thus, muscle inhibition could serve to override low baseline excitation by inactive B-class neurons, allowing the opposite side to relax fully. Indeed, in the continuous model presented in Section 8.4.5, muscle inhibition is required, but is not sufficient without neural inhibition (not shown). Secondly, muscle inhibition could play a role in resolving competition between the forward and backward circuits, as may occur during a switch in direction. After all, D-class neurons are innervated both by B-class (forward locomotion) and A-class (backward locomotion) motor neurons. Thus, when both B- and A-class neurons are actively competing, D-class inhibition could counteract muscle activation by the “weaker” circuit, and allow the “stronger” circuit to take over.

The importance of neural inhibition (and the sufficiency of one-way inhibition) for symmetry breaking in the model is illustrated in Section 9.3.2. The fact that the model requires these VD to VB connections could be seen as a limitation, particularly in light of the relatively small number of identified connections between these classes (see Figure 2.6). It could certainly be argued that these are simply spurious connections with no behavioural role. It is also possible, however, that a few of these connections may have been missed, and that this is a real motif in the worm’s neural circuit. Weight is given to this idea by the fact that, at least in the anterior of the worm where connection data is expected to be more reliable, most of the VBs do receive at least one such connection. Furthermore, the fact that virtually no equivalent connections exist between DD and DB makes the connections on the ventral side seem more significant. The model therefore makes the novel prediction that these connections are in fact functional. More specifically, the model predicts that while a lack of direct muscle inhibition is likely to underlie the shrinker phenotype on agar, it is a lack of neural inhibition that underlies the swimming defect of GABA pathway defective worms.

10.3.2 Experimental result

While the aforementioned prediction is likely to be controversial, it can at least be tested. Together with Sophie Bamps of the Hope Laboratory, we have devised a genetic experiment that is currently under way. While the details of the molecular biology techniques are beyond the scope of this thesis, the basic approach is to start with an *unc-49* null mutant which lacks a functional GABA receptor. These worms exhibit the usual phenotypes of GABA pathway defects, including shrinking and the inability to swim. The next step is to rescue the GABA receptor selectively in either the muscles or a relevant subset of the nervous system. This is accomplished by expressing a functional copy of *unc-49* under the control of suitable promoters. If the model's prediction is correct, the neural rescue will be sufficient to rescue the swimming defect (and not the shrinker phenotype) while the muscle rescue will rescue the shrinker phenotype (but not the swimming defect). At the time of writing, the experiment was still ongoing. However, one promising interim result is the finding that B-class motor neurons do naturally express *unc-49*, and could therefore be receptive to inhibition by D-class neurons.

10.4 Masking effect

If D-class neurons are in fact required for forwards locomotion, one must ask why this phenotype largely disappears on agar. One interesting possibility is that the physical forces imposed by the substrate could help to stabilize the body shape of defective animals. The reliance of the proposed locomotion mechanism on non-local proprioceptive feedback means that an improved body posture would provide more appropriate sensory feedback to the rest of the body, possibly leading to a self-reinforcing effect.

10.4.1 Model prediction

To investigate this possibility, I returned to the model and performed a set of simulation experiments in which the anterior 3/4 of the worm is normal, but muscles in the posterior 1/4 of the body are flaccidly paralysed. I found that while this defect is clearly visible in water, it is much harder to detect on agar (see Figure 10.2, Supplementary movies C10_5 and C10_6). This confirms that, in the context of the model, the physical forces exerted on the worm by stiff gel or agar-like substrates serve to stabilize the body shape, hence facilitating more effective locomotion.

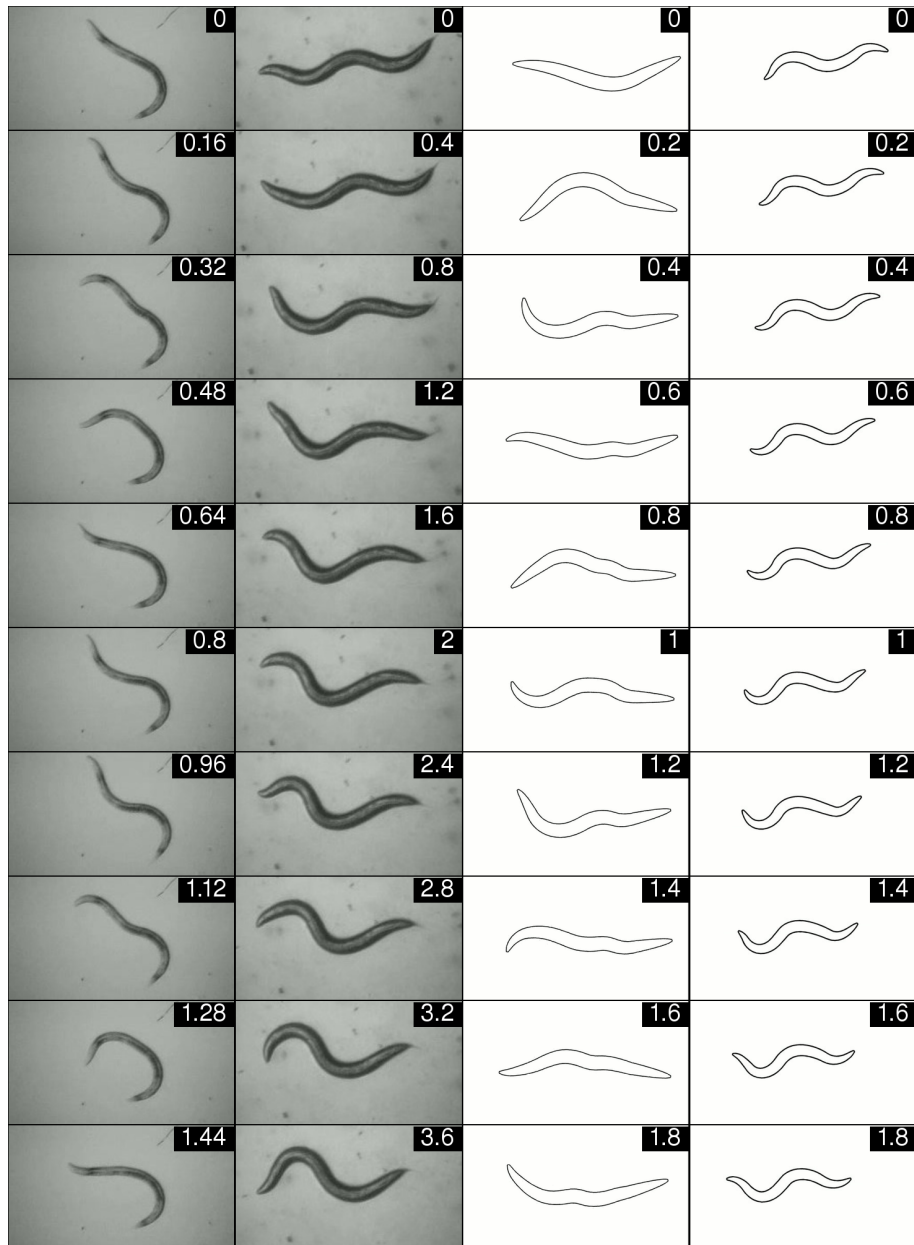


Figure 10.2: Stills taken from movies of real and simulated defective worms, with frame times (in seconds). Columns are (from left) *unc-8 (e49)* mutant worm in water, *unc-8 (e49)* mutant worm on agar, model worm with paralysed tail in water and model worm with paralysed tail on agar.

10.4.2 Experimental result

To explore whether the masking phenomenon observed for GABA pathway defective worms is more generic, we performed the same set of experiments on mutants defective in *unc-8* (a gene unrelated to GABA function that is implicated in the regulation of locomotion [119]). We found that *unc-8 (e49)* mutant worms have only a subtle phenotype on agar yet become severely uncoordinated as the medium becomes more dilute (see Figure 10.2 and Supplementary movie C10_7). Like the GABA⁻ mutants, *unc-8 (e49)* mutant worms are unable to make progress or propagate a coordinated undulation in a liquid environment. They are mostly immobile and very loopy in water; when attempting forward locomotion, the anterior third of the body will sometimes undulate, with the remainder of the body forming a hook-like shape; backward locomotion, when it occurs in water, appears normal. Thus, while the exact defect underlying the *unc-8* mutant phenotype is unclear, it does seem to manifest more severely towards the posterior of the worm much like the virtual mutant described above. This result, together with those presented in Section 10.2, suggest that the physical properties of and agar substrate are able to mask a variety of locomotion defects to varying degrees.

Chapter 11

Discussion and conclusions

In this chapter I will bring the thesis to a close by discussing the major contributions of my research, beginning with a brief review of the preliminary investigations presented in Part II. Following this I will discuss the implications of the model that is at the heart of my work, before considering the more general matter of my methodology. Finally I will outline some possible directions for future work.

11.1 Preliminary investigation

The results of the individual investigations were discussed at the ends of the relevant chapters, so here I briefly summarise the results in the context of the open questions outlined in Section 2.3.7.

Locomotion in different media

One of the most important results of this thesis is the finding, presented in Chapter 4, that “swimming” and “crawling” represent snapshots out of a continuum of locomotion behaviours. To those outside the field this may seem like an unsurprising result, but it goes counter to the conventional wisdom within much of the *C. elegans* community. Indeed, given that some worm biologists are somewhat sceptical of models, this result may turn out to be the most influential contribution of my work. As I have argued, a continuous transition implies a single underlying neural mechanism, which means that models should

account for this entire range of behaviours. With respect to the experimental community, the main implications relate to the way in which behaviour is assessed and phenotypes are interpreted. Specifically, locomotion is one of the main behaviours that is evaluated when looking for mutant phenotypes. These assays generally take one of two forms: either worms are placed in water and the number of body bends per minute are counted; or the worm is placed on agar and the waveform is evaluated in various ways. Our work suggests that locomotion could be more thoroughly evaluated by using a range of media. This is particularly important in light of the results of Sections 10.2 and 10.4, suggesting that some phenotypes may manifest differently in the two environments. If such a phenotype is found in an assay that focusses on certain environments, one might conclude that the gene in question is only required for locomotion in that medium. But by including intermediate environments in the assay (and in the context of our single gait finding) one may instead conclude, for example, that the phenotype is frequency dependent. When attempting to infer the actual role of the gene in question, such a change in interpretation could well be important.

The importance of body physics

In light of the result discussed above, it seemed likely that the physics of body and environment would be significant. In Chapter 5 this was addressed in the context of a pre-existing neural model [21]. The results demonstrate that body physics could be a major factor in determining the frequency of oscillation, but that they also introduce long range interactions that impose additional constraints on the control system. This implies that the neural circuit should, where possible, be studied in the context of the body and environment. Models of locomotion should certainly include a quantitative physical model. This point will be revisited in the context of the integrated model below.

Role of body wall muscles

A previous locomotion model [67] as well as experimental data from *Ascaris* [132] had suggested that the body wall muscles, and specifically the gap junction coupling between them, could play an active role in the patterning of locomotion. The investigation in Chapter 6 suggests that this is unlikely, which is supported by the results of Ref. [25]. Thus, as is the case in most organisms, the worm's neural circuit (in conjunction with the body) appears to be the primary rhythm generating component of the system.

The locomotion mechanism

This question was not addressed as part of the preliminary investigation, but will instead be discussed in the context of the integrated model.

11.2 Model

This section deals with the integrated model of Part III that forms the core of this thesis. I will start by outlining the achievements and limitations of the model, before delving into a discussion of the scientific implications of the work.

11.2.1 Achievements

The high level goal of this model was to further our understanding of *C. elegans* forwards locomotion by consolidating biological data from a wide variety of sources into a working hypothesis for the underlying mechanism. Furthermore, it was hoped that the model would motivate poignant experiments to address unanswered questions and test predictions. From all these perspectives the model has been successful, as will be discussed in Section 11.2.3. In this section, however, I focus on the model's achievements from a behavioural point of view.

Behaviourally, the goal of the model was to reproduce *C. elegans* locomotion in a range of media from water to agar, motivated by the results of Chapter 4. In this respect it has also been successful. Specifically, the binary version of the model is able to reproduce crawling on agar and swimming in water with quite realistic frequencies and wave forms. Consistent with our experimental results, the model exhibits a continuous transition between these two behaviours, although this transition is not perfect (see Section 11.2.2). Compared to the binary model, the continuous model introduced in Section 8.4.5 performs less well, but the fact that the fundamental mechanism still works with more realistic neurons is an important proof of concept. What is quite remarkable, however, is the extent to which the binary model generalises to heterogeneous environments. Specifically, it has been quite successful in reproducing locomotion in microfluidic post arrays (see Section 9.2.3). This is interesting as it demonstrates the robustness of the proposed mechanism and its suitability for controlling locomotion in variable and inhomogeneous environments (i.e. the real world).

This model represents a significant advance over those that have come before it for two main reasons. It is the first biologically grounded model to address swimming in water, and is certainly the first to account for the swim-crawl transition and locomotion

in microfluidic post arrays. It is also the most comprehensively integrated model to date, including a quantitatively grounded model of the body and environment as well as biologically grounded models of the muscles, neurons (particularly the continuous version) and the neural circuit. However, as is usually the case with models, this one is not without its limitations. These are discussed in the following section.

11.2.2 Limitations

The main limitation of the model is the fact that the wavelength/frequency relationship in Figure 9.5B is not linear. Unfortunately I have not been able to determine why the wavelength initially increases as the medium becomes more resistive. It is possible that this could be solved by some form of parameter optimization applied to the neural parameters, but it may require a change to some of the equations that define the model. Specifically, many of the equations in the physical and neural models are linear (for simplicity) but there may be some important non-linearities in the real worm that have not been taken into account. Probably linked to the limitations with the transition, there is also a fairly minor problem that the undulation frequency in water is a bit too high. Any strategy that was able to improve the transition would almost certainly be able to solve this problem as well. Another potential limitation is the fact that the model does not produce coordinated locomotion for all the combinations of C_{\parallel} and C_{\perp} that were tested (see Figure 9.6). While it is possible that the real worm would also exhibit uncoordinated locomotion in an environment with those combinations of drag coefficients, this seems somewhat unlikely. A useful first step would be to determine the effective drag coefficients for gelatin solutions of various concentrations experimentally, allowing more accurate quantitative modelling of intermediate environments. But even so, it would be preferable for the model's locomotion to be coordinated in all virtual media. Finally it is worth noting that the behaviour of the continuous model is quantitatively inferior to that of the binary model. This version would be likely to benefit even more from parameter optimization.

11.2.3 Implications

While it is rewarding to see one's model reproduce the desired behaviours, this is not particularly valuable from a scientific point of view. Of much greater significance is the insight that the model provides into the underlying biological system. In this section I discuss the main implications of the model in terms of the advancement of *C. elegans* science.

Proprioception

Probably the biggest unanswered question in *C. elegans* locomotion is about the relative contributions of sensory feedback (proprioception) and endogenous central pattern generator (CPG) control. CPG circuits, which generate rhythmic outputs in absence of rhythmic input, are generally thought to be involved in most if not all rhythmic animal behaviours, including locomotion [46, 58]. While these circuits are often studied in isolation from the animal, it has long been known that sensory feedback plays an important role in modulating the output pattern and compensating for external perturbations [45]. Alternatively it has been suggested that CPG circuits could act more like predictive filters, processing feedback signals and correcting for imperfect sensors [70].

Given the prevalence of CPG circuits in controlling animal behaviour, it is natural to assume that the same is true of *C. elegans* locomotion. But of course, the natural world is full of exceptions and the accumulating evidence necessitates that we consider the possibility that the worm could rely entirely on sensory feedback. Indeed one of the main questions addressed by this work is the plausibility of such a mechanism for the generation and modulation of the locomotion waveform. By successfully reproducing a broad range of locomotory behaviours, the model demonstrates that, in principle, proprioceptive feedback is sufficient in this case. Of course, demonstrating sufficiency of sensory feedback does not in any way preclude the involvement of a CPG, which may in fact exist. Nonetheless, it is interesting to take this idea a bit further and speculate why the worm might be so unusual in this regard, *if* indeed it is.

In Ref. [70], Kuo points out that pure feedback control is optimal for responding to external perturbations, but suffers when feedback signals are imperfect. For a small organism with a compliant body and simple mode of locomotion, that must move through a variety of heterogeneous environments, perhaps external perturbations are more of a concern than precise control of body shape. Another interesting point made by Grillner [45] is that feedback based control suffers when the sensory signals are slow relative to the behaviour. For a 1 mm long worm in which the motor neurons themselves perform the sensory function, and whose behaviour occurs at time scales on the order of seconds, it seems likely that feedback delays would not be an issue. Finally there is the fact that the entire worm only has 302 neurons to work with, so neural economy is paramount. Thus, while it is *far* too soon to rule out the involvement of a CPG, it does seem plausible that *C. elegans* locomotion could be an exception to this very common principle.

Inhibition

One of the major contributions of this work has been to our understanding of the role of inhibition in *C. elegans* locomotion. Body bending is the result of anti-phase activation of dorsal and ventral muscles, activated by DB and VB neurons respectively. This requires that the activity in DB and VB neurons also oscillate in anti-phase. One common way of ensuring anti-phase oscillation is through mutual inhibition. It is therefore quite surprising that the D-class neurons were thought to be non-essential for forwards locomotion [21, 129, 138]. In contrast, the model predicted that D-class neurons are required for locomotion in less resistive media like water, leading to the experiment described in Section 10.2 which confirmed this prediction. The fact that the uncoordinated phenotype associated with their removal is largely masked in a highly resistive environment is also significant, and led us to address the possibility that agar might mask locomotion defects more generally (see Section 10.4). As an aside, this implies that agar is not the ideal environment to use when looking for locomotion phenotypes. Nonetheless, in the context of the single-gait finding presented in Chapter 4, this suggests that the D-class neurons should be considered part of the “core” circuit for forwards locomotion.

Of greater significance, however, is the insight the model has provided into the relative roles of neural and muscle inhibition. Typically, the direct inhibition of B-class neurons has not been considered significant, and was not included in the original connectivity diagrams due to White et al. [136]. Indeed, the argument that inhibition of opposing muscles would facilitate the correct dorso-ventral phase relationship seemed entirely reasonable, and therefore rendered the neural inhibition redundant. It is therefore interesting that the model predicts that muscle inhibition would have an effect opposite to that which is required, suggesting that the neural inhibition might be significant after all. Unfortunately, at the time of writing this thesis the results of our experiment (described in Section 10.3) were not yet available, although the finding that B-class neurons do express *unc-49* is certainly encouraging. If the results end up supporting this hypothesis, this will represent a very significant change in our understanding of the locomotion circuit.

Oscillatory mechanism

One fundamental requirement for generating the alternating dorso-ventral muscle contraction that underlies the worm’s body wave is the presence of one or more oscillators of some form. In principle, a single oscillator somewhere in the system could control the entire body via time delayed signals that would provide the correct phase lag to establish the spatial wavelength. Alternatively, as is the case in the present model (and similarly

in the lamprey [27]), there could be a chain of coupled oscillators along the animal that control local bending and are synchronised with appropriate phase lags. In either case, the requirement for one or more oscillators remains. As it happens, oscillators have been extensively studied in the context of dynamical systems, providing a theoretical basis for the study of oscillations [115]. One important distinction to point out is between linear oscillators (such as an undamped mass-spring system), in which there is no preference for the amplitude of the oscillation, and non-linear (or limit cycle) oscillators that exhibit sustained oscillations of fixed amplitude, such that perturbations soon die away. For the purposes of locomotion, the oscillations must be of the latter type. In the present model, it is the combination of the B-class dynamics (that have a threshold and hysteresis) and delayed inhibition mediated by the stretch receptor feedback in conjunction with the body properties that satisfy the requirements for sustained oscillation (see Section 7.3.2).

However, it is important to note that the model's oscillatory mechanism does not fundamentally require that the threshold be a property of the B-class neurons. This is simply one way to ensure that the neuron's response to body stretch be strongly non-linear and one that appears plausible in light of the experimental data to date [77, 85]. Another plausible locus for the nonlinearity is the stretch receptors themselves, as is the case in the model due to Bryden and Cohen [21].

11.3 Methodology

In Section 1.2 I advocated an integrated approach to the study of biological systems, and this thesis has applied such approach to the study of *C. elegans* locomotion. Here I will briefly discuss two aspects of the work that exemplify the power of this methodology.

Consider first the investigation of the effects of neural and muscle inhibition. The hypothesis that muscle inhibition imposes an anti-phase relationship between dorsal and ventral contractions sounds very convincing, so it is no surprise that it is quite widely accepted. However, in the context of the model, this inhibition was found to have a different effect, motivating the experiment described in Section 10.3. While it is entirely possible that the model will turn out to be wrong in this respect, we will soon have experimental confirmation one way or the other. If the experiment confirms the model prediction, this will represent a major discovery that would probably not otherwise have been made. If this is not the case, we instead have stronger evidence as to the role of muscle inhibition (and the insignificance of neural inhibition), so a new model can be developed that takes this into account. Either way, we end up with a better picture of the locomotion system.

The second example relates to the results presented in Section 9.4.4. As they stand,

the results of Liu et al. [77] suggest that the cholinergic ventral cord neurons have graded dynamics, in contrast to the plateau potentials of RMD neurons [85]. But by constructing a detailed (continuous as distinct from binary) model, I was able to demonstrate that the results of Liu et al. are not inconsistent with RMD-like B-class behaviour. Conversely, it also implies that the behaviour of the RMD neurons is not entirely all-or-none and that the high and low states, though distinct, are themselves graded functions of the input current. While it is entirely plausible that the B-class dynamics are nothing like those of RMD, this work still shows that a well grounded model can provide new interpretations for data and possibly resolve apparent inconsistencies.

11.4 Future work

While the results of this project have certainly advanced the field, we are still a long way from the ultimate goal of a complete understanding of *C. elegans* locomotion. Below I will outline some directions for future work that may prove fruitful.

Model optimization

The most obvious avenue for future investigation is to apply an automated optimization algorithm to the model in an attempt to improve its behaviour. This is particularly appealing for the continuous version, which has the advantage of being more biologically realistic. If the model's limitations can be overcome in this way, that will strengthen the results of this work and suggest that the model is a good reflection of the worm's locomotion mechanism. If a satisfactory solution cannot be found, this will suggest that a more significant qualitative change should be made. In either case it will be highly informative. The main difficulties will be to find a suitable fitness function, to find an optimization algorithm that can handle the multi-dimensional search space and to implement this in a way that yields results in a reasonable time frame.

Integration of new data

Enormous advances in experimental techniques are constantly being made, and it is only a matter of time before the dynamics of the ventral cord motor neurons are characterized in detail. Furthermore, we can hope that at some point direct evidence will be found for the existence of motor neuron stretch receptors. Perhaps it will even be possible to characterize their properties. As more data becomes available, new models will need to be developed that incorporate these findings. Having argued for the importance of a well

grounded physical model, experiments that more accurately characterise the body and environment would also be of great benefit for future models.

Integration with higher level behaviour

One of the motivations for choosing to model locomotion was the central role that it plays in the worm's behaviour. Having developed a fairly well grounded and successful locomotion model, an important next step is to integrate this with models of higher level goal directed control. Granted, this will also require extending the model to include backwards locomotion, pirouettes and other orienting behaviours. Our group is already beginning to incorporate models of chemotaxis, and the preliminary results are promising. Specifically, it has been possible to demonstrate gentle turning in response to chemical gradients using the present model coupled to a simple model of chemosensation. As models of the sensory system and motor control become more advanced, integrating these subcomponents into a full, reactive model of the worm is likely to become a fruitful area of research.

11.5 Concluding remarks

It was the intention of this thesis to demonstrate the potential of a holistic, multidisciplinary approach to biology, and to contribute to our understanding of *C. elegans* locomotion in particular. In both these respects I hope it has been successful. For such a simple organism, the worm is remarkably difficult to tease apart, so we all still have much work to do. But if the experimental and modelling communities can learn to work effectively together, this combined effort can yield results far beyond what could be achieved by either approach alone. We therefore need to make a concerted effort to understand both perspectives and pull in the same direction. Modellers cannot afford to shy away from the biological reality, and experimentalists should have a grasp of the principles of computational modelling, keeping these in mind when designing experiments. Finally, we must all learn to recognise each other's strengths as well as our own weaknesses.

Bibliography

- [1] R. McN. Alexander. Bending of cylindrical animals with helical fibres in their skin or cuticle. *J. Theor. Biol.*, 124:97–110, 1987.
- [2] R. McN. Alexander. Optimization and gaits in the locomotion of vertebrates. *Physiol. Rev.*, 69:1199–1227, 1989.
- [3] R. McN. Alexander. Personal Communication, 2008. reporting that Reynolds numbers as high as 3 are still within the “low” regime where drag forces are approximately proportional to velocity.
- [4] Z. F. Altun and D. H. Hall. *Alimentary System*. <http://www.wormatlas.org/hermaphrodite/alimentary/Alimframeset.html>, 2008.
- [5] Z. F. Altun and D. H. Hall. *Handbook of C. elegans Anatomy*. <http://www.wormatlas.org/hermaphrodite/hermaphroditehomepage.htm>, 2008.
- [6] Z. F. Altun and D. H. Hall. *Introduction to C. elegans Anatomy*. <http://www.wormatlas.org/hermaphrodite/introduction/Introframeset.html>, 2008.
- [7] Z. F. Altun and D. H. Hall. *Muscle System*. <http://www.wormatlas.org/hermaphrodite/muscleintro/MusIntroframeset.html>, 2008.
- [8] Z. F. Altun and D. H. Hall. *Nervous System*. <http://www.wormatlas.org/hermaphrodite/nervous/Neuroframeset.html>, 2008.
- [9] A. Azuma. *The Biokinetics of Flying and Swimming*. Springer-Verlag, Tokyo, 1992.
- [10] C. I. Bargmann. Neurobiology of the *Caenorhabditis elegans* genome. *Science*, 282:2028–2033, 1998.

- [11] C. I. Bargmann. *Chemosensation in C. elegans*. WormBook, doi/10.1895/wormbook.1.123.1, <http://www.wormbook.org>, 2006.
- [12] T. M. Barnes and S. Hekimi. The *Caenorhabditis elegans* avermectin resistance and anesthetic response gene *unc-9* encodes a member of a protein family implicated in electrical coupling of excitable cells. *J. Neurochem.*, 69:2251–2260, 1997.
- [13] S. Berri, J. H. Boyle, M. Tassieri, I. A. Hope, and N. Cohen. Forward locomotion of the nematode *C. elegans* is achieved through modulation of a single gait. *HFSP J.*, 3:186–193, 2009.
- [14] J. H. Boyle, J. A. Bryden, and N. Cohen. An integrated neuro-mechanical model of *C. elegans* forward locomotion. In M. Ishikawa, K. Doya, H. Miyamoto, and T. Yamakawa, editors, *LNCS: Neural Information Processing, Part 1*, volume 4984, pages 37–47. Springer-Verlag Berlin, 2008.
- [15] J. H. Boyle and N. Cohen. The role of body wall muscles in *C. elegans* locomotion. In N. Crook and T. olde Scheper, editors, *Proc. IPCAT 7*, pages 364–375. Oxford Brookes University, 2007.
- [16] J. H. Boyle and N. Cohen. *C. elegans* body wall muscles are simple actuators. *Biosystems*, 94:170–181, 2008.
- [17] S. Brenner. The genetics of *Caenorhabditis elegans*. *Genetics*, 77:71–94, 1974.
- [18] S. Brenner. Nature’s gift to science, 2002. http://nobelprize.org/nobel_prizes.
- [19] J. A. Bryden. A simulation model of the locomotion controllers for the nematode *Caenorhabditis elegans*. Master’s thesis, University of Leeds, 2003.
- [20] J. A. Bryden and N. Cohen. A simulation model of the locomotion controllers for the nematode *Caenorhabditis elegans*. In S. Schaal, A. J. Ijspeert, A. Billard, S. Vijayakumar, J. Hallam, and J-A. Meyer, editors, *Proceedings of the eighth international conference on the simulation of adaptive behavior*, pages 183–192. MIT Press / Bradford Books, 2004.
- [21] J. A. Bryden and N. Cohen. Neural control of *Caenorhabditis elegans* forward locomotion: the role of sensory feedback. *Biol. Cybern.*, 98:339–351, 2008.
- [22] J. Burr, A. H and C. Gans. Mechanical significance of obliquely striated architecture in nematode muscle. *Biol. Bull.*, 194:1–6, 1998.

- [23] M. Chalfie. GFP: Lighting up life, 2008. http://nobelprize.org/nobel_prizes.
- [24] M. Chalfie, J. E. Sulston, J. G. White, E. Southgate, J. N. Thomson, and S. Brenner. The neural circuit for touch sensitivity in *Caenorhabditis elegans*. *J. Neurosci.*, 5:956–964, 1985.
- [25] B. Chen, Q. Liu, Q. Ge, J. Xie, and Z. W. Wang. Unc-1 regulates gap junctions important to locomotion in *C. elegans*. *Curr. Biol.*, 17:1334–1339, 2007.
- [26] B.L. Chen, D.H. Hall, and D.B. Chklovskii. Wiring optimization can relate neuronal structure and function. *Proc. Natl. Acad. Sci. (USA)*, 103:4723–4728, 2006.
- [27] A. H. Cohen, P. J. Holmes, and R. H. Rand. The nature of the coupling between segmental oscillators of the lamprey spinal generator for locomotion: A mathematical model. *J. Math. Biol.*, 13:345–369, 1982.
- [28] N. Cohen. *The development of spontaneous beating activity in cultured heart cells: from cells to networks*. PhD thesis, Israel Institute of Technology, Kislev, 5761, Haifa, December 2000.
- [29] *C. elegans* Sequencing Consortium. Genome sequence of the nematode *C. elegans*: A platform for investigating biology. *Science*, 282:2012–2018, 1998.
- [30] G. N. Cox, M. Kusch, and R. S. Edgar. Cuticle of *Caenorhabditis elegans*: Its isolation and partial characterization. *J. Cell Biol.*, 90:7–17, 1981.
- [31] R. G. Cox. The motion of long slender bodies in a viscous fluid part 1. general theory. *J. Fluid Mec.*, 44:791–810, 1970.
- [32] R. E. Davis and A. O. W. Stretton. Signalling properties of *Ascaris* motoneurons: Graded active responses, graded synaptic transmission, and tonic transmitter release. *J. Neurosci.*, 9:415–425, 1989.
- [33] Mario de Bono and Andres Villu Maricq. Neuronal substrates of complex behaviors in *C. elegans*. *Annu. Rev. Neurosci.*, 28:451–501, 2005.
- [34] S. J. Dixon and P. J. Roy. Muscle arm development in *Caenorhabditis elegans*. *Development*, 132:3079–3092, 2005.
- [35] J. C. Doll, N. Harjee, N. Klejwa, R. Kwon, S. M. Coulthard, B. Petzold, M. B. Goodman, and B. L. Pruitt. SU-8 force sensing pillar arrays for biological measurements. *Lab Chip*, 9:1449–1454, 2009.

- [36] P. Erdős and E. Niebur. The neural basis of the locomotion of nematodes. *Lect. Notes Phys.*, 368:253–267, 1990.
- [37] B. D. Ermentrout and N. Kopell. Frequency plateaus in a chain of weakly coupled oscillators, I. *SIAM J. Math. Anal.*, 15:215–237, 1984.
- [38] G. B. Ermentrout. n:m phase-locking of weakly coupled oscillators. *J. Math. Biol.*, 12:327–342, 1981.
- [39] A. Z. Fire. Gene silencing by double stranded RNA, 2006. http://nobelprize.org/nobel_prizes.
- [40] M. B. Goodman. *Mechanosensation*. WormBook, doi/10.1895/wormbook.1.62.1, <http://www.wormbook.org>, 2006.
- [41] J. Gray. Undulatory propulsion. *Q. J. Microsc. Sci.*, 94:551–578, 1953.
- [42] J. Gray and G. J. Hancock. The propulsion of sea-urchin spermatozoa. *J. Exp. Biol.*, 32:802–814, 1955.
- [43] J. Gray and H. W. Lissmann. The locomotion of nematodes. *J. Exp. Biol.*, 41:135–154, 1964.
- [44] J. M. Gray, J. J. Hill, and C. I. Bargmann. A circuit for navigation in *Caenorhabditis elegans*. *Proc. Natl. Acad. Sci.*, 102:3184–3191, 2005.
- [45] S. Grillner. The motor infrastructure: from ion channels to neuronal networks. *Nat. Neurosci.*, 4:573–586, 2003.
- [46] S. Grillner, L. Cangiano, G. Y. Hu, T. R. Hill, and P. Wallén. The intrinsic function of a motor system - from ion channels to networks and behaviour. *Brain Res.*, 886:224–236, 2000.
- [47] S. Grillner, P. Wallén, K. Saitoh, A. Kozlov, and B. Robertson. Neural bases of goal-directed locomotion in vertebrates – an overview. *Brain Res. Rev.*, 57:2–12, 2008.
- [48] D. H. Hall and Z. F. Altun. *Nervous system*. Cold Spring Harbour Laboratory Press, Cold Spring Harbour, New York, 2008.
- [49] D. H. Hall and R. L. Russell. The posterior nervous system of the nematode *Caenorhabditis elegans*: Serial reconstruction of identified neurons and complete pattern of synaptic interactions. *J. Neurosci.*, 11:1–22, 1991.

- [50] A. K. Han, C. Kurrer, and Y. Kuramoto. Dephasing and bursting in coupled neural oscillators. *Phys. Rev. Lett.*, 75:3190–3193, 1995.
- [51] G. J. Hancock. The self-propulsion of microscopic organisms through liquids. *Proc. R. Soc. A*, 217:96–121, 1953.
- [52] R. M. Harris-Warrick. Pattern generation. *Curr. Opin. Neurobiol.*, 3:982–988, 1993.
- [53] A. C. Hart. *Behaviour*. WormBook, doi/10.1895/wormbook.1.87.1, <http://www.wormbook.org>, 2006.
- [54] E. M. Hedgecock and R. L. Russel. Normal and mutant thermotaxis in the nematode *Caenorhabditis elegans*. *Proc. Natl. Acad. Sci.*, 72:4061–4065, 1975.
- [55] A. V. Hill. The heat of shortening and the dynamic constants of muscle. *Proc. R. Soc. London, B*, 126:136–195, 1938.
- [56] A. Hindmarsh, A. Taylor, and R. Serban. Sundials. <http://www.llnl.gov/CASC/sundials/>.
- [57] J. Hodgkin. Male phenotypes and mating efficiency in *Caenorhabditis elegans*. *Genetics*, 103:43–64, 1983.
- [58] S. L. Hooper. *Central Pattern Generators*. John Wiley and Sons, Ltd, 2001.
- [59] H. R. Horvitz. Worms, life and death, 2002. http://nobelprize.org/nobel_prizes.
- [60] J. D. Huizinga, L. W. C. Liu, M. G. Blennerhassett, L. Thuneberg, and A. Molleman. Intercellular communication in smooth muscle. *Cell. Mol. Life Sci.*, 48:932–941, 1992.
- [61] A. J. Ijspeert. A connectionist central pattern generator for the aquatic and terrestrial gaits of a simulated salamander. *Biol. Cybern.*, 84:331–348, 2001.
- [62] C. D. Johnson and A. O. Stretton. Localization of choline acetyltransferase within identified motoneurons of the nematode *Ascaris*. *J. Neurosci.*, 5:1984–1992, 1985.
- [63] R. E. Johnson and C. J. Brokaw. Flagellar hydrodynamics. *Biophys. J.*, 25:113–127, 1979.

- [64] M. Jospin, V. Jacquemond, M. C. Mariol, L. Segalat, and B. Allard. The L-type voltage-dependent Ca²⁺ channel EGL-19 controls body wall muscle function in *Caenorhabditis elegans*. *J. Cell Biol.*, 159:337–347, 2002.
- [65] M. Jospin, M. C. Mariol, L. Segalat, and B. Allard. Characterisation of K⁺ currents using an *in situ* patch clamp technique in body wall muscle cells from *Caenorhabditis elegans*. *J. Physiol.*, 544.2:373–384, 2002.
- [66] J. Karbowski, C. J. Cronin, A. Seah, J. E. Mendel, D. Cleary, and P. W. Sternberg. Conservation rules, their breakdown, and optimality in *Caenorhabditis* sinusoidal locomotion. *J. Theor. Biol.*, 242:652–669, 2006.
- [67] J. Karbowski, G. Schindelman, C.J. Cronin, A. Seah, and P.W. Sternberg. Systems level circuit model of *C. elegans* undulatory locomotion: mathematical modeling and molecular genetics. *J. Comp. Neurosci.*, 24:253–276, 2008.
- [68] N. Kopell and G. B. Ermentrout. Symmetry and phaselocking in chains of weakly coupled oscillator. *Commun. Pur. Appl. Math.*, 39:623–660, 1986.
- [69] J. Korta, D. A. Clark, C. V. Gabel, L. Mahadevan, and A. D. Samuel. Mechanosensation and mechanical load modulate the locomotory gait of swimming *C. elegans*. *J. Exp. Biol.*, 210:2383–2389, 2007.
- [70] A. D. Kuo. The relative roles of feedforward and feedback in the control of rhythmic movements. *Motor Control*, 6:129–145, 2002.
- [71] G. La Spina, M. Sfakiotakis, D. P. Tsakiris, A. Menciassi, and P. Dario. Polychaete-like undulatory robotic locomotion in unstructured substrates. *IEEE Trans. Robot.*, 23:1200–1212, 2007.
- [72] W. Li, Z. Feng, P. W. Sternberg, and X. Z. S. Xu. A *C. elegans* stretch receptor neuron revealed by a mechanosensitive TRP channel homologue. *Nature*, 440:684–687, 2006.
- [73] J. Lighthill. Large-amplitude elongated-body theory of fish locomotion. *Proc. R. Soc. Lond. B.*, 179:125–138, 1971.
- [74] J. Lighthill. Flagellar hydrodynamics. *SIAM Rev.*, 18:161–230, 1976.
- [75] J. Liu, B. Schrank, and R. H. Waterston. Interaction between a putative mechanosensory membrane channel and a collagen. *Science*, 273:361–364, 1996.

- [76] Q. Liu, B. Chen, E. Gaier, J. Joshi, and Z. W. Wang. Low conductance gap junctions mediate specific electrical coupling in body-wall muscle cells of *Caenorhabditis elegans*. *J. Biol. Chem.*, 281:7881–7889, 2006.
- [77] Q. Liu, G. Hollopeter, and E. M. Jorgensen. Graded synaptic transmission at the *Caenorhabditis elegans* neuromuscular junction. *Proc. Natl. Acad. Sci. (USA)*, 106:10823–10828, 2009.
- [78] S. R. Lockery, K. J. Lawton, J. C. Doll, S. Faumont, S. M. Coulthard, T. R. Thiele, N. Chronis, K. E. McCormick, M. B. Goodman, and B. L. Pruitt. Artificial dirt: microfluidic substrates for nematode neurobiology and behavior. *J. Neurophysiol.*, 99:3136–3143, 2008.
- [79] A. Looss. The anatomy and life history of agckylostoma dub. pt. ii. *Cairo Records Eg. Govt. Sch. Med.*, 4:167–507, 1911.
- [80] W. Ludwig. Zur theorie der flimmerbewegung (dynamik, nutzeffekt, energiebilanz). *Zeitschrift fuer Vergleichende Physiologie*, 13:397–504, 1930.
- [81] E. Marder. Motor pattern generation. *Curr. Opin. Neurobiol.*, 10:691–698, 2000.
- [82] E. Marder and R. L. Calabrese. Principles of rhythmic motor pattern generation. *Physiol. Rev.*, 76:687–717, 1996.
- [83] S. L. McIntire, E. Jorgensen, and H. R. Horvitz. Genes required for GABA function in *Caenorhabditis elegans*. *Nature*, 364:334–337, 1993.
- [84] S. L. McIntire, E. Jorgensen, J. Kaplan, and H. R. Horvitz. The GABAergic nervous system of *Caenorhabditis elegans*. *Nature*, 364:337–341, 1993.
- [85] J. E. Mellem, P. J. Brockie, D. M. Madsen, and A. V. Maricq. Action potentials contribute to neuronal signaling in *C. elegans*. *Nat. Neurosci.*, 11:865–867, 2008.
- [86] C. C. Mello. Return to the RNAi world: Rethinking gene expression and evolution, 2006. http://nobelprize.org/nobel_prizes.
- [87] B. J. Milligan, N. A. Curtin, and Q. Bone. Contractile properties of obliquely striated muscle from the mantle of squid (*Alloteuthis subulata*) and cuttlefish (*Sepia officinalis*). *J. Exp. Biol.*, 200:2425–2436, 1997.

- [88] E. Niebur and P. Erdős. Computer simulation of networks of electrotonic neurons. In R. M. J Cotterill, editor, *Computer simulation in brain science*, pages 148–163. Cambridge University Press, Cambridge, UK, 1988.
- [89] E. Niebur and P. Erdős. Theory of the locomotion of nematodes: Dynamics of undulatory progression on a surface. *Biophys. J.*, 60:1132–1146, 1991.
- [90] S. Park, H. Hwang, S. W. Nam, F. Martinez, R. H. Austin, and W. S. Ryu. Enhanced *Caenorhabditis elegans* locomotion in a structured microfluidic environment. *PLoS ONE*, 3:e2550, 2008.
- [91] S. J. Park, M. B. Goodman, and B. L. Pruitt. Analysis of nematode mechanics by piezoresistive displacement clamp. *Proc. Natl. Acad. Sci.*, 104:17376–17381, 2007.
- [92] P. Phelan and T. A. Starich. Innexins get into the gap. *BioEssays*, 23:388–396, 2001.
- [93] J. T. Pierce-Shimomura, B. L. Chen, J. J. Mun, R. Ho, R. Sarkis, and S. L. McIntire. Genetic analysis of crawling and swimming locomotory patterns in *C. elegans*. *Proc. Natl. Acad. Sci. (USA)*, 105:20982–20987, 2008.
- [94] J. T. Pierce-Shimomura, M. Dores, and S. R. Lockery. Analysis of the effects of turning bias on chemotaxis in *C. elegans*. *J. Exp. Biol.*, 208:4727–4733, 2005.
- [95] J. T. Pierce-Shimomura, T. M. Morse, and S. R. Lockery. The fundamental role of pirouettes in *Caenorhabditis elegans* chemotaxis. *J. Neurosci.*, 19:9557–9569, 1999.
- [96] K. Price and R. Storn. Differential evolution. *Dr. Dobb's Journal*, April:18–24, 1997.
- [97] E. M. Purcell. Life at low reynolds number. *Am. J. Phys.*, 45:3–11, 1977.
- [98] D.V. Ramana Reddy, A. Sen, and G. L. Johnston. Time delay induced death in coupled limit cycle oscillators. *Phys. Rev. Lett.*, 80:5109–5112, 1998.
- [99] J. B. Rand and M. L. Nonet. *Neurotransmitter assignments for specific neurons*, pages 1049–1052. Cold Spring Harbour Laboratory Press, 1997.

- [100] J. E. Richmond and E. M. Jorgensen. One GABA and two acetylcholine receptors function at the *C. elegans* neuromuscular junction. *Nat. Neurosci.*, 2:791–797, 1999.
- [101] M. Rönkkö and G. Wong. Modelling the *C. elegans* nematode and its environment using a particle system. *J. Theor. Biol.*, 253:316–322, 2008.
- [102] K. Sakata and R. Shingai. Neural network model to generate head swing in locomotion of *Caenorhabditis elegans*. *Network-Comp. Neural*, 15:199–216, 2004.
- [103] P. Sauvage. *Etude de la locomotion chez C. elegans et perturbations mecaniques du mouvement*. PhD thesis, Universite Paris, Diderot-Paris 7, September 2007.
- [104] E. R. Sawin, R. Ranganathan, and H. R. Horvitz. *C. elegans* locomotory rate is modulated by the environment through a dopaminergic pathway and by experience through a serotonergic pathway. *Neuron*, 26:619–631, 2000.
- [105] A. Selverston. Modulation of circuits underlying rhythmic behaviours. *J. Comp. Physiol. A*, 176:139–147, 1995.
- [106] A. Shapere and F. Wilczek. Geometry of self-propulsion at low Reynolds number. *J. Fluid Mech.*, 198:557–585, 1989.
- [107] A. Sherman and J. Rinzel. Rhythmogenic effects of weak electrotonic coupling in neuronal models. *Neurobiology*, 89:2471–2474, 1992.
- [108] O. Shimomura. Discovery of green fluorescent protein, GFP, 2008. http://nobelprize.org/nobel_prizes.
- [109] F. Simmer, M. Tijsterman, S. Parrish, S. P. Koushika, M. L. Nonet, A. Fire, J. Ahringer, and R. H. A. Plasterk. Loss of the putative RNA-directed RNA polymerase RRF-3 makes *C. elegans* hypersensitive to RNAi. *Curr. Biol.*, 12:1317–1319, 2002.
- [110] T. Starich, M. Sheehan, J. Jadrlich, and J. Shaw. Innexins in *C. elegans*. *Cell Commun. Adhes.*, 8:311–314, 2001.
- [111] T. A. Starich, A. Miller, R. L. Nguyen, D. H. Hall, and J. E. Shaw. The *Caenorhabditis elegans* innexin INX-3 is localized to gap junctions and is essential for embryonic development. *Devel. Biol.*, 256:403–417, 2003.

- [112] T. Stiernagle. *Maintenance of C. elegans*. WormBook, doi/10.1895/wormbook.1.101.1, <http://www.wormbook.org>, 2006.
- [113] A. O. W. Stretton, R. E. Davis, J. D. Angstadt, J. E. Donmoyer, and C. D. Johnson. Neural control of behaviour in *Ascaris*. *TINS*, 8:294–300, 1985.
- [114] A. O. W. Stretton, R. M. Fishpool, E. Southgate, J. E. Donmoyer, J. P. Walrond, J. E. R. Moses, and I. S. Kass. Structure and physiological activity of the motoneurons of the nematode *Ascaris*. *Proc. Natl. Acad. Sci.*, 75:3493–3497, 1978.
- [115] S. H. Strogatz. *Nonlinear dynamics and chaos*. Perseus Books, Reading, Massachusetts, 1994.
- [116] J. E. Sulston. The cell lineage and beyond, 2002. http://nobelprize.org/nobel_prizes.
- [117] J. E. Sulston and S. Brenner. The DNA of *Caenorhabditis elegans*. *Genetics*, 77:95–104, 1974.
- [118] M. Suzuki, T. Tsuji, and H. Ohtake. A model of motor control of the nematode with neuronal circuits. *Artif. Intel. Med.*, 35:75–86, 2005.
- [119] N. Tavernarakis, W. Shreffler, S. Wang, and M. Driscoll. *unc-8*, a DEG/ENaC family member, encodes a subunit of a candidate mechanically gated channel that modulates *C. elegans* locomotion. *Neuron*, 18:107–119, 1997.
- [120] G. I. Taylor. Analysis of the swimming of microscopic organisms. *Proc. R. Soc. A*, 209:447–461, 1951.
- [121] G. I. Taylor. Analysis of the swimming of long and narrow animals. *Proc. R. Soc. A*, 214:158–183, 1952.
- [122] R. Y. Tsien. Constructing and exploiting the fluorescent protein paintbox, 2008. http://nobelprize.org/nobel_prizes.
- [123] L. R. Varshney, B. L. Chen, E. Paniagua, D. H. Hall, and D. Chklovskii. Structural properties of the *Caenorhabditis elegans* neuronal network. arXiv:0907.2373v2 [q-bio.NC], 2009.
- [124] S. E. Von Stetina, M. Treinin, and D. M. Miller III. The motor circuit. *Int. Rev. Neurobiol.*, 69:125–167, 2005.

- [125] H. R. Wallace. The movement of eelworms. i. *Ann. Appl. Biol.*, 46:74–85, 1958.
- [126] H. R. Wallace. Movement of eelworms in water films. *Ann. Appl. Biol.*, 47:366–370, 1959.
- [127] H. R. Wallace. Movement of eelworms. vi. the influence of soil type, moisture gradients and host plant roots on the migration of the potato root eelworm *Heterodera rostochiensis* wollemoerber. *Ann. Appl. Biol.*, 48:107–120, 1960.
- [128] H. R. Wallace. Wave formation by infective larvae of the plant parasitic nematode *Meloidogyne javanica*. *Nematologica*, 15:65–75, 1969.
- [129] W. W. Walthall, L. Li, J. A. Plunkett, and C. Y. Hsu. Changing synaptic specificities in the nervous system of *Caenorhabditis elegans*: differentiation of the DD motoneurons. *J. Neurobiol.*, 24:1589–1599, 1993.
- [130] Z. W. Wang. Personal Communication, 2007. reporting that no spiking was observed in recordings of *C. elegans* body wall muscles in acutely dissected preparations.
- [131] D. A. Weisblat, L. Byerly, and R. L. Russel. Ionic mechanisms of electrical activity in somatic muscle of the nematode *Ascaris lumbricoides*. *J. Comp. Physiol.*, 111:93–113, 1976.
- [132] D. A. Weisblat and R. L. Russell. Propagation of electrical activity in the nerve cord and muscle syncytium of the nematode *Ascaris lumbricoides*. *J. Comp. Physiol.*, 107:293–307, 1976.
- [133] J. G. White. *The Anatomy*, pages 81–122. Cold Spring Harbor Laboratory Press, Cold Spring Harbor, New York., 1988.
- [134] J. G. White, D. G. Albertson, and M. A. R. Anness. Connectivity changes in a class of motoneurone during the development of a nematode. *Nature*, 271:764–766, 1978.
- [135] J.G. White, E. Southgate, J.N. Thomson, and S. Brenner. The structure of the ventral nerve cord of *Caenorhabditis elegans*. *Philos. Trans. R. Soc. Lond., B, Biol. Sci.*, 275:327–348, 1976.
- [136] J.G. White, E. Southgate, J.N. Thomson, and S. Brenner. The structure of the nervous system of the nematode *Caenorhabditis elegans*. *Philos. Trans. R. Soc. London B Biol. Sci.*, 314:1–340, 1986.

- [137] M. F. Yanik, H. Cinar, H. N. Cinar, A. Gibby, A. D. Chisholm, Y. Jin, and A. Ben-Yakar. Nerve regeneration in *Caenorhabditis elegans* after femtosecond laser axotomy. *IEEE Journal of selected topics in quantum electronics*, 12:1283–1291, 2006.
- [138] M. F. Yanik, H. Cinarm, H. N. Cinarm, A. D. Chisholm, Y. Jin, and A. Ben-Yakar. Neurosurgery: Functional regeneration after laser axotomy. *Nature*, 432:822, 2004.

Appendix A

Publications

The following publications, produced from the work in this thesis, are included.

- J. H. Boyle and N. Cohen**, “The role of body wall muscles in *C. elegans* locomotion”, *Proc. IPCAT 7*, (2007) 364–375.
- J. H. Boyle and N. Cohen**, “*C. elegans* body wall muscles are simple actuators”, *Biosystems*, 94 (2008) 170–181.
- J. H. Boyle, J. A. Bryden and N. Cohen**, “An integrated neuro-mechanical model of *C. elegans* forward locomotion”, *LNCS: Neural Information Processing, Part 1*, 4984 (2008) 37–47.
- S. Berri, J. H. Boyle, M. Tassieri, I. A. Hope and N. Cohen**, “Forward locomotion of the nematode *C. elegans* is achieved through modulation of a single gait”, *HFSP J.*, 3 (2009) 186–193.
- N. Cohen and J. H. Boyle**, “Swimming at low Reynolds numbers: a beginners guide to undulatory locomotion”, *Contemp. Phys.*, 51 (2010) 103–123.